Caractérisation expérimentale et modélisation des phénomènes d'évaporation sur les parois d'une enceinte réfrigérée

Logan Lecoq

THESE DE DOCTORAT

préparée à l'Institut des sciences et industries du vivant et de l'environnement (AgroParisTech)

pour obtenir le grade de

Docteur de l'Institut agronomique vétérinaire et forestier de France

Spécialité : Génie des procédés

École doctorale n°581
Agriculture, alimentation, biologie, environnement et santé (ABIES)

par

Logan LECOQ

Caractérisation expérimentale et modélisation des phénomènes d'évaporation sur les parois d'une enceinte réfrigérée

Directeur de thèse : **Onrawee LAGUERRE**
Co-directeur de la thèse : **Denis FLICK**

Thèse présentée et soutenue à AgroParisTech le 6 octobre 2016 :

Composition du jury :

Mr. Patrick PERRÉ, Professeur, École Centrale Paris	Président
Mr. Alain KONDJOYAN, Directeur de recherche, Inra	Rapporteur
Mr. Alain LE BAIL, Professeur, ONIRIS Nantes	Rapporteur
Mr. Laurent GUILLIER, Chargé de projets scientifiques, Anses	Examinateur
Mme. Onrawee LAGUERRE, Directeur de recherche, Irstea	Directeur de thèse
Mr. Denis FLICK, Professeur, AgroParisTech	Codirecteur de thèse

IRSTEA
1 rue Pierre-Gilles de Gennes CS 10030 92761 Antony cedex

Remerciements

Je tiens à remercier toutes les personnes qui m'ont soutenu et qui ont rendu la réalisation de travail possible.
Tout d'abord mes directeurs de thèse, Onrawee Laguerre et Denis Flick. Leur présence d'esprit, disponibilité et conseils ont rendu ces 3 années très agréable à la fois dans le travail mais aussi humainement.
Je tiens aussi à remercier tout particulièrement Hong-Minh Hoang et Evelyne Derens pour leur aide tout au long de cette période. Ce fut de très belles années particulièrement grâce à elles.
Je remercie Alain Le Bail et Alain Kondjoyan d'avoir accepté de rapporter ce travail. Merci également à Patrick Perré d'avoir accepté de présider mon jury et à Laurent Guillier pour sa participation en tant que membre du jury mais aussi pour les connaissances qu'il a pu m'apporter lors la thèse.
Je tiens ensuite à remercier toutes les personnes ayant participées au projet EcoSec et tout particulièrement Olivier Firmesse qui a dirigé ce projet pendant 4 années. L'ambiance dans ce projet était vraiment agréable et la collaboration avec des personnes venant de divers milieux a été très enrichissante.
Je remercie également Laurence Fournaison de m'avoir accueilli dans l'unité GPAN d'Irstea et plus généralement toutes les personnes présentes dans l'unité. Grâce à eux, l'ambiance de travail y est exceptionnelle.

Résumé

L'objectif de cette thèse est de développer une méthodologie permettant de prédire la cinétique de séchage des parois d'un atelier agro-alimentaire.

Cette méthodologie se base sur des études à différentes échelles dans le but d'analyser les phénomènes liés aux échanges thermique et massique (eau) dans un atelier. Trois études en laboratoire ont été réalisées : dans une boîte ventilée (~0.001 m ^{3}), une soufflerie (~0.02 m^3), une cellule d'essai (~30 m^3) et une étude sur site dans un atelier agro-alimentaire (~450 m^3). Des modèles numériques (Comsol) et analytiques ont été développés permettant de prédire le taux d'évaporation d'eau sur une surface (inox, PVC) et validés avec les données expérimentales obtenues en soufflerie et en cellule d'essai. Pour les conditions expérimentales étudiées, les résultats ont montré que l'humidité relative était le facteur le plus influant sur le taux d'évaporation.

Ces études ont permis le développement d'un modèle simplifié des échanges thermique et massique permettant de prédire l'évolution de la masse d'eau sur les parois d'un atelier en fonction des conditions ambiantes. Ce modèle se base sur une approche zonale en considérant trois parois : un mur, un sol et un équipement. Cela a permis d'étudier l'influence de l'implantation d'un déshumidificateur d'air. Les résultats expérimentaux et numériques ont mis en évidence l'intérêt de l'utilisation d'un tel appareil pour améliorer le séchage des parois. L'humidité relative de l'air dans l'atelier était réduite de 90% à 60% avec un déshumidificateur, ce qui diminuait le temps de séchage d'un facteur 1,5. Il a été montré que l'équipement séchait le plus lentement à cause de sa faible inertie thermique, par conséquent, il restait encore de l'eau même après 2h (durée de séchage de l'atelier). Pour augmenter le taux d'évaporation sur l'équipement, il a été estimé par le modèle qu'un apport de chaleur de 50 W.m^{-2} serait suffisant pour sécher les équipements.

Ce modèle a ensuite été couplé avec un modèle de microbiologie prévisionnelle dont les paramètres ont été identifiés en utilisant les données expérimentales de la cultivabilité de la *Listeria monocytogenes* à différentes humidités relatives dans la boîte ventilée (collaboration l'UMR PAM et l'ANSES). Les résultats ont montré que l'inactivation bactérienne était la plus importante pour une humidité relative aux alentours de 68% et qu'un apport de chaleur à l'équipement de 50 W.m^{-2} permettait d'atteindre un minimum de charge bactérienne au bout de 5 heures au lieu de 12 heures sans apport de chaleur.

Mots clés : atelier agro-alimentaire, évaporation, transfert thermique et massique, modèle simplifié, déshumidification

Abstract

The aim of this Ph.D. thesis is to develop a methodology to predict drying rate on walls in a food processing plant.

This methodology is based on studies at different scales to analyze the heat and mass (water) exchanges in a food plant. Three laboratory studies were performed: a ventilated box (~0.001 m^3), a wind tunnel (~0.02 m^3), a cold room (~30 m^3) and one in a food processing plant (~450 m^3). Numerical (Comsol) and analytical models were developed to predict water evaporation rate on a solid surface (stainless steel, PVC) and validated with experimental data obtained in the wind tunnel and the cold room. For the experimental conditions studied, the results shown that relative humidity was the most influential factor on the evaporation rate.

A simplified heat and mass transfer model was developed to predict the water mass evolution on the walls of a food plant in function of ambient conditions. This model is based on a zonal approach that considers three walls: wall, floor and equipment. The influence of a dehumidifier was studied. The experimental and numerical results showed that the dehumidifier allowed the reduction of relative humidity in the room from 90% to 60% which reduced the drying time by about 1.5 times. It was shown that the equipment dries the slowest due to its low thermal inertia, consequently, water was still remained after 2h (drying duration in the food plant). In order to increase the evaporation rate on the equipment, it was estimated by the model that 50 $W.m^{-2}$ of heat supply could be provided to complete drying.

Finally, this model was coupled to predictive microbiology model where the parameters were identified using the experimental data of the *Listeria monocytogenes* cultivability exposed to different relative humidity in the ventilated box (UMR PAM and ANSES collaboration). The results showed that the inactivation was the highest at 68% of relative humidity and that with the heat supplied to equipment of 50 $W.m^{-2}$, the minimal of bacterial load would be reached after 5 hours instead of 12 hours without heat supply.

TABLE DES MATIERES

CHAPITRE 1 : INTRODUCTION GENERALE

Cette thèse s'inscrit dans le projet national EcoSec : réduction de l'impact environnemental des opérations d'hygiène dans les ateliers agro-alimentaires réfrigérés par une utilisation optimale de la déshumidification de l'air (2013-2016). L'objectif de ce projet est de proposer un moyen écologique et économique pour réduire *Listeria monocytogènes* dans les ateliers agro-alimentaires à l'aide d'une réduction de l'humidité relative. Ce projet comprend 7 partenaires : ANSES Maisons-Alfort (Coordinateur), Irstea Antony, UMR PAM Dijon, INRA Theix, MF conseil, Dessica, Groupe Labeyrie.

Listeria monocytogènes est une bactérie pathogène que l'on retrouve principalement dans l'industrie du saumon, dans les produits prêts à consommer etc… Elle peut être la cause de maladies graves (listériose) avec des taux de mortalité d'environ 20% (EFSA 2015). Cette bactérie a une température minimale de croissance aux alentours de 0°C, elle peut croître tant que l'activité de l'eau est supérieure à 0.92 et avec un pH compris entre 4.6 et 9.5 (Buchanan et al. 2004), ce qui la rend omniprésente dans les ateliers agro-alimentaires. Elle peut facilement être transférée d'une surface à une autre, contaminant l'ensemble de la pièce et principalement les équipements servant à la production (Løvdal 2015). Sa présence amène à la destruction de beaucoup de produits alimentaires. Pour limiter la prolifération bactérienne, des opérations d'hygiène sont effectuées tous les jours après la période de production. Lors de ces opérations, une quantité importante d'eau et de produit désinfectant est utilisée et malgré cela, *Listeria monocytogènes* est capable de résister (Muhterem-Uyar et al. 2015, Vogel et al. 2001). Des petites fissures ou des équipements légèrement endommagés où l'eau peut stagner et où une quantité létale de produit désinfectant n'est pas atteinte servent de refuges aux bactéries (Carpentier & Cerf 2011). La présence d'eau sur les parois de l'atelier ou une humidité relative très importante (> 92%) permet la survie de la bactérie. Pour éviter la présence d'eau stagnante pendant la production, la maitrise de l'étape de séchage juste après le nettoyage est cruciale. Pour cela il est important de comprendre les phénomènes de transfert massique et thermique dans un atelier agro-alimentaire.

De nombreuses études des transferts thermiques et des écoulements dans des équipements frigorifiques ont déjà été réalisées par l'unité de recherche génie des procédés frigorifiques GPAN à Irstea. Des méthodologies expérimentales et numériques permettant la prédiction des champs de température et de vitesse ont été développées et appliquées dans des enceintes réfrigérées avec ou sans ventilation. Les applications concernent les réfrigérateurs domestiques (Laguerre & Flick 2010), les meubles frigorifiques de vente (Laguerre et al. 2012), les véhicules frigorifiques (Hoang et al. 2012) et les chambres froides (Laguerre et al. 2014). L'ensemble de ces études a permis de mettre en évidence l'évolution de la température d'un produit le long de la chaîne du froid jusqu'au réfrigérateur domestique. L'un des objectifs était par exemple de cibler les étapes portant un risque de contamination bactérienne et d'analyser l'impact d'un meilleur contrôle de la température sur la réduction de ce risque (Duret et al. 2014). Pour cela, des approches CFD (Computational Fluid Dynamics) et des modèles simplifiés ont été développés. L'approche CFD permet d'avoir des résultats sur les écoulements et transferts de chaleur en tout point du dispositif étudié. Cependant elle demande un temps de calcul généralement très long. Par exemple pour la modélisation d'un véhicule frigorifique, le temps de calcul de l'approche CFD était estimé à 60h (Moureh et al.

2009) tandis que le modèle simplifié sur ce même dispositif prenait moins d'une minute (Hoang et al. 2012). Les modèles simplifiés, basés sur une approche zonale, permettent aussi de déduire les évolutions de paramètres tels que la température ou encore l'humidité relative mais uniquement en certains points stratégiques du domaine étudié. L'approche zonale consiste à décomposer le domaine d'étude en différentes zones et à exprimer les interactions entre ces zones à l'aide de bilans de chaleur ou de masse par exemple. Les modèles simplifiés, ayant un temps de calcul très court, ils permettent une analyse plus rapide de l'influence de différentes conditions (température de consigne, ouverture de portes, isolation,…) sur les paramètres étudiés (évolution des températures d'air, de parois, des produits,…). Dans les études antérieures, l'influence de l'humidité relative dans le couplage des transferts thermique et massique n'avait pas encore été étudiée tout comme l'étape dans la chaine du froid qui précède le transport des produits : celui d'un atelier de production alimentaire.

Cette thèse apporte une connaissance complémentaire aux études déjà réalisées par GPAN sur 2 points :

- L'étude analyse l'évaporation de l'eau sur différentes surfaces dont la cinétique est fonction des champs de vitesse, température et humidité.
- L'étude porte sur une enceinte réfrigérée de grand volume. Il s'agit d'une application à un atelier agro-alimentaire de volume de l'ordre de 500m^3. Les écoulements, les transferts de chaleur et d'eau sont plus complexes dans cette configuration que dans des réfrigérateurs domestiques, des meubles frigorifiques de vente, des véhicules frigorifiques ou des chambres froides.

De manière plus générale, à notre connaissance il n'y a pas d'étude dans la littérature portant sur l'influence de la déshumidification de l'air soufflé dans un atelier agro-alimentaire sur l'humidité relative de l'air et le taux d'évaporation sur les différentes surfaces (sols, murs, équipements). La quantité d'eau à sécher dans les ateliers après le nettoyage n'a jamais été mesurée à notre connaissance. L'installation d'un déshumidificateur est rarement effectuée dans les ateliers agro-alimentaires et lorsque c'est le cas, elle est réalisée de manière empirique. C'est pourquoi plusieurs expérimentations dans un atelier agro-alimentaire ont été mises en place lors de cette thèse dans le but d'avoir les connaissances nécessaires pour analyser le séchage d'un atelier après son nettoyage.

L'évaporation étant un phénomène endothermique, le taux d'évaporation est influencé par le transfert de chaleur dans la phase liquide à l'interface liquide/vapeur (Hu & Wu 2015, Maa 1967, Mozurkewich 1986, Yang et al. 2014). Le transfert de chaleur lors de l'évaporation est principalement dirigé par le gradient de température entre la surface et l'air environnant tandis que le transfert de masse est lui dirigé par le gradient de concentration de vapeur dans l'air. Dans le cas d'une convection forcée, la vitesse d'air et la turbulence ont aussi un impact sur l'évaporation (Navaz et al. 2008, Raimundo et al. 2014, Vik & Reif 2011). En plus des conditions ambiantes, le type de surface (hydrophobe, hydrophile, faible ou grande conductivité…), de liquide, et la répartition initiale de l'eau ont aussi une influence sur le taux d'évaporation (Beysens 1995, Birdi et al. 1989, Chandra et al. 1996, Croce et al. 2005, Hsu et al. 2015). Des études expérimentales et numériques ont été mises au point dans le but

d'étudier l'influence de toutes ces conditions et d'en déduire des corrélations sur le temps de séchage en fonction de celles-ci.

Parmi les études citées précédemment, certaines ont analysé le refroidissement d'une plaque chaude par évaporation (Chandra et al. 1996, Hsu et al. 2015). Dans leur étude, Chandra et al. 1996 ont analysé l'évaporation d'une goutte d'eau sur une plaque chauffée en inox soumise à une convection naturelle. Ils ont montré l'influence de la surface mouillée sur l'évaporation en ajoutant à la goutte d'eau un surfactant pour diminuer l'angle de contact. Cela a permis de mettre en évidence le fait que l'échange de chaleur entre la goutte et la plaque ainsi que l'évaporation était plus important lorsque la surface mouillée était plus grande. Lors de cette thèse, nous nous sommes focalisés sur l'évaporation de plusieurs gouttes sur une surface à température ambiante (de 5 à 20°C) soumise à un écoulement d'air en prenant en compte la conduction dans la surface, ce qui a rarement été étudié. Pour cela, nous avons utilisé des méthodes empiriques, analytiques et numériques (milieu continu). Certaines études se rapprochent du cas que nous étudions mais des conditions restent différentes. Hu and Wu (2015), Yang et al. (2014) ont étudié l'évaporation d'une goutte d'eau sur une plaque (chauffée ou non chauffée) soumis à différentes humidités relatives et température de plaque. Ils ont développé un modèle numérique et des corrélations semi-empiriques pour prédire notamment le temps de séchage. Cependant leur étude s'applique au cas d'une convection naturelle et non forcée. Navaz et al. (2008) ont étudié particulièrement l'influence de la turbulence dans l'évaporation d'une goutte d'agent chimique sur une surface soumise à une convection forcée et ont développé des corrélations semi-empirique pour prédire la cinétique d'évaporation. Seulement dans leur étude, la conduction dans la surface étudiée n'était pas prise en compte. Le tableau suivant résume les différentes études qui se rapprochent de ce que nous avons réalisé au cours de cette thèse et les différences par rapport à notre cas d'étude.

Ref.	Liquide	Surface	Paramètres variés	Modèle	Conduction (plaque)	Convection
Chandra et al. (1996)	1 goutte d'eau	Plaque chauffée inox	T_{plaque}, angle de contact eau/inox	Numérique	oui	Naturelle
Yang et al. (2014)	1 goutte d'eau	Surface solide	Conductivité, volume goutte, angle de contact	Numérique	oui	Naturelle
Hu and Wu (2015)	1 goutte d'eau	Cuivre et aluminium Chauffée et non chauffée	T_{plaque}, HR_{air}, rayon goutte	Numérique et semi empirique	oui	Naturelle
Navaz et al. (2008)	1 goutte (agent chimique « HD, mustard »)	Surface solide	T_{air}, V_{air}, Turbulence, volume goutte	Semi empirique	non	Forcée
Présente étude	1 (plusieurs) goutte(s), film d'eau	Inox et PVC	T_{air}, HR_{air}, V_{air}, %surface mouillée, Conductivité et épaisseur de plaque	Semi empirique, numérique, théorique	oui	Forcée

Dans le cadre du projet EcoSec, l'impact d'un stress hydrique sur la *Listeria monocytogenes* a été étudié par les partenaires du projet (l'ANSES Maisons-Alfort, l'UMR PAM Dijon, l'INRA Theix). Grâce aux différentes études réalisées, un couplage entre un modèle thermique/massique avec la microbiologie prévisionnelle dans un atelier agro-alimentaire a pu être mis en place. Selon CAC (Codex Alimentarius Commission, 2007) et European Regulation (2002), la microbiologie prédictive est un outil complémentaire pour assurer la qualité et la sureté des produits. C'est une approche qui donne un ordre de grandeur du développement microbien permettant ainsi d'éviter un grand nombre d'expérimentations difficiles à mettre en œuvre et d'optimiser les procédés industriels par un meilleur contrôle de la température par exemple (VamImpe et al. 1995). Les études réalisées auparavant ont principalement utilisé un modèle de microbiologie prévisionnelle pour analyser l'influence de la température sur le développement microbien (Nicolaï & VanImpe 1996, VamImpe et al. 1995, VanImpe et al. 1992). Ici, l'originalité est d'analyser le développement microbien sur les surfaces d'un atelier agro-alimentaire soumis à une dessiccation.

Objectifs de la thèse :

L'objectif scientifique de cette thèse est de développer un outil de prédiction des champs de vitesse, température et humidité d'air ainsi que de la cinétique d'évaporation de l'eau sur différentes surfaces dans une enceinte réfrigérée en fonction des conditions opératoires. Le couplage avec la microbiologie prévisionnelle doit alors permettre de prédire l'évolution de la charge microbienne. Ainsi, les positions chaudes et humides favorables au développement microbien pourront être identifiées.

Grâce à cela, les conditions optimales pour sécher l'eau le plus rapidement possible après nettoyage pourront être proposées. L'impact de l'implantation d'un déshumidificateur d'air dans un atelier agro-alimentaire sur la cinétique d'évaporation d'eau au niveau des différentes surfaces (sol, mur et équipement) sera notamment étudié, représentant l'objectif technologique de cette thèse.

Ceci permettra à terme de réduire la présence de *Listeria monocytogenes* dans ces ateliers et donc dans les produits fabriqués.

Méthodologie développée dans la thèse :

Pour mener à bien ce projet et répondre aux objectifs, divers dispositifs ont été mis en place. Du fait de la complexité des transferts de chaleur et de masse dans un atelier agro-alimentaire, des études à quatre échelles très différentes ont été réalisées. Dans ces quatre échelles, le phénomène d'évaporation de l'eau sur une surface soumis à un écoulement d'air a été étudié. Nous sommes d'abord partis d'une échelle très petite (~0.001 m^3) pour nous rapprocher au fur et à mesure d'un atelier agro-alimentaire (~450 m^3) :

Echelle 1 : **Une boîte hermétique ventilée d'un volume d'environ 0.001 m^3 dans laquelle est placée une boîte de Pétri contenant une goutte d'eau.** Ce dispositif a été utilisé au sein du projet EcoSec par l'équipe de microbiologie de l'UMR PAM à Dijon. Nous étions chargés d'étudier la cinétique de séchage d'une goutte en fonction de l'humidité relative et d'extrapoler les résultats à d'autres conditions opératoires (volume de la goutte, température…). La collaboration avec cette équipe a permis d'établir un lien entre l'évaporation et la décroissance de la cultivabilité bactérienne (article 1).

Echelle 2 : **Une soufflerie d'un volume d'environ 0.02 m^3 dans laquelle est placée une plaque (15 cm x 15 cm) sur laquelle sont déposées quelques dizaines de gouttes d'eau.** Cela permet d'étudier la cinétique d'évaporation des gouttes (masse, surface mouillée) dans des conditions (température, humidité, vitesse d'air, nombre et taille des gouttes) parfaitement maîtrisées. Cette étude a été réalisée dans le but de comprendre plus précisément l'impact de chacun des paramètres sur l'évaporation et d'en déduire des corrélations sur le taux d'évaporation, les évolutions de surface mouillée et température de plaque. Ceci nous a aidé par la suite dans la réalisation d'un modèle thermique et massique d'un atelier. Dans l'objectif de proposer des abaques prédisant le temps de séchage en fonction des conditions opératoires, des simulations par éléments finis de l'évaporation d'une goutte sur une surface ont été réalisées sur le logiciel Comsol et validées avec les expérimentations. Ce logiciel a été choisi car il est adapté pour l'étude de problèmes multi physiques, dans notre cas : évaporation,

convection, conduction et rayonnement. Le temps de calcul d'une simulation étant très court pour le système étudié (quelques minutes), nous avons pu analyser rapidement l'influence d'autres paramètres sur l'évaporation que ceux étudiés expérimentalement (épaisseur de la plaque, conductivité, émissivité, inertie thermique, angle de contact solide/liquide…) pour créer les abaques.

Echelle 3 : **Une cellule d'essai de volume d'environ 30 m^3 à température dirigée dans laquelle est placée une plaque (50 cm x 50 cm) mouillée de quelques dizaines de gouttes d'eau ou dans laquelle le sol est entièrement mouillé.** Dans la cellule d'essai la température, la ventilation et l'humidité relative (un déshumidificateur y a été installé) peuvent être contrôlées. Les vitesses d'air y sont comparables à celles observées dans l'atelier industriel. Cela permet de s'approcher des conditions réelles d'un atelier sans avoir les contraintes de la mesure sur le site. Avec cette échelle nous avons pu faire le lien entre les études réalisées en soufflerie et dans un atelier agro-alimentaire. Dans l'étude où l'on mouille une plaque de 50 cm x 50 cm, qui représente l'évaporation sur un équipement dans un atelier, les mêmes paramètres que dans la soufflerie ont été étudiés dans la cellule d'essai. Les résultats trouvés auparavant (corrélation sur le taux d'évaporation, évolutions de surface mouillée et température de plaque) ont pu être confirmés pour une plus grande échelle (où les conditions sont moins bien maîtrisées), ce qui a facilité l'analyse des études suivantes. L'étude consistant à mouiller entièrement le sol a permis de reproduire les conditions de séchage d'un atelier après son nettoyage (où température et humidité évoluent) et ainsi d'étudier précisément cette étape sans avoir les difficultés que l'on peut retrouver lors des expérimentations sur site (installation du matériel compliquée, mesures limitées, reproductibilité des expériences difficile,…). Un premier modèle simplifié, basé sur un bilan thermique/massique, a été construit sur Matlab pour prédire l'évaporation de la masse d'eau déposée sur le sol de la cellule. Cette configuration étant moins complexe que celle de l'atelier, cela nous a donné une première approche pour le développement d'un modèle zonal dans un atelier agro-alimentaire.

Echelle 4 : **Un atelier alimentaire de volume 450 m^3 dont les équipements, le sol et les murs viennent d'être nettoyés à l'eau chaude.** Un modèle simplifié des échanges thermique et massique basé sur une approche zonale a pu être développé sur Matlab grâce aux connaissances acquises lors des expérimentations précédentes (échelle soufflerie et cellule d'essai) ainsi que des expérimentations réalisées sur le terrain (mesure sur le site des conditions de température, d'humidité relative, de quantité d'eau à sécher). A cela a pu être ajouté un modèle de microbiologie prévisionnelle grâce aux corrélations développées entre le temps de séchage et la décroissance de la cultivabilité bactérienne lors de l'étude réalisée par l'UMR PAM à l'échelle de la boîte hermétique. Ceci a permis de prédire le temps de séchage en fonction des conditions ambiantes et l'impact sur la charge microbienne. Ainsi les conditions optimales pour la destruction bactérienne dans l'atelier ont pu être proposées.

Ci-dessous est représenté un tableau récapitulatif des différentes échelles avec les conditions, paramètres étudiés et méthodes utilisées :

Nomenclature :

h	Coefficient de transfert convectif	$W.m^{-2}.K^{-1}$
HR	Humidité relative de l'air	Sans dimension
m(t)	Evolution de la masse d'eau sur une surface	kg
$\dot{m}$	Taux d'évaporation	$kg.s^{-1}$
n	Nombre de *Listeria monocytogenes* par m²	m^{-2}
r	Rayon d'une goutte d'eau	m
T	Température	°C
t_s	Temps de séchage	s
β	Surface mouillée sur la surface totale	Sans dimension

Souscrits :

0	initiale
pl	plaque

Dispositif	Echelle	Dimensions (m) Long. x larg. x hauteur	Conditions	Paramètres mesuré/prédit	Méthodes
Boîte ventilée	1	0.25 x 0.11 x 0.06	HR(%) : 11-85 T_{air} (°C) : 20 h (W.m^{-2}.K^{-1}) : 50 r_0 matériau : boîte de Pétri (polyéthylène)	t_s	Expérimentale : Mesure d'évaporation d'une goutte
				n	Expérimentale (microbiologique) : UMR PAM Dijon
Soufflerie	2	0.60 x 0.19 x 0.19	HR(%) : 51-85 T_{air} (°C) : 5-20 h (W.m^{-2}.K^{-1}) : 13-40 β_0 (%) : 10-94 matériaux : inox et PVC	$\dot{m}$ t_s β T_{pl}	Expérimentale : Mesure d'évaporation de plusieurs gouttes Théorique : Développement de corrélations Numérique : Comsol
Cellule d'essai	3	3.6 x 3.6 x 2.5	HR(%) : 30-90 T_{air} (°C) : 5-20 h (W.m^{-2}.K^{-1}) : 8-14 β_0 (%) : 7-28 matériaux : inox et inox recouvert de plastique *Conditions expérimentales comparable à celles de la soufflerie*	$\dot{m}$ β T_{pl}	Expérimentale : Mesure d'évaporation de plusieurs gouttes (plaque mouillée, reste de la cellule sec) Théorique : Développement de formules analytiques
			Avec ou sans déshumidificateur $T_{initiale}$ (°C) : 20 $T_{consigne}$ (°C) : 5 $h_{moy\ (sol)}$ (W.m^{-2}.K^{-1}) : 10 β_0 *(%)* : 100 matériau : béton *Reproduction laboratoire des mesures sur site*	t_s HR T_{air} T_{sol} $m(t)$	Expérimentale : Mesure d'évaporation d'un sol entièrement mouillé Numérique : Matlab Première approche au modèle simplifié : prédiction T_{sol} et $m(t)$
Atelier	4	15.5 x 8.2 x 3.6	Avec ou sans déshumidificateur $T_{consigne}$ (°C) : 5	t_s HR T_{air} T_{mur} T_{sol} $T_{équipement}$ $m(t)$ n *(prédit)*	Expérimentale : Mesure sur site de l'évaporation sur trois surfaces : mur, sol et équipement Numérique (approche zonale) : Matlab Développement d'un modèle thermique et massique couplé à la microbiologie prévisionnelle

L'étude à différentes échelles a permis de réaliser 7 articles que nous présentons dans l'organigramme ci-dessous.

1.1. Organisation de la thèse

CHAPITRE 1 : Introduction

CHAPITRE 2 : Etude de l'évaporation d'une goutte d'eau dans une boite ventilée et relation avec l'inactivation microbienne

Volume d'étude ~ 0,001 m^3

Art. 1
Influence of air relative humidity on the evolution of a liquid droplet on a solid plate and relation with microbial destruction

CHAPITRE 3 : Etude de l'évaporation de plusieurs gouttes d'eau dans une soufflerie

Volume d'étude ~ 0,02 m^3

Art. 2
Etude expérimentale
Study of the water evaporation rate on stainless steel plate in controlled conditions

Art.3
Etude numérique
Droplet evaporation on a solid surface exposed to forced convection: experiments, simulation and dimensional analysis

CHAPITRE 4 : Etude de l'évaporation d'eau dans une cellule d'essai

Volume d'étude ~ 30 m^3

Art. 4
Study of the drying process of wetted surfaces in food processing like conditions

CHAPITRE 5 : Application à un atelier agro-alimentaire

Volume d'étude ~ 450 m^3

Art. 5
Simplified heat and mass transfer modeling in a food processing plant

Art. 6
Influence of air dehumidification on water evaporation in a food plant

Art. 7
Influence of the relative humidity on the water drying rate and on microbial growth and inactivation in a food processing plant: Numerical study

CHAPITRE 6 : Conclusion – Perspectives

Nous présentons ici un résumé en français des méthodologies, des principaux résultats et nous mettons en perspective les relations entre les articles.

1.2. Etude de l'évaporation d'une goutte d'eau dans une boîte ventilée (~0.001 m^3)

1.2.1. Introduction

Le séchage, causant un stress hydrique, amène à la destruction microbienne (Dupont et al. 2014). La compréhension des liens entre séchage et inactivation microbienne est ainsi nécessaire dans l'objectif de prévenir la contamination bactérienne dans les ateliers agro-alimentaires. Pour cela, cette étude a été réalisée en collaboration avec l'UMR PAM (Procédés Alimentaires et Microbiologiques, Dijon) dans le but d'analyser le mécanisme d'évaporation d'une goutte et de déduire une corrélation simple pour prédire le temps de séchage en fonction de la température et de l'humidité relative ambiante. Ensuite, une analyse associant le temps de séchage et la perte de cultivabilité de *Listeria monocytogenes* a été réalisée pour différentes humidités relatives, la température d'air étant fixée à 20°C.

1.2.2. Matériels et méthodes

Des expériences ont été réalisées dans une boîte hermétique en polypropylène (longueur x largeur x hauteur = 25 x 11 x 6 cm^3, Figure 1) dans laquelle la température, la vitesse et l'humidité relative étaient contrôlées. L'humidité relative était imposée à l'aide d'une solution de sel saturée : 11% (LiCl), 43% (K_2CO_3), 76% (NaCl), 85% (KCl). Pour homogénéiser l'air dans la boîte, un ventilateur (5 volts) était placé à l'intérieur. La boîte hermétique était dans une cellule où la température y était contrôlée ce qui permettait de maîtriser la température à l'intérieur de la boîte à 20°C.

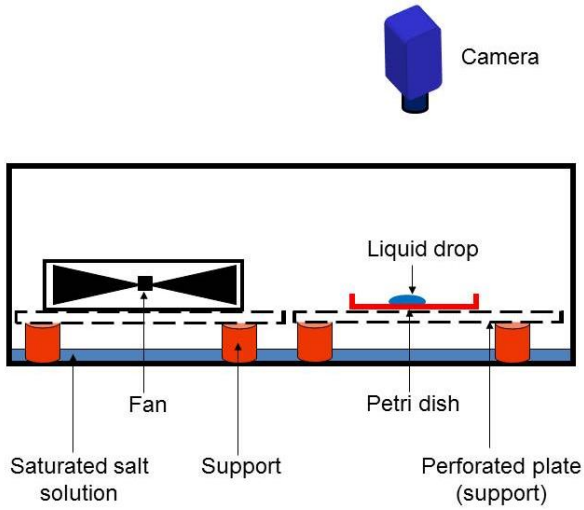

Figure 1 : Schéma du dispositif expérimental (boîte hermétique) dans lequel une goutte de liquide est déposée dans une boîte de Pétri.

Deux types de liquide ont été étudiés : de l'eau distillée et de l'eau mélangée avec une substance nutritive (du « jus » de saumon).

Dans la boîte hermétique, une goutte de liquide (eau distillée ou jus de saumon) d'environ 360 µL était placée sur une boîte de Pétri (en polypropylène) à l'aide d'une pipette. Pour suivre l'évolution de la surface projetée de la goutte au cours de l'évaporation, une caméra était positionnée au-dessus de la boîte, au niveau de la goutte. Des images étaient prises à un

intervalle de temps régulier et à l'aide d'un logiciel d'analyse d'image (Image J), la surface projetée de la goutte était déterminée.
Le même type de boîte contenant différentes solutions saturées de sel a été utilisé dans des expériences de cultivabilité de *Listeria monocytogènes* par l'UMR PAM. La température était fixée à 25°C et une goutte de 10 µL contenant des cellules en suspension était déposée sur une boîte de Pétri. La cultivabilité, exprimée en $\log_{10}$ du nombre de bactérie à l'instant t sur le nombre initial de bactérie a été mesurée toutes les 30 min pendant les 3 premières heures puis à 16 et 24h.

1.2.3. Résultats et perspectives

Les résultats expérimentaux sur l'évaporation ont permis de proposer une corrélation donnant le temps de séchage en fonction du coefficient de transfert de chaleur convectif (lié à la ventilation) (h), du rayon initial de la goutte (r_0) et des températures d'air et de bulbe humide (T_a et T_{wb}). Il est à noter que le temps de séchage semble être inversement proportionnel à la différence de température entre l'air et le bulbe humide (équation 1).

$$t_{drying} = \gamma \frac{r_0}{h(T_a - T_{wb})} \quad (1)$$

Avec γ=1.18x10^9 J.m^{-3} pour un angle de contact de 70 degrés (paramètre identifié avec les données expérimentales).

Grâce à cette relation, les temps de séchage des expériences permettant d'étudier la cultivabilité ont pu être estimés et un lien entre la cinétique d'évaporation (fonction de l'humidité relative) et l'inactivation microbienne a été établi. Il a été remarqué que plus l'humidité relative était élevée, plus le temps de séchage était long et plus la cinétique d'inactivation bactérienne était lente.

Publication :

Cette étude est présentée en détails dans l'article 1 « Influence of air relative humidity on the evolution of a liquid droplet on a solid plate and relation with microbial destruction » : influence de l'humidité relative sur le séchage d'une goutte et relation avec la destruction microbienne (Soumis à Food Research International le 5 Avril 2016).
Les résultats expérimentaux de l'inactivation microbienne ont par ailleurs permis de modéliser la cinétique et la fraction résiduelle en fonction de l'humidité relative, puis, ce modèle a été inclus dans le modèle thermique et massique d'un atelier agro-alimentaire. Cela a permis de prédire l'évolution de la *Listeria monocytogènes* sur les surfaces d'un atelier agro-alimentaire en fonction des conditions ambiantes (présenté dans l'article 7).

1.3. Etude de l'évaporation de plusieurs gouttes d'eau dans une soufflerie (~0.02m^3)

1.3.1. Introduction

Dans un atelier agro-alimentaire le matériau utilisé pour fabriquer les équipements est principalement l'inox. Afin de comprendre le mécanisme d'évaporation de l'eau sur cette surface, des expériences ont été réalisées dans une soufflerie de section 19 x 19 cm² (volume d'environ 0.02 m^3) où la température, la vitesse d'air et l'humidité relative sont bien maitrisées. Lors de cette étude, une méthodologie expérimentale a été développée pour caractériser le taux d'évaporation de l'eau déposée sur une plaque en inox à différentes conditions ambiantes. Un modèle empirique prédisant la cinétique de l'évaporation en fonction de la température, la vitesse, l'humidité de l'air et la répartition initiale de l'eau sur la plaque en inox a été établi.

Deux études numériques considérant l'évaporation d'une goutte d'eau sur une plaque dans les mêmes conditions que celles expérimentales ont, par la suite, été réalisées. La première est une modélisation simplifiée en régime quasi-statique (changement géométrique de la goutte et terme transitoire, $C_p \frac{\partial T}{\partial t}$, négligés). La conduction dans la plaque et dans la goutte ainsi que les échanges convectifs (chaleur, masse) avec l'air sont pris en compte. Une simulation quasi-statique a pu être envisagée car il a été observé lors des expériences que le taux d'évaporation était quasiment constant pendant la plupart du temps. Les taux d'évaporation expérimentaux et numériques pendant cette période ont été comparés pour valider le modèle. Ensuite un second modèle en régime transitoire a été mis au point pour étudier l'évaporation de façon plus approfondie. L'influence des caractéristiques du matériau de la plaque (épaisseur, inox ou PVC) et des gouttes (taille, fraction de surface mouillée) sur le taux d'évaporation a été étudiée. La simulation a été réalisée en utilisant la méthode des éléments finis sur le logiciel Comsol (version 5.0).

1.3.2. Matériels et méthodes

La soufflerie (Figure 2) était placée dans une cellule dans laquelle la température de l'air et l'humidité relative étaient maîtrisées. Pour vérifier ces paramètres dans la soufflerie, un hygromètre capacitif (Testo 174H, $\pm$ 3%) et des thermocouples type T (1 mm diamètre, $\pm$ 0.2°C précision) étaient placés à l'intérieur de la veine. L'évolution de la surface mouillée au cours de l'évaporation était suivie par la prise d'images avec une caméra et à l'aide d'un logiciel d'analyse d'image. La masse d'eau sur la plaque était mesurée pendant l'expérience à l'aide d'une balance (précision ± 0.001 g). La vitesse d'air était mesurée sur une section de la soufflerie juste avant la plaque avec un anémomètre à fil chaud (TESTO 435-2, plage de valeurs 0-20 m.s^{-1}, ± 0.03 m.s^{-1} précision). Le coefficient de transfert convectif sur la plaque était mesuré en utilisant un fluxmètre (Captec, largeur x hauteur x épaisseur: 4 cm x 4 cm x 450 µm).

Dans cette étude, *HR* était variée de 51 à 85%, T_{air} de 5 à 20°C, h de 13 à 40 W.m^{-2}.K^{-1} et β_0 de 10 à 94%. Les conditions utilisées sont détaillées dans l'article 2, Tableau 1.

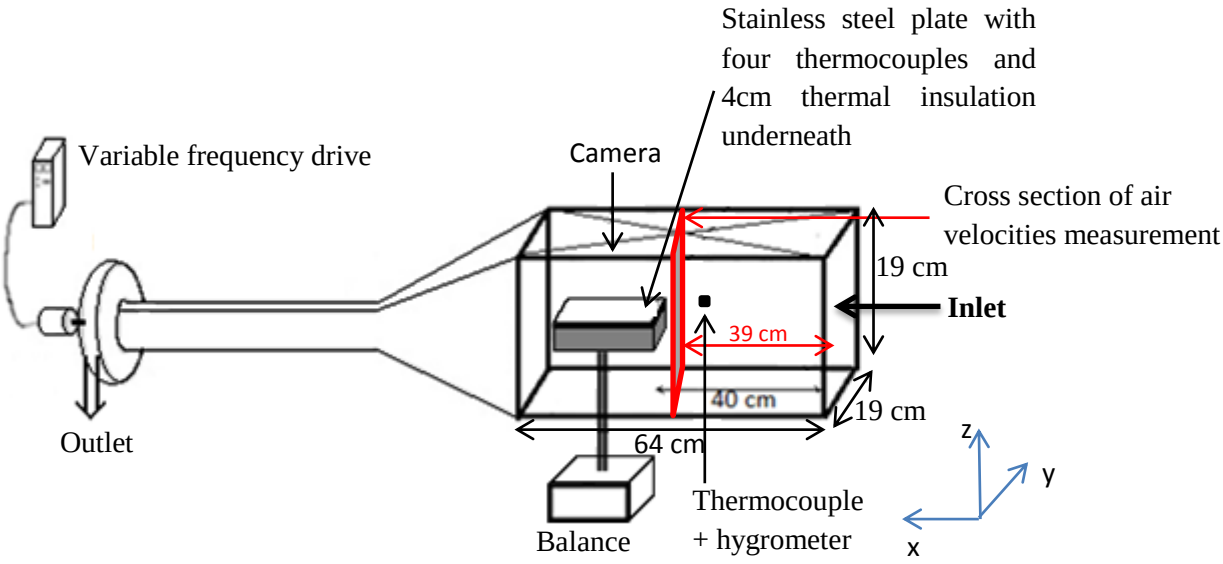

Figure 2 : Schéma de la soufflerie

1.3.3. Résultats de l'étude expérimentale

Il a été constaté que l'évaporation de l'eau sur une surface en inox est composée de deux périodes : la première où la surface de contact entre l'eau et la plaque reste constante, période pendant laquelle le taux d'évaporation reste quasiment constant ; la seconde où cette surface de contact diminue progressivement entraînant un taux d'évaporation de plus en plus faible.

Par rapport à l'expérience réalisée dans la boîte ventilée sur une boîte de Pétri, il y a deux différences notables : la première période est quasi inexistante pour la boîte de Pétri du fait de la nature hydrophobe du matériau (polyéthylène) et la conduction dans ce matériau est négligeable contrairement à celle de l'inox. Ceci fait que les corrélations obtenues ont des formes différentes.

L'étude expérimentale a permis de mettre en évidence que le taux d'évaporation était proportionnel à la différence entre la température de l'air (T_a) et celle de la plaque (T_{pl}). Cette différence dépend de l'humidité relative de l'air et de la répartition de l'eau sur la plaque. Plus la plaque est couverte d'eau, plus sa température est proche de la température humide (T_{wb}). Les expériences réalisées ont permis de développer une corrélation empirique pour modéliser ce phénomène sur une plaque en inox (conductivité supposée infinie) :

$$\frac{T_a - T_{pl}}{T_a - T_{wb}} = f(\beta_0) \approx \frac{3 \cdot \beta_0}{1 + 2 \cdot \beta_0} \qquad (2)$$

où β_0 est le rapport entre la surface mouillée initiale et la surface totale de la plaque (S).

Ceci a permis d'en déduire une corrélation simple pour estimer le taux d'évaporation ($\dot{m}$) en fonction de la différence entre la température de l'air et la température humide, de la surface mouillée sur la surface de la plaque (β_0) et du coefficient de transfert convectif *h* (équation 3). Ce coefficient h dépend de la vitesse d'air dans la soufflerie. Pendant la première période de l'évaporation (surface mouillée constante), on a :

$$\dot{m} = \frac{S \cdot f(\beta_0) \cdot (T_a - T_{wb}) \cdot h(v)}{\Delta H_v} \quad (3)$$

En complément de l'étude précédente réalisée pour une goutte dans une boîte ventilée, il a été montré l'influence majeure de la surface mouillée sur le taux d'évaporation.

Des expériences similaires ont été réalisées sur une plaque en PVC. Les différents résultats expérimentaux ont ensuite été comparés avec les valeurs numériques des simulations présentées ci-dessous.

1.3.4. Résultats de l'étude numérique

1.3.4.1. Modélisation en régime quasi-statique

Les comparaisons des taux d'évaporation expérimentaux et numériques ont montré que pour la première période d'évaporation, l'hypothèse d'un régime quasi-statique était valide (écart relatif moyen entre les deux résultats de 7.8%). L'avantage de ce modèle est de fournir une bonne estimation du taux d'évaporation dans les conditions étudiées tout en utilisant un modèle simple. De plus, l'évaporation de l'eau sur une surface moins conductrice peut aussi être estimée avec ce modèle, ce qui n'est pas le cas avec la corrélation empirique développée expérimentalement (équation 3) valable pour une conduction supposée infinie.

Publication :

L'étude expérimentale ainsi que ce modèle sont présentés en détails dans l'article 2 «Study of the water evaporation rate on stainless steel plate in controlled conditions » : influence des conditions ambiantes (humidité relative, température, vitesse d'air) et de la surface mouillée sur l'évaporation de gouttes d'eau déposées sur une plaque en inox : développement d'un modèle empirique et numérique (Soumis à *International Journal of Thermal Sciences* le 12 Février 2016).

1.3.4.2. Modélisation en régime transitoire

Les caractéristiques physiques des phases liquide et solide ont un impact important sur l'angle de contact liquide/solide, les dimensions de la goutte (rayon, hauteur) et de ce fait sur l'évaporation. Dans le cas d'une surface hydrophobe, l'évaporation de l'eau peut entrainer directement une diminution de la surface de contact. Dans l'objectif de comprendre cette influence, une simulation en régime transitoire a été réalisée. Les changements géométriques de la goutte (diminution du volume de la calotte sphérique puis de la surface de contact entre l'eau et la plaque) ont été simulés pendant toute la durée de l'évaporation et les résultats ont été comparés avec les valeurs expérimentales (voir 1.3.2 et 1.3.3). Dans la littérature, les modèles numériques qui sont développés ne prennent en compte généralement que la première période de l'évaporation (rayon constant, diminution de l'angle de contact) (Hu & Wu 2015, Yang et al. 2014), contrairement à cette étude qui modélise les deux périodes. Le modèle a aussi permis d'effectuer par la suite une analyse des paramètres adimensionnels ayant une influence sur le taux d'évaporation et d'établir des abaques permettant d'estimer les temps de séchage dans des cas pratiques variés.

Lors de ces études (expérimentale et numérique) il a pu être mis en évidence une relation reliant l'évolution de la surface mouillée pendant les deux périodes de l'évaporation (constante pendant la 1ère période et dépendant de la masse d'eau pendant la seconde) :

$$\beta(t) = \min\left(\beta_0, \frac{m(t)^{\frac{2}{3}}}{(0{,}15 \cdot m_0)^{\frac{2}{3}}} \cdot \beta_0\right) \quad (4)$$

Lorsque la masse d'eau atteint 15% de la masse initiale, la seconde période commence. Cette équation (4) a été validée lors des expériences réalisées en cellule d'essai (en ambiance moins contrôlée) et a pu être appliquée lors de la réalisation d'un modèle des échanges thermique et massique dans un atelier agro-alimentaire pour prédire la cinétique de séchage sur les surfaces. En effet, la connaissance de l'évolution de ce coefficient β est nécessaire pour prédire la température de la surface et ainsi l'évolution de la masse d'eau pendant les deux périodes de l'évaporation.

Publication :

Cette étude est présentée en détails dans l'article 3 « Droplet evaporation on a solid surface exposed to forced convection: experiments, simulation and dimensional analysis » : évaporation d'une goutte sur une surface solide soumise à une convection forcée : expériences, simulation et analyse dimensionnelle (soumission à *International Journal of Heat and Mass Transfer* prévue en Juillet 2016).

1.4. Etude de l'évaporation d'eau dans une cellule d'essai (~30 m^3)

1.4.1. Introduction

Dans une cellule d'essai ayant un volume d'environ 30 m^3, les conditions ambiantes (vitesse d'air, température et humidité relative) sont moins bien maîtrisées que pour les études réalisées en soufflerie mais restent mieux contrôlées que dans un atelier agro-alimentaire. Deux types d'expériences ont été effectués.

Expérience A

Cette expérience est similaire au séchage d'un équipement (généralement en inox) où les conditions ambiantes étudiées sont semblables à celles que l'on retrouve dans un atelier agro-alimentaire. Des mesures de cinétique d'évaporation d'eau sur une plaque en inox placée à différentes positions dans la cellule ont été réalisées. Les corrélations développées en soufflerie ont été utilisées dans cette configuration pour vérifier leurs validités dans un environnement plus proche d'un atelier agro-alimentaire.

Expérience B.

Cette expérience a été réalisée pour étudier le processus de séchage sur la surface (le sol) où la quantité la plus importante d'eau est observée après nettoyage. Les conditions ambiantes choisies étaient proches de celles d'un atelier agro-alimentaire et l'impact d'un déshumidificateur a été étudié. L'expérience consiste à verser une quantité d'eau connue sur toute la surface du sol de la cellule (quantité d'eau similaire à ce que l'on retrouve dans un atelier) et d'étudier la vitesse de séchage au sol avec et sans déshumidificateur d'air. Un premier modèle simplifié, basé sur un bilan thermique/massique au niveau du sol, a été construit sur Matlab pour prédire l'évaporation de la masse d'eau déposée sur le sol de la cellule. Cette configuration étant moins complexe que celle de l'atelier, cela nous a donné une première approche pour le développement d'un modèle zonal dans un atelier agro-alimentaire.

1.4.2. Matériels et méthode

La cellule (3.6 x 3.6 x 2.5 m^3, Figure 3) était régulée en température et en humidité relative à l'aide d'un évaporateur et d'un déshumidificateur. La vitesse d'air en sorti des évaporateurs pouvait être ajustée avec un variateur de fréquence.

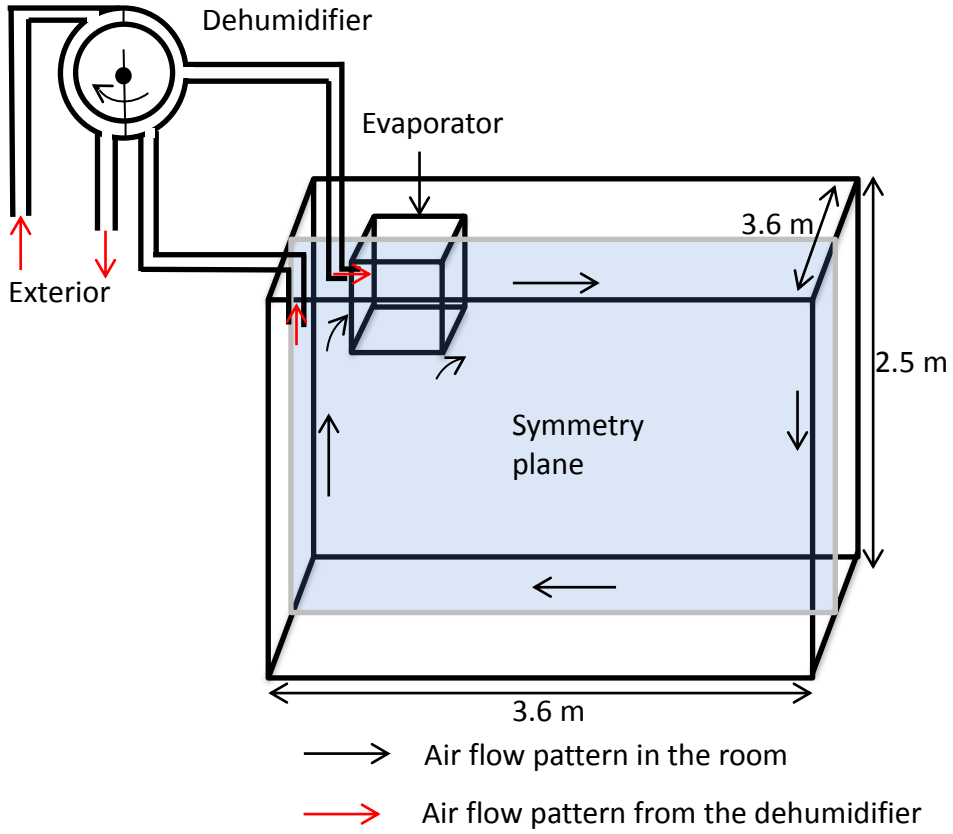

Figure 3 : Schéma de la cellule d'essai avec les écoulements d'air

Expérience A : Evaporation de gouttes d'eau sur une plaque en inox

Des gouttes d'eau de 0.5 mL (100 gouttes) ont été déposées sur la plaque avec une pipette. La plaque était placée sur une balance (précision ± 0.001 g) et la mesure de la masse d'eau pendant l'évaporation était effectuée toutes les 10s jusqu'à ce qu'il ne reste plus d'eau. La température dans la pièce était mesurée à l'aide de thermocouples de type T (1 mm diamètre, ± 0.2°C précision) qui étaient placés au soufflage, à la reprise de l'évaporateur et deux autres proches de la plaque (10 cm au-dessus de la plaque). L'humidité relative était mesurée aux mêmes emplacements à l'aide d'hygromètre capacitif (Testo 174 H, ± 3%). La vitesse d'air était mesurée à la reprise et au soufflage de l'évaporateur avec un anémomètre à fil chaud (TESTO 435-2, plage de mesures 0-20 $m.s^{-1}$, ± 0.03 $m.s^{-1}$ précision). La vitesse était variée de 2.0 à 4.8 $m.s^{-1}$ correspondants à un débit d'air dans la pièce allant de 1000 à 2400 $m^3.h^{-1}$. Pour étudier l'influence de la position de la plaque dans la cellule, celle-ci a été placée à différents endroits. Les emplacements des capteurs et les positions de la plaque dans la cellule sont indiqués plus précisément dans l'article 4, Figure 2. Le coefficient de transfert convectif sur la plaque correspondant aux différentes vitesses d'air ou positions a été mesuré en utilisant un fluxmètre (Captec, largeur x hauteur x épaisseur: 4 cm x 4 cm x 450 µm).

Dans cette étude, *HR* était variée de 30 à 90%, T_{air} de 5 à 20°C, h de 8 à 14 $W.m^{-2}.K^{-1}$ et β_0 de 7 à 20%. Les conditions utilisées sont détaillées dans l'article 4, Tableau 1.

Expérience B : Sol entièrement mouillé

Dans cette expérience, 230 g.m^{-2} d'eau (similaire à la mesure effectuée sur site) a été déposée au sol, représentant 3 kg d'eau au total. Une autre expérience a été réalisée en ne déposant que 1 kg d'eau, représentant la quantité d'eau qu'il reste si le sol est raclé par des techniciens. Pour mesurer la masse d'eau sur le sol, des lingettes étaient utilisées pour essuyer toute la surface et ensuite pesées avec une balance (Sartorius, CPA34001P, ± 0.1 g). Par exemple, pour 3kg d'eau initialement déposé au sol et sans déshumidificateur, l'expérience a été réalisée 7 fois avec les mêmes conditions initiales (masse d'eau, température, humidité relative) et arrêtée pour prélever toute la masse d'eau au sol au bout de 30min, 1h, 3h, 5h, 10h, 16h20, 20h, permettant de connaître son évolution au cours du séchage. La température et l'humidité relative était mesurées dans la pièce (reprise, soufflage de l'évaporateur et 3 autres à 1m de hauteur à différentes positions dans l'axe de symétrie : 0.2m, 1.8m et 3.4m) en utilisant des capteurs Testo (174H, ± 3%RH, ±0.5 °C précision). La température au sol était mesurée à l'aide de thermocouples type T (1 mm diamètre, ± 0.2°C précision) avec 4 mm d'isolant sur les capteurs. Les emplacements des capteurs sont indiqués plus précisément dans l'article 4, Figure 1. Le coefficient de transfert convectif a été mesuré à 7 positions différentes au sol en utilisant un fluxmètre (Captec, largeur x hauteur x épaisseur: 4 cm x 4 cm x 450 µm) pour estimer la valeur globale de ce coefficient. La vitesse d'air soufflée par l'évaporateur était fixée à 2.0 m.s^{-1} pour cette expérience.

Les températures initiales (air et parois) étaient fixées à 20°C, l'humidité relative initiale à 40-50% et la température de consigne était réglée à 5°C. Pour étudier l'influence d'un déshumidificateur, les expériences (1 kg et 3 kg d'eau initialement déposée sur le sol) ont été réalisées avec et sans déshumidificateur. Lorsqu'il était en fonctionnement, la valeur de la consigne pour l'humidité relative était de 45%.

1.4.3. Résultats

Expérience A : Evaporation de gouttes d'eau sur une plaque en inox

Lors de cette étude les mêmes phénomènes ont pu être observés que lors de celle réalisée en soufflerie, c'est-à-dire, un rayon de goutte constant puis un angle de contact constant pendant l'évaporation. Les différents paramètres ayant une influence sur le débit d'évaporation ont été analysés (HR, T_{air}, h et β_0) pour cette échelle. Dans les conditions expérimentales étudiées, la diminution de l'humidité relative de 90% à 30% a augmenté le débit d'évaporation d'un facteur de 5.2 (débit d'évaporation mesuré pendant la 1ère période d'évaporation, où il est quasiment constant). Le changement des autres paramètres (température, vitesse de l'air, surface mouillée) n'a permis une augmentation du débit d'évaporation que de 2.3 au maximum dans les plages de valeurs étudiées. Ainsi, il semblerait que la réduction de l'humidité relative par l'utilisation d'un déshumidificateur soit une solution efficace pour augmenter de façon signifiante le débit d'évaporation et ainsi réduire le temps de séchage. En effet, dans un atelier agro-alimentaire, lorsqu'il n'y a pas déshumidificateur, l'humidité relative est souvent au-dessus de 85% ce qui est extrêmement défavorable pour le séchage.

Les corrélations empiriques développées (eq. 2 et 3) en soufflerie ont pu être appliquées dans cette étude. Le débit d'évaporation calculé avec ces formules (pendant la 1ère période où la cinétique d'évaporation est quasiment constante) a montré un bon accord avec les résultats expérimentaux, l'erreur relative étant en moyenne de 16%. Une formule théorique basée sur un bilan de chaleur sur la plaque et l'analogie de Lewis a aussi été développée lors de cette étude pour prédire le débit d'évaporation. La formule théorique a montré de meilleurs résultats avec une erreur relative de 9%. L'évolution de la masse d'eau pendant les deux

périodes d'évaporation a aussi pu être prédite avec une bonne précision en utilisant l'équation (4) développée avec les études réalisées en soufflerie. Cette étude a donc aussi montré l'applicabilité des résultats trouvés en soufflerie pour de plus grand volume, dans des ambiances moins bien contrôlées.

Expérience B : Sol entièrement mouillé

Lors de cette expérience, l'impact d'un déshumidificateur a pu être étudié pour le séchage d'un sol entièrement mouillée. Il a été remarqué que, du fait d'une inertie thermique importante du sol, le débit d'évaporation était du même ordre de grandeur avec et sans déshumidificateur au début du séchage. L'impact du déshumidificateur était notable pour les 20% d'eau restante sur le sol. Par exemple, lorsque 3 kg d'eau était déposée au sol, après 20 h il restait encore quelques grammes (23 g) sans déshumidificateur, alors que le sol était quasiment sec au bout de 10 h avec déshumidificateur. Le fait d'avoir cet appareil permettait de conserver une humidité relativement basse (~50%) alors qu'elle montait jusqu'à 90% sans déshumidificateur. De ce fait, lorsque l'inertie thermique n'était plus assez grande pour apporter la chaleur pour faire évaporer l'eau, le séchage des 20% d'eau restant au sol était quasiment impossible sans déshumidificateur.

Un modèle qui se base sur un bilan thermique et massique au sol a été développé lors de cette expérience en utilisant aussi l'équation (4) (évolution de la surface mouillée pendant l'évaporation) permettant de prédire l'évolution de la température et de la masse d'eau sur le sol. En plus de l'utilité d'un déshumidificateur sur le séchage des surfaces, ce modèle a permis de mettre en évidence l'impact de la qualité de la surface sur l'évaporation. Si la surface en question est abîmée ou bondée et permet à l'eau de s'accumuler à certaines positions, le séchage complet ne pourra pas être réalisé en deux heures (temps moyen pour l'étape de séchage d'un atelier agro-alimentaire) même avec un déshumidificateur. Il y aura toujours de l'eau stagnante, ce qui favorisera le développement microbien, un des problèmes important pour les industries.

La résolution des équations pour les expériences A et B a été effectuée sur le logiciel Matlab (vR2012a; The MathWorks Inc., Natick, MA, USA).

Publication :

Cette étude est présentée en détail dans l'article 4 « Study of the drying process of wetted surfaces in food processing like conditions » : Etude du séchage de surfaces mouillées dans des conditions semblables à celles d'un atelier agro-alimentaire (revue visée : *International Journal of Refrigeration*, soumission prévue en Juillet 2016).

1.5. Etude du séchage après nettoyage dans un atelier agro-alimentaire et de son influence sur la prolifération bactérienne (~450 m^3)

1.5.1. Introduction

Deux expérimentations dans un atelier agro-alimentaire de volume d'environ 450m^3 ont été réalisées. La première a été mise en place (mai 2013) dans le but de connaître les conditions opératoires, la durée des étapes (production, nettoyage, séchage) et la masse d'eau à sécher dans la pièce après le nettoyage de l'atelier. Les résultats de cette expérimentation et ceux de la soufflerie et cellule d'essai (paragraphe 1.3 et 1.4) ont été utilisés pour élaborer un modèle simplifiée (2D) des échanges de chaleur et de masse dans l'atelier agro-alimentaire (paragraphe 1.5.3). Ce modèle permet de déterminer la cinétique d'évaporation de l'eau déposée sur les surfaces lors du nettoyage. Après validation, ce modèle a pu être utilisé pour prédire l'évolution du séchage sur les parois dans d'autres conditions (humidité relative au soufflage différente par exemple).

Par la suite, un déshumidificateur d'air a été installé dans l'atelier. Pour voir l'impact de son implantation sur le séchage, une deuxième expérimentation sur le terrain a été effectuée sur deux jours (avril 2015). Le premier jour, le déshumidificateur dans l'atelier était en fonctionnement et des mesures de température, vitesse, humidité relative et masse d'eau ont été prises. Le deuxième jour, le déshumidificateur n'était plus en fonctionnement et les mêmes mesures que lors du premier jour ont été réalisées. Le modèle développé précédemment a été légèrement modifié pour s'adapter à la nouvelle configuration de l'atelier et a permis d'étudier l'influence de nouvelles conditions.

Pour finir, la microbiologie prévisionnelle a été incluse dans le modèle de transfert thermique et massique pour prédire l'évolution de la charge de *Listeria monocytogenes* à différents endroits dans l'atelier. Ainsi, nous pouvons évaluer les risques sanitaires et envisager des solutions pour réduire la prolifération bactérienne.

1.5.2. Matériels et méthodes

Les mesures de température et d'humidité relative dans l'atelier ont été prises avec des thermistances (Testo 171, $\pm$ 0.2°C) et des hygromètres capacitifs (Testo 174H, $\pm$ 3%), respectivement. Les mesures ont été réalisées à plusieurs endroits de manière à obtenir une bonne connaissance de l'évolution de ces paramètres dans la pièce. Les vitesses d'air ont aussi été relevées à la reprise d'un évaporateur et du déshumidificateur avec un anémomètre à fil chaud (Testo 435-2, plage de mesure : 0-20 $m.s^{-1}$, $\pm$ 0.03 $m.s^{-1}$ précision) permettant d'estimer les débits d'air : ~12 000 $m^3.h^{-1}$ au niveau de l'évaporateur et ~3000 $m^3.h^{-1}$ au niveau du déshumidificateur. Pour avoir une estimation de la quantité d'eau à sécher sur les différentes surfaces de l'atelier après le nettoyage et l'évolution de cette quantité pendant le séchage, des prélèvements d'eau ont été effectués sur trois surfaces : le mur, le sol et un équipement. Pour mesurer la masse d'eau présente, des lingettes étaient utilisées pour essuyer une surface de 25 cm x 50 cm sur le sol et 50 cm x 50 cm sur le mur et un équipement. Après prélèvements, les lingettes étaient déposées dans un sac plastique fermé. Elles étaient ensuite pesées à l'aide d'une balance (Sartorius, CPA34001P, $\pm$ 0.1 g). Cette démarche était répétée toutes les 30

min sur les surfaces adjacentes aux premiers prélèvements pendant les deux heures de séchage permettant de suivre l'évolution de la charge en eau.

L'implémentation des modèles simplifiés des échanges de chaleur et de masse ainsi que le modèle de microbiologie prévisionnelle relatif à cet atelier agro-alimentaire a été réalisé sur le logiciel Matlab (vR2012a; The MathWorks Inc., Natick, MA, USA).

1.5.3. Développement d'un modèle simplifié des échanges de chaleur et de masse

Dans le but d'optimiser le processus de séchage, un modèle simplifié basé sur les données d'un atelier agro-alimentaire (géométrie, température de consigne dans la pièce, humidité relative au soufflage…) a été développé. Il permet la prédiction des températures et humidités relatives de l'air en différents points de l'atelier (1 à 6, Figure 4) ainsi que de l'évolution des températures et des masses d'eau sur le mur, le sol et un équipement.

La figure ci-dessous montre schématiquement l'écoulement d'air et les échanges qui ont lieu dans une section de l'atelier.

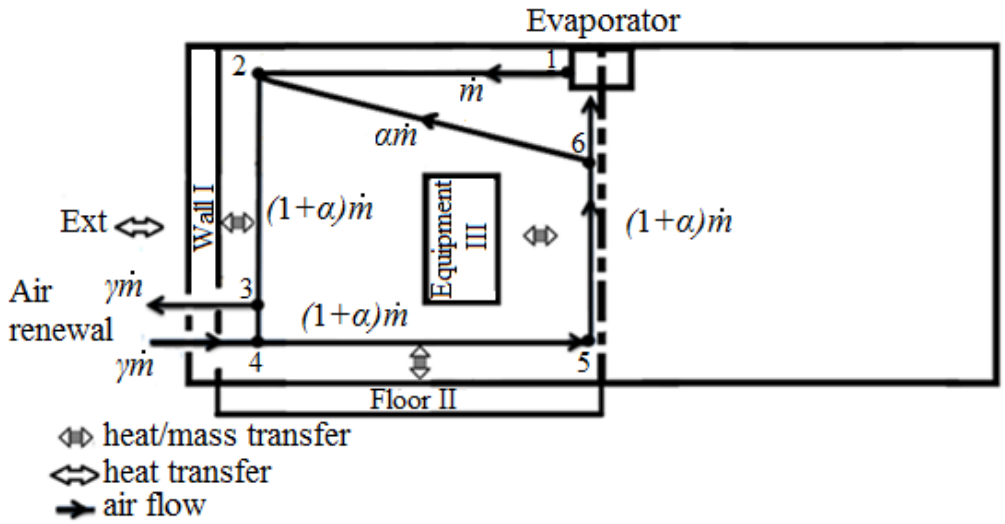

Figure 4 : Modèle d'écoulement d'air simplifié, transferts de chaleur et de masse dans un atelier agro-alimentaire (vue de côté)

Sur chacun des points 1 à 6 et pour les trois surfaces (mur, sol et équipement), un bilan de chaleur et de masse est réalisé.

Le modèle a été validé en comparant les résultats obtenus pour l'évolution des masses d'eau et des températures d'air avec les données expérimentales récoltées lors du premier essai dans l'atelier. Par la suite, l'influence sur les cinétiques d'évaporation d'autres conditions ambiantes a été étudiée numériquement. Il a été observé que l'humidité relative au soufflage était l'un des paramètres clés pour améliorer le séchage. Lorsque l'on imposait une humidité relative au soufflage de 50% (ordre de grandeur de l'humidité relative d'un atelier avec déshumidificateur en fonctionnement) au lieu de 85% (condition usuelle sans déshumidificateur), le taux d'évaporation sur les surfaces était environ 1,5 fois plus important (cf. paragraphe 1.5.4.).

Le modèle développé dans cette étude peut être généralisé à d'autres ateliers, à partir du moment où certaines caractéristiques propres à l'atelier en question sont connues. Les différents paramètres à connaître pour appliquer le modèle sont donnés sur le tableau suivant :

Tableau 1 : Paramètres à connaitre pour appliquer le modèle à un autre atelier

Atelier	• Géométrie (surfaces, m²)
Surfaces (mur, sol, équipement)	• Inertie thermique ($J.K^{-1}$) • Température initiale (°C) • Masse d'eau initiale $kg_{water}.m^{-2}$, répartition (% surface mouillée) • Vitesse proche des surfaces ($m.s^{-1}$)
Evaporateur	• Puissance (W) • Débit d'air ($m^3.h^{-1}$) • Température de consigne (°C) • Humidité relative de l'air soufflé (%)
Déshumidificateur	• Puissance (W) • Débit d'air ($m^3.h^{-1}$) • Température (°C) et humidité soufflé (%)

Publication :

Cette étude est présentée en détails dans l'article 5 « Simplified heat and mass transfer modeling in a food processing plant » : mise en place d'un modèle simplifié d'échanges de masse et de chaleur dans un atelier agro-alimentaire : prédiction de l'évaporation d'eau sur les parois (Journal of Food Engineering, 2016, v. 171, p. 1–13).

1.5.4. Etude expérimentale et numérique de l'impact sur le séchage de la mise en place d'un déshumidificateur dans un atelier

Dans les ateliers agro-alimentaires, il est rare que des déshumidificateurs soient installés et lorsqu'ils le sont, c'est souvent de manière empirique. Les expérimentations réalisées dans l'atelier (un jour avec déshumidificateur et un jour sans) nous ont permis de constater que l'humidité relative de l'air dans la pièce sans déshumidificateur était très élevée : aux alentours de 85-90%, impliquant un séchage relativement lent sur les surfaces étudiées (>120 min). Alors que quand le déshumidificateur était en marche, l'humidité relative de l'air était d'environ 60% assurant un séchage de la pièce plus rapide (~100 min). Cependant, dans les deux cas (avec ou sans déshumidificateur), de l'eau pouvait encore être présente à la fin des

deux heures de séchage, notamment dans les coins de l'atelier et sur des équipements complexes, là où les vitesses d'air sont plus faibles. De plus, nous avons pu constater que les équipements étaient de manière générale les surfaces qui séchaient le plus lentement du fait d'une plus faible inertie thermique comparés au sol et aux murs. Le nettoyage étant réalisé avec de l'eau chaude (~40°C) les températures d'air et de surface sont plus élevées que la température de consigne de la batterie froide (5°C). Lorsque l'étape de séchage commence, la température de l'air diminue rapidement. La surface d'un équipement (en inox) se refroidit plus rapidement que le sol et les murs. Ainsi moins de chaleur est disponible pour faire évaporer l'eau.

Lors de cette étude, le modèle simplifié développé précédemment a été légèrement modifié pour répondre aux changements effectués du fait de l'installation d'un déshumidificateur (coefficient convectifs, conditions aux limites,…). Le modèle a été validé en comparant les résultats obtenus pour l'évolution des masses d'eau et des températures de surface (mur, sol et équipement). Ensuite, le séchage d'un équipement a été simulé avec un apport de chaleur de 50 $W.m^{-2}$ pour un équipement (ayant une surface de 2 m^2). Il a été observé qu'avec cet apport, l'équipement serait sec au bout de 100 min avec déshumidificateur et 150 min sans déshumidificateur. Sans l'apport de chaleur, le temps de séchage dépasserait 150 min avec et sans déshumidificateur.

Cette étude a également apporté des éléments pour le dimensionnement d'une installation efficace de séchage après nettoyage. Le déshumidificateur doit avoir une capacité suffisamment importante pour récupérer toute l'eau évaporée dans la pièce. Pour cela, nos expérimentations ont permis de donner l'ordre de grandeur de la quantité à évaporer après le nettoyage. Il faut aussi que les surfaces aient assez d'inertie thermique pour apporter la chaleur latente de vaporisation de l'eau. Si ce n'est pas le cas, il faut envisager un apport de chaleur.

Publication :

Cette étude est présentée en détails dans l'article 6 « Influence of air dehumidification on water evaporation in a food plant » : étude de l'influence de l'implantation d'un déshumidificateur sur le séchage d'un atelier agro-alimentaire (Soumis à *International Journal of Refrigeration* le 30 Mai 2016).

1.5.5. Couplage du modèle thermique et massique avec la microbiologie prévisionnelle

Au modèle simplifié des échanges de chaleur et de masse développé lors de la première étude (paragraphe 1.5.3) a été ajouté un modèle permettant de prédire la croissance ou l'inactivation d'une population de *Listeria monocytogènes* pendant les étapes de séchage et de production d'un atelier (simulation sur 20 h). Le modèle de transfert thermique et massique développé précédemment permet de prédire les évolutions de la température (air et surfaces), de l'humidité relative et de la surface mouillée sur le sol, le mur et un équipement. Ces valeurs sont utilisées comme paramètres d'entrée du modèle de microbiologie prévisionnelle : si une surface est mouillée ou si l'humidité relative proche de la surface est supérieure à 92%, il y a croissance bactérienne (Buchanan et al. 2004) en fonction de la température. Dans le cas contraire, il y a inactivation et celle-ci dépend de l'humidité relative de l'air proche de la

surface (Zoz et al. 2016). Ainsi, la prédiction de l'évolution de la surface mouillée est un facteur déterminant la croissance ou l'inactivation. Les résultats des expériences effectuées par l'UMR PAM à Dijon dans une boîte hermétique (paragraphe 1.2.) ont été utilisés pour en déduire les paramètres d'inactivation bactérienne (la vitesse d'inactivation et la fraction de bactérie capable de résister au stress).

Cette approche associant les modèles thermique, massique et microbiologique permet par exemple, d'évaluer l'influence de l'humidité relative au soufflage de l'évaporateur sur l'évolution de la surface mouillée et de la population bactérienne. Trois simulations ont été effectuées : à 50% d'humidité relative, 68% et 85%. Il a été remarqué qu'une humidité relative de 68% induisait une plus grande destruction bactérienne mais avec une cinétique de destruction légèrement plus lente qu'à 50%. De plus, les études précédentes ont montré que l'évaporation sur l'équipement était plus lente du fait de sa faible inertie thermique. Cela implique que l'inactivation s'effectue le plus lentement sur cette surface (~12h à 68% pour atteindre le minimum de population bactérienne sur l'équipement contre ~2h30 sur le mur et le sol). Pour augmenter la cinétique de séchage, il a été montré que l'on pouvait apporter de la chaleur (paragraphe 1.5.4.). Dans les conditions étudiées, avec un apport de chaleur de 50 $W.m^{-2}$ pour un équipement de 2 m^2, la population de *Listeria monocytogènes* atteint son minimum en 5h contre 12h sans apport de chaleur.

Publication :

Cette étude est présentée en détails dans l'article 7 « Influence of drying rate on microbial destruction in food plant » : Couplage d'un modèle thermique et massique dans un atelier agro-alimentaire avec la microbiologie prévisionnelle : prédiction de la charge microbienne sur les surfaces d'un atelier (Soumis à *Journal of Food Engineering* le 7 Juillet 2016).

Ces deux dernières études ont montré qu'une humidité relative au soufflage aux alentours de 60% combiné avec un apport de chaleur au niveau des équipements semble être un bon compromis pour sécher rapidement l'atelier et détruire un grand nombre de bactéries.

1.6. Valorisation des travaux de thèse

1.6.1. Articles dans des revues internationales

Article 1	
Titre	Influence of air relative humidity on the evolution of a liquid droplet on a solid plate and a relation with microbial destruction
Auteur	Laguerre O., Zoz F., Flick D., Lecoq L., Beney L., Guyot S.
Journal	Food Research International
Statut	Soumis - 5 Avril 2016
Article 2	
Titre	Study of the water evaporation rate on stainless steel plate in controlled conditions
Auteur	Lecoq L., Flick D., Laguerre O.
Journal	International Journal of Thermal Sciences
Statut	Soumis - 12 Février 2016
Article 3	
Titre	Droplet evaporation on a solid surface exposed to forced convection: experiments, simulation and dimensional analysis
Auteur	Doursat C., Lecoq L., Laguerre O., Flick D.
Journal	International Journal of Heat and Mass Transfer
Statut	Soumission prévue : Juillet 2016
Article 4	
Titre	Study of the drying process of wetted surfaces in food processing like conditions
Auteur	L. Lecoq, D. Flick, O. Laguerre
Journal	Revue visée : International Journal of Refrigeration
Statut	Soumission prévue : Juillet 2016
Article 5	
Titre	Simplified heat and mass transfer modeling in a food processing plant
Auteur	Lecoq L., Flick D., Derens E., Hoang H. M., Laguerre O.
Journal	Journal of Food Engineering
Statut	Paru - 2016 (v. 171, p. 1–13)
Article 6	
Titre	Influence of air dehumidification on water evaporation in a food plant
Auteur	Lecoq L., Flick D., Derens E., Laguerre O.
Journal	International Journal of Refrigeration
Statut	Soumis - 30 Mai 2016
Article 7	
Titre	Influence of drying rate on microbial destruction in food plant
Auteur	Lecoq L., Guillier L., Fritsch L., Derens E., Laguerre O., Flick D.
Journal	Journal of Food Engineering
Statut	Soumis - 7 Juillet 2016

1.6.2. Article dans une revue technique

Impact d'un déshumidificateur d'air sur la cinétique de séchage des parois d'un atelier agro-alimentaire. *Revue générale du froid*. En préparation

1.6.3. Conférences internationales

Conférence	ICCC : 3rd IIR International Conference on Sustainability and the Cold Chain, 2014, Londres
Type de présentation	Une présentation orale
Titre	Characterization of evaporation rate and temperature, velocity, humidity fields in a cold chamber
Auteurs	L. Lecoq, D. Flick, A. Plana-Fattori, D. Flick, O. Laguerre
Conférence	ICR : The 24th IIR International Congress of Refrigeration, 2015,
Type de présentation	Deux présentations orales
Titres	-Simplified heat and mass transfer modelling in a food processing plant -Experimental study of the water evaporation rate on stainless steel plate in a wind tunnel
Auteurs	- L. Lecoq, D. Flick, E. Derens, H.M. Hoang, O. Laguerre - L. Lecoq, D. Flick, O. Laguerre
Conférence	ICCC : 4th IIR International Conference on Sustainability and the Cold Chain, 2016, Auckland
Type de présentation	Une présentation orale
Titre	Influence of air dehumidification on water evaporation in a food plant
Auteurs	L. Lecoq, D. Flick, E. Derens, O. Laguerre

Références:

2002. No 178/2002 of the European parliament and of the council of 28 January 2002 laying down the general principles and requirements of food law, establishing the European Food Safety Authority and laying down procedures in matters of food safety. *(OJ L 31, 1.2.2002)*

Beysens D. 1995. The formation of dew. *Atmos. Res.* 39

Birdi K. S., Vu D. T., Winter A. 1989. A study of the evaporation rates of small water drops placed on a solid surface. *J. Phys. Chem.* 93: 3702–03

Buchanan R., Lindqvist R., Ross T., Smith M., Todd E., Whiting R. 2004. Risk assessment of Listeria monocytogenes in ready-to-eat foods. *Food and Agriculture Organisation of the United Nations* Microbiological Risk Assessment Series, 4

CAC. Codex Alimentarius Commission, 2007. Principles and guidelines for the conduct of Microbiological Risk Management (MRM). *CAC/GL* 63-2007

Carpentier B., Cerf O. 2011. Review — Persistence of Listeria monocytogenes in food industry equipment and premises. *International Journal of Food Microbiology* 145: 1-8

Chandra S., Marzo M. d., Qiao Y. M., Tartarini P. 1996. Effect of liquid-solid contact angle on droplet evaporation. *Fire Safety Journal* 27: 141-58

Croce G., D'agaro P., Mora F. D. 2005. Numerical simulation of glass fogging and defogging. *International Journal of Computational Fluid Dynamics* 19: 437-45

Dupont S., Rapoport A., Gervais P., Beney L. 2014. Survival kit of *Saccharomyces cerevisiae* for anhydrobiosis. *Appl Microbiol Biot* 98: 8821-34

Duret S., Guillier L., Hoang H. M., Flick D., Laguerre O. 2014. Identification of the significant factors in food safety using global sensitivity analysis and the accept-and-reject algorithm: application to the cold chain of ham. *International Journal of Food Microbiology* 180: 39-48

EFSA. 2015. The European Union summary report on trends and sources of zoonoses, zoonotic agents and food-borne outbreaks in 2013. *EFSA Journal* 13: 3991, 162 pp

Hoang H.-M., Laguerre O., Moureh J., Flick D. 2012. Heat transfer modelling in a ventilated cavity loaded with food product: Application to a refrigerated vehicle. *Journal of Food Engineering*, 113: 389-98

Hsu C. C., Su T. W., Wu C. H., Kuo L. S., Chen P. H. 2015. Influence of surface temperature and wettability on droplet evaporation. *Applied Physics Letters* 106

Hu D., Wu H. 2015. Numerical study and predictions of evolution behaviors of evaporating pinned droplets based on a comprehensive model. *International Journal of Thermal Sciences* 96: 149-59

Laguerre O., Duret S., Hoang M. H., Guillier L., Flick D. 2014. Simplified heat transfer modelling in a cold room filled with food products. *Journal of Food Engineering* in press

Laguerre O., Flick D. 2010. Temperature prediction in domestic refrigerator: association of deterministic and stochastic approaches. *International Journal of Refrigeration* 33: 41-51

Laguerre O., Hoang M. H., Flick D. 2012. Heat transfer modelling in a refrigerated display cabinet: the influence of operating conditions. *Journal of Food Engineering* 108: 353–64

Løvdal T. 2015. The microbiology of cold smoked salmon. *Food Control* 54: 360-73

Maa J. R. 1967. Evaporation coefficient of liquids. *Industrial Engineering Chemical Fundamentals* 6: 504-18

Moureh J., Tapsoba M. S., Derens E., Flick D. 2009. Air velocity characteristics within vented pallets loaded in a refrigerated vehicle with and without air ducts. *International Journal of Refrigeration* 32(2): 220-34

Mozurkewich M. 1986. Aerosol growth and the condensation coefficient for water: a review. *Aerosol Science and Technology* 5: 223-36

Muhterem-Uyar M., Dalmasso M., Bolocan A. S., et, al. 2015. Environmental sampling for Listeria monocytogenes control in food processing facilities reveals three contamination scenarios. *Food Control* 51: 94–107

Navaz H. K., Chan E., Markicevic B. 2008. Convective evaporation model of sessile droplets in a turbulent flow—comparison with wind tunnel data. *International Journal of Thermal Sciences* 47: 963-71

Nicolaï B. M., VanImpe J. F. 1996. Predictive food microbiology: A probabilistic approach. *Mathematics and Computers in Simulation* 42: 287-92

Raimundo A., Gaspar A., Oliveira A. V. M., Quintela D. 2014. Wind tunnel measurements and numerical simulations of water evaporation in forced convection airflow. *International Journal of Thermal Sciences* 86: 28-40

VamImpe J. F., Nicolaï B. M., Schellekens M., Martens T., Baerdemaeker J. D. 1995. Predictive microbiology in a dynamic environment: a system theory approach. *International Journal of Food Microbiology* 25: 227-49

VanImpe J. F., Nicolaï B. M., Martens T., Baerdemaeker J. D., Vandewalle J. 1992. Dynamic mathematical model to predict microbial growth and inactivation during food processing. *Applied and Environmental Microbiology* 58 (9): 2901-09

Vik T., Reif B. A. P. 2011. Modeling the evaporation from a thin liquid surface beneath a turbulent boundary layer. *International Journal of Thermal Sciences* 50: 2311–17

Vogel B. F., Huss H. H., Ojeniyi B., Ahrens P., Gram L. 2001. Elucidation of Listeria monocytogenes contamination routes in cold-smoked salmon processing plants detected by DNA-based typing methods. *Appl. Environ. Microbiol.* 67: 2586–95

Yang K., Hong F., Cheng P. 2014. A fully coupled numerical simulation of sessile droplet evaporation using Arbitrary Lagrangian–Eulerian formulation. *International Journal of Heat and Mass Transfer* 70: 409-20

Zoz F., Iaconelli C., Lang E., Iddir H., Guyot S., Grandvalet C., Gervais P., Beney L. 2016. Control of Relative Air Humidity as a Potential Means to Improve Hygiene on Surfaces: A Preliminary Approach with Listeria monocytogenes. *Plos One* 11

CHAPITRE 2 : ETUDE DE L'EVAPORATION D'UNE GOUTTE D'EAU DANS UNE BOITE VENTILEE

Article 1: Influence of air relative humidity on the evolution of a liquid droplet on a solid plate and relation with microbial destruction (soumis à Food Research International)

Influence of air relative humidity on the drying of a liquid droplet on a solid plate and relation with microbial destruction

Laguerre O.[a*], Lecoq L.[a,b], Zoz F.[c], Guyot S.[c], Beney L.[c], Flick D.[b]

[a] Irstea, UR GPAN, 1 rue Pierre-Gilles de Gennes, 92761 Antony, France

[b] AgroParisTech, UMR Ingénierie Procédés Aliments AgroParisTech, INRA, Université Paris-Saclay,

F-91300 Massy, France

[c] UMR A 02.102 PAM, équipe Procédés Microbiologiques et Biotechnologiques, Université de Bourgogne Franche-Comté/AgroSup Dijon, 1 Esplanade Erasme, 21000 Dijon, France

Abstract

This study was carried out to develop an experimental methodology using a camera to monitor the evolution of the surface of a liquid droplet deposited on a solid surface made of polypropylene. The droplet was exposed to different ambient relative humidity (11.3%, 43.2%, 68.9% and 75.3%). Two types of liquid were investigated: distilled water and water containing nutritive substances (salmon "juice"). At 11.3% relative humidity, it takes 40% more times to evaporate a water droplet (initial weight 0.36g, volume 360µL, radius $6.5x10^{-3}$m) than a salmon "juice" droplet (3H40 min for distilled water, 2h50min for salmon "juice"). For distilled water droplet, the wet surface decreases progressively and completely disappears at the end. For salmon "juice" droplet, the wet surface is constant for about 2h and then it decreases progressively because of the drying from the border to the center of the droplet. A simple correlation to predict the drying rate was proposed. Main measurements of loss of cultivability were recently published (Zoz, F., Iaconelli, C., Lang, E., Iddir, H., Guyot, S., Grandvalet, C., Gervais, P. & Beney, L. (2016). Control of air relative humidity as a potential means to improve hygiene on surfaces: a preliminary approach with Listeria monocytogenes. PloS One, 11(2): e0148418) and reused in the present paper. The relation between the relative humidity, droplet drying time and loss of cultivability of *Listeria monocytogenes* was analyzed. It seems that for 11.3%, 43.2% and 68.9% relative humidity, the drying time and the rate of bacterial death can be correlated, while at 75.3% relative humidity, the phenomena seems more complex.

Keywords: droplet, evaporation, drying rate, relative humidity, *Listeria monocytogenes*

[*] Corresponding author: Tel: 33 1 40 96 90 04, Fax: 33 1 40 96 60 75, E-mail: onrawee.laguerre@irstea.fr

Nomenclature

A	Projected surface of droplet on solid plate (m^2)
g	Gravitational acceleration (9.81 $m.s^{-2}$)
h	Droplet height (m)
h_c	Convective heat transfer coefficient ($W.m^{-2}.C^{-1}$)
$\dot{q}$	Heat flux ($W.m^{-2}$)
N	Number of *L. monocytogenes* at a given time
N_0	Initial number of *L. monocytogenes*
r	Droplet cap radius (m)
r_0	Droplet cap initial radius (m)
R	Sphere radius (m)
RH	Relative humidity of air (%)
S	Cap surface of droplet (m^2)
T_a	Air temperature (°C)
T_{fm}	Mean temperature measured by fluxmeter (°C)
T_{wb}	Wet bulb temperature (°C)
t_{drying}	Droplet drying time (s)
V	Droplet volume (m^3)
ΔH_v	Latent heat of evaporation ($J.kg^{-1}$)

Greek symbol

α	Contact angle (°)
β	Slope of drying rate correlation ($s^{-1}C^{-1}$)
ρ	Liquid density of ($kg.m^{-3}$)
γ	Coefficient depending on contact angle ($J.m^{-3}$)

Introduction

In food industry, controlling the ambient humidity has three major issues: product sanitary quality, personal wellness and energy consumption of equipment. The development and/or destruction of microorganisms in a food production plant depend on the characteristics, concentration of the microorganisms and on the types of adhered surface. It also depends on the properties of the ambient air (temperature, velocity and humidity) which are the determining factors for water evaporation rate from the surface. This evaporation creates the microorganism hydric stress and consequently the cell lethality. The beneficial effect of using air of low relative humidity to dry the surfaces after cleaning and disinfection to limit microbial growth has already been observed by the manufacturers, but the choice of operating condition is still empirical in practice. Understanding the mechanisms of heat and mass exchanges between a wet surface and the ambient air is, thus, necessary for microbial growth control.

The first objective of this study is to develop an experimental methodology to monitor the evolution of the surface of a liquid droplet exposed to different ambient relative humidity. Two types of liquid were investigated: pure water and water containing nutritive substances (salmon "juice"). The analysis of the experimental result allows the understanding of the mechanism of evaporation and the development of a simple correlation to predict the drying rate. The second objective is to develop a relation between the drying rate and the cultivability of *Listeria monocytogenes* for different relative humidity. The relation between the relative humidity, droplet drying time and loss of cultivability of *Listeria monocytogenes* was analyzed.

1. Literature review

In food plants, the presence of water vapour in air, of water droplet in air and on walls (materials, room and floor) is favourable for microbial growth. The presence of this water (or vapour) may be due to the water pulverization during cleaning and the condensation which takes place when the wall temperature is lower than the dew temperature of surrounding air. After cleaning, drying can be carried out by blowing warm and dry air in the room to reduce humid zones. The presence of food residues in conjunction with water is favorable for the microbial growth (Guinebretiere et al., 2008). Nortj et al. (1990); Patterson (1969) reported the surface contamination of walls, tables, floors and equipment used for food processing. Several studies have shown the presence of *Listeria* monocytogenes in production plants and along the food chain. Cox et al, 1989 investigated 17 food factories representing six different product groups and reported that *Listeria* spp. was found in drains, floors, residues and food-contact surfaces, in descending order of frequency. These authors concluded that dry conditions and the restriction of food residues contribute to the control of these microorganisms. Cold smoked salmon can present a risk to human health if it is contaminated with pathogens along the food chain (Garrido et al, 2008). Rotariu et al (2014) conducted an analysis of the current practices in 16 plants of the Scottish smoked salmon that can affect the *Listeria monocytogenes* contamination in products. They reported a risk of ceiling condensation dripping onto product, particularly in the small plants. Evans et al (2004) have made sampling on foodstuffs, evaporator and condenser in 15 cold rooms in UK. The microbial contamination was observed on all investigated cold rooms. The authors reported a significant influence of the temperature, humidity and air-blowing velocity on the contamination. Despite regular evaporator cleaning procedures, this is not efficient in reducing contamination. By wiping in 23 domestic refrigerators and microbial analysis, Carpentier et al (2012) found that the highest bacterial contamination was found on the

surfaces when both condensation and food traces were visible (mean of 10^4 CFU/cm^2) against clean surfaces and dry surfaces with food traces (mean of 32 CFU/cm^2). Consequently, the recommendations for consumers are to avoid condensation and to clean up food spills as soon as possible.

During evaporation, heat is lost from a liquid surface. The evaporation rate is influenced by the heat transfer in the liquid phase and at the liquid/vapour interphase which is the controlling factor (Barrett and Clement, 1988; Mozurkewich, 1986; Hickman, 1965; Maa, 1967). The evaporation rate increases exponentially greatly depends on temperature and air humidity (Eames et al., 1997).

When a liquid is carefully placed on the surface of a given solid, it remains as a drop with the formation of a contact angle between the liquid and solid phases. The magnitude of the contact angle depends on the physical characteristics of both the liquid and the solid phases. The higher value of the contact angle of a given volume of a liquid always gives a thicker drop with a smaller base radius. The contact angle plays therefore an important role in the rate of evaporation of the drop. The rate of evaporation is linearly proportional to the radius of the liquid-solid interface and for water drop resting on a glass surface, evaporation is a stationary process (constant rate of evaporation (Birdi et al, 1989).

According to Beysens (1995), the evaporation of a droplet may be distinguished into 2 periods (Figure 1).

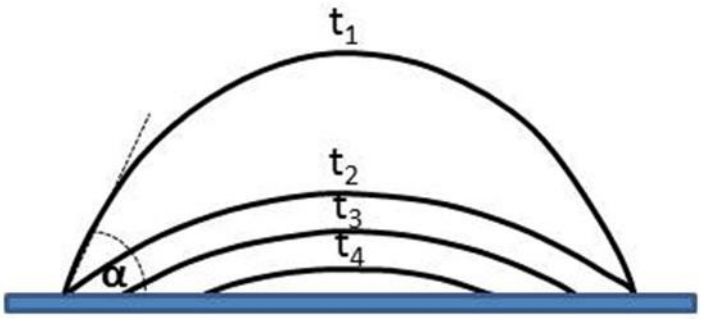

Figure 1: Droplet shape evolution during evaporation.

The first period during which the base area of the droplet is constant while the contact angle (α) decreases until the receding value is reached: the evaporation rate is almost constant (time t_1 and t_2 on Figure 1). The second period, during which the contact angle is constant: the wet area and the evaporation rate decrease (time t_3 and t_4). Hsu et al. (2015) investigated experimentally water droplets on hydrophilic, hydrophobic and mixed wettability surfaces. The measurement of the contact angle and volume evolution was undertaken over the evaporation time. The results revealed that the surface wettability plays a critical role in evaporation rate.

The drying leads to microbial destruction because of the hydric stress (loss of water). Desiccation induces several damages to biological cells that are related to mechanical, structural and oxidative constraints. All these mechanisms are detailed in a recent review (Dupont et al., 2014). Briefly, mechanical constraint is related to water transfer by osmosis between intracellular space and external medium caused by increased concentration of solutes. It causes cell shrinkage, molecular confinement and possible alteration of cell membranes by invagination and rupture (Dupont et al., 2010). The structural constraint is related to the contribution of water to the structure of many biological molecules and

molecular assemblies. For example, desiccation promotes phase transitions in biological membranes that lead to the alteration of membrane barrier properties (Laroche et al., 2005; Lemetais et al., 2012). This constraint is also implied in the change of protein spatial organization and functions. The oxidative constraint is related to the increased exposure to air (when drying is performed in ambient conditions) resulting from water evaporation and also to possible structural and functional alteration of cellular enzymes involved in the management of oxidative stress. This constraint induces chemical degradation of cell lipids, proteins, and nucleic chains.

2. Materials and methods

2.1. Experiment of wet surface evolution

The experiment was conducted in a hermetic box (internal dimension length x width x height = 25 x 11 x 6cm, wall thickness 2 mm) made of polypropylene (Figure 2a).

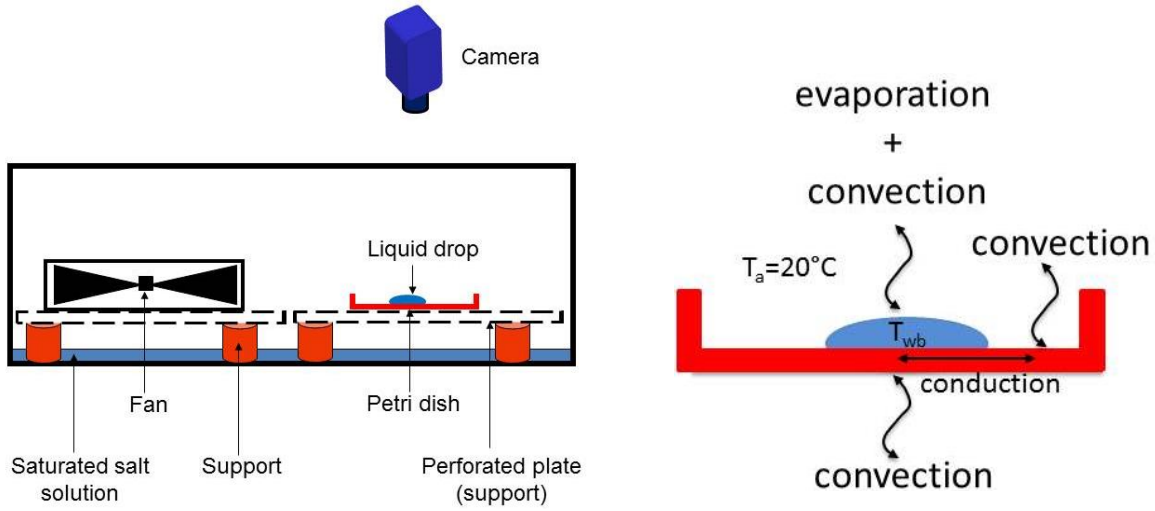

(a) (b)

Figure 2: (a) Experimental device (side view of the controlled relative humidity box) in which a droplet of liquid was deposited in a petri dish (b) zoom on the liquid droplet showing the exchange modes.

To control the relative humidity in the box, 100 ml of saturated salt solution was placed at the bottom. Four salt solutions were used (Table 1) allowing the relative humidity in the box to be 11.3, 43.2, 68.9 and 75.3.

Table 1: Relative humidity of different saturated salt solutions (20-25°C) used in the experiment of wet surface evolution (Source International Organization of Legal Metrology)

Saturated salt solution	% Relative humidity
Lithium Chloride (LiCl)	11.3±0.3
Potassium carbonate (K_2CO_3)	43.2±0.3
Potassium iodide (KI)	68.9±0.2
Sodium Chloride (NaCl)	75.5±0.1

A fan (power supply 5 volts) was used to homogenize the air. A liquid droplet was placed in a petri dish made of polypropylene (3.4cm internal diameter, 1cm height, 1mm wall thickness) using a pipette, then, the box was closed immediately while the fan was turn on. Images of the wet surface were taken using a high definition camera (Kappa DXP 1154) and a zoom (Navitar TenX) located outside the box and just over the droplet position. The time interval between 2 images was 30, 45, 120 and 180 seconds for the experiment of relative humidity in the box 11.3, 43.2, 68.9 and 75.3%, respectively. Two types of liquid droplet were studied: distilled water and salmon "juice". The distilled water droplet was used as a reference experiment and the salmon "juice" represents the splash of "juice" in a cutting plant. The initial weight of the droplet was 0.36g, its volume was 360µL and its top view radius was $6.5x10^{-3}$ m, averagely. The experiment was carried out in a test room in which the temperature was set at 20°C. It is to be emphasized that 2 measurements were carried out for a given relative humidity.

During the experiment, there are heat and mass exchanges by convection between the liquid droplet and the air, heat transfer by convection between the dry surface and air (over and under the petri dish) and by conduction inside the petri dish wall (Figure 2b). Because the air is stagnant under the petri dish, the convection at this position can be considered as negligible. Because of low thermal conductivity of polypropylene (0.1 $Wm^{-1}K^{-1}$) and low wall thickness (1mm), the conduction inside the petri dish wall is also negligible. Using this hypothesis, the droplet temperature can be considered as close to the wet bulb temperature of air (T_{wb}). The driving force of the evaporation is, thus, the difference between the air temperature (20°C) and droplet temperature (T_{wb}).

2.2. Wet surface measurement

The wet surface was determined from the images taken at different times until the end of drying using ImageJ (open software). Of course, a calibration was previously carried out to obtain the relationship between the number of pixels and a distance.

2.3. Heat transfer coefficient measurement

Evaporation and heat transfer depend on the ventilation inside the box. In order to quantify the exchanges between the surface of petri dish and air in the box, a fluxmeter was used (Trade name Captec, width x height x depth: 4 cm x 4 cm x 450 µm, Figure 3).

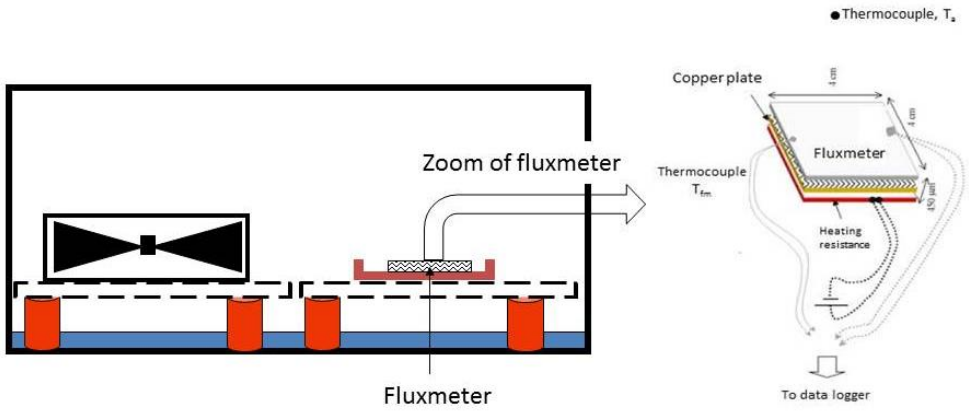

Figure 3: Fluxmeter for heat transfer coefficient measurement inside the box.

This fluxmeter (equipped with a thermocouple) was placed on the support at the same position of the petri dish. Three experiments were carried out using 3 different heating powers (1.0W, 1.5W and 2.7W) supplied to this fluxmeter. The fluxmeter temperature (T_{fm}), the air temperature (T_a, measured at 1 cm from the surface of the fluxmeter) and the output signal of the fluxmeter ($\dot{q}$, W/m^2) were recorded every 2 min until a steady state was obtained (about 10h). Then, the mean values were calculated over 1 h of stabilization period. It is to be emphasized that the emissivity of this fluxmeter is close to zero; thus, the radiative exchange can be neglected in the measurement.

The heat transfer coefficient between the surface of petri dish and the air (h_c,$Wm^{-2}K^{-1}$), was calculated using the equation (1):

$$h_c = \frac{\dot{q}}{T_{fm} - T_a} \quad (1)$$

Where,

$\dot{q}$ = mean value of measured heat flux, $W.m^{-2}$

T_{fm} = mean temperature measured by the fluxmeter, °C

T_a = mean air temperature in the box, °C

2.4. Experiment of *Listeria monocytogenes* cultivability

Five experiments were carried out in the same type of hermetic box equipped with fan (Figure 1) as previously described by Zoz et al. (2016). Briefly, the relative humidity in the box was controlled by using several saturated salt solutions while the room temperature was set at 25°C (Table 1). Cultures of *L. monocytogenes* EGDe strains (serotype 1/2a) in Tryptic Soy Broy (TSB, Sigma Aldrich) were centrifuged for 10 min at 3.645 × *g* and washed once with Phosphate-Buffered Saline (PBS containing 0.01M phosphate, 0.0027M KCl and 0.137M NaCl, Sigma-Aldrich). A droplet of 10 µL of cell suspension with PBS (droplet radius $2x10^{-3}$ m) was deposited onto polypropylene petri dish with a final concentration of 10^9 $CFUmL^{-1}$. *L. monocytogenes* strains were dried during 0.5, 1.0, 1.5, 2.0, 3.0, 16 and 24 h. Measurements performed between 0.5-16 h were previously published by Zoz et al. (2016) and so reused in the present study. Bacterial cells were rehydrated with 1 mL of PBS and were detached from the polypropylene petri dish by aspirating and dispensing samples 30 times using a micropipette. The cultivability of bacteria was estimated using the CFU method. After

rehydration, cell suspensions were serially diluted and appropriate 10-fold dilutions were plated on Tryptic Soy Agar (TSA). Colonies were counted after incubation for 48 h at 25 °C and recorded as $CFUmL^{-1}$. Results were expressed as $\log_{10}(N/N_0)$, where N represents the final cell concentration and N_0 represents the initial cell concentration.

3. Results and discussion

3.1. Wet surface evolution

Figure 4 shows the images of a droplet of distilled water and salmon "juice" at different times until the end of drying for 11.3% relative humidity in the box. For distilled water droplet, the wet surface decreases progressively and completely disappears at the end. For salmon "juice" droplet, the wet surface is constant for about 2h and then it decreases progressively because of the drying from the border to the center of the droplet. At the end of drying, traces of dry matters (proteins and solutes) are observed.

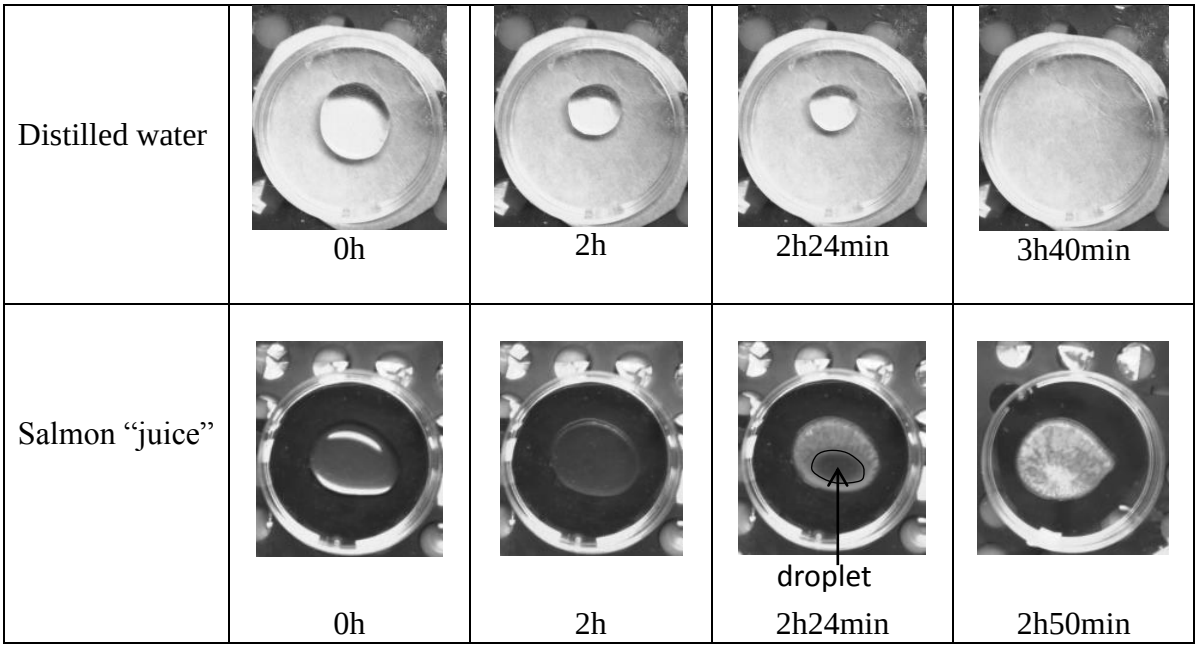

Figure 4: Images at different times of a droplet of distilled water and salmon "juice" exposed to the ambient relative humidity of 11%.

It was observed that the water droplet evolution is different from that of salmon "juice" (Figure 5). For water, the radius of wet surface decreases while the contact angle is almost constant during drying. This can be explained by the high interfacial tension of the water droplet deposited on the petri dish made of polypropylene which is a hydrophobic surface. For salmon "juice", the wet surface is more spread on the petri dish because of the presence of dry matters in the "juice" leading to lower interfacial tension of droplet. The wet surface is constant for about 2h (for 11.3% RH) while the contact angle decreases, after that the wet surface decreases.

Water droplet
-constant contact angle

Salmon "juice"
-constant wet surface

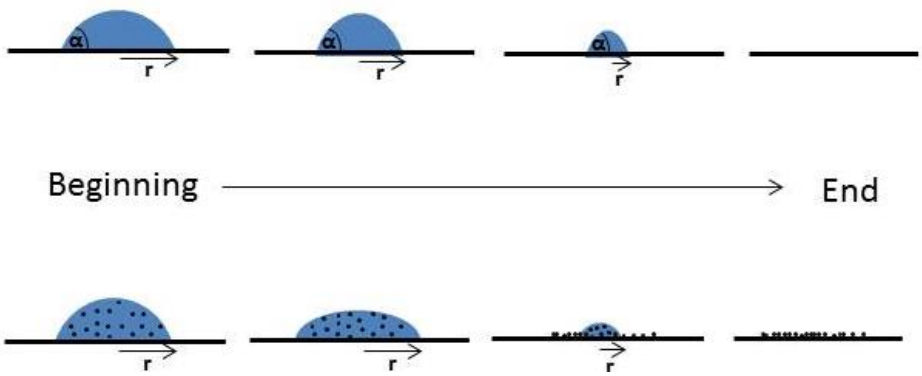

Figure 5: Two different mechanisms of wet surface evolution during drying of a droplet of water and salmon "juice".

The evolution of wet surface of distilled water and salmon "juice" droplets (measured by the ImageJ software) is presented in Figure 6 for the relative humidity of 11.3%.

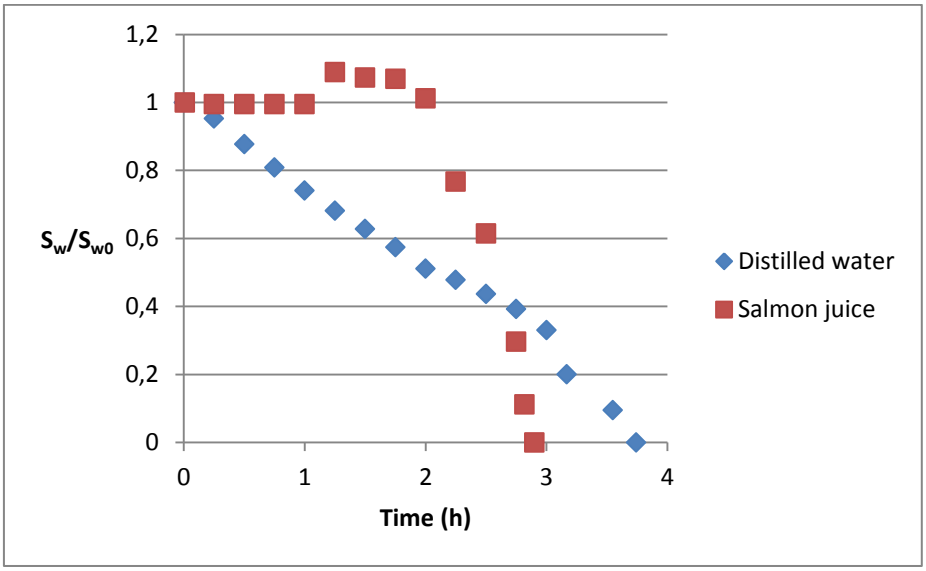

Figure 6: Evolution of the ratio of wet surface and initial wet surface (S_w/S_{w0}) of a droplet of distilled water and salmon "juice" exposed to the ambient of 11.3% relative humidity.

To be able to compare the results of the both cases, the ratio of the wet surface at a given time (S_w) to the initial one (S_{w0}) is reported in this figure. The drying time of the droplet of salmon "juice" is about 50 min less than the one of water (2H50 for salmon "juice" and 3H40 for water). This can be explained by the fact that, for the same volume, the droplet of salmon "juice" is more spread because of lower interfacial tension. The slight surface increase of the salmon "juice" droplet during 1.2 and 1.8 hours observed experimentally may be explained by the decrease of the interfacial tension because of solute concentration rise.

3.2. Convective heat transfer coefficient

The convective heat transfer coefficient (h_c) was estimated as presented in the section 2.3 by using the equation (1). The results are shown in Table 2. The mean value of the 3 experiments with different heating power applied to the fluxmeter is 50.3 $Wm^{-2}K^{-1}$.

Table 2: Experimental results of heat transfer coefficient inside the box equipped with a fan.

Heating power applied to fluxmeter (W)	T_{fm} (°C)	T_a (°C)	$\dot{q}$ ($W.m^{-2}$)	$h_c = \frac{\dot{q}}{T_{fm} - T_a}$ ($Wm^{-2}C^{-1}$)
1.0	26.8	20.7	310.6	50.9
1.5	32.0	22.1	497.8	50.3
2.7	38.1	23.6	721.9	49.7

3.3. Drying rate prediction for water droplet

Figure 7 presents the experimental drying time (t_{drying}) for a water droplet exposed to 11.3, 43.2, 68.9 and 75.3% relative humidity. The higher the relative humidity, the higher is the drying time. It takes about 5 folds more time to dry a water droplet when the relative humidity increases from 11.3%RH (3.7 hours) to 75.3 % (19.8 hours).

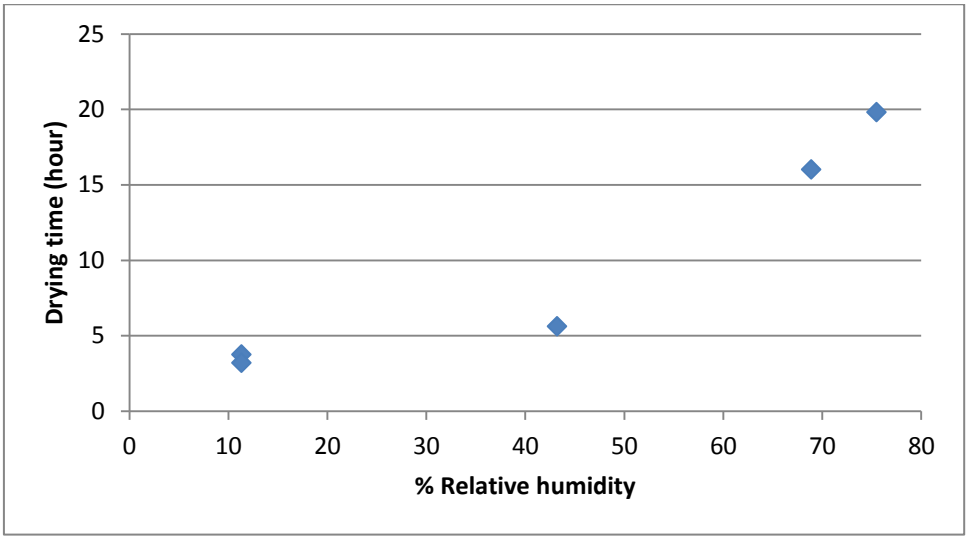

Figure 7: Experimental values of drying time of a water droplet in function of the relative humidity.

The values of drying time (t_{drying}) shown in Figure 7 were used to calculate the drying rate ($1/t_{drying}$) and reported as a function of the difference between the air temperature (T_a) and the wet bulb temperature (T_{wb}, temperature of the water droplet) in Figure 8.

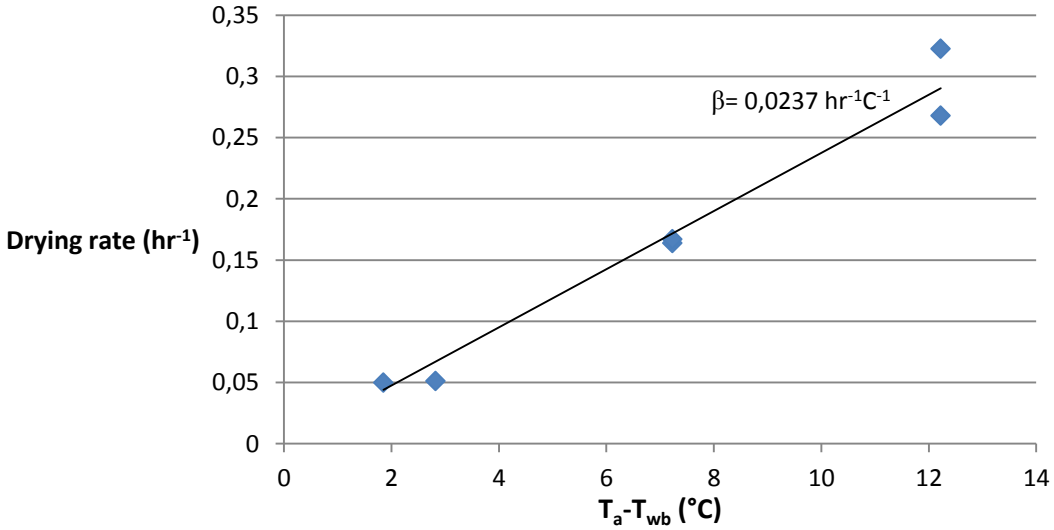

Figure 8: Drying rate as a function of the difference between the air temperature (T_a=20°C) and the wet bulb temperature (T_{wb}).

Using a diagram of humid air for the air temperature of 20°C, the wet bulb temperatures are 7.8, 12.8, 16.3 and 17.1°C, for relative humidity of 11.3, 43.2, 68.9 and 75.3%, respectively. By adjusting a linear relationship between the drying rate and the temperature difference (T_a - T_{wb}), considered as a driving force, the following equation to predict the drying rate is proposed:

$$\text{Drying rate} = \frac{1}{t_{drying}} = \beta(T_a - T_{wb}) \quad (2)$$

$$\text{Where the slope of the curve } (\beta) = 0.0237\ \text{hr}^{-1}\text{C}^{-1} = 6.58\text{x}10^{-6}\ \text{s}^{-1}\text{C}^{-1}$$

The equation (2) can be only applied to predict the water drying rate under similar conditions: water droplet of volume (V) 360µL (initial radius, r_0=6.5x10^{-3}m) on a hydrophobic surface, heat transfer coefficient of about 50.3 W.m^{-2}.K^{-1}, negligible conduction and convection inside and under this surface, respectively. Under these conditions, the convection and evaporation are the dominant exchange modes between the droplet and the air (temperature T_a) and the droplet temperature is close to the wet bulb temperature.

In order to extrapolate this result to other conditions (different ventilation and initial droplet radius…), a simple evaporation model was developed. As a first approach, it is assumed that heat is only exchanged between air (T_a) and droplet (T_{wb}) through surface (S) with a heat transfer coefficient (h). This exchange is equal to the evaporation rate ($\rho\, dV/dt$) multiplied by the latent heat of vaporization (ΔH_v)

$$\frac{dV}{dt} = \frac{hS(T_a - T_{wb})}{\rho \Delta Hv} \quad (3)$$

Where V = droplet volume, m^3

S = exchange surface area between the droplet and air, m^2

ΔH_v = Latent heat of vaporization, Jkg^{-1}

Considering a droplet as a spherical cap of radius r with a given contact angle α, $S = Kr^2$ and $V = K'r^3$, where K and K' are coefficients (depending on α). By replacing S and V in the equation (3), the equation (4) is obtained.

$$\frac{dr}{dt} = \frac{K}{3K'}\frac{h(T_a - T_{wb})}{\rho \Delta Hv} \quad (4)$$

The integration of the equation (4) gives the equation (5).

$$r = r_0 - \frac{h}{\gamma}(T_a - T_{wb})t \quad (5)$$

When the droplet is totally evaporated (r=0), the drying time (t_{drying}) can be calculated by the equation (6).

$$t_{drying} = \gamma \frac{r_0}{h(T_a - T_{wb})} \quad (6)$$

Where r_0 = initial radius and $\gamma = 3K'\rho\Delta H_v/K$ depends on the contact angle.

The value of γ was identified using the equation (2), $\gamma = 1.18x10^9 Jm^{-3}$.

The equation (6) can be used to predict the drying time if r_0 and h are known. For example, in a colder ambiance T_a=10°C, RH=70% (corresponding to T_{wb}=7.5°C) with a lower ventilation in the box (h=15 $Wm^{-2}K^{-1}$) and for smaller droplet ($r_0=2x10^{-3}$m), the drying time can be estimated as follows:

$$t_{drying} = 1.18x10^9 \frac{2.10^{-3}}{15(10 - 7.5)} = 62933s = 17.5\ hr$$

This illustrates how the results can be extrapolated in conditions closer to that of a production plant of chilled foods.

3.4. Drying rate prediction in the conditions of microbiological experiments

The microbiological experiments were carried out with PBS (Phosphate-Buffered Saline). If the PBS droplet (at 25°C) has the same contact angle (α) as that of water droplet at 20°C (Figure 9), the equation (6) developed for a water droplet drying can be applied. To calculate the contact angle, the mathematical development is as follows.

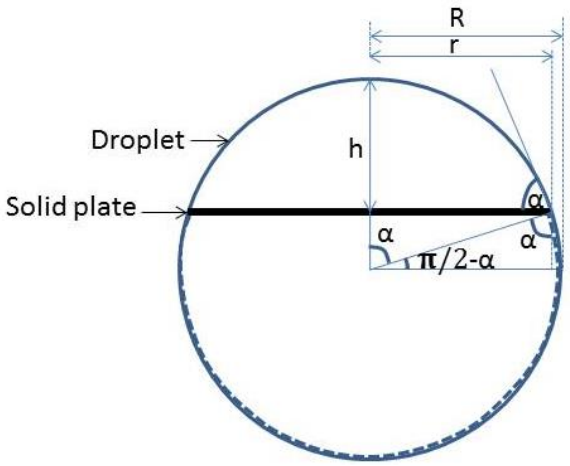

Figure 9: Side view of a droplet with the height "h" and the contact angle "α" on a solid plate.

The volume of a droplet considered as a spherical cap is expressed by the equation (7).

$$V = \frac{\pi h^2(3R - h)}{3} = \frac{\pi}{3}R^3(1 - \cos\ \alpha)^2(2 + \cos\alpha) \quad (7)$$

where $r = R\sin\alpha$ and $h = R(1 - \cos\alpha)$

By dividing the equation 7 by the contact area between the droplet and the plate (A), the equation (8) is obtained.

$$\frac{V^{1/3}}{A^{1/2}} = \left(\frac{1}{3\sqrt{\pi}}\right)^{1/3} \frac{((1 - \cos\alpha)^2(2 + \cos\alpha))^{1/3}}{\sin\alpha} \quad (8)$$

where $A = \pi[R\ \sin\alpha]^2$

Using the equation 8, Figure 10 shows a relation between $\frac{V^{1/3}}{A^{1/2}}$ and α.

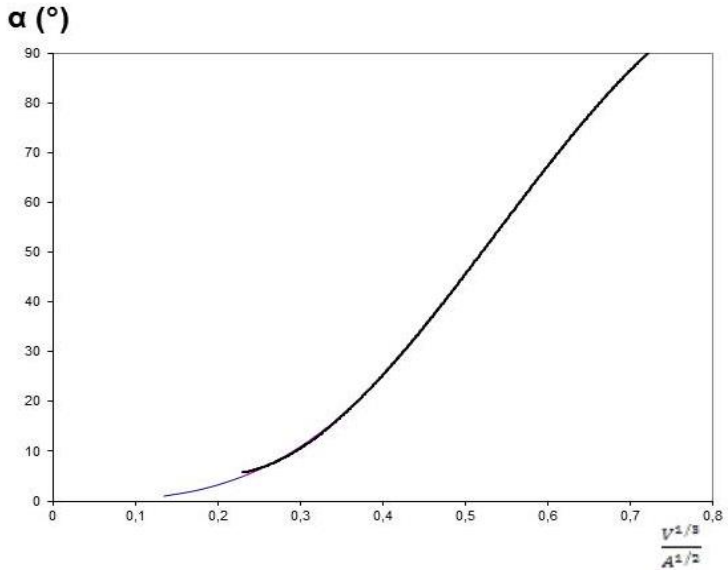

Figure 10: Relation between $\frac{V^{1/3}}{A^{1/2}}$ and α.

By adjustment of the curve shown in Figure 10 by a polynomial equation (3th order), the following equation is proposed:

$$\alpha = -672\left(\frac{V^{1/3}}{A^{1/2}}\right)^3 + 1080\left(\frac{V^{1/3}}{A^{1/2}}\right)^2 - 363\left(\frac{V^{1/3}}{A^{1/2}}\right) + 40.1 \quad (9)$$

Using the equation (9) to calculate the contact angle (α), the result in Table 3 shows the same order of magnitude for these 2 types of droplet. This signifies that the drying rate of PBS droplet exposed to different relative humidity (for the air temperature of 25°C) can be predicted by the equation (6).

Table 3: Characteristic of a droplet of water and PBS.

Droplet characteristic	Experimental values				Predicted value of α (°)
	Initial volume, V (µL)	Initial radius, r (m)	A (m^2)	$\frac{V^{1/3}}{A^{1/2}}$	
Water droplet (20°C)	360	$6.5x10^{-3}$	132.7	0.62	70
PBS droplet (25°C)	10	$2.0x10^{-3}$	12.6	0.61	68

Using the equation (6), the drying time of PBS droplets was calculated and reported in Table 4.

Table 4: Prediction of drying time of a droplet of PBS ($r_0 = 2.0x10^{-3}$m, γ =$1.18x10^9$ Jm^{-3} and h_c=50.3 $Wm^{-2}C^{-1}$

Solution of saturated salt	T_a (°C)	RH (%)	T_{wb} (°C)	t_{drying} (hour)
LiCl	25	11.3	10.68	0.91
K2CO3	25	43.2	16.70	1.57
KI	25	68.9	20.82	3.11
NaCl	25	75.3	21.81	4.09

3.5. Relation between drying time, ambient relative humidity and loss of cultivability of *Listeria monocytogenes*

The predicted drying time (see Table 4) is reported on the curves representing the loss of cultivability of *L. monocytogenes* (exposed to different relative humidity) with time (Figure 11).

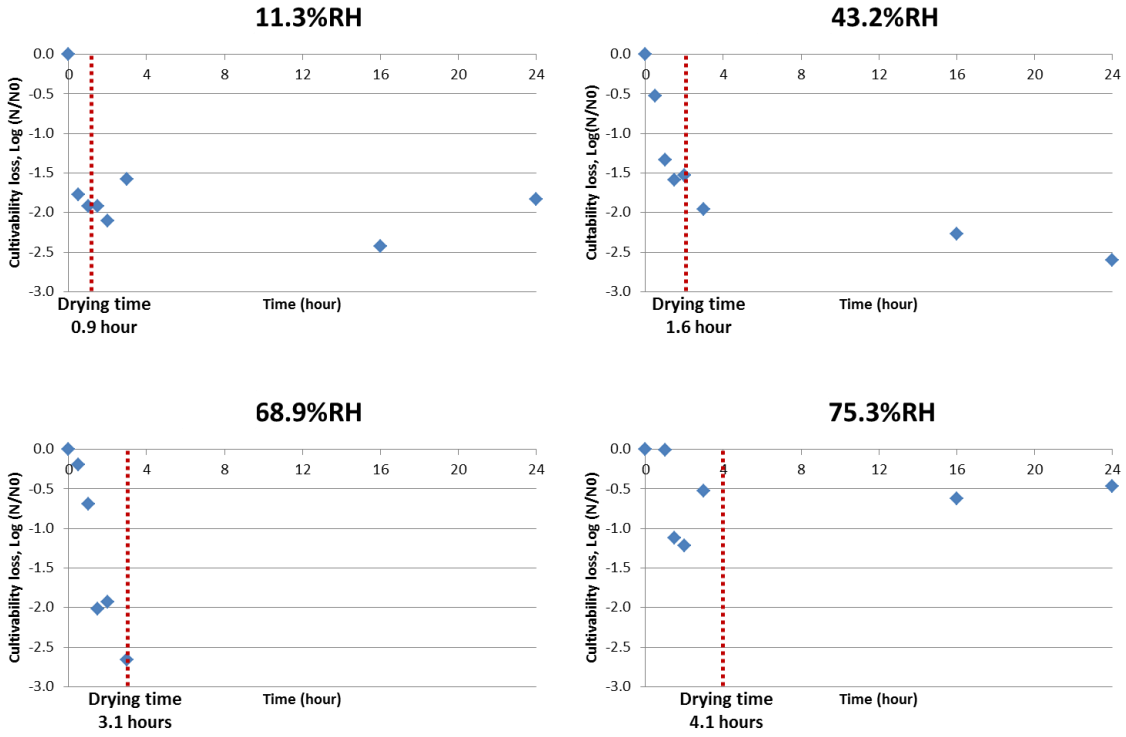

Figure 11: Average loss of cultivability of *Listeria monocytogenes* (EGDe strain) exposed to ambient relative humidity of 11.3, 43.2, 68.9 and 75.3% for air temperature fixed at 25°C. (Data reproduced with permission of PLoS One).

The relation of the loss of cultivability (previously published by Zoz et al., 2016) with the predicted drying time appears to be an interesting way to evaluate its relevance in the field of food microbiology. The loss of cultivability is defined as Log (N/N_0), where N is the number of *L. monocytogenes* at a given time and N_0 is the initial number. The reported values represent the average of 4 repetitions of *L. monocytogenes* (EGDe strain). For 68.9% relative humidity, the experiment was ended at 3 h because the loss of cultivability reaches the maximum value (lethality of *Listeria*).

In an ambience of 11.3, 43.2 and 68.9% RH, the loss of cultivability seems to relate with the drying time. The higher the relative humidity, the higher the time after which the cultivability reached a plateau of lowest value. This can be explained by the fact that dehydration/desiccation constraints to cells both depend on the drying kinetics and RH level (Lemetais et al., 2012). Transitional phase of drying has an impact on cell survival and could be explained by the dependence of the survival to amplitude and dehydration rate. In an ambience of 75.3%RH, the peak of loss of cultivability is about 2hr while the drying time is 4hr. However, bacterial cells remained in liquid after drying at 75.3%RH, probably due to the presence of cellular and external solutes that significantly affects the kinetic of drying compared to that of pure water. Moreover, PBS contains NaCl and K+ and allows during drying to 75.3% RH to develop a saturated salt solution. As shown by Zoz et al. (2016), it is

important to note that the dehydration step is not the only parameter involved in bacterial death as cell death could occur during the rehydration step. Indeed, the faster the rehydration rate, the higher the cell death. In the light of this consideration, future works should take into account the rehydration step in order to establish a predictive model.

4. Conclusions

An experimental methodology using a camera to monitor the evolution of the surface of a liquid droplet deposited on a hydrophobic solid surface (petri dish made of polypropylene) was developed. The droplet was exposed to different ambient relative humidity (11.3%, 43.2%, 68.9% and 75.3%). Two types of liquid were investigated: distilled water and water containing nutritive substances (salmon "juice"). For the same droplet volume, it takes more time to evaporate distilled water compared to that of salmon "juice". The geometry change of droplet during evaporation was also different. For distilled water droplet, the wet surface decreases progressively and completely disappears at the end. For salmon "juice" droplet, the wet surface is constant for about 2 hours and then it decreases progressively because of the drying from the border to the center of the droplet. A development of a correlation to predict the drying rate at different relative humidity was proposed. An experiment of cultivability of a strain of *L. monocytogenes* exposed to different relative humidity and at different times was carried out. The relation between the relative humidity, droplet drying time and loss of cultivability of *L. monocytogenes* was analyzed. It seems that for 11.3%, 43.2% and 68.9% relative humidity, the drying time and the rate of bacterial death can be correlated, while at 75.3% relative humidity, the phenomena seems more complex.

Acknowledgement:

The research has received funding from the French National Research Agency (EcoSec Project, ANR-12-ALID-0005-04)

References

Barrett, J.C. & Clement, C.F. (1988). Growth rates for liquid drops. *Journal of Aerosol Science, 19*, 223-242.

Beysens, D. (1995). The formation of dew. *Atmosphere Research, 39*, 215–237.

Birdi, K. S., Vu, D. T. & Winter A. (1989). A Study of the Evaporation Rates of Small Water Drops Placed on a Solid Surface. *The Journal of Physical Chemistry, 93*, 3702-3703.

Carpentier, B., Lagendijk, E., Chassaing, D., Rosset, P., Morelli, E. & Noël, V. (2012). Factors impacting microbial load of food refrigeration equipment. *Food Control*, *25*, 254-259.

Cox, L. J., Kleiss, T., Cordier, J. L., Cordellana, C., Konkel, P., Pedrazzini, C., Beumet, R. & Siebenga, A. (1989). Listeria spp. in food processing, non-food and domestic environments. *Food Microbiology*, *6*, 49-61.

Dupont, S., Beney, L., Ritt, J.F., Lherminier, J. & Gervais, P. (2010). Lateral reorganization of plasma membrane is involved in the yeast resistance to severe dehydration. *Biochim. Biophys. Acta*, *1798*, 975-985.

Dupont, S., Rapoport, A., Gervais, P. & Beney, L. (2014). Survival kit of Saccharomyces cerevisiae for anhydrobiosis. *Appl Microbiol Biot*, *98*, 8821-8834.

Eames, I. W., Marr, N. J. & Sabir, H. (1997). The evaporation coefficient of water: a review. *International Journal of Heat and Mass Transfer*, *40*, 2963-2973.

Evans, J.A., Russell, S.L., James, C., Corry & J. E.L. (2004). Microbial contamination of food refrigeration equipment. *Journal of Food Engineering*, *62*, 225–232

Garrido, V., Torroba, L., Garcia-Jalon, I., & Vitas, A. I. (2008). Surveillance of listeriosis in Navarre, Spain, 1995-2005 epidemiological patterns and characterisation of clinical and food isolates. Euro Surveillance: Bulletin Europeen sur les Maladies Transmissibles, *European communicable disease bulletin*, *13*, 1-6.

Guinebretiere, M. H., Thompson, F. L., Sorokin, A., Normand, P., Dawyndt, P. & Ehling-Schulz, M. (2008). Ecological diversification in the Bacillus cereus group. *Environmental Microbiology*, *10*, 851-865.

Hickman, K.C.D., (1965). Evaporation coefficients of liquids, First International Symposium on Water Desalination, Washington.

Hsu, C. C., Su, T. W., Wu, C. H., Kuo, L. S. & Chen, P. H. (2015). Influence of surface temperature and wettability on droplet evaporation. *Applied Physics Letters*, 106.

Laroche, C., Simonin, H., Beney, L. & Gervais, P. (2005). Phase transitions as a function of osmotic pressure in Saccharomyces cerevisiae whole cells, membrane extracts and phospholipid mixtures. *Bba-Biomembranes, 1669*, 8-16.

Lemetais, G., Dupont, S., Beney, L. & Gervais, P. (2012). Air-drying kinetics affect yeast membrane organization and survival. *Appl Microbiol Biot, 96*, 471-480.

Maa, J.R. (1967). Evaporation coefficient of liquids. *Industrial Engineering Chemical Fundamentals*, *6*, 504-518.

Mozurkewich, M. (1986). Aerosol growth and the condensation coefficient for water: a review. *Aerosol Science and Technology, 5,* 223-236.

Nortje, G. L., Nel, L., Jordan, E., Badenhorst, K., Goedhart, G., Holzapfel, W. H. & Grimbeek, R. J. (1990). A quantitative survey of a meat production chain to determine the microbial profile of the final product. *Journal of Food Protection, 53,* 411–417.

Patterson, J. T. (1969). Meat Hygiene: II. Hygiene during slaughter and subsequent treatment of the carcass. *Veterinary Research, 85,* 536–541.

Rotariu, O., Thomas, D., Goodburn, K., Hutchison, M. & Strachan N. (2014). Smoked salmon industry practices and their association with *Listeria monocytogenes*. *Food Control*, *35,* 284-292.

Zoz, F., Iaconelli, C., Lang, E., Iddir, H., Guyot, S., Grandvalet, C., Gervais, P. & Beney, L. (2016). Control of air relative humidity as a potential means to improve hygiene on surfaces: a preliminary approach with Listeria monocytogenes. *PloS One*, 11(2): e0148418.

CHAPITRE 3 : ETUDE DE L'EVAPORATION DE PLUSIEURS GOUTTES D'EAU DANS UNE SOUFFLERIE

3.1. Article 2 : Study of the water evaporation rate on stainless steel plate in controlled conditions (Soumis à International Journal of Thermal Sciences)

Study of the water evaporation rate on stainless steel plate in controlled conditions

L. Lecoq [abc*], D. Flick [bc], O. Laguerre [a]

[a] Irstea, UR GPAN, 1 rue Pierre-Gilles de Gennes, 92761 Antony, France

[b] AgroParisTech, UMR1145 Ingénierie Procédés Aliments, F-75005 Paris, France

[c] INRA, UMR1145 Ingénierie Procédés Aliments, F-91300 Massy, France

ABSTRACT

The evaporation of water droplets is involved in many applications: fire extinction, building and greenhouse. On the equipment of a food plant (mostly made of stainless steel), bacterial contamination can cause the deterioration of food quality and safety. To avoid this problem, cleaning by water and subsequent drying are often performed. Water stagnation, however, is observed at certain positions if the ambient conditions during the drying process are not well-controlled. The water evaporation rate depends on the room conditions (temperature, velocity, humidity). It is thus necessary to understand the evaporation mechanism of water droplets on solid surfaces and the influence of the room conditions on the evaporation rate. Experiments were performed in a wind tunnel, in which the air velocity, temperature and relative humidity were controlled. Water droplets were deposited onto a stainless steel plate (15 cm x 15 cm x 0.1 cm). This plate, placed in a work zone, was exposed to several air velocities (0.5 $m.s^{-1}$ to 2.0 $m.s^{-1}$), relative humidities (50% to 85%) and temperatures (4°C to 20°C). The evolution of the wet surface on the plate was observed using a camera, and the evolution of the water weight was determined using a digital balance. The influence of the initial percentage of wet surface on the water evaporation rate was studied at various ambient conditions. It was observed that the air relative humidity is the factor that has the greatest influence on the evaporation rate.

Keywords: water, evaporation droplet, humidity, temperature, air velocity

[*] Corresponding author: Tel: 33 1 40 96 90 04, Fax: 33 1 40 96 60 75, E-mail: logan.lecoq@irstea.fr

Nomenclature

C_{sat}	Concentration of saturated water vapour	kg.m^{-3}
C_{wa}	Concentration of water vapour in air	kg.m^{-3}
e	Plate thickness	m
h	Heat transfer coefficient	W.m^{-2}.K^{-1}
k	Mass transfer coefficient	m.s^{-1}
l	Half distance between two drops	m
$\dot{m}$	Evaporation rate	kg.s^{-1}
$\dot{q}$	Mean value of measured heat flux	W.m^{-2}
RH	Relative humidity	%
S	Total surface of the plate	m²
T	Temperature	°C
v	Air velocity	m.s^{-1}
α_{diff}	Thermal diffusivity	m².s^{-1}
β	Wet surface over total surface	Dimensionless
ε	Emissivity	Dimensionless
Φ	Heat flux density	W.m^{-2}
λ	Thermal conductivity	W.m^{-1}.K^{-1}
ΔH_v	Heat of water evaporation	J.kg^{-1}

Subscripts

a	air
d	dry zone of plate
i	initial
pl	plate
w	wet zone of plate
wb	wet-bulb

1. Introduction

The evaporation of water droplets is involved in many applications. In a closed display cabinet, condensation and evaporation on the glass door are often observed [1]. For fire extinction, the cooling of solid surfaces can be performed thanks to the evaporation of water droplets [2, 3], as well as the enhancement of heat exchanges [4, 5]. For fruit and vegetable humidification, the use of small water droplets accelerates the product temperature decrease because of water evaporation from the product [6, 7, 8, 9]. Heat and moisture transfer is a determining factor of the food product cooling rate [10, 11] and heating rate [12]. Humidity control (evaporation, condensation) has a significant impact on the well-being of humans indoors [13].

In a food plant, after production, cleaning by water is often practiced, which leads to high humidity in the air and to the presence of water droplets on walls (e.g., equipment and floor). These conditions are favourable for microbial growth, such as *Listeria Monocytogenes*, a serious foodborne pathogen [14]. Equipment that is mostly made of stainless steel can be contaminated, causing a threat to food quality and safety [15]. Several studies have shown the presence of *Listeria* in production plants and along the food chain [16, 17]. These authors investigated food factories and found the presence of *Listeria* inside the production room (on the evaporators, floors, drains, food-contact surfaces…). The influence of temperature, humidity and air-blowing velocity on the contamination was noted. Despite the cleaning, which requires large amounts of water and chemical substances that remain, microbial contamination was observed. They concluded that dry conditions and the restriction of food residues contribute to the control of these microorganisms. The presence of water must be eliminated by drying, especially right after cleaning, to limit contamination; thus, the evaporation phenomenon of a liquid deposited onto a solid surface has to be well-understood.

The main objective of this work is to study the influence of the following factors on the water evaporation rate: ambient conditions (relative humidity, temperature, velocity) and percentage of wet surface. A correlation for the evaporation rate as a function of these parameters is proposed.

A literature review of a liquid evaporating on a solid surface is carried out for better understanding of this phenomenon.

Evaporation of a liquid is a phenomenon that occurs in many industrial operations (refrigeration, spray cooling, drying processes…). Because evaporation is endothermic, the evaporation rate is influenced by the heat transfer in the liquid phase and at the liquid/vapour interface [18, 19]. The heat transfer during evaporation is mainly driven by the temperature gradient, while the mass transfer, by the concentration gradient. In the case of forced convection, air velocity and turbulence also influence the evaporation process [20, 21, 22]. These studies showed the influence of the neighbouring environment on evaporation. The initial deposition of the droplets on the solid surface is another parameter that has an impact on the evaporation rate. This deposition depends on different parameters, such as the droplet size and the droplet impact velocity [23] during water pulverization. When a liquid is carefully placed on a surface of a given solid, it remains as a drop with the formation of a contact angle between the liquid and solid phases. The magnitude of the contact angle depends on the physical characteristics of both the liquid and the solid phases [24, 25]. For a given drop volume, a higher value of the contact angle produces a thicker drop with a smaller base radius. The contact angle plays, therefore, an important role in the rate of evaporation of the drop. Birdi et al. (1989) [24] reported that the rate of evaporation is linearly proportional to the radius of the liquid-solid interface. According to Beysens (1995) [26] and Croce et al.

(2005) [27], the evaporation of a droplet may be distinguished into 2 periods. During the first period, the base area of the droplet is constant while the contact angle decreases until the receding value is reached: the evaporation rate is almost constant. During the second period, the contact angle is constant: the wet area decreases, which modifies the evaporation rate. Therefore, the change in the evaporation rate when the water surface varies has to be considered. Hsu et al. (2015) [28] investigated experimentally water droplets on hydrophilic, hydrophobic and mixed wettability surfaces. The measurement of the contact angle and volume evolution was undertaken over the evaporation time. The results revealed that surface wettability plays a critical role not only in vapour bubble formation but also in evaporation rate.

2. Materials and Methods

Experiments were carried out in a wind tunnel, in which velocity, temperature and relative humidity of the air were controlled. In the work zone of this wind tunnel, a stainless steel plate wetted by water was exposed to several air conditions. The water mass and the wet surface evolutions were examined.

2.1. Description of the wind tunnel

The experimental device consists of a wind tunnel (length x height x width = 64 cm x 19 cm x 19 cm, Figure 1) made of PVC, except the upper wall, which is made of Plexiglas. This device is located in a test room where temperature and relative humidity can be controlled. In the work zone, a stainless steel plate (15 cm x 15 cm x 0.1 cm) is placed on a balance. Underneath this plate, extruded polystyrene (4 cm thickness) is used as thermal insulation. In this way, the result interpretation is facilitated because the exchange with air is undertaken only between the upper surface of the stainless steel and the air. This plate, wetted by water (procedure explained in section 2.2), was exposed to different ambient conditions: air temperature (4.2°C to 19.6°C), relative humidity (51% to 85%) and air velocity (0.45 to 2.0 $m.s^{-1}$). During the experiments, the air and plate temperatures, the air velocity, the relative humidity in the tunnel, the water weight and the wet surface on the stainless steel plate were measured.

Figure 1: Schematic representation of the experimental setup.

Positions of the air velocity measurements, (a)- position of the cross section in the wind tunnel, (b)- positions of the measurements in the section

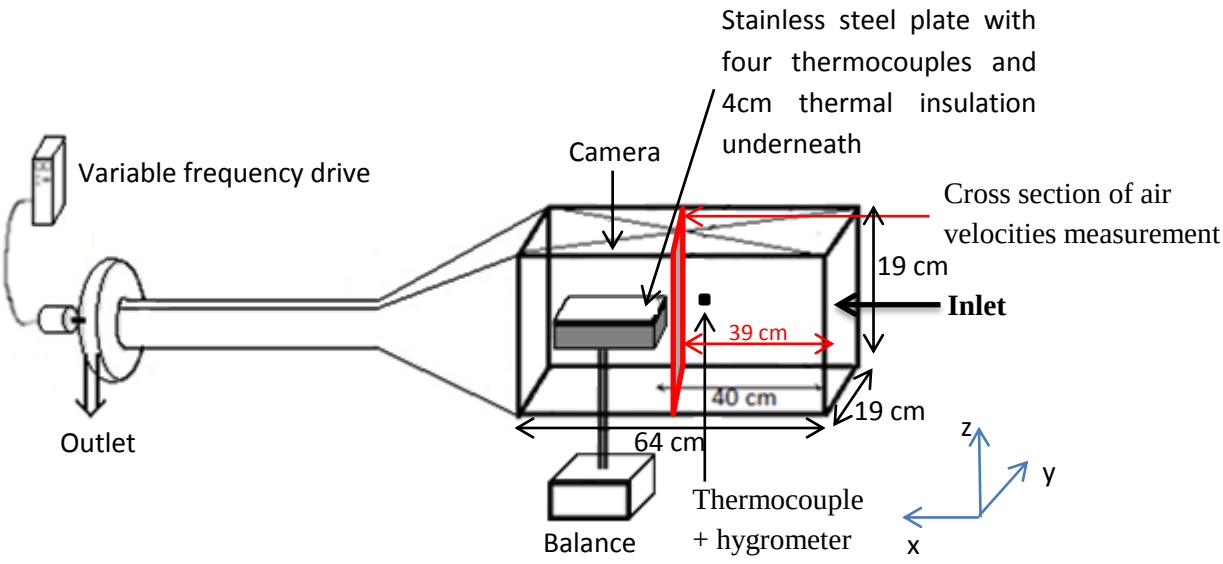

(a)

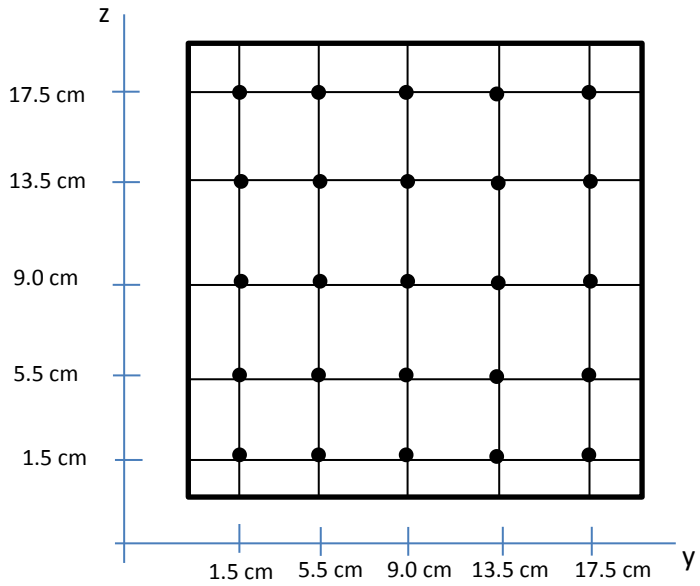

(b)

2.2. Parameters measurement

Water droplets of 0.1 mL (30 droplets, 60 droplets, 100 droplets, using a pipette), puddles and a film were deposited onto the stainless steel plate (Figure 2). Moreover, another experiment was carried out with smaller droplets: 60 droplets of 0.05 mL. The water weight on the plate was recorded every 5 seconds using an electronic balance (Sartorius, 3410028, +/-0.001 g

precision) connected to a data-logger (Agilent 34970A). Measurement was carried out until all the water was evaporated.

Figure 2: Different water distributions on the stainless steel plate used in the experiment (β_0=percentage of wet surface over total surface). A spot at the center is a fixing screw.

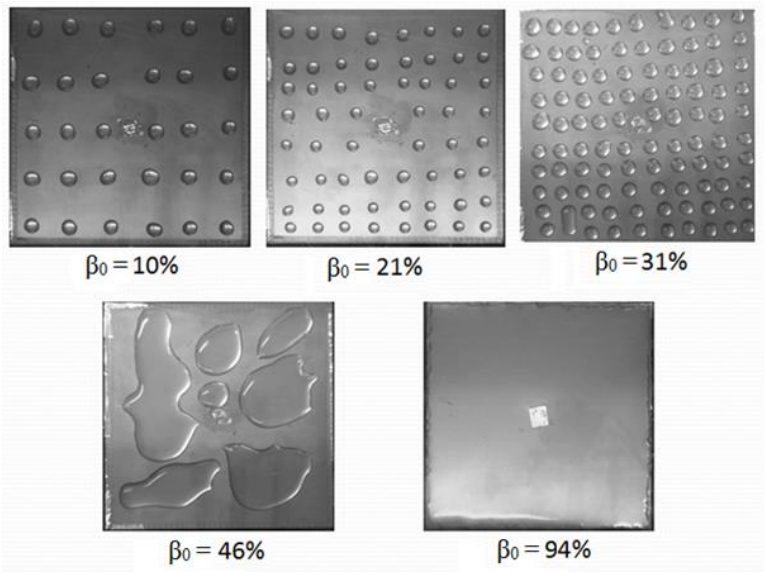

The air temperature inside the wind tunnel and the plate temperature were measured using calibrated T-type thermocouples (1 mm diameter, +/- 0.1°C precision) during the evaporation. One thermocouple was put in the wind tunnel to measure the air temperature and 4 thermocouples were put underneath the plate (between the stainless steel and polystyrene plates).

The air relative humidity was measured using a capacitive humidity sensor TESTO 174H (+/- 3% precision).

The air velocity in the wind tunnel was varied from 0.45 to 2.0 $m.s^{-1}$ using a variable frequency drive. To stabilize, as much as possible, the air inside the wind tunnel, ventilation was operated in aspiration mode. Moreover, a honeycomb (tubes of 3 mm in diameter) was placed at the cross-section of the inlet. The air velocity was measured one centimetre before the plate at 25 positions in this cross-section (Figure 1), and the average velocity was calculated for different powers of the variable frequency drive (reported in Table 1). At each point, the velocity was taken every second during 2 min using a hot wire anemometer (TESTO 435-4, +/- 0.03 $m.s^{-1}$ precision).

To monitor the evolution of the wet surface on the plate during the evaporation, images were taken using a high definition camera (KAPPA DXP 1154) and a zoom (NavitarTenX) located outside the wind tunnel and just above the plate (Figure 1). The time interval between 2 images was 5 min. Image treatment, using the open source software ImageJ, allowed for the determination of the wet surface. The results were reported in terms of percentage of wet surface over the total plate surface: β.

Table 1: Summary of the experimental conditions.

Studied parameter	Air temperature[1] (°C)	Air relative humidity[2] (%)	Air velocity ($m.s^{-1}$)[3]	β_0[4] (%)
Influence of air temperature	4.2 (+/- 0.1)	51 (+/- 3)	1.0 (+/-0.03)	~10 (30 droplets of 0.1 mL)
	10.2 (+/- 0.1)			
	19.6 (+/- 0.1)			
Influence of air relative humidity	4.2 (+/- 0.1)	51 (+/- 3)	1.0 (+/-0.03)	~10 (30 droplets of 0.1 mL)
		65 (+/- 3)		
		85 (+/- 3)		
Influence of air velocity	4.2 (+/- 0.1)	51 (+/- 3)	0.45 (+/-0.03)	~10 (30 droplets of 0.1 mL)
			0.7 (+/-0.03)	
			1.0 (+/-0.03) three repetitions	
			2.0 (+/-0.03)	
Influence of % of wet surface (β_0)	4.2 (+/- 0.1)	51 (+/- 3)	1.0 (+/-0.03)	~10 (30 droplets of 0.1 mL)
				~13 (60 droplets of 0.05 mL)
				~21 (60 droplets of 0.1 mL)
				~31 (100 droplets of 0.1 mL)
				~46 (Puddles)
				~94 (Film)

[1] average value of the air temperature during 5 to 23 hours (depending of the experimental conditions) with an acquisition frequency of 0.2Hz.

[2] average value of the relative humidity during 5 to 23 hours (depending of the experimental conditions) with an acquisition frequency of 0.2Hz.

[3] average value of 25 positions (during 2 min for each position with a frequency of 1 Hz).

[4] measurements by camera and image treatment by software

Additionally, to quantify the exchanges between the plate and air in the wind tunnel, a fluxmeter, equipped with a thermocouple, was used (Trade name Captec, width x height x depth: 4 cm x 4 cm x 450 µm, Figure 3). It was placed in the middle of the plate and supplied

by 10 W of heating power (insulated underneath). The fluxmeter temperature ($T_{fluxmeter}$), the air temperature (T_a, measured at 5 cm from the surface of the fluxmeter) and the output signal of the fluxmeter (q̇, W.m^{-2}) were recorded every second until a steady state was obtained. Then, the mean values were calculated over 30 min of a stabilization period. Note that the emissivity of this fluxmeter is close to zero; thus, the radiative exchange can be neglected in the measurement. The heat transfer coefficient between the surface and the air (h, W.m^{-2}.K^{-1}) was calculated using equation 1:

$$h = \frac{\dot{q}}{T_{fluxmeter} - T_a} \quad (1)$$

Figure 3: Fluxmeter for convective heat transfer coefficient measurement between the plate and the air in the wind tunnel

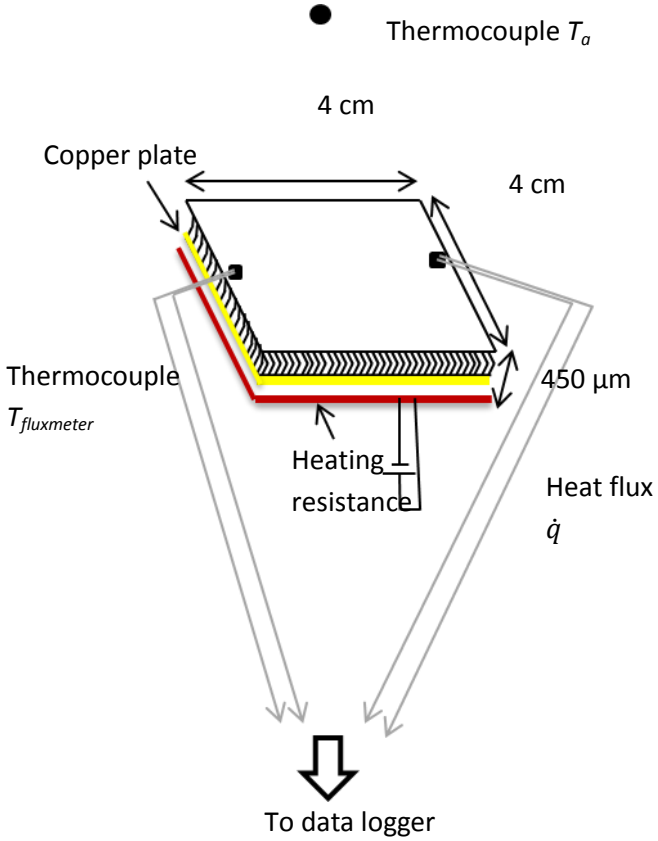

2.3. Experimental conditions

Once the air temperature and relative humidity were stabilized at the desired values inside the wind tunnel, the plate with the droplets, puddles or film was placed on the balance. Then, the data were recorded (air and plate temperatures, relative humidity, water weight and wet surface). To study the influence of ambient conditions on the evaporation rate, 15 experiments were carried out. The average values of the air temperature and relative humidity from 5 to 23 hours (depending on the experimental conditions), with an acquisition frequency of 0.2 Hz, are reported in Table 1, as well as the air velocity and the initial value of β (measurements by camera and image treatment by software).

2.4. Numerical simulations

In addition to the experiments, numerical simulations using the finite element method (Comsol software, version 3.5) were performed as a first approach to highlight some phenomena. The simulations were notably carried out to analyse temperature difference between the wet/dry areas and to predict evaporation rate. Note that the simulations give only an approximation for the period during which the wetted surface remains constant. During this period, it can be observed from the experimental results for the reference case (Figure 4) that the water mass decreases linearly during the first three hours of the evaporation (similar observation for the other cases in Figure 5). The evaporation rate is thus about constant during this period. The studied geometry is composed of a water droplet deposited onto a stainless steel plate (Figure 6), considering axial symmetry.

Figure 4: Parameters evolution on the stainless steel plate (ratio of initial wet surface: β_0 ~10%) exposed to ambient conditions of 51%*RH*, 4.2°C, 1.0m.s^{-1}. Three repetitions were performed and an average value of these repetitions ± standard deviation are shown (a)-Water mass (b)-Percentage of wet surface over total surface: β (c)-Temperature difference between air and plate.

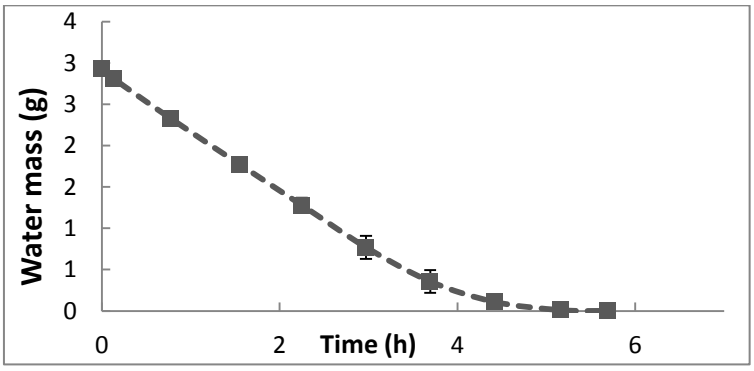

(a)

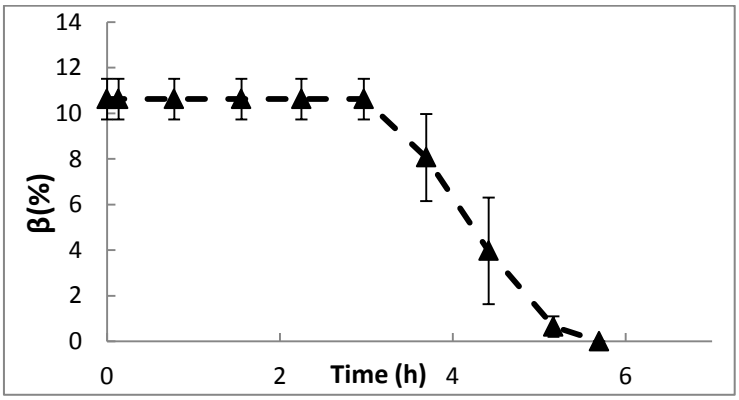

(b)

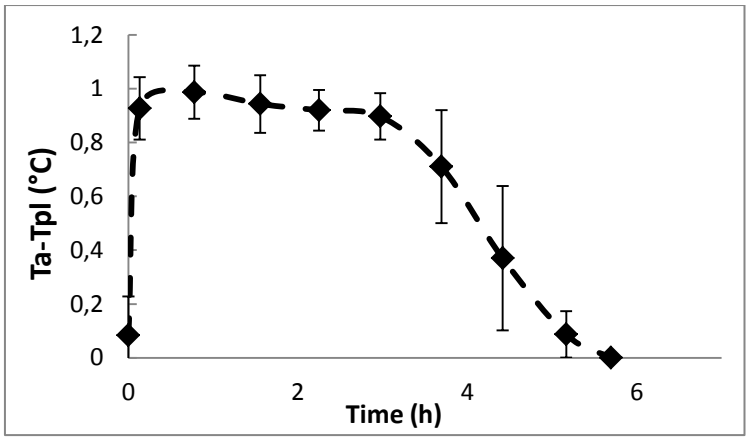

(c)

Figure 5: Influence on the evaporation rate of (a)-the air relative humidity (for experimental conditions of 4.2°C, 1.0 m.s^{-1} and β_0~10%) (b)-the air temperature (for experimental conditions of 51%*RH*, 1.0 m.s^{-1}, β_0~10%) (c)-the air velocity (for experimental conditions of 4.2°C, 51%*RH*, β_0~10%)

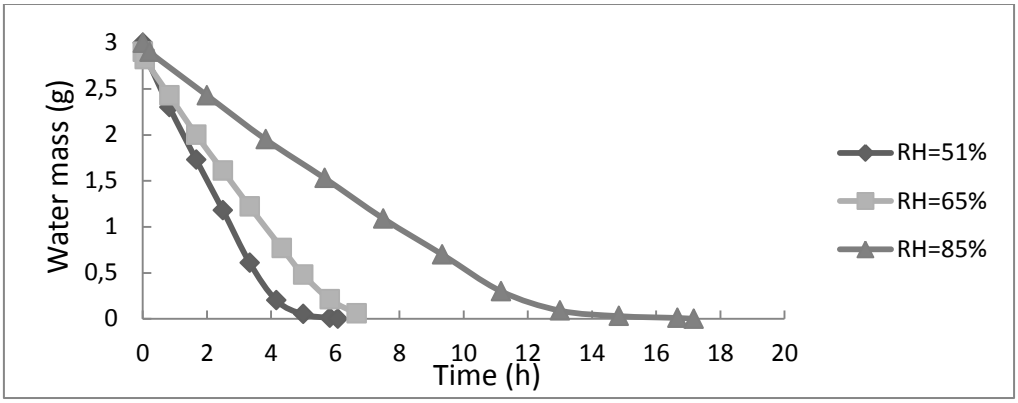

(a)

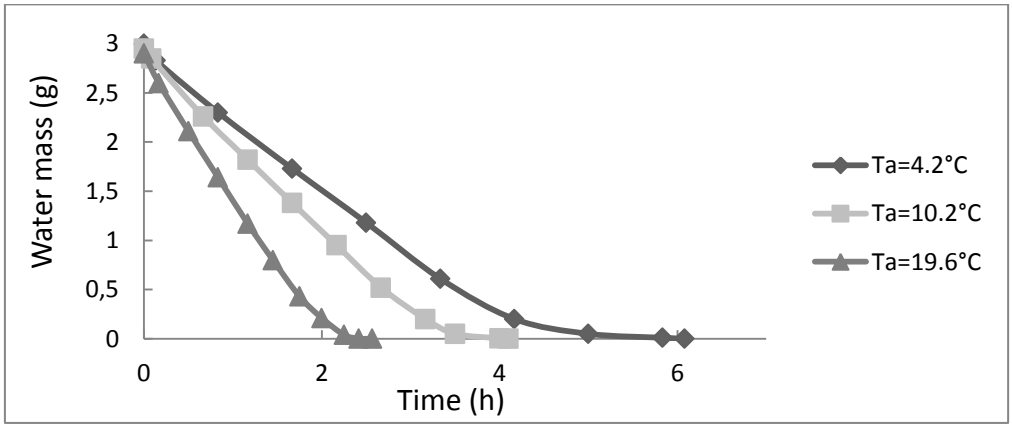

(b)

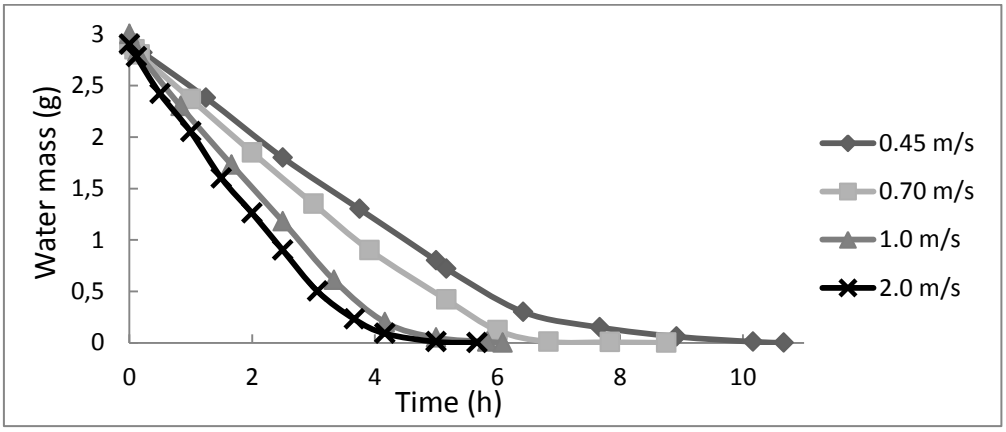

(c)

Figure 6: Temperature distribution inside a water droplet and a stainless plate for the reference case: 4.2°C, 51% *RH*, 1.0 m.s^{-1}, β_0~10%.

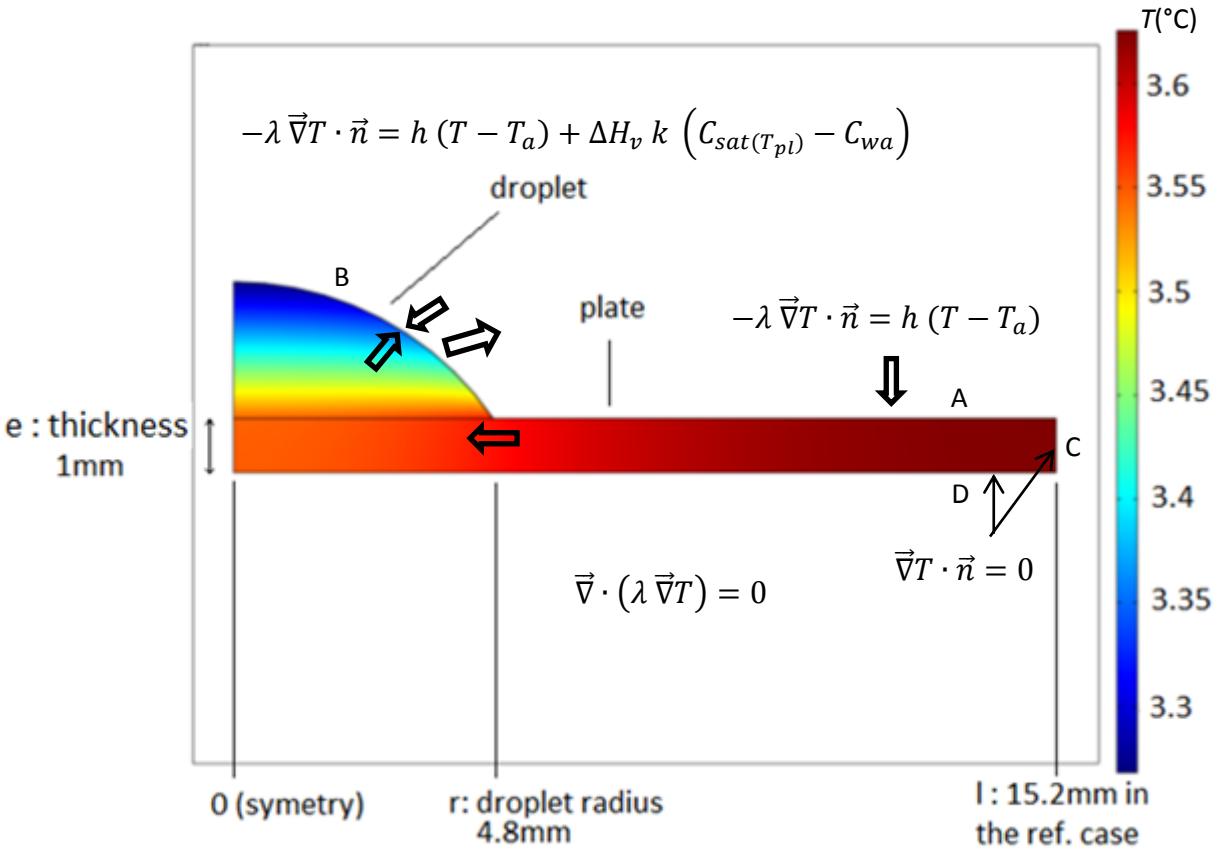

Because these simulations were performed to compare the evaporation rate with the experimental results during constant evaporation rate period, a quasi-steady-state approximation was applied. Thus, during this period, geometrical change of the drop was ignored and the transient thermal term ($\rho\,C_p\,\frac{\partial T}{\partial t}$) was neglected. Indeed, it could be observed (Figure 4) that the plate temperature remains almost constant during this period. Moreover, the characteristic times of thermal diffusion are low compared to the evaporation time (several hours):

For the droplet, the characteristic diffusion time is: $\frac{e^2{}_{droplet}}{\alpha_{diff.water}} \approx 30s$

For the stainless steel: $\frac{l^2}{\alpha_{diff.stainless\ steel}} \approx 25s$

Therefore, steady state conduction was considered in the stainless steel plate and in water.

$$\vec{\nabla}\cdot(\lambda\,\vec{\nabla}T)=0 \qquad (2)$$

At the dry surface (A in Figure 6), convection occurs (radiation is neglected due to the low emissivity of stainless steel).

$$-\lambda\,\vec{\nabla}T\cdot\vec{n}=h\,(T-T_a) \qquad (3)$$

where h is the convective heat transfer coefficient measured by a fluxmeter and T_a is the average air temperature measured in the wind tunnel during the experiment.

At the water-air interface (B in Figure 6), the latent heat of evaporation is additionally taken into account.

$$-\lambda \vec{\nabla}T \cdot \vec{n} = h\,(T - T_a) + \Delta H_v\, k\, \left(C_{sat(T_{pl})} - C_{wa}\right) \quad (4)$$

where $C_{sat(T_{pl})}$ is the concentration of saturated water vapour at the plate temperature.

The Lewis analogy (Le) was used to estimate the mass transfer coefficient k (evaporation).

$k = \frac{h}{\rho.Cp_{air}.Le^{2/3}}$ with $Le = \frac{a_{diff}}{D} \approx 0.85$

a_{diff} is the thermal diffusivity of water vapor = $18.6 \cdot 10^{-6}$ m².s^{-1} at 0°C,

D is the mass diffusivity of water vapor in air = $21.8 \cdot 10^{-6}$ m².s^{-1} at 0°C [29].

As a first approach, radiation was also ignored at the water-air interface. This approximation is reasonable only if the fraction of wetted surface is low (for the reference case, β=10%) and if convection is dominant. This point is discussed in section 3.7.

Perfect insulation is assumed at the bottom and lateral faces of the stainless steel plate (C and D in Figure 6):

$$\vec{\nabla}T \cdot \vec{n} = 0 \quad (5)$$

The evaporation rate is obtained by integration over the water-air surface

$$\dot{m} = \int_B k\left(C_{sat(T)} - C_{wa}\right) dS \quad (6)$$

The initial radius of the droplet and the average half distance between two droplets, l, were calculated for all experiments. These values were used as input parameters. The output parameters were the dry (T_d), wet (T_w), and average plate (T_{pl}) temperatures and the evaporation rate during the first period (constant rate). Simulations were performed using a direct stationary solver and meshing was performed with triangular quadratic elements. In order to verify the mesh independence on the results, two numbers of elements were used (1552 and 6208), it was found that the difference is negligible in terms of evaporation rate. The comparison between the numerical (6208 elements) and experimental results is shown in section 3.8.

3. Results and Discussion

3.1. Reference experiment

To assure result repeatability, three experiments were performed using the same conditions: air temperature of 4.2°C, relative humidity of 51%, velocity of 1.0 m.s^{-1} and 30 droplets of 0.1 mL (β_0~10%). The evolution of the water mass, the wet surface and the difference between the plate temperature and the air temperature are shown in Figure 4a, 4b and 4c, respectively. It can be observed that the results are relatively close for these 3 experiments.

During the evaporation, it is possible to distinguish 2 periods (Figure 4a). During the first period (~3 h), the evaporation rate is constant, and then it decreases progressively. The first period corresponds to the time during which the wet surface (the surface occupied by water on the plate) (Figure 4b) and the temperature difference between the air and the plate (Figure 4c) are almost constant. This observation leads to the conclusion that only the contact angle of the droplets decreases in the first period while the wet surface is constant. Then, because of the uneven transfer intensity on the plate (the hydrodynamic boundary layer thickness evolves along the plate), some droplets evaporate faster than others, which reduces the wet surface during the second period. In fact, the percentage of wet surface over the total surface of the stainless steel plate influences the plate temperature and, consequently, the temperature difference (air-plate), a determining factor of the evaporation rate. Note that at the beginning of the evaporation, the plate and air temperatures are the same. However, because of the low heat capacity of the plate (mCp≈90 J.K^{-1}), the time for the plate to reach its temperature during the first period (approximately 10 minutes) is negligible compared to the time needed to entirely evaporate the water (approximately 6 hours, Figure 4c). These phenomena are examined in the following sections.

3.2. Influence of the relative humidity on the evaporation rate

Figure 5a shows the influence of the relative humidity on the evaporation rate for 30 droplets of 0.1 mL (β~10%), an air temperature of 4.2°C and air velocity of 1.0 m.s^{-1}. For every relative humidity (51%, 65% and 85%), the same evolution trends are observed for the water mass (Figure 5a). Additionally, it can be observed that the higher the relative humidity, the lower the evaporation rate, which leads to an increase of the drying duration (Table 2).

Table 2: Influence of air relative humidity on the evaporation of 3g of water droplets (for experimental conditions of 4.2°C, 1.0 m.s^{-1}, β_0 ~10%).

***RH* (%)**	T_a (°C)	T_{wb} (°C)	T_{pl}^* (°C)	T_a-T_{pl} (°C)	Duration of constant evaporation rate (h)	Duration of drying (h)
51	4.15	0.72	3.29	0.86	3.3	6.1
65	4.19	1.73	3.59	0.60	4.3	8.2
85	4.28	3.26	3.96	0.32	9.3	17.2

T_{pl}^*: Mean value of the plate temperature during the constant evaporation rate (first period).

By reducing the relative humidity from 85% to 51%, the time to evaporate the same amount of water was reduced by a factor of 2.8. This can be explained by the fact that a higher relative humidity corresponds to a higher wet bulb temperature (0.72°C for 51% *RH*, 1.73°C for 65% *RH*, 3.26°C for 85% *RH*); consequently, the plate temperature increases. The difference between the air and the plate temperatures decreases; thus, the time for total evaporation increases. Indeed, a smaller temperature difference between the air and the plate induces a lower driving force for the heat transfer (eq. 7) and therefore a longer time to transfer the latent heat of vaporization.

$$\Phi_{convection} = h \cdot (T_a - T_{pl}) \quad (7)$$

3.3. Influence of the air temperature on the evaporation rate

Three experiments were performed to study the air temperature influence. The air temperature was set at 4.2°C, 10.2°C and 19.6°C (51% *RH*, 1.0 m.s^{-1}, and β~10% for the three experiments). The water mass evolutions are shown in Figure 5b. The results are also summarized in Table 3.

Table 3: Influence of the air temperature on the evaporation of 3g of water droplets (for experimental conditions of 51% *RH*, 1.0 m.s^{-1}, β_0 ~10%).

RH (%)	T_a **(°C)**	T_{wb} (°C)	T_{pl} (°C)	T_a-T_{pl} (°C)	Duration of constant evaporation rate (h)	Duration of drying (h)
51	**4.15**	0.72	3.29	0.86	3.3	6.1
50	**10.16**	5.66	8.76	1.40	2.2	4.1
51	**19.57**	13.56	17.56	2.01	1.5	2.6

It can be observed that when T_a-T_{pl} decreases by 2.3 times (from 2.01°C to 0.86°C), the duration of drying increases by 2.3 times. The results show that the higher the air temperature, the higher the air-plate temperature difference (for constant *RH*), which indicates, as explained previously, a higher evaporation rate. Moreover, the evaporation rate seems to increase linearly with this difference.

3.4. Influence of the air velocity on the evaporation rate

Air velocity has an influence on the heat transfer: higher air velocity leads to higher heat exchange. Four experiments were performed, using air velocities of 0.45, 0.70, 1.0 and 2.0 m.s^{-1} (51% *RH*, T_a=4.2°C and β~10% for all experiments). Figure 5c shows that higher air velocity leads to higher evaporation rate. However, the influence of air velocity on the temperature difference between the air and plate is not significant (Table 4).

Table 4: Influence of the air velocity on the evaporation of 3g of water droplets (for experimental conditions of 4.2°C, 51% *RH*, β_0 ~10%).

v **(m.s^{-1})**	*RH* (%)	T_a (°C)	T_{wb} (°C)	T_{pl} (°C)	T_a-T_{pl} (°C)	Duration of constant evaporation rate (h)	Duration of drying (h)
0.45	52	4.29	0.91	3.44	0.85	5.2	10.7
0.70	51	4.25	0.79	3.38	0.87	3.9	8.8
1.0	51	4.15	0.72	3.29	0.86	3.3	6.1
2.0	52	3.81	0.50	3.05	0.76	2.5	5.7

An increase in the air velocity will increase the heat transfer coefficient *h*, which leads to more exchange for water evaporation (eq. 7).

A correlation between air velocity and heat transfer coefficient was proposed using these experimental results on the basis of the following development:

The heat balance for a constant evaporation rate (considering T_d-T_w << T_a-T_{pl} and neglecting the heat capacity of the stainless steel plate) becomes:

$$\dot{m} \cdot \Delta Hv = h \cdot S \cdot (T_a - T_{pl}) \quad (8)$$

Thus, the heat transfer coefficient h can be determined as follows:

$$h = \frac{\dot{m} \cdot \Delta Hv}{S \cdot (T_a - T_{pl})} \quad (9)$$

where $\dot{m} = \frac{dm}{dt}$ is the evaporation rate during the first period (kg.s^{-1}), which is the slope of the linear part of the curves shown in Figure 5c, and T_{pl} is the average plate temperature during this period.

The heat transfer coefficient, calculated by using equation 9 as a function of the air velocity, is shown in Figure 7. This curve, fitted by a power law, shows that:

$$h = 22.7\, v^{0.53} \quad (10)$$

(h in W.m^{-2}.K^{-1}, v in m.s^{-1})

Figure 7: Relation between the heat transfer coefficient and the air velocity

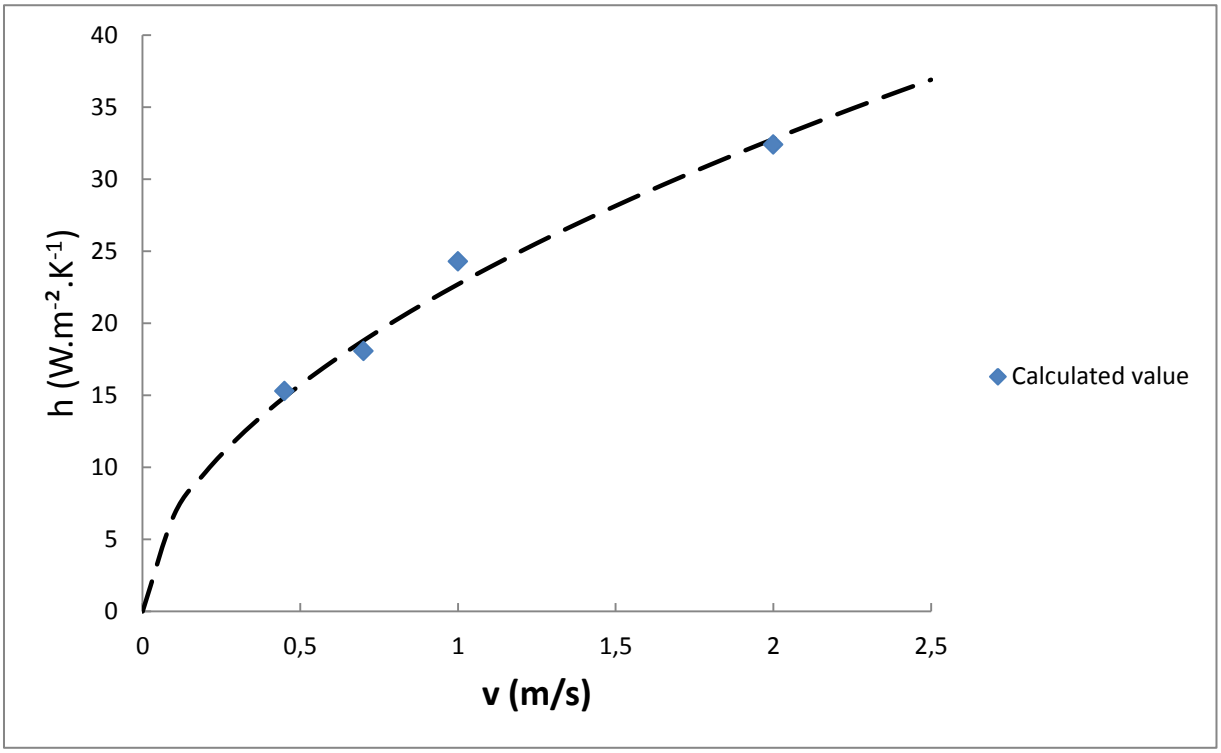

The heat transfer coefficient is almost proportional to the square root of the velocity, which corresponds to the expected laminar boundary layer: the maximal Reynolds number relative to the development of the hydrodynamic boundary layer along a plate (length, L= 0.15 m) for an air velocity V of 2.0 m.s^{-1} is $Re = \frac{V \cdot L}{\nu} \approx 2.10^4$. This value is less than 5.10^5, which is considered as the beginning of the turbulent boundary layer [30].

The values of h obtained from the evaporation experiments (eq. 9) were compared to the ones measured by the fluxmeter (as explained in section 2.2) and exposed to the same air velocities (Figure 8). The results are close, except for the air velocity of 2.0 m.s^{-1}, where the value

calculated (32 $Wm^{-2}K^{-1}$) is lower than the one measured with the fluxmeter (40 $Wm^{-2}K^{-1}$). This can be explained by the more significant influence of conduction in the stainless steel plate (λ=15 $W.m^{-1}K^{-1}$, e= 1 mm, h=40 $W.m^{-2}K^{-1}$) for higher heat fluxes:

$$\frac{T_d - T_w}{T_a - T_{pl}} \approx \frac{h \cdot l^2}{2 \cdot \lambda \cdot e} = 0.31$$

Figure 8: Comparison between the heat transfer coefficients calculated using the evaporation experiments and the ones measured by a fluxmeter.

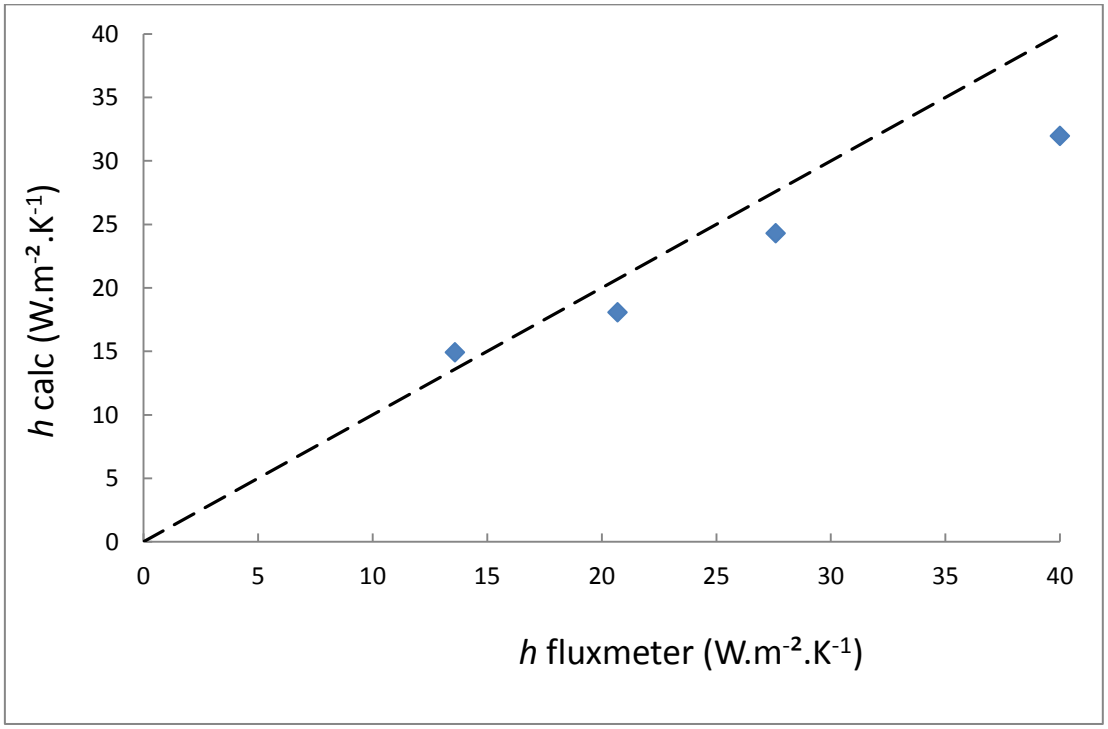

3.5. Influence of the droplet volume

An experiment was carried out to study the influence of the droplet volume for the same initial water weight (3 g) as in the reference experiment: 60 droplets of 0.05 mL were deposited onto the plate instead of 30 droplets of 0.1 mL. Table 5 shows the duration of drying and the temperature difference T_a-T_{pl}.

Table 5: Influence of the initial droplet volume on the evaporation of 3g of water droplets (for experimental conditions of 51% *RH*, 1.0 $m.s^{-1}$, β_0 ~10%).

Droplet volume (mL)	β_0 (%)	*RH* (%)	T_a (°C)	T_{wb} (°C)	T_{pl} (°C)	T_a-T_{pl} (°C)	Duration of constant evaporation rate (h)	Duration of drying (h)
0.1	9.8	51	4.15	0.72	3.29	0.86	3.3	6.1
0.05	12.8	54	4.16	0.94	3.09	1.07	2.5	5.3

It can be observed that the evaporation is slightly faster for the 60 droplets experiment because the temperature difference (air-plate) is slightly higher. This can be explained by the fact that for the case of 60 droplets, β_0 is 12.8%, while for the 30 droplets case, β_0 is 9.8%.

3.6. Influence of initial wet surface ratio, β_0

β_0 is defined as the initial percentage of wet surface over the total surface of the stainless steel plate. Experiments were made at the same ambient conditions (temperature at 4.2°C, relative humidity at 51%, air velocity at 1.0 m.s^{-1}) for different initial wet surfaces (10%, 21%, 31%, 46% and 94% of the total plate surface, see Figure 2). Figure 9a and 9b show the water weight evolution and the temperature difference between the air and the plate, respectively. The higher the initial percentage of wet surface, β_0, the higher the temperature difference (air-plate) (Table 6), and, as explained previously, a larger temperature difference will lead to a higher evaporation rate.

Table 6: Influence of the percentage of initial wet surface (β_0) on the water evaporation (for experimental conditions of 4.2°C, 51% *RH*, 1.0 m.s^{-1}).

β_0 (%)	*RH* (%)	T_a (°C)	T_{wb} (°C)	T_{pl} (°C)	T_a-T_{pl} (°C)	Duration of constant evaporation rate (h)	Duration of drying (h)
9.8	51	4.15	0.72	3.29	0.86	3.3	6.1
21.4	52	4.27	0.89	2.73	1.54	3.4	6.8
30.9	50	4.12	0.62	1.82	2.30	3.2	8.9
46.2	51	4.25	0.79	1.82	2.43	10.0	19.4
94.3	51	4.26	0.80	1.44	2.82	13.5	22.7

It can be observed that the evaporation rate (g/s), corresponding to the slope in Figure 9a, increases with β_0. However, the rate is almost the same for β_0=31% (100 droplets of 1 mL) and β_0=46% (puddles). Note that the surface taken into consideration for β (measured by a camera) is the projected surface of the droplets (surface in contact with plate). In the case of droplets (e.g., β_0=31%), the liquid/air interface where the evaporation occurs is higher than the projected surface, whereas for puddles (β_0=46%), the two surfaces are close.

Figure 9: Influence of the initial wet surface on (a)- evaporation rate (b)- temperature difference between plate and air (for experimental conditions of 51%*RH*, 4.2°C, 1.0 m.s^{-1})

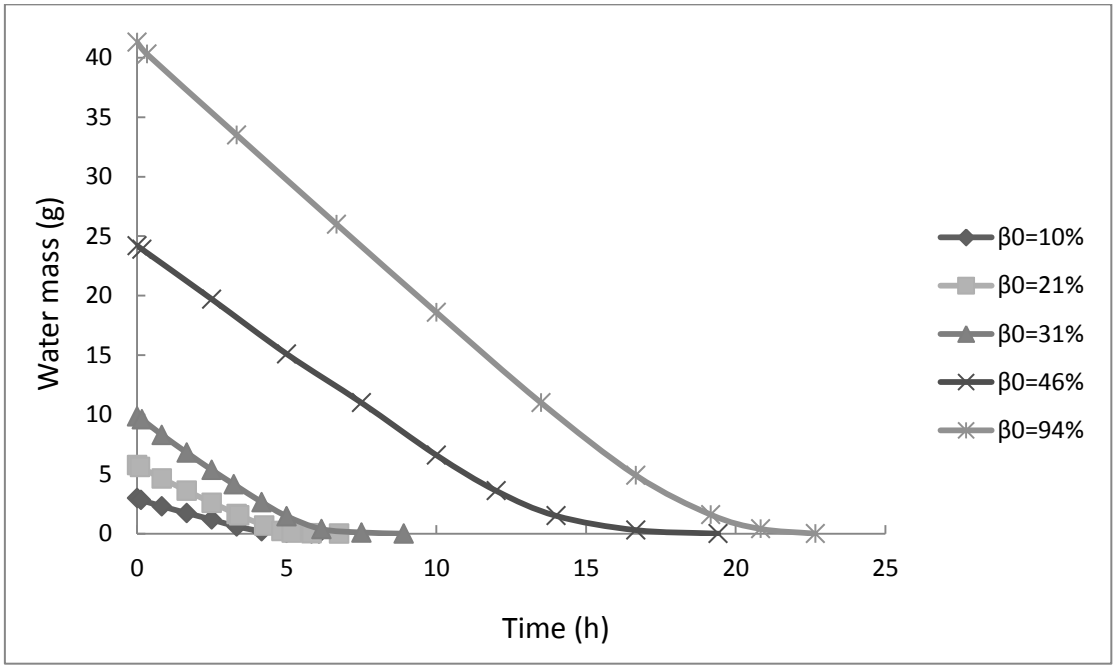

(a)

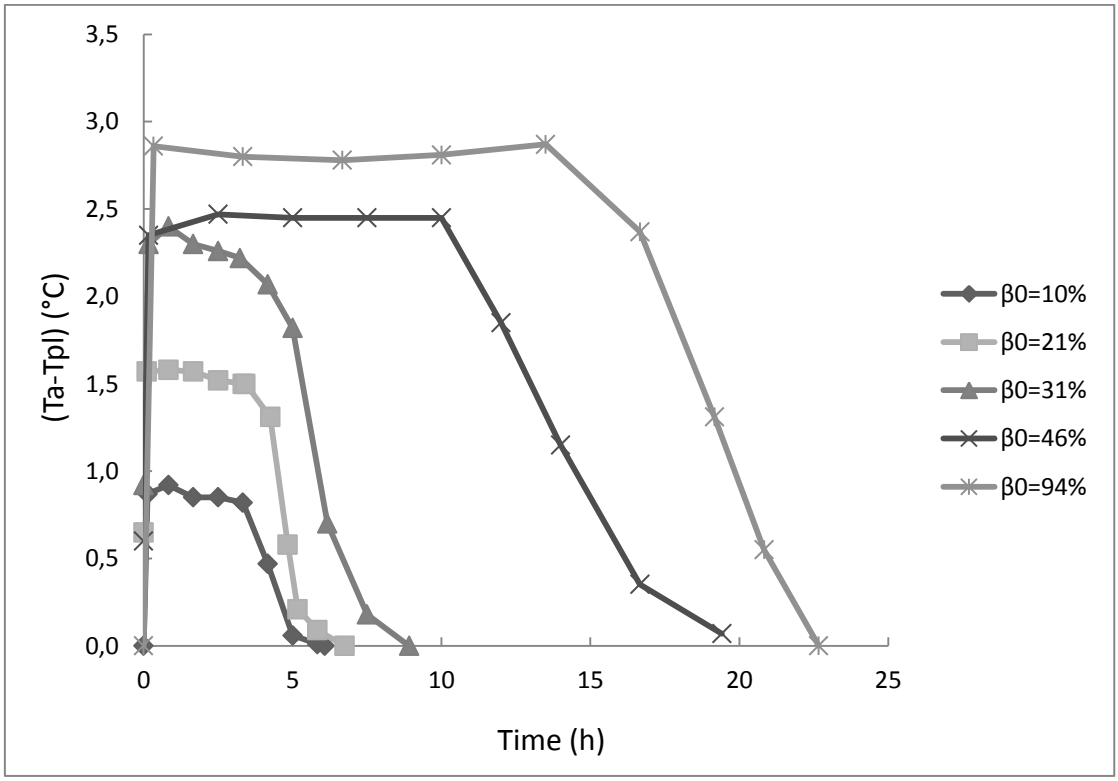

(b)

3.7. Analysis of exchange phenomena

Figure 10 present schematically the exchange phenomena.

Figure 10: Heat and mass transfer during experiment of wet stainless steel plate exposed to air in the wind tunnel, (a)-film of water on the plate, (b)-droplets or puddles on the plate.

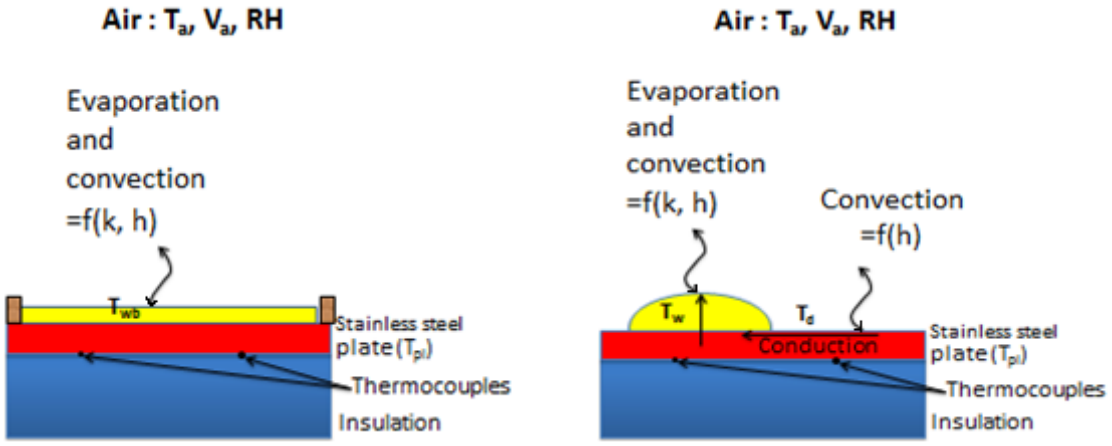

(a) (b)

Between the wet surface and the air, there are exchanges by evaporation and convection, which are functions of the mass transfer coefficient (k) and the heat transfer coefficient (h), respectively. Between the dry surface and air there is only convection. Inside the stainless steel, heat is transferred by conduction. In the case of a film of water (Figure 10a), the plate temperature tends toward the wet bulb temperature (T_{wb}). In the case of droplets and puddles (Figure 10b), the wet area temperature (T_w) is slightly lower than the dry area temperature (T_d) inside the stainless steel plate. The plate temperature (T_{pl}), defined as the average temperature, is influenced by the presence of the wet and dry surfaces, which change during drying. Taking into account this phenomena and for better representation of the plate temperature, 4 measurement positions were undertaken underneath the stainless steel plate and the average value was used. However, the temperature difference between wet and dry zones is expected to be small in our case, with the following order of magnitude:

$$conductive\ flux\ inside\ the\ plate = convective\ flux\ from\ air\ to\ plate$$

$$\lambda \cdot 2\pi \cdot l/2 \cdot e \cdot \frac{T_d - T_w}{l/2} \approx h \cdot \pi \cdot l^2 \cdot (T_a - T_{pl})$$

$$\frac{T_d - T_w}{T_a - T_{pl}} \approx \frac{h \cdot l^2}{2 \cdot \lambda \cdot e} \qquad (11)$$

where l is the half distance between two drops, e is the plate thickness and λ is the stainless steel conductivity ($15\ W.m^{-1}K^{-1}$ at 20°C). This ratio is most often lower than 0.2. This approximation was validated numerically (see section 3.8).

Note that because the surface used is smooth stainless steel, the emissivity is low; thus, the exchange by radiation can be neglected. However, when water covers a significant surface of the plate, the emissivity, thus the radiation, becomes more important and might slightly impact the evaporation rate. The emissivity of the stainless plate is approximately 0.1, and the one of water is 0.95. When a water film with a thickness above 10 µm recovers a surface, it can be considered as optically thick (Mitchell & Salvaggio 2003). In our case, the water film

or droplet thickness was approximately 2 mm; thus, its emissivity can be considered equal to the one of water, 0.95. The order of magnitude of the radiative heat flux density with and without water can be calculated as follows:

$$\Phi_{radiation} = \varepsilon \cdot \sigma \cdot \left(T_a{}^4 - T_{pl}{}^4\right) \quad (12)$$

where σ is Stefan's constant ($=5.67 \cdot 10^{-8}\ \mathrm{W.m^{-2}.K^{-4}}$) and ε is the average emissivity, which is a function of the fraction of wetted surface β_0:

$$\varepsilon = \varepsilon_{water} \cdot \beta_0 + \varepsilon_{stainless\ steel} \cdot (1 - \beta_0) \quad (13)$$

Moreover, the convective heat flux density is expressed by:

$$\Phi_{convection} = h \cdot \left(T_a - T_{pl}\right) \quad (14)$$

Table 7 compares the convective and radiative fluxes for different values of β_0.

Table 7: Influence of the radiation at different initial wet surface (β_0)

β_0 (%)	T_a (°C)	T_{pl} (°C)	Emissivity ε	radiative flux ($W.m^{-2}$)	convective flux ($W.m^{-2}$)	% radiation part
9.8	4.15	3.29	0.19	0.8	20.9	**3.7**
21.4	4.27	2.73	0.28	2.1	37.4	**5.3**
30.9	4.23	1.93	0.36	4.0	55.9	**6.7**
46.2	4.25	1.82	0.49	5.7	59.0	**8.8**
94.3	4.26	1.44	0.90	12.1	68.5	**15.0**

It can be observed that for the experiments where β_0 is approximately 10%, the contribution of the radiative flux density represents less than 4%, which can be considered negligible. Then, when the water surface increases, the radiation contribution increases too. When β_0 is approximately 21 and 31%, it represents, respectively, 5.3 and 6.7%. For the cases where water forms puddles (β_0=46%) or a film (β_0=94%) rather than droplets, the contribution of radiation becomes even greater, i.e., 8.8% and 15.0%, respectively, which means that in these cases, even if convection remains the main factor, radiation could have a significant impact on the evaporation.

To summarize, if the plate is entirely covered by water (β=1), the plate temperature is expected to be close to the wet bulb temperature (T_{wb}). When the plate is completely dry (β=0), its temperature is close to the one of air (T_a). For a partially wet plate ($0<\beta<1$), its temperature is intermediate between T_{wb} and T_a.

3.8. Comparison between experimental and numerical results

Simulations were performed for the conditions corresponding to all the experiments with droplets ($\beta \leq 31\%$). From these simulations it was possible to predict the dry (T_d), wet (T_w) and average temperatures of the plate (T_{pl}) and the evaporation rate. Thus, the ratio $\frac{T_d - T_w}{T_a - T_{pl}}$ could be determined. Figure 6 shows the temperature distribution in the droplet and in the plate

obtained from the simulation for the reference condition (4.2°C, 51% *RH*, 4.2°C, 1.0 m.s^{-1}, β_0~10%). The temperature inside the droplet is slightly different (3.3°C at the top and 3.5°C at the base), while the plate temperature variation is low (<0.05 °C). An order of magnitude of the heat flux density given by this temperature difference can be calculated:

$$\lambda_{water} \cdot \frac{\Delta T}{e_{droplet}} \approx 0.6 \frac{0.2}{10^{-3}} = 120 \text{ W.m}^{-2}$$

This value divided by the latent heat of water evaporation ΔH_v (2491 kJ/kg at 4°C) is of the same order of magnitude as the evaporation rate found in the experiments:

$$\frac{\dot{m}}{S} \approx \frac{\Phi}{\Delta H_v} \approx 5 \cdot 10^{-2} \text{ g.s}^{-1}\text{.m}^{-2}$$

Thus, it can be considered that the temperature difference inside the droplet is high enough for its evaporation. The order of magnitude of $\frac{T_d - T_w}{T_a - T_{pl}}$ given by equation 11, i.e., $\frac{h \cdot l^2}{2 \cdot \lambda \cdot e}$, was verified by these simulations (Figure 11).

Figure 11: Verification of the approximation made for the equation 1 $\left(\frac{T_d - T_w}{T_a - T_{pl}} \approx \frac{h \cdot l^2}{2 \cdot \lambda \cdot e}\right)$ by simulation using Comsol. The experimental conditions corresponding to each symbol are shown below.

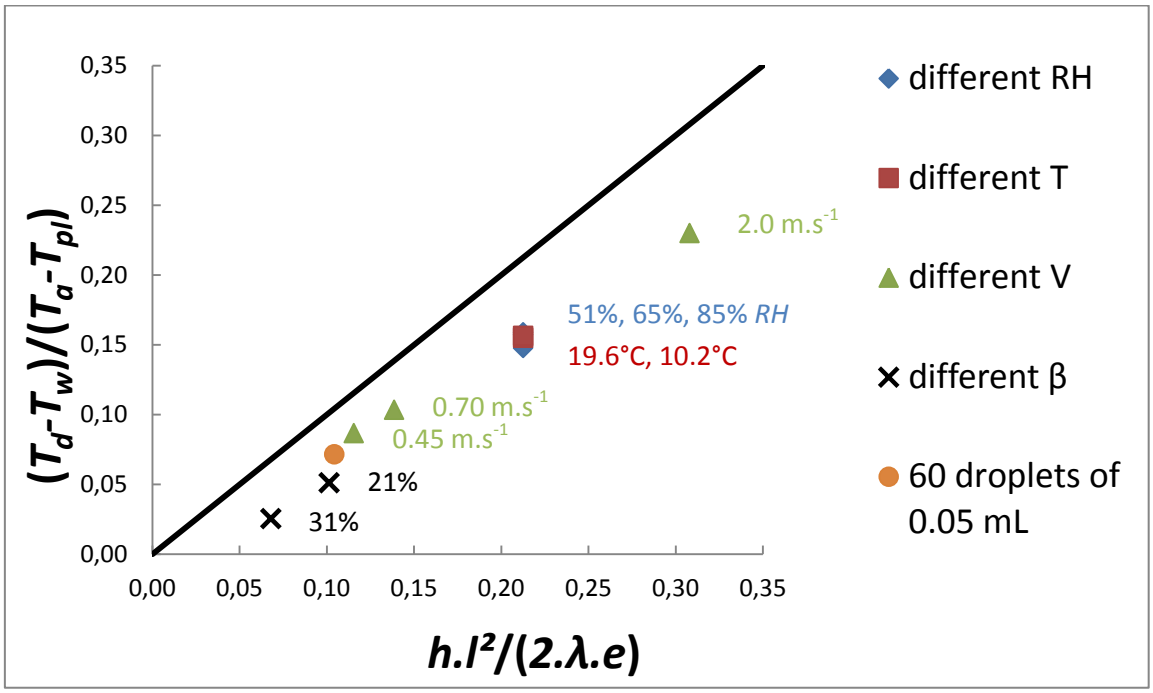

Symbol	Experimental conditions			
	Ta (°c)	*v* (m.s^{-1})	*RH* (%)	θ_0 (%)
◆	4.2	1.0	51 65 85	10
●	4.2	1.0	51	13
■	10.2 19.6	1.0	51	10
▲	4.2	0.45 0.70 2.0	51	10
×	4.2	1.0	51	21 31 46 94

For the figures 13 and 14

Figure 12 compares the evaporation rate obtained from the experiments (for the first period, when it is constant) and from the simulations. The experimental conditions corresponding to each symbol in Figure 12 are summarized in the table of Figure 11. The experimental evaporation rates are presented on the abscise, and the numerical ones, on the ordinate.

Figure 12: Comparison between the experimental and numerical (using Comsol) evaporation rates. The experimental conditions corresponding to each symbol are the same as in Figure 11.

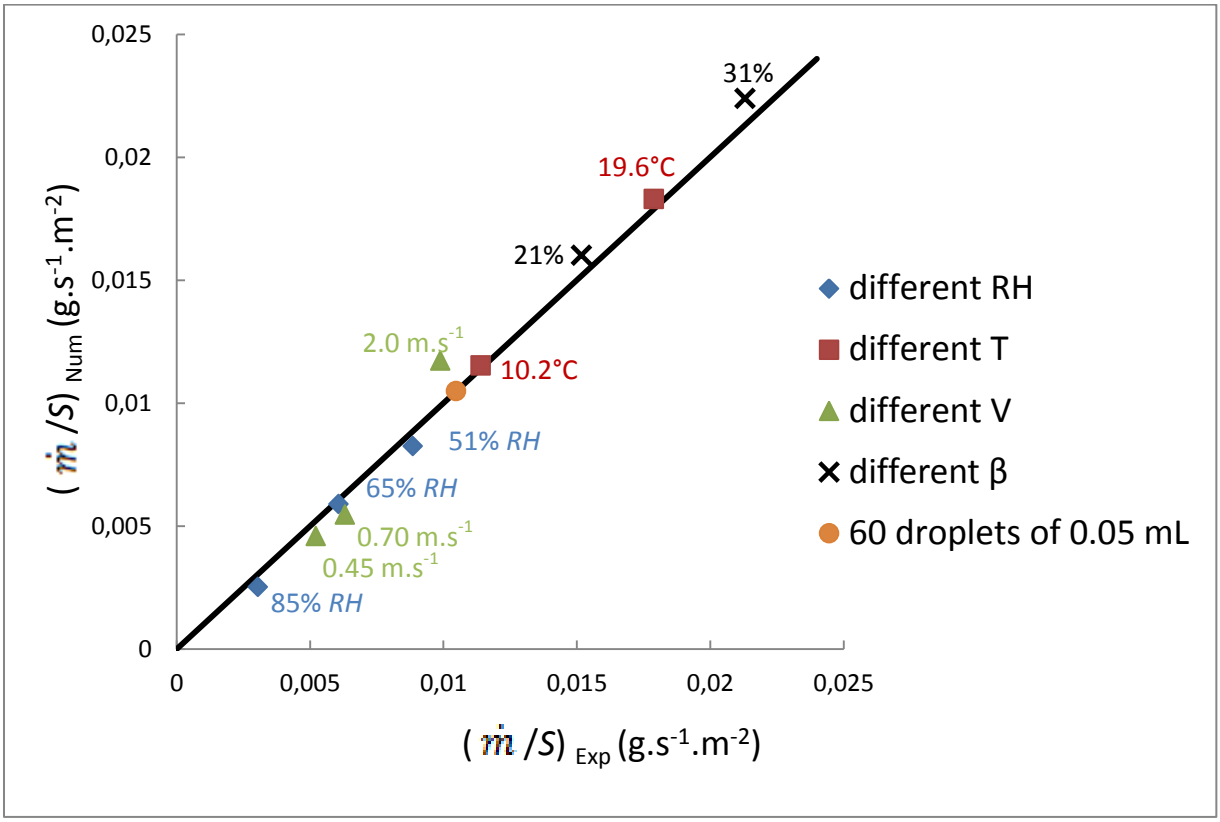

Low discrepancy between numerical and experimental values can be observed: high coefficient of determination R^2 (0.98) and low average relative error (7.8%). This leads to conclude that in spite of the simplification of the numerical model (quasi steady-state, no radiation), it gives a good estimation of the evaporation rate during the period of constant wet surface.

In the cases where β is higher, radiation should have a larger impact on the evaporation rate. Because it is validated, the numerical approach could be used for other types of plate material (less conductive than steel).

3.9. General observation

The relationship between the temperature difference (air-plate) and the evaporation rate during the first period seems to be linear (Figure 13) for different relative humidities, air temperatures and percentages of wet surface at a given velocity (1.0 $m.s^{-1}$), i.e., at given heat and mass transfer coefficients.

Figure 13: Evaporation rate during the first period (constant rate) in function of the air-plate temperature difference. The experimental conditions corresponding to each symbol are summarized in the table Figure 11.

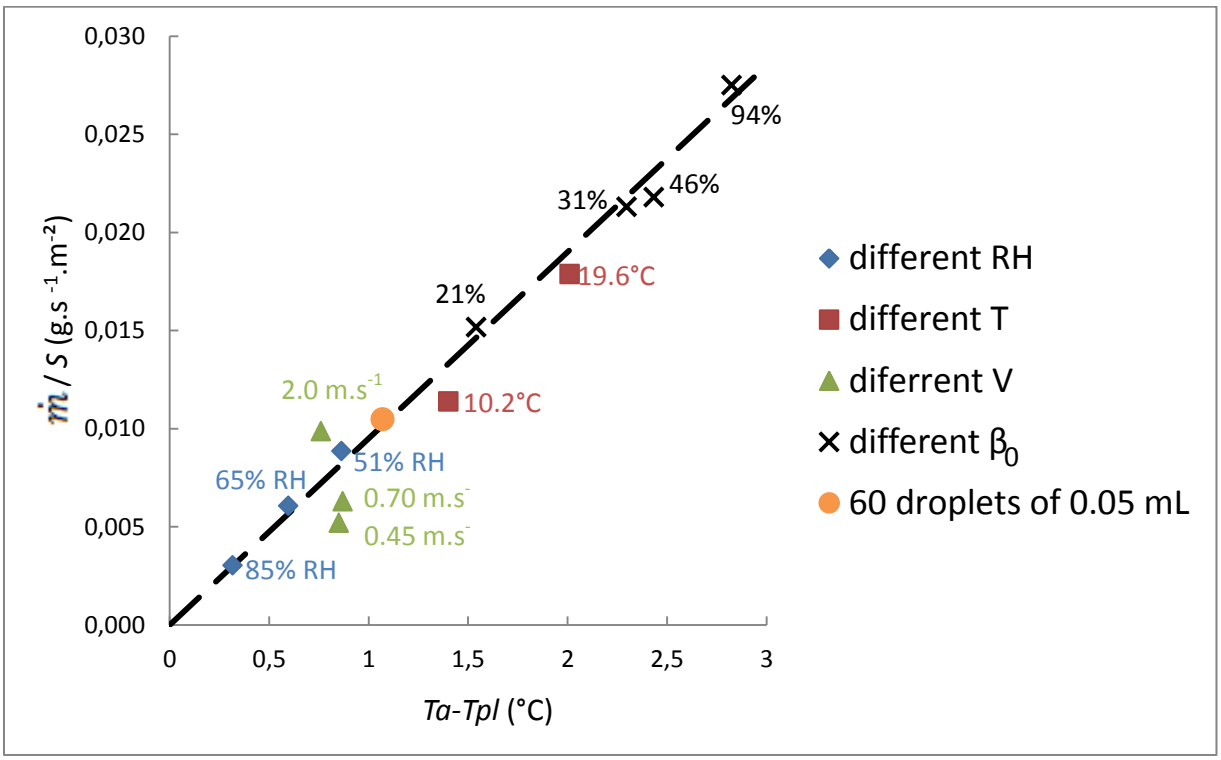

The heat balance on the plate, neglecting its thermal inertia, leads to equation (15), which shows that the evaporation rate is proportional to the temperature difference (for a given velocity):

$$\dot{m} = \frac{S \cdot (T_a - T_{pl}) \cdot h(v)}{\Delta H_v} \tag{15}$$

Moreover, the percentage of wet surface (β) has an effect on the temperature difference between the air and the plate, which in turn has an effect on the evaporation rate. Figure 14 shows the evolution of the dimensionless temperature $(T_a - T_{pl})/(T_a - T_{wb})$ as a function of β_0.

Figure 14: Evolution of the temperature difference (air-plate) over the temperature difference (air- wet bulb) with β_0 in different experiments. The points at different *RH* and different velocity are overlapped. The experimental conditions corresponding to each symbol are summarized in the table Figure 11.

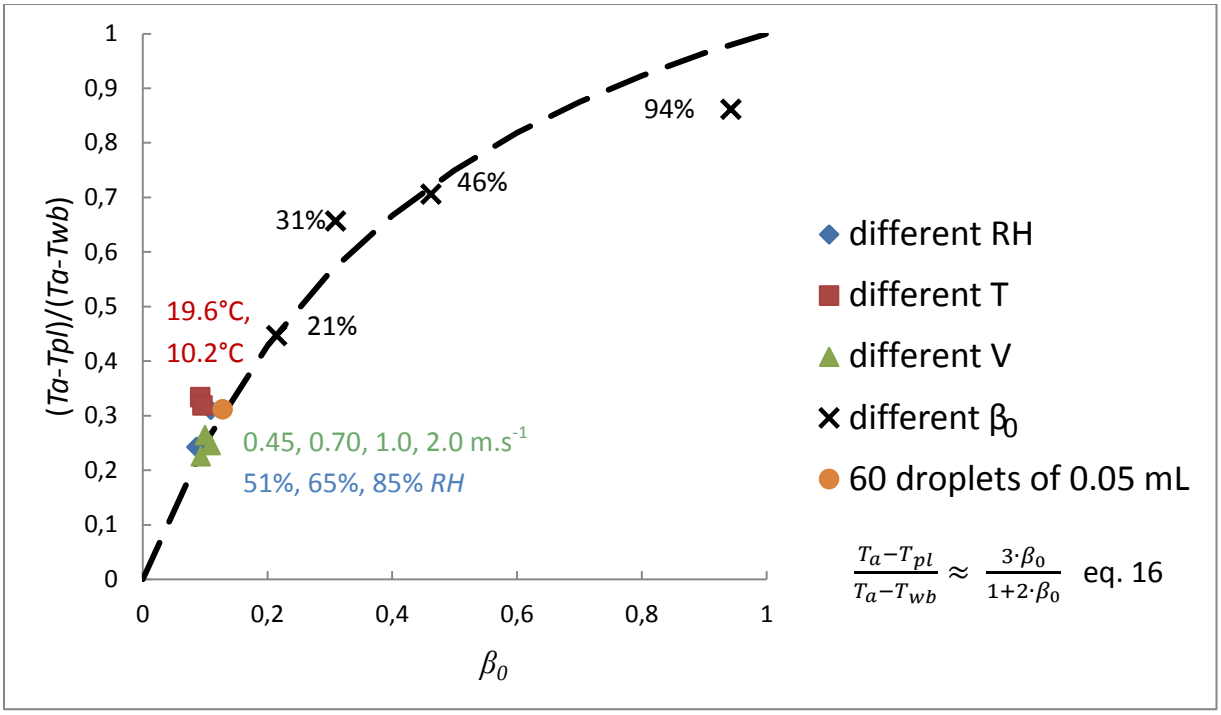

The average values during the first period (constant evaporation rate), when the wet surface and the plate temperature were constant, were used in this figure. It can be observed that this relation is not linear. When β_0 is low, the plate temperature is close to the air temperature. When β_0 is high, the plate temperature tends toward the wet-bulb temperature. The relationship seems almost independent of the velocity, the *RH*, the temperature of air and the droplet size (points overlap). The following correlation can be proposed:

$$\frac{T_a - T_{pl}}{T_a - T_{wb}} = f(\beta_0) \approx \frac{3 \cdot \beta_0}{1 + 2 \cdot \beta_0} \qquad (16)$$

When the plate is recovered by a film of water (β_0=94%), the experimental result does not exactly fit this function, but this may be explained by the radiation effect when water covers the whole plate, as discussed in section 3.7. This radiative exchange induces a lower temperature difference between the air and the plate (higher plate temperature).

Figure 15 shows the evolution of the percentage of wet surface (β) as a function of the mass of water, which evolves with time (for different β_0). It can be observed that when the mass of water reaches approximately 25% of the initial value, the wet surface starts to decrease, as well as the evaporation rate.

Figure 15: Evolution of the percentage of wetted surface with the mass of water over its initial value

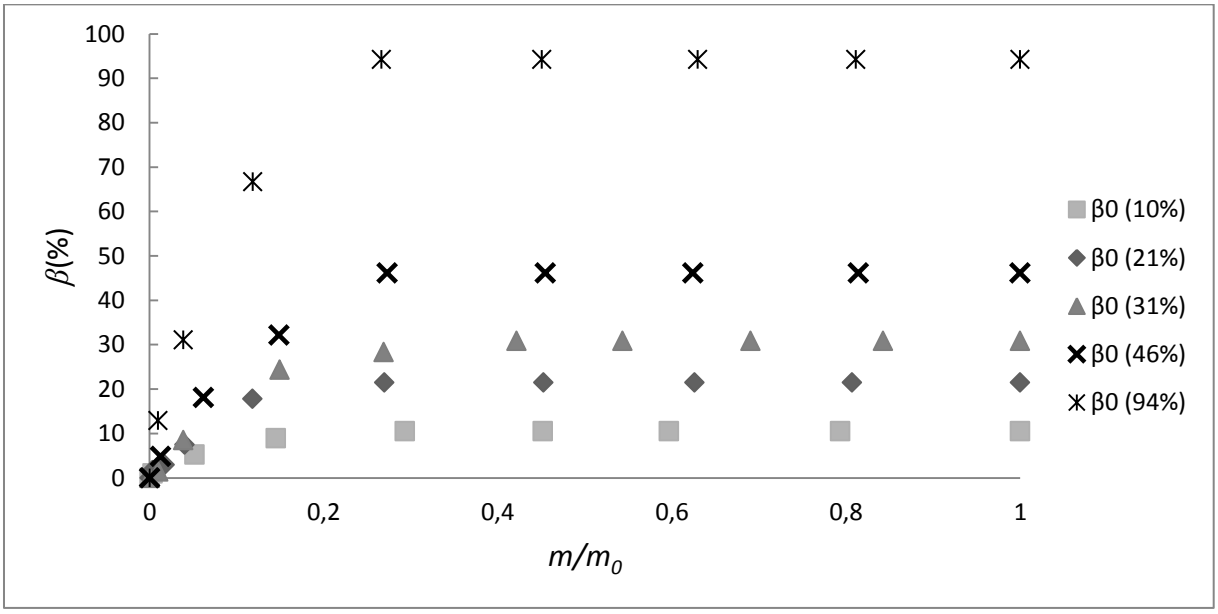

From these experiments, an equation of the evaporation rate in the first period could be proposed. This equation involves the difference between air and wet bulb temperatures (T_a-T_{wb}), the initial wet surface ratio (β_0) and the heat transfer coefficient (h):

$$\dot{m} = \frac{S \cdot (T_a - T_{pl}) \cdot h(v)}{\Delta H_v} = \frac{S \cdot f(\beta_0) \cdot (T_a - T_{wb}) \cdot h(v)}{\Delta H_v} \quad (17)$$

where $f(\beta_0)$ can be obtained from eq. 16 and $h(v)$ from eq. 10.

4. Conclusions

4.1. General conclusion

An experimental methodology was developed to characterize the evaporation rate of water deposited onto a stainless steel plate exposed to different ambient conditions (i.e., air velocity, temperature and relative humidity). Experiments were carried out in a wind tunnel, during which measurements of plate temperature, wet surface area and evaporation rate were performed. The results showed that the relative humidity is the factor that most influences the evaporation rate. The evaporation rate, which was constant during the first period, varied linearly with the difference between air and plate temperatures and with the square root of the air velocity. Additionally, it was shown that the air-plate temperature difference was proportional to the air and wet bulb temperature difference and depended on the percentage of wet surface. The empirical approach (eq. 17) can be used as long as the plate conductivity is considered as infinite. In the case where this hypothesis cannot be made, the finite element method developed with Comsol in this study can gives a good estimation of the evaporation rate even though the model was simplified. The development of another model taking into account the geometrical change of the droplet during evaporation (spherical cap and wet surface decrease) and radiation is in progress. It will allow better prediction of the evaporation rate during the entire droplet evaporation. This model will be used to study the influence of the surface nature (stainless steel and PVC for example) and the droplet thermo-physical proprieties (pure water and syrup) on the evaporation rate.

4.2. Application

Inside a chilled food production plant, the ambient conditions are in the range of this study (room temperature of approximately 5°C, relative humidity of 70%-90% and air velocity from 0.1 to 2.0 $m.s^{-1}$, personal measurement in a food factory). It was shown that by reducing the relative humidity from 85% to 51%, the time to evaporate the same amount of water was reduced by a factor of 2.8. When the air velocity was increased from 0.45 to 1.0 $m.s^{-1}$, the time to evaporate the same amount of water was reduced by a factor of 1.8. These results can be applied to limit the presence of water in food production plants, given that dry surfaces (floor, wall and equipment) are less favourable to bacterial growth. The developed model could help to forecast if only dehumidification is enough to dry surfaces inside a room or if complementary devices for heating and ventilation inside the food plants are necessary.

Moreover, this study could be applied in other domains, e.g., the thermal calculation of buildings, considering the heat loss from evaporation after a rainy period, or fire safety, where the knowledge of the evaporation rate in the flame zone as a function of the droplet parameters is crucial.

ACKNOWLEDGEMENT

The research leading to this result has received funding from the French National Research Agency (EcoSec Project, ANR-12-ALID-0005-04)

REFERENCES

[1] D'agaro P., Croce G., Cortella G. 2006. Numerical simulation of glass doors fogging and defogging in refrigerated display cabinets. *Applied Thermal Engineering* 26: 1927–34

[2] Marzo M. d., Tinker S. 1996. Evaporative cooling due to a sparse spray. *Fire Safety Journal* 27: 289-303

[3] Tartarini P., Corticelli M. A., Tarozzi L. 2007. Dropwise cooling: Experimental tests by infrared thermography and numerical simulations. *Applied Thermal Engineering* 29: 1391-97

[4] Boulet P., Tissot J., Trinquet F., Fournaison L. 2013. Enhancement of heat exchanges on a condenser using an air flow containing water droplets. *Applied Thermal Engineering* 50: 1164-73

[5] Montazeri H., Bert B., Hensen J. L. M. 2015. CFD analysis of the impact of physical parameters on evaporative cooling by a mist spray system. *Applied Thermal Engineering* 75: 608-22

[6] Allais I., Alvarez G. 2001. Analysis of heat transfer during mist chilling of a packed bed of spheres simulating foodstuffs. *Journal of Food Engineering* 49: 37-47

[7] Allais I., Letang G. 2009. Influence of mist-chilling on post-harvest quality of fresh strawberries Cv. Mara des Bois and Gariguette. *International Journal of Refrigeration* 32: 1495 – 504

[8] Delele M. A., Schenk A., Ramon H., Nicolaï B. M., Verboven P. 2009. Evaluation of a chicory root cold store humidification system using computational fluid dynamics. *Journal of Food Engineering* 94: 110-21

[9] Hung D. V., Tong S., Tanaka F., Yasunaga E., Hamanaka D., Hiruma N., Uchino T. 2011. Controlling the weight loss of fresh produce during postharvest storage under a nanosize mist environment. *Journal of Food Engineering* 106: 325-30

[10] Hu Z., Sun D.-W. 2000. CFD simulation of heat and moisture transfer for predicting cooling rate and weight loss of cooked ham during air-blast chilling process. *Journal of Food Engineering* 46: 189-97

[11] Sun D. W., Hu Z. 2003. CFD simulation of coupled heat and mass transfer through porous foods during vacuum cooling process. *International Journal of Refrigeration* 26: 19 –27

[12] Simal S., Femenia A., Llull P., Rossello C. 2000. Dehydration of aloe vera: simulation of drying curves and evaluation of functional properties. *Journal of Food Engineering* 43: 109–14

[13] Teodosiu R. 2013. Integrated moisture (including condensation) - energy-airflow model within enclosures: Experimental validation. *Building and Environment* 61: 197-209

[14] Buchanan R., Lindqvist R., Ross T., Smith M., Todd E., Whiting R. 2004. Risk assessment of Listeria monocytogenes in ready-to-eat foods. *Food and Agriculture Organisation of the United Nations* Microbiological Risk Assessment Series, 4

[15] Carpentier B., Cerf O. 2011. Review — Persistence of Listeria monocytogenes in food industry equipment and premises. *International Journal of Food Microbiology* 145: 1-8

[16] Cox L. J., Kleiss T., Cordier J. L., Cordellana C., Konkel, C. P. P., Beumet R., Siebenga A. 1989. Listeria spp. in food processing, non-food and domestic environments. *Food Microbiology* 6: 49-61

[17]Evans J. A., Russell S. L., James C., Corry J. E. L. 2004. Microbial contamination of food refrigeration equipment. *Journal of Food Engineering* 62: 225–32

[18] Maa J. R. 1967. Evaporation coefficient of liquids. *Industrial Engineering Chemical Fundamentals* 6: 504-18

[19] Mozurkewich M. 1986. Aerosol growth and the condensation coefficient for water: a review. *Aerosol Science and Technology* 5: 223-36

[20] Navaz H. K., Chan E., Markicevic B. 2008. Convective evaporation model of sessile droplets in a turbulent flow—comparison with wind tunnel data. *International Journal of Thermal Sciences* 47: 963-71

[21] Raimundo A., Gaspar A., Oliveira A. V. M., Quintela D. 2014. Wind tunnel measurements and numerical simulations of water evaporation in forced convection airflow. *International Journal of Thermal Sciences* 86: 28-40

[22] Vik T., Reif B. A. P. 2011. Modeling the evaporation from a thin liquid surface beneath a turbulent boundary layer. *International Journal of Thermal Sciences* 50: 2311–17

[23] Rymkiewicz J., Zapalowicz Z. 1993. Analysis of the evaporation process for water droplet on flat heated surface. *Int. Commun. Heat Mass Transfer* 20: 687–97

[24] Birdi K. S., Vu D. T., Winter A. 1989. A study of the evaporation rates of small water drops placed on a solid surface. *J. Phys. Chem.* 93: 3702–03

[25] Chandra S., Marzo M. d., Qiao Y. M., Tartarini P. 1996. Effect of liquid-solid contact angle on droplet evaporation. *Fire Safety Journal* 27: 141-58

[26] Beysens D. 1995. The formation of dew. *Atmos. Res.* 39

[27] Croce G., D'agaro P., Mora F. D. 2005. Numerical simulation of glass fogging and defogging. *International Journal of Computational Fluid Dynamics* 19: 437-45

[28] Hsu C. C., Su T. W., Wu C. H., Kuo L. S., Chen P. H. 2015. Influence of surface temperature and wettability on droplet evaporation. *Applied Physics Letters* 106

[29] Bimbenet J.-J., Duquenoy A., Trystram G. 2002. Génie des procédés alimentaires : Des bases aux applications.

[30] Incropera F. P., DeWitt D. P. 1990. Fundamentals of Heat and Mass Transfer. *John Wiley & Sons, 3rd ed.*

3.2. Article 3 : Droplet evaporation on a solid surface exposed to forced convection: experiments, simulation and dimensional analysis (En préparation)

Droplet evaporation on a solid surface exposed to forced convection: experiments, simulation and dimensional analysis

Christophe Doursat[1*], Logan Lecoq[1,2], Onrawee Laguerre[2], Denis Flick[1]

[1]UMR Ingénierie Procédés Aliments, AgroParisTech, Inra, Université Paris-Saclay, F-91300 Massy, France

[2]Irstea, UR GPAN, 1 rue Pierre-Gilles de Gennes, 92761 Antony, France

Abstract

Experiments were carried out to study the evolution of mass and wetted surface during evaporation of pure water droplets on stainless steel and PVC plates exposed to force air convection. The developed numerical model takes into account the coupled heat and mass transfer phenomena and the change of droplet geometry for both pinning and receding periods. The comparison between experimental results and simulation shows a good agreement. The model is able to reproduce the influence of the plate properties of the plate and of relative humidity. A dimensional analysis was performed and dimensionless charts were developed to predict the drying time for water droplets on stainless steel in a large range of operating conditions.

Keywords:

droplet, evaporation, water, model, dimensional analysis.

Highlight:

- The model takes into account droplet geometry changes during pinning and unpinning periods, coupled heat transfer (conduction, convection, radiation) and mass transfer.
- Good agreement with experiments with stainless steel and PVC plates
- Charts based on dimensional analysis allow estimating drying time in various conditions.

*Corresponding author: E-mail: christophe.doursat@agroparistech.fr

Nomenclature

A	Surface (m^2)
c	Water vapor concentration in air (kg water. m^{-3})
C	Heat capacity ($J.kg^{-1}.K^{-1}$)
e	Thickness (m)
h	Convective heat transfer coefficient ($W.m^{-2}.K^{-1}$)
h_m	Convective mass transfer coefficient ($m.s^{-1}$)
H	Height (m)
m	Mass (kg)
L	Latent heat of water evaporation (J/kg)
r	Radius (m)
t	Time (s)
T	Temperature (K)
V	Volume (m^3)

Greek symbol

ε	Emissivity (dimensionless)
α	Contact angle (°)
ρ	Density ($kg.m^{-3}$)
β	Fraction of wet surface (dimensionless)
σ	Stefan-Boltzmann constant ($W.m^{-2}.K^{-4}$)
λ	Heat conductivity ($W.m^{-1}.K^{-1}$)
φ	Evaporation flux ($kg.m^{-2}.s^{-1}$)

Subscript

a	air
evap	evaporation
d	droplet or drying
p	plate
sat	saturation
w	water
wb	wet bulb
v	vapor
r	receding angle
rad	radiation
0	Initial

Dimensionless numbers

Bi	Biot number
St	Stefan number
E_v	Evaporation number
Le	Lewis number

1. Introduction

The evaporation of water droplets is involved in many applications. For fire extinction, efficient cooling of solid surfaces can be performed because of the evaporation of water droplets [1, 2] which enhance the heat exchanges [3, 4]. The use of fogging during fruit and vegetable sale allows maintaining of product freshness because of less product dehydration [5, 6, 7, 8]. In supermarket, condensation and evaporation on the glass door of a closed display cabinet are often observed because of humidity entrance during door opening [9]. In food factories, after production, cleaning by water leads to the presence of water droplets on equipment (mostly made of stainless steel) which is favorable for bacterial growth such as *Listeria Monocytogenes,* a serious food borne pathogen [10, 11]. Therefore, it is important to dry rapidly the equipment to achieve the microbial destruction by hydric stress (desiccation induces damages to biological cells). In all these situations, the phenomena involved during the evaporation of liquid droplets deposited on a solid surface have to be well-understood.

The main objective of this work was to study phenomena such as the droplet geometry change and evaporation rate evolution occurring during evaporation of a pure water droplet on a solid plate submitted to force air convection. Modeling of these phenomena was carried out and compared with experimental results in the case of a stainless steel plate for different relative humidity and for a PVC plate. Then, the influence of different parameters was studied numerically and by dimensional analysis. This allowed establishing charts giving the drying time for various conditions.

2. Literature review

When a liquid is carefully placed on a surface of a given solid, it remains as a drop with the formation of a contact angle between the liquid and solid phases. The magnitude of the contact angle depends on the physical characteristics of both the liquid and the solid phases [12, 13]. For a given drop volume, a higher value of the contact angle produces a thicker drop with a smaller base radius. The contact angle plays, therefore, an important role in the rate of evaporation of the drop. According to many authors [e.g. 14, 15], the evaporation of a droplet may be distinguished into 2 periods. During the first period, called pinning stage, the base area of the droplet is constant while the contact angle decreases until the receding value is reached, the evaporation rate is almost constant. During the second period, called unpinning stage, the contact angle is constant while the wet area decreases, the evaporation rate decreases. Therefore, the change in the evaporation rate when the water surface varies has to be considered.

Evaporation is endothermic; thus, the evaporation rate is influenced by the heat transfer in the liquid phase and at the liquid/vapor interface [16, 17]. The heat transfer during evaporation is mainly driven by the temperature gradient, while the mass transfer, by the concentration gradient of water vapor in surrounding air. In the case of forced convection, air velocity and turbulence also influence the evaporation process [18, 19, 20]. Navaz et al (2008) [18] proposed a semi-empirical model were the parameters were identified for evaporation of HD (mustard) droplets; conduction in the solid was not taken into account. These studies showed the influence of the neighboring environment on evaporation.

The initial deposition of the droplets on the solid surface is a parameter that has an impact on the evaporation rate. This deposition depends on several parameters such as the droplet size and the droplet impact velocity during water pulverization [21]. Hsu et al. (2015) [22] investigated experimentally water droplets on hydrophilic, hydrophobic and mixed wettability

surfaces. The measurement of the contact angle and volume evolution was undertaken over the evaporation time. The results revealed that surface wettability plays a critical role on evaporation rate.

Most available models focus on the initial pinning stage [23], several considers only water vapor diffusion in stagnant air [e.g. 24], some include conjugated heat transfer [e.g. 25] and free convection [e.g. 26]. The model developed in the present study applies for forced convection and includes coupled heat/mass transfer for both periods (pinned and unpinned).

3. Experiments

Experiments were carried out in a wind tunnel, in which velocity, temperature and relative humidity of the air were controlled. In the work zone of this wind tunnel, a stainless steel or PVC plate wetted by water was exposed to several air conditions. The water mass and the wet surface evolutions were examined.

The wind tunnel (length x height x width = 64cm x 19cm x 19cm, Fig. 1) was made of PVC, except the upper wall made of Plexiglas. This device is located in a controlled temperature and relative humidity test room. In the work zone, a stainless steel plate (15cm x 15cm x 0.1cm) or PVC plate (15 cm x 15 cm x 0.2 cm) was placed on a balance. Underneath this plate, extruded polystyrene (4cm thickness) is used as thermal insulation. In this way, the results interpretation is facilitated because the exchange with air is undertaken only between the upper surface of the plate and the air.

The stainless steel or PVC plate was wetted by water using a pipette. Thirty water droplets of 0.1mL were uniformly deposited on the plate. The plate was exposed to an air flow 1 m/s at 4.1°C with variable relative humidity (51% to 85%). During the experiments, the air and plate temperatures, the air velocity, the relative humidity in the work zone, the water weight and the wet surface on the plate were measured.

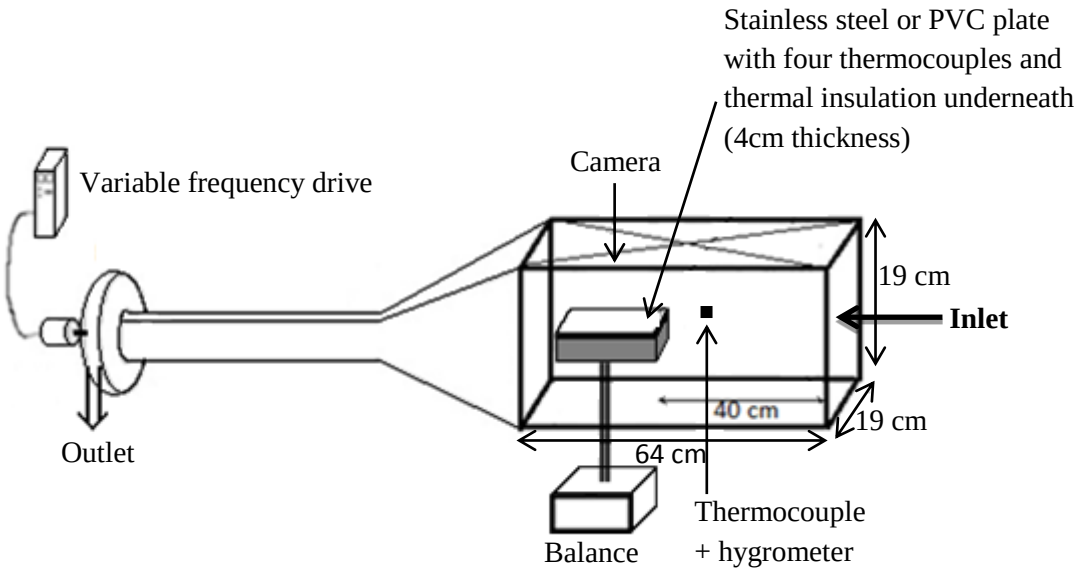

Fig. 1. schematic representation of the experimental setup

The water weight on the plate was recorded every 5 seconds using an electronic balance (Sartorius, 3410028, ±0.001 g precision) connected to a data-logger (Agilent 34970A). Measurement was carried out until all the water was evaporated.

The air temperature inside the wind tunnel and the plate temperature during the evaporation were measured using calibrated T-type thermocouples (1 mm diameter, ± 0.1°C precision). One thermocouple was put in the wind tunnel to measure the air temperature and 4 thermocouples were put underneath the plate (between the stainless steel or PVC plate and the polystyrene).

The air relative humidity was measured using a capacitive humidity sensor TESTO 174H (± 3% precision).

The air velocity was measured one centimetre before the plate at 25 positions in this cross-section and the average velocity was calculated. At each point, the velocity was taken every second during 2 min using a hot wire anemometer (TESTO 435-4, ± 0.03 $m.s^{-1}$ precision). To stabilize, as much as possible, the air inside the wind tunnel, ventilation was operated in aspiration mode. Moreover, a honeycomb (tubes of 3 mm in diameter) was placed at the cross-section of the inlet.

To monitor the evolution of the wet surface on the plate during the evaporation, images were taken using a high definition camera (KAPPA DXP 1154) and a zoom (Navitar TenX) located outside the wind tunnel and just above the plate (Fig. 1). The time interval between 2 images was 5 min. Image treatment, using the open source software ImageJ, allowed for the determination of the wet surface. The results were reported in terms of percentage of wet surface over the total plate surface: β.

Additionally, the heat exchanges between the plate and air in the wind tunnel was measured by a fluxmeter equipped with a thermocouple (Trade name Captec, width x height x depth: 4 cm x 4 cm x 450 µm, Fig. 3). This fluxmeter placed at the middle of the plate was supplied by 10 W of heating power. The fluxmeter temperature, the air temperature (measured at 5 cm from the surface of the fluxmeter) and the measured flux were recorded every second until a steady state was obtained. Then, the mean values were calculated over 30 min of a stabilization period allowing the estimation of the heat transfer coefficient. It is to be noticed that the emissivity of this fluxmeter is close to zero; thus, the radiative exchange can be neglected. The estimated value for an air velocity of 1 m/s was 22.7 (+/- 0.4) $W.m^{-2}.K^{-1}$.

Once the air temperature and relative humidity were stabilized at the desired values inside the wind tunnel, the plate with the droplets was placed on the balance and the data were recorded.

Table 1: Summary of the experimental conditions.

Plate material	Air temperature* (°C)	Air relative humidity* (%)	Air velocity ($m.s^{-1}$) Heat transfer coefficient ($W.m^{-2}.K^{-1}$)	β_0 (%)
Stainless steel	4.1 (± 0.1)	51 (± 3) 3 repetitions	1.0 (±0.03) 22.7 (±0.4)	~10 (30 droplets of 0.1 mL)
		65 (± 3)		
		85(± 3)		
PVC plate	4.1 (± 0.1)	51 (± 3)	1.0 (±0.03) 22.7 (±0.4) 2 repetitions	~8 (30 droplets of 0.1 mL)

* average value during the drying time.

4. Model

The aim of the model development is to predict the evolution of the mass of water droplets deposited on a plate (insulated at the bottom) exposed to forced airflow.

4.1. Main assumptions

The initial fraction of the surface of the plate in contact with droplets (β_0) and the initial base radius (radius of the interface of one droplet with the plate : r_0) are assumed to be known, as well as the air temperature (T_a) and relative humidity (RH). All the droplets on the surface are considered to dry approximately in the same conditions. So only, one droplet and the corresponding part of the plate are considered.

The droplet is assumed to have a spherical cup shape all along the drying. During a first period (pinning stage), the contact surface with the plate remains constant whereas the contact angle: α (at the solid/liquid/gas angle meeting point) varies. Then, when this angle reaches the receding angle value: α_r, the angle remains constant whereas the contact surface with the plate decreases.

Heat in transferred inside the water and inside the plate only by conduction. Free convection is neglected inside the droplet. Heat is transferred from air to the surface of the dry zone of the plate by convection, with a given uniform heat transfer coefficient (h). Heat is also transferred by convection at the interface between water and air. The heat transfer coefficient at this interface (h_d) is higher than the one on the dry part of the plate (h). To ovoid too much complexity, h_d is assumed to be uniform (in reality it is higher on the upwind face but the conduction in the water droplet is damping this effect). This allows considering axisymetric geometry (Fig. 2). Radiation is assumed to occur between the dry part of the plate (emissivity ε_p) or the surface of the droplet (emissivity ε_w close to unity) and a black body at temperature T_{rad}.

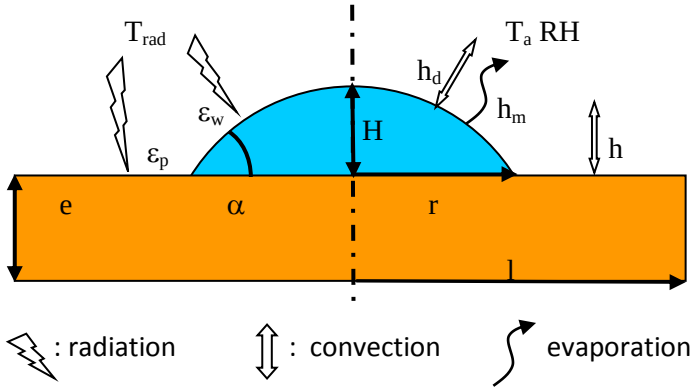

Fig. 2. Schematic view of one droplet and of the corresponding plate

Water evaporates from the droplet/air interface with a mass transfer coefficient (h_m) which can be deduced from the heat transfer coefficient by the Lewis analogy. The volume of the droplet decreases according to the evaporation leading to a moving boundary condition.

4.2. Governing equations

The unsteady conduction equation (inside the water and inside the plate) is:

$$\rho C \frac{\partial T}{\partial t} = \vec{\nabla}.\left(\lambda \vec{\nabla} T\right) \quad (1)$$

At the water/air interface :

$$\varphi_{evap} = h_m (c_{sat(T)} - RH.c_{sat(Ta)}) \quad (2)$$

and

$$-\lambda_w \vec{\nabla} T.\vec{n} + h_d (T_a - T) + \varepsilon_w \sigma (T_{rad}^4 - T^4) = \varphi_{evap} L \quad (3)$$

where $c_{sat(T)}$ is the saturated water vapor concentration in air at temperature T, and L is the latent heat of water vaporization

The droplet volume varies according to following equation:

$$\frac{dV}{dt} = -\iint_{water/air} \frac{\varphi_{evap}}{\rho_w} dS \quad (4)$$

At the plate/air interface:

$$-\lambda_{pl} \vec{\nabla} T.\vec{n} + h(T_a - T) + \varepsilon_p \sigma (T_{rad}^4 - T^4) = 0 \quad (5)$$

At the bottom of the plate and at its lateral edge:

$$\vec{\nabla} T.\vec{n} = 0 \quad (6)$$

Geometrical equations also determine the radius (r) and the height (H) of the droplet knowing its volume.

While $\alpha>\alpha_r$ (pinning period) :

$$r=r_0 \text{ and } H=\left(\frac{3V}{\pi}+\left(r_0^{\,6}+\left(\frac{3V}{\pi}\right)^2\right)^{\frac{1}{2}}\right)^{\frac{1}{3}}+\left(\frac{3V}{\pi}-\left(r_0^{\,6}+\left(\frac{3V}{\pi}\right)^2\right)^{\frac{1}{2}}\right)^{\frac{1}{3}} \quad (7)$$

When the receding angle is reached

$$H_{lim}=r_0\frac{1-\cos(\alpha_r)}{\sin(\alpha_r)} \text{ and } V_{lim}=\frac{\pi H_{lim}}{6}\left(H_{lim}^2+3r_0^{\,2}\right) \quad (8)$$

Then $\alpha=\alpha_r$ (unpinning period) and the geometry remains homothetic:

$$r=r_0\left(\frac{V}{V_{lim}}\right)^{\frac{1}{3}} \text{ and } H=H_{lim}\left(\frac{V}{V_{lim}}\right)^{\frac{1}{3}} \quad (9)$$

These partial derivative equations were solved with the finite element method using the Comsol software (version 5.2). After a mesh sensitivity analysis, a mesh of 2400 elements was chosen. The geometry and mesh were continuously adapted using the 'deformed mesh' method.

4.3. Estimation of the heat transfer coefficient on the droplet/air interface

In order to estimate the ratio of heat transfer coefficient on the droplet/air interface and on the plate/air interface: h_d/h, a complementary simulation was carried out with a fixed geometry and without evaporation.

A plate with 6 deposited droplets was considered in terms of air flow (laminar flow near the plate) and heat transfer from the droplet and plate surface to air (Fig. 3). All the surface temperatures were set at 1 K higher than the upwind air temperature. Airflow of 1 m/s at 4.1°C was considered.

In this way, the mean heat transfer coefficient on the droplet/air interface and on the plate/air interface could easily be determined by integrating the interfacial heat flux. The value of the so obtained ratio h_d/h was 1.44. This value was later applied in the unsteady coupled heat transfer /evaporation model.

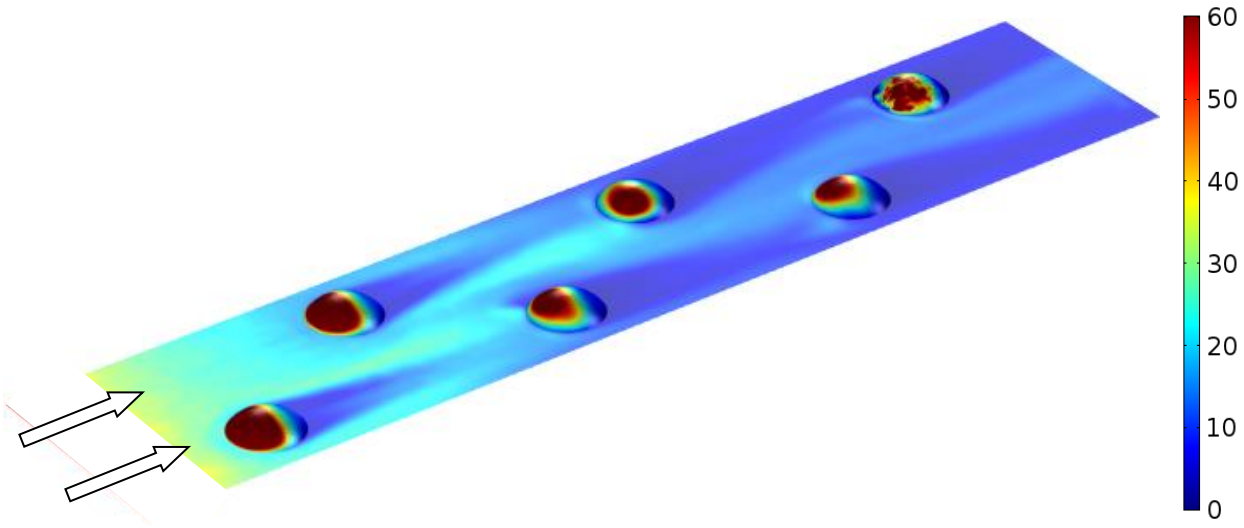

Fig. 3. Heat transfer coefficient ($W.m^{-2}.K^{-1}$) on the air/water and air/plate interfaces

5. Comparison with experimental results

5.1. Reference case (stainless steel plate, RH:51%)

For the stainless steel plate simulation, the initial contact angle (deduced from imposed droplet volume: 0.1mL, and measured initial base radius: 4.8 mm) was 55°. The receding angle was 10° [13]. The properties of water and steel are presented in table 2

Table 2 : Properties of water, stainless steel and PVC plates

	Water	Stainless steel	PVC
Density : ρ	1000 $kg.m^{-3}$	7960 $kg.m^{-3}$	1380 $kg.m^{-3}$
Heat capacity : c	4185 $J.kg^{-1}.K^{-1}$	480 $J.kg^{-1}.K^{-1}$	1046 $J.kg^{-1}.K^{-1}$
Conductivity : λ	0.6 $W.m^{-1}.K^{-1}$	15 $W.m^{-1}.K^{-1}$	0.2 $W.m^{-1}.K^{-1}$
Thickness : e		1 mm	2 mm
Latent heat of vaporization at 4°C	2492 $kJ.kg^{-1}$		
Emissivity	0.95	0.1	0.95

The comparison between the evolutions of the mass of the droplet obtained from the simulation and from the three experimental repetitions shows a good agreement (Fig. 4). During the first period, the evaporation rate is almost constant and 85% of the initial mass evaporates during this period. It takes 120 min to evaporate half of the initial mass. During the second period the evaporation rate decreases continuously up to complete drying. The total

drying time is difficult to identify precisely on this graph because of the small variations at the end of drying.

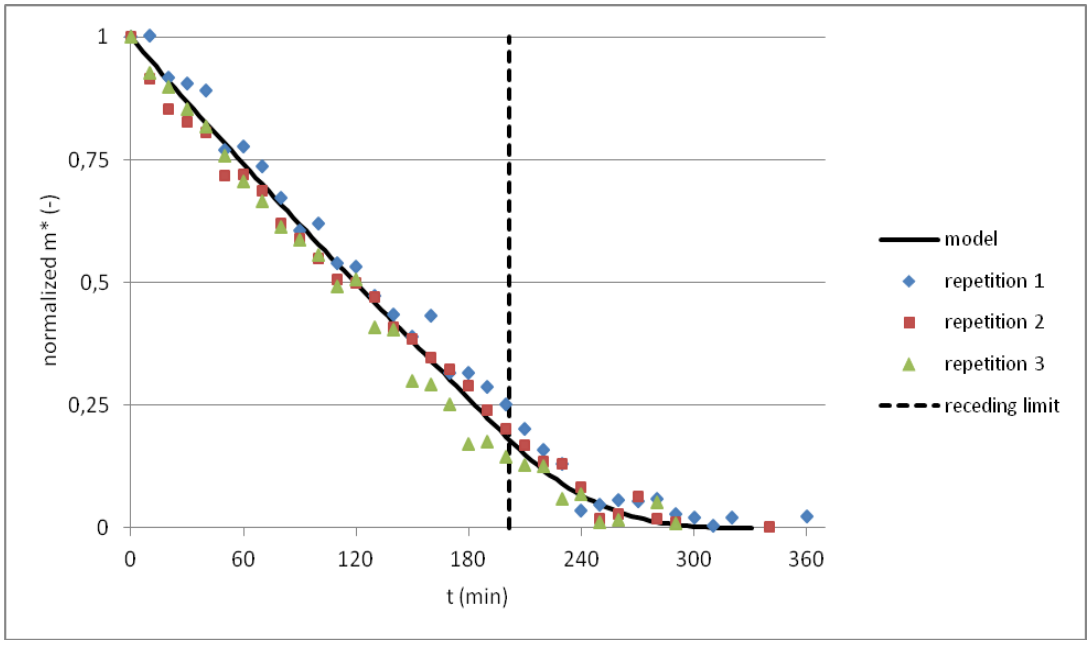

Fig. 4. Droplet mass evolution on stainless steel plate ($m^* = m(t)/m_0$).

The comparison between the measured and predicted evolutions of the base radius (radius of the water/plate interface) shows quite good agreement (Fig. 5). It can be observed that during the second period the radius evolution is almost linear. The total drying time in this reference case is 330 min.

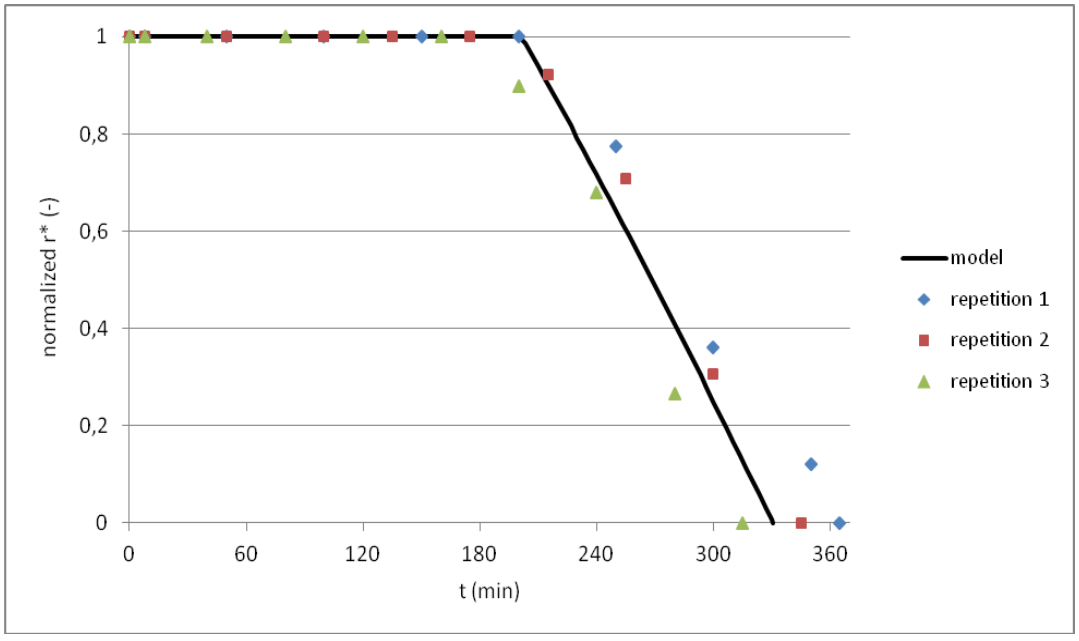

Fig. 5. Base radius evolution on stainless steel plate ($r^*=r(t)/r_0$).

Fig. 6 presents the plate temperature evolution. If the plate was completely covered by water and radiation was negligible, the plate temperature would tend toward the wet bulb temperature: 0.7°C. From simulation and experiments it can be observed that very rapidly, the plate temperature becomes intermediate between the dry and wet bulb temperature. This means that, for thin plate (e=1mm) the thermal inertia is small. During the first period, the plate temperature is almost constant. During the second period it increases and tends toward the dry air temperature.

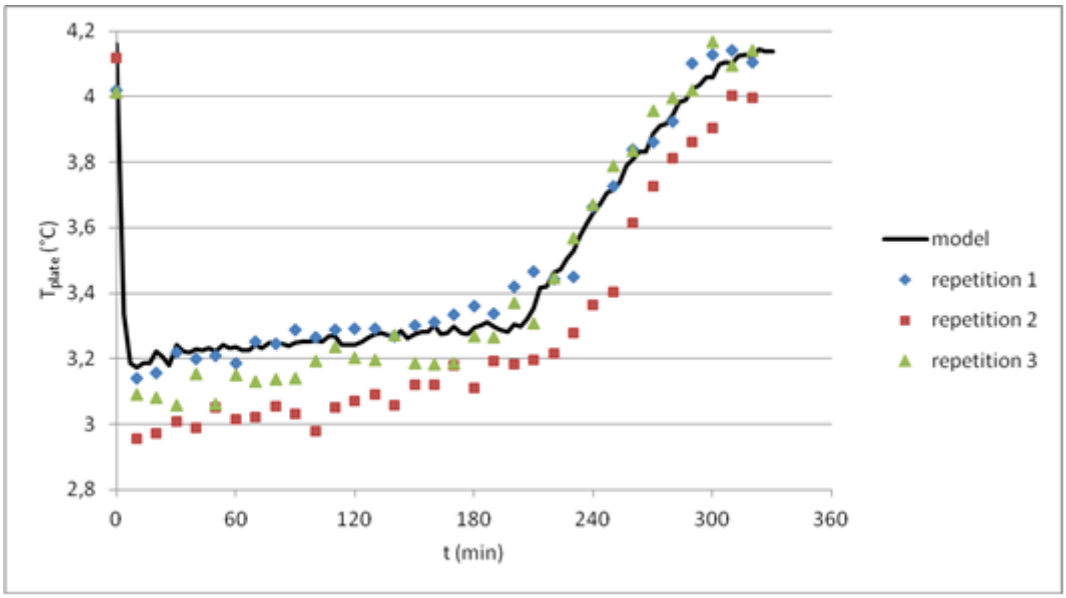

Fig. 6. Stainless steel plate temperature evolution (T_a=4.1°C; T_{wb} = 0.7 °C).

Fig. 7 presents the simulated temperature field at 3 instants: 3min, 200 min (end of the pinning period) and 270 min. It can be observed that, for this good conducting plate material (λ_p=15 $W.m^{-1}.K^{-1}$ for stainless steel), the temperature differences inside the plate or inside the water droplets are small all along the drying compared to the difference between plate and air temperature.

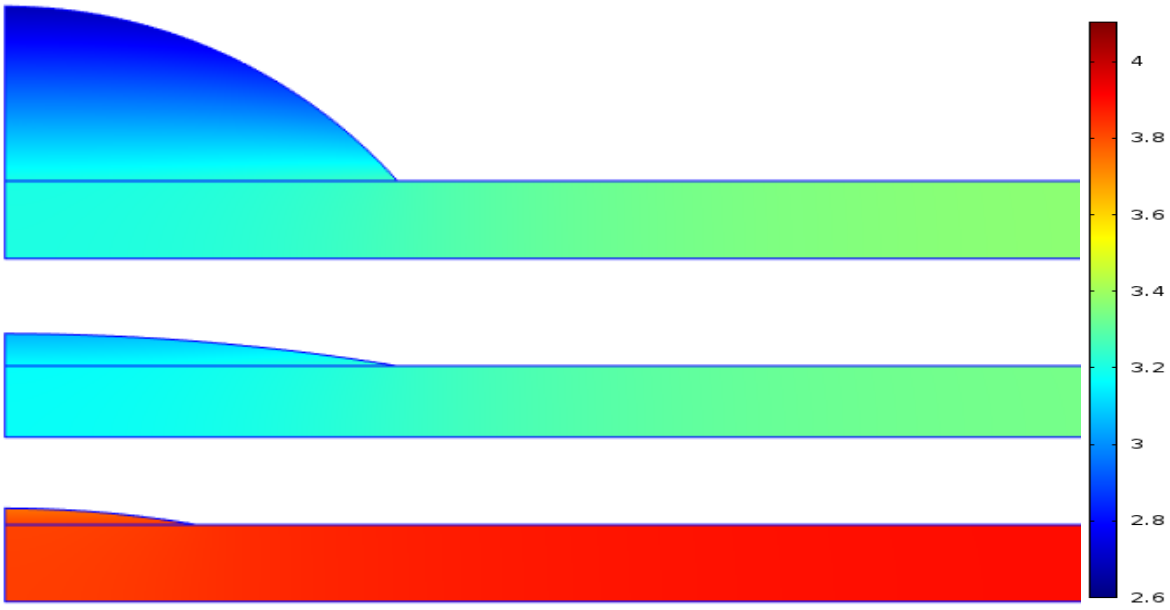

Fig. 7. Temperature field after 3 min, 200 min (end of the pinning period) and 270 min
Stainless steel plate, Air temperature : 4.1 °C (red) , Wet bulb temperature : 0.7 °C.

5.2. Influence of air relative humidity (stainless steel plate)

Fig. 8 presents the influence of relative air humidity on half and total drying time. The half drying time is determined from the mass evolution and the total drying time from the base radius evolution. The model takes correctly into account the influence of relative humidity. For the highest experimental humidity value (RH = 85%) the drying time is almost 3 times higher than in the reference case (RH = 51%)

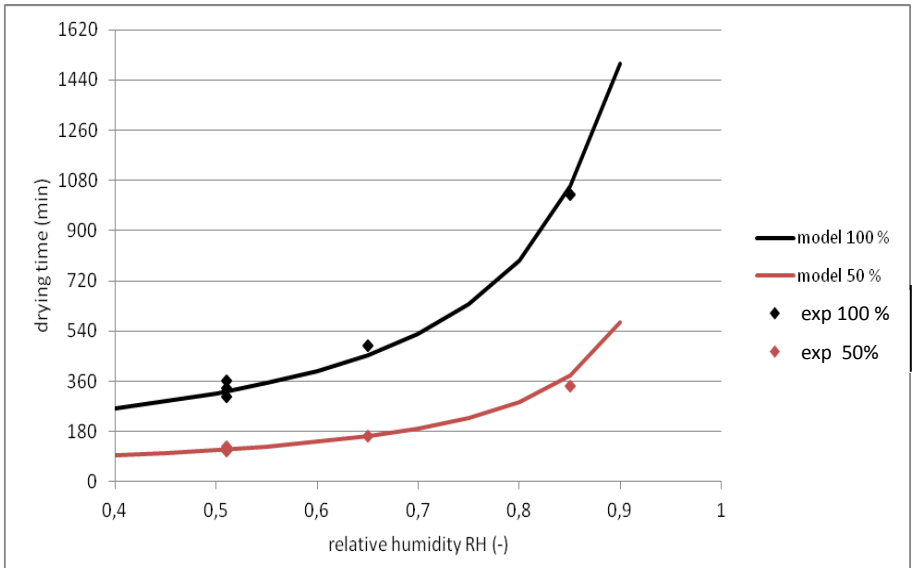

Fig. 8. Influence of relative humidity on drying time of water droplets on stainless steel plate.

5.3. Influence of plate material (PVC plate)

For the PVC plate simulation, the initial contact angle (deduced from imposed droplet volume: 1mL, and measured initial base radius: 4.4 mm) was 67°. The receding angle was estimated of about 30°. The properties of PVC are presented in table 2.

The comparison between the evolutions of the mass of the droplet obtained from the simulation and from the two experimental repetitions shows a good agreement (Fig. 9). The evaporation rate is globally lower than that on stainless steel. This is due firstly to the lower conductivity of PVC (even if the plate thickness is twice) and secondly to the higher contact angles (initial value and receding value) since PVC is rather hydrophobic. This leads to a lower water/air interface area for a given droplet volume on a PVC plate.

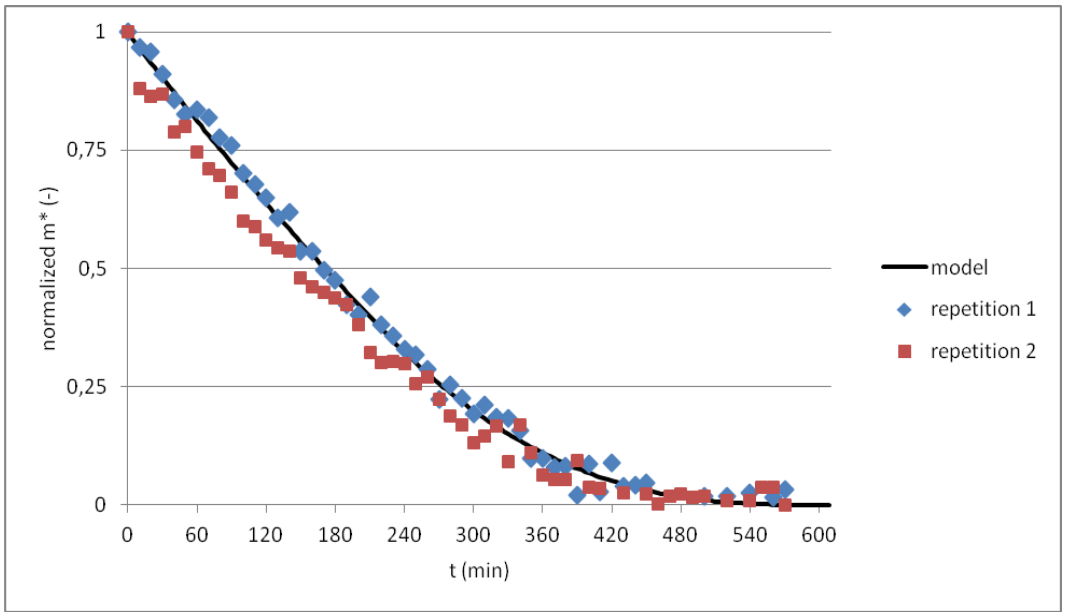

Fig. 9. Droplet mass evolution on PVC plate ($m^* = m(t)/m_0$).

Fig. 10 presents the evolution of the droplet base radius on PVC plate. It can be observed that the experimental values decrease progressively at the beginning while a constant value was observed for the stainless steel plate (Fig. 5). The radius evolution is not as simply as for the steel plate. The assumption of first constant base radius and then constant angle does not strictly apply for PVC plate. In fact wetting during evaporation is complicated phenomenon [Yu and al 2015]. However, the global trend is predicted by the model.

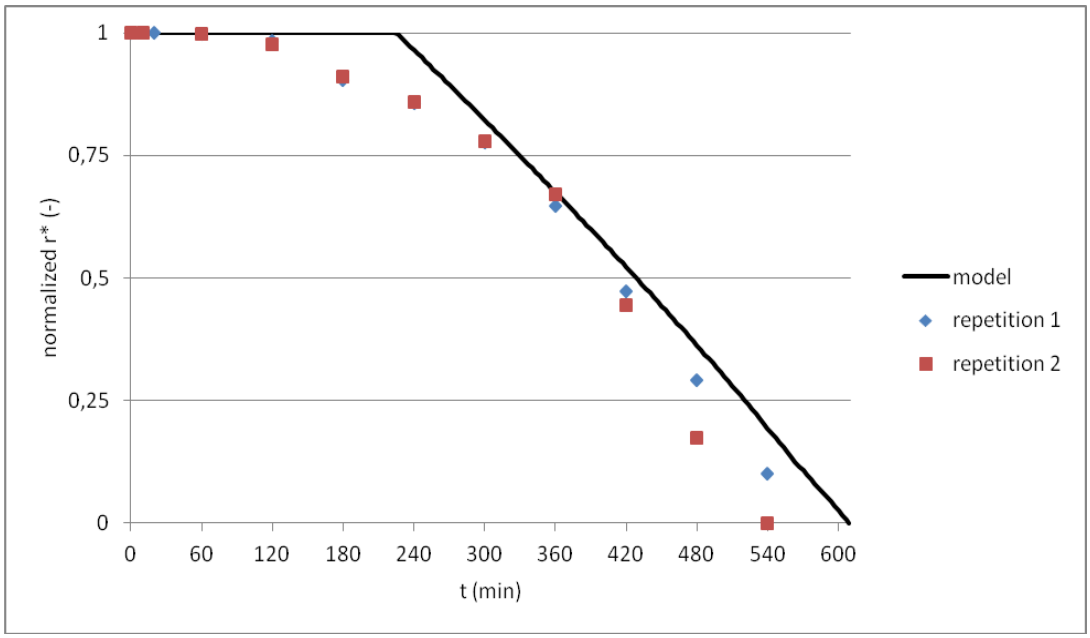

Fig. 10. Droplet base radius evolution on PVC plate ($r^*=r(t)/r_0$).

Fig. 11 presents the temperature field at 3 instants: 7 min, 220 min (end of the pinning period) and 460 min. It can be observed a higher temperature gradient in the PVC plate than that in stainless steel because of the much lower conductivity.

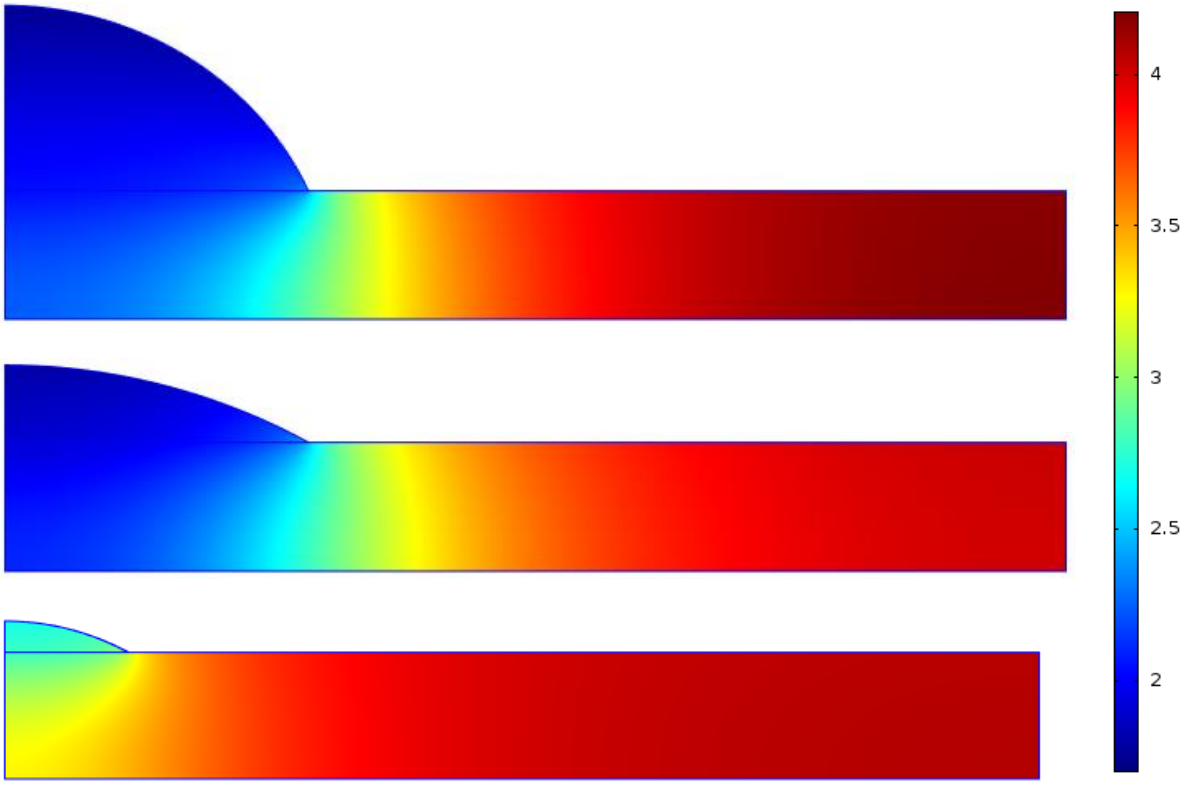

Fig. 11. Temperature field after 7 min, 220 min (end of the pinning period) and 460 min.
PVC plate, Air temperature : 4.1 °C (red) , Wet bulb temperature : 0.7 °C

6. Dimensional analysis

In order to generalize the numerical results obtained in specific cases, a dimensional analysis was carried out. Let us begin the analysis with the case of negligible radiation and with initial water and plate temperatures equal to air temperature. In order to simplify the analysis we also consider a linear approximation of the saturated water vapour concentration in air.

$$c_{sat(T)} \approx c_{sat(Ta)} + \frac{dc_{sat}}{dT}(T - T_{a)} \tag{10}$$

Considering the Lewis analogy, the evaporation flux can then be expressed as follows:

$$\varphi_{evap} = h_m (c_{sat(T)} - HR.c_{sat(Ta)}) = \frac{h_d}{(\rho C_p)_a Le^{2/3}} \frac{dc_{sat}}{dT}(T - T_{dp}) \tag{11}$$

where T_{dp} is the dew point temperature defined by: $c_{sat(Tdp)} = HR.c_{sat(Ta)}$

The heat flux necessary for the evaporation is then:

$$\varphi_{evap} L = E_v h_d (T - T_{dp}) \quad \text{with} \quad E_v = \frac{L}{(\rho C_p)_a Le^{2/3}} \frac{dc_{sat}}{dT} \tag{12}$$

E_v is a dimensionless number, called 'evaporation number', which relates heat and mass transfer.

If a plate entirely covered by water is considered, its temperature tends toward the wet bulb temperature, T_{wb} , which can be defined by following equation :

$$\varphi_{evap} L = \frac{hL}{(\rho C_p)_a Le^{2/3}} (c_{sat(Twb)} - HRc_{sat(Ta)}) = h(T_a - T_{wb})$$

$$\Leftrightarrow \frac{hL}{(\rho C_p)_a Le^{2/3}} \frac{dc_{sat}}{dT}(T_{wb} - T_{dp}) = h(T_a - T_{wb}) \Leftrightarrow \frac{T_a - T_{wb}}{T_{wb} - T_{dp}} = E_v \tag{13}$$

From this preliminary analysis, it can be observed that beside all the thermal aspects, the coupling with evaporation can be taken into account by the evaporation number E_v and a characteristic temperature difference such as (T_a-T_{wb}). In addition, the time forentirely evaporate a single droplet of initial radius r_0 or to evaporate a height r_0 of water recovering entirely a plate is simply related to (T_a-T_{wb}) by following equation:

$$\tau = \frac{(\rho_w L) r_0}{h(T_a - T_{wb})} \text{ or } \tau = \frac{(\rho_w L) H}{h(T_a - T_{wb})} \tag{14}$$

In a more general case, including radiation between the plate (emissivity ε_p) or the droplet (emissivity close to unity) and a wall (emissivity close to unity) at same temperature as the air, the drying time t_d of a droplet is dependent on 15 following parameters

$$t_d = f\{ T_a\text{-}T_{wb}, T_0\text{-}T_a , E_v, \alpha_0 , \alpha_r , \beta_0 , \varepsilon_p , r_0 , e_p , h, \lambda_w , \lambda_p, \rho_w L ,(\rho C)_w , (\rho C)_p \} \tag{15}$$

Three fundamental units are involved (m, s, K); in addition there is no conversion of mechanical energy into heat, so the thermal energy unit (J) can also be considered. Therefore, the dimensionless drying time $t^*=t_d/\tau$ can be expressed in function of 11 dimensionless numbers.

$$t^* = \frac{t_d h(T_a - T_{wb})}{\rho_w L r_0} = f\left\{\alpha_0, \alpha_r, \varepsilon_p, \frac{\lambda_p}{\lambda_w}, \frac{(\rho C)_p}{(\rho C)_w}, \frac{e_p \lambda_p \beta_0}{h.r_0^2}, \beta_0, \frac{hr_0}{\lambda_w}, \frac{C_w(T_a - T_{wb})}{L}, E_v, \frac{T_0 - T_a}{T_a - T_{wb}}\right\} \quad (16)$$

The first five numbers are specific to the material of the plate.

The dimensionless plate thickness $e^*= \frac{e_p \lambda_p \beta_0}{h.r_0^2}$ and the initial wetted surface β_0 are expected to have the largest effect (the half average distance between two droplets is indirectly taken into account because its value is $l = r_0 / \sqrt{\beta_0}$).

The Biot number $\frac{hr_0}{\lambda_w}$ represents the ratio of the heat transfer resistance in the droplet and the convection heat transfer resistance; this ratio is generally small in practice (< 0.3)

The Stefan number $\frac{C_w(T_a - T_{wb})}{L}$ represents the ratio of the sensible heat variation and the latent heat of vaporization, this ratio is always very low (<0.01).

The evaporation number $E_v = \frac{L}{(\rho C_p)_{air} Le^{2/3}} \frac{dc_{sat}}{dT} = \frac{T_a - T_{wb}}{T_{wb} - T_{dp}}$ depends on the range of temperature because dc_{sat}/dT is increasing with T.

The last number : $\frac{T_0 - T_a}{T_a - T_{wb}}$ takes into account the fact that the plate is not always initially at the air temperature; but in the present study only the case where $T_0=T_a$ is considered.

7. Dimensionless results

For engineering applications, it can be interesting to have charts providing for a given plate material, the drying time in function of plate thickness, initial wetted surface, initial droplet radius, heat transfer coefficient, air temperature and humidity. This can be achieved based on the dimensional analysis presented previously.

Fig. 12 presents the drying time, in function of the plate thickness and the initial fraction of wetted surface for a stainless steel plate, both in dimensional and dimensionless forms. This figure was obtained by taking a reference case very close to the experimental one: m_0=0.1g, T_a=4°C, RH=50%, h=20 $W.m^{-2}.K^{-1}$ and by varying the plate thickness from e=0.1 to 10 mm. The results for the reference case (e=1 mm) is indicated by a diamond sign.

The values of the following dimensionless parameters are fixed:

$$\frac{\lambda_p}{\lambda_w} = 25 \quad , \quad \frac{(\rho C)_p}{(\rho C)_w} = 0.91 \quad , \quad \varepsilon_p = 0.1 \; , \quad \alpha_0 = 55° \quad , \quad \alpha_r = 10°$$

$$Bi = \frac{hr_0}{\lambda_w} = 0.16 \qquad St = \frac{C_w (T_a - T_{wb})}{L} = 5.8\ 10^{-3} \qquad E_v = \frac{T_a - T_{wb}}{T_{wb} - T_{dp}} = 0.57$$

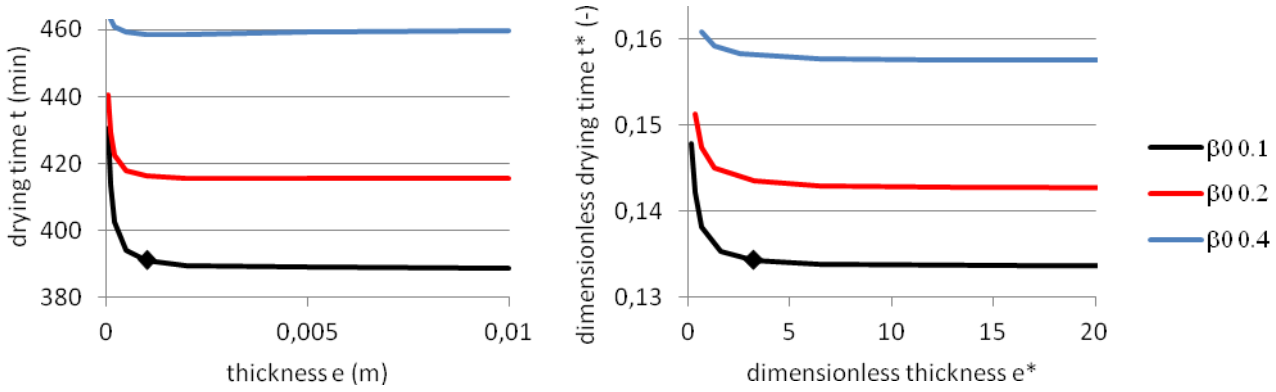

Fig. 12. Drying time versus plate thickness (dimensional /dimensionless)
(Bi=0.16 ,St=5.8 10^{-3}, E_v=0.57)

It can be observed that, whatever β_0, the drying time tends rapidly toward an asymptotic value. For a thin or low conductivity plate, heat conduction inside the plate can be a limiting phenomenon; but for thick or high conductivity plate, the conductive resistance becomes negligible.

The asymptotic value is typically reached when e*>10 and depends on initial wetted surface ratio β_0. The higher β_0, that is the closer are the droplets on the plate, the higher is the drying time. This can be explained by the fact that the plate around the droplet acts like a fin. The larger the area of the plate around a droplet (i.e. the fin) the higher the heat flux provided for the latent heat of evaporation.

Fig. 13, 14 and 15 present, the influence of the Biot, Stefan and evaporation numbers on the asymptotic dimensionless drying time (e*>10).

Fig. 13 was constructed by varying the heat transfer coefficient around the reference value (h=20 W.m^{-2}.K^{-1}, indicated by a diamond sign) from 5 to 40 W.m^{-2}.K^{-1}. The dimensionless drying time is almost independent of the Biot number; this means that drying time is almost inversely proportional to the heat transfer coefficient. The small effect is due to the contribution of radiation.

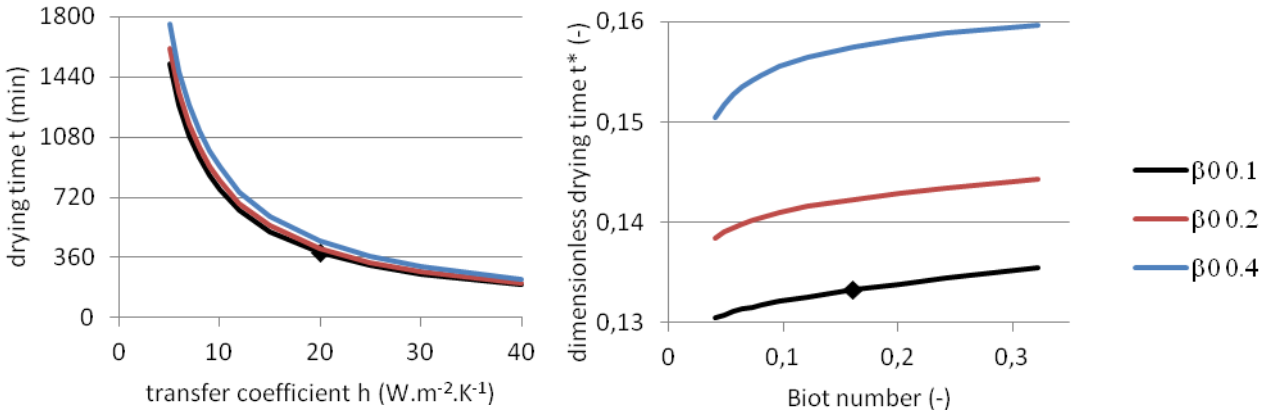

Fig. 13. Influence of heat transfer coefficient/Biot number on drying time (dimensional / dimensionless) (β_0=0.1, St=5.8 10^{-3}, E_v=0.57, e*>10)

Fig. 14 was constructed by varying the relative humidity from 40 to 90% (wet bulb temperature varying from -0.1 to 3.4°C). For Stefan number higher than 0.002 which corresponds to relative humidity lower than 80%; the dimensionless drying time is almost independent of the relative humidity. This means that drying time is almost inversely proportional to (T_a-T_{wb}). For higher relative humidity; the convective heat flux decreases (because droplet/air temperature difference decreases) and radiation cannot be ignored. In fact, for droplet exposed to radiation, the equilibrium temperature is no more the wet bulb value.

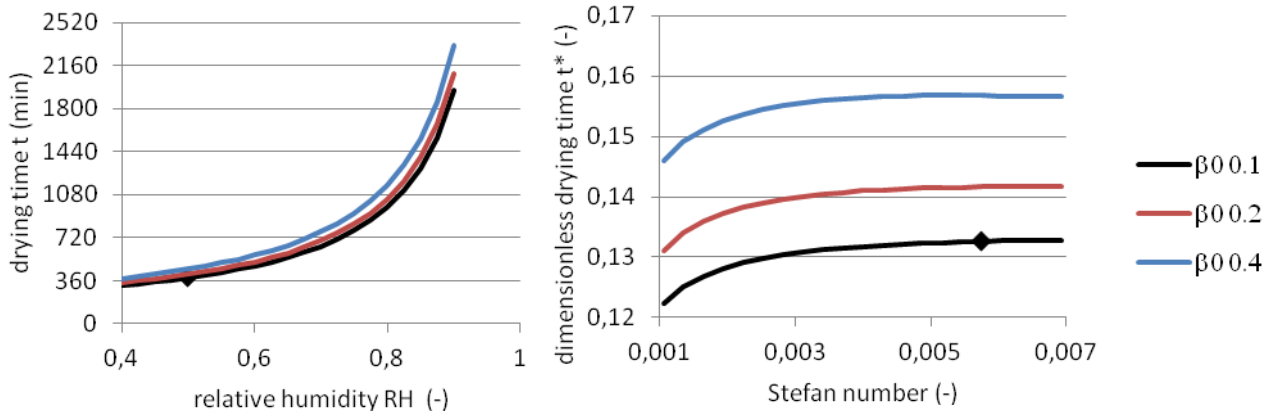

Fig. 14. Influence of relative humidity/Stefan number on drying time (dimensional / dimensionless) (β_0=0.1, Bi=0.16, E_v=0.57, e*>10)

Fig. 15 was constructed by varying the dry air temperature from 4 to 20°C and by maintaining the same difference with wet bulb temperature: (T_a-T_{wb}) = 3.44°C. The dimensionless drying time decreases because of the non-linearity of saturated vapour pressure versus temperature (dP_{sat}/dT increases with T).

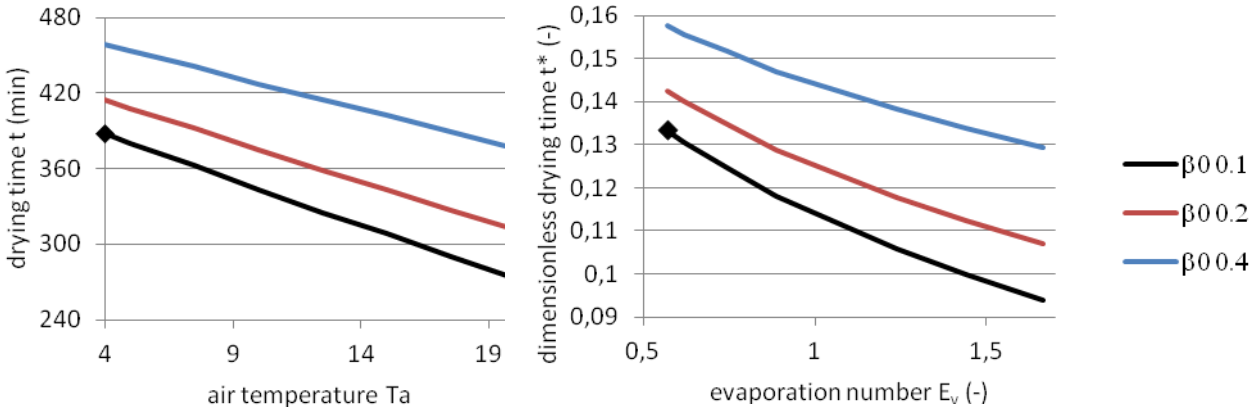

Fig. 15. Influence of air temperature/evaporation number on drying time (dimensional / dimensionless) (β_0=0.1, Bi=0.16 ,St=5.8 10^{-3}, e*>10)

For pratical use, for stainless steel plate, if e*>2, β<0.4, 0.5<E_v<1.5 and St>0.002, which correspond to most of the encountered cases, the dimensionless drying time can be roughly estimated by folowing equation : $t^* \approx 1.65\ \beta_0^{0.17}\ E_v^{-0.26}$. Similar chart could also be obtained for type of material encountered in industrial case like PVC, glass, wood, concrete etc.

8. Conclusion

A model was developed to predict the drying of liquid droplets deposited on a solid plate submitted to forced convection. The model takes into account change of geometry for both pinning and receding periods. Comparison with experiments using stainless steel and PVC plates showed a good agreement. A dimensional analysis was performed and dimensionless charts were developed to predict the drying time for water droplets on stain less steel in a large range of operating conditions.

ACKNOWLEDGEMENT

The research leading to this result has received funding from the French National Research Agency (EcoSec Project, ANR-12-ALID-0005-04).

References

[1] Marzo M. D., Tinker S. 1996. Evaporative cooling due to a sparse spray. *Fire Safety Journal* 27: 289-303.

[2] Tartarini P., Corticelli M. A., Tarozzi L. 2007. Dropwise cooling: Experimental tests by infrared thermography and numerical simulations. *Applied Thermal Engineering* 29: 1391-97.

[3] Boulet P., Tissot J., Trinquet F., Fournaison L. 2013. Enhancement of heat exchanges on a condenser using an air flow containing water droplets. *Applied Thermal Engineering* 50: 1164-73.

[4] Montazeri H., Bert B., Hensen J. L. M. 2015. CFD analysis of the impact of physical parameters on evaporative cooling by a mist spray system. *Applied Thermal Engineering* 75: 608-22.

[5] Allais I., Alvarez G. 2001. Analysis of heat transfer during mist chilling of a packed bed of spheres simulating foodstuffs. *Journal of Food Engineering* 49: 37-47

[6] Allais I., Letang G. 2009. Influence of mist-chilling on post-harvest quality of fresh strawberries Cv. Mara des Bois and Gariguette. *International Journal of Refrigeration* 32: 1495 – 1504.

[7] Delele M. A., Schenk A., Ramon H., Nicolaï B. M., Verboven P. 2009. Evaluation of a chicory root cold store humidification system using computational fluid dynamics. *Journal of Food Engineering* 94: 110-21.

[8] Hung D. V., Tong S., Tanaka F., Yasunaga E., Hamanaka D., Hiruma N., Uchino T. 2011. Controlling the weight loss of fresh produce during postharvest storage under a nanosize mist environment. *Journal of Food Engineering* 106: 325-30.

[9] D'agaro P., Croce G., Cortella G. 2006. Numerical simulation of glass doors fogging and defogging in refrigerated display cabinets. *Applied Thermal Engineering* 26: 1927–34.

[10] Cox L. J., Kleiss T., Cordier J. L., Cordellana. C., Konkel P., Pedrazzini C., Beumet R., Siebenga A., 1989, Listeria spp. in food processing, non-food and domestic environments, *Food Microbiology,* 6, 49-61.

[11] Zoz F., Iaconelli C., Lang E., Iddir H., Guyot S., Grandvalet C, Gervais P., Beney L, 2016, Control of Relative Air Humidity as a Potential Means to Improve Hygiene on Surfaces: A Preliminary Approach with Listeria monocytogenes, PLOS ONE, DOI:10.1371/ journal.pone.0148418).

[12] Birdi K. S., Vu D. T., Winter A., 1989. A Study of the Evaporation Rates of Small Water Drops Placed on a Solid Surface, *The Journal of Physical Chemistry*, 93(9)3702-3703.

[13] Chandra S., Marzo M. D., Qiao Y. M., Tartarini P. 1996. Effect of liquid-solid contact angle on droplet evaporation. *Fire Safety Journal* 27: 141-58.

[14] Picknett R.G., Baxon R. 1977, The evaporation of sessile or pendant drops in still air. *J Colloid Interface Sci*.61,336-350.

[15] Yu D.I., Kwak H.J., Doh S.W., Kang H.C., Ahn H.S., Kiyofumi M., Park H.S. and Kim M.H., 2015, Wetting and evaporation of water droplets on textured surfaces. *International Journal of Heat and Mass Transfer*. 90, 191-200.

[16] Maa J. R. 1967. Evaporation coefficient of liquids. *Industrial Engineering Chemical Fundamentals* 6: 504-18.

[17] Mozurkewich M. 1986. Aerosol growth and the condensation coefficient for water: a review. *Aerosol Science and Technology* 5: 223-36.

[18] Navaz H. K., Chan E., Markicevic B. 2008. Convective evaporation model of sessile droplets in a turbulent flow—comparison with wind tunnel data. *International Journal of Thermal Sciences* 47: 963-71.

[19] Raimundo A., Gaspar A., Oliveira A. V. M., Quintela D. 2014. Wind tunnel measurements and numerical simulations of water evaporation in forced convection airflow. *International Journal of Thermal Sciences* 86: 28-40.

[20] Vik T., Reif B. A. P. 2011. Modeling the evaporation from a thin liquid surface beneath a turbulent boundary layer. *International Journal of Thermal Sciences* 50: 2311–17.

[21] Rymkiewicz J. Zapalowicz Z., 1993, Analysis of the evaporation process for water droplet on flat heated surface. *International communications in heat and mass transfer*, 20, 687-697

[22] Hsu C. C., Su T. W., Wu C. H., Kuo L. S., Chen P. H. 2015. Influence of surface temperature and wettability on droplet evaporation. *Applied Physics Letters* 106.

[23] Nguyen T. A. H. , Nguyen A.V., Hampton M.A., Xu Z.P., Huang L., Rudolph V., 2012, Theoretical and experimental analysis of droplet evaporation on solids surfaces. *Chemical Engineering Science* 69, 522-529.

[24] Hu H, Larson R.G. 2002, Evaporation of a sessile droplet on a substrate. *J. Phys.Chem B.* 106, 1334-1344.

[25] Dunn G.J., Wilson S.K., Duffy B.R., David S., Sefian K., 2008, A mathematical model for the evaporation of a thin sessile liquid droplet : comparison between experiment and theory. *Colloids Surfaces A: Physiochem. Eng. Aspects* 323, 50-55

[26] Hu D., Wu H., 2015, Numerical study and predictions of evolution behaviors of evaporating pinned droplets based on a comprehensive model. *International Journal of Thermal Sciences* 96, 149-159.

CHAPITRE 4 : ETUDE DE L’EVAPORATION D’EAU DANS UNE CELLULE D’ESSAI

Article 4 : Study of the drying process of wetted surfaces in food processing like conditions (En preparation)

Study of the drying process of wetted surfaces in food processing like conditions

L. Lecoq [ab*], D. Flick [b], O. Laguerre [a]

[a] Irstea, UR GPAN, 1 rue Pierre-Gilles de Gennes, 92761 Antony, France

[b], UMR Ingénierie Procédés Aliments, AgroParisTech, INRA, Université Paris-Saclay, 91300 Massy, France

ABSTRACT

Experiments were carried out inside a cold room to study the drying of wetted surfaces in conditions similar to the ones encountered in food processing plants. Two experiments were performed: one where evaporation of water droplets on stainless steel was studied at different ambient conditions in the room. Another where the floor was entirely wetted with water to reproduce conditions of drying period inside a food processing plant and water mass evolution was measured with and without dehumidifier. Models predicting the evaporation in the two kinds of experiment were developed. The comparison with the experimental data shows good agreements. Relative humidity was shown to have the most impact on evaporation rate in the ranges of conditions studied and implantation of dehumidifier was found to be efficient to enhance drying.

Keywords: evaporation, droplet, water film, model, drying

Highlights:

- Experimental results showed the importance of relative humidity to control drying
- Use of dehumidifier was studied as a solution to enhance evaporation on wet floor
- Models were developed to predict water mass evolution in function of ambient conditions
- Good agreements were found between the models and the experimental data

* Corresponding author: Tel: 33 1 40 96 90 04, Fax: 33 1 40 96 60 75, E-mail: logan.lecoq@irstea.fr

Nomenclature

C_{sat}	Concentration of saturated water vapor	$kg.m^{-3}$
C_{wa}	Concentration of water vapor in air	$kg.m^{-3}$
h	Overall heat transfer coefficient	$W.m^{-2}.K^{-1}$
h_c	Convection heat transfer coefficient	$W.m^{-2}.K^{-1}$
h_r	Radiative heat transfer coefficient	$W.m^{-2}.K^{-1}$
k	Mass transfer coefficient	$m.s^{-1}$
m	Water mass	kg
$\dot{m}$	Evaporation rate	$kg.s^{-1}$
M	Molar mass	$kg.mol^{-1}$
RH	Relative humidity	%
R	Ideal gas constant	$J.K^{-1}.mol^{-1}$
S	Total surface of the plate	m^2
T	Temperature	°C
t	time	s
X	Water content	$kg_{water}.kg_{dry\ air}^{-1}$
β	Wet surface over total surface	Dimensionless
β_c	Spherical cap surface over total surface	Dimensionless
ε	Emissivity	Dimensionless
ΔH_v	Latent heat of water evaporation	$J.kg^{-1}$

Subscripts

a	air	0	initial
pl	plate	w	water
wb	wet-bulb		

1. Introduction

In a food processing plant, cleaning and disinfection are performed daily to prevent bacteria growth. However bacteria such as *Listeria monocytogenes* still persist even through the best disinfection practice (Muhterem-Uyar et al. 2015, Vogel et al. 2001). In order to make this operation as efficient as possible, complete drying of the room must be performed. Indeed, during cleaning and disinfection, a lot of water is used and water remaining will allow bacteria to survive (Carpentier & Cerf 2011, Zoz et al. 2016). In practice, if study to improve cleaning and disinfection have been performed, drying is still done empirically. The solutions to enhance drying such as the installation of air drying device (dehumidifier) to lower relative humidity in the room have yet to be studied.

In this study, experiments were performed at laboratory (in a cold room) where similar conditions as the one in a food plant (water mass, relative humidity, temperature…) were applied. Evaporation of water on two surfaces was studied: on a stainless steel plate (to represent evaporation on equipment) and on the whole floor of the cold room. The influence of a dehumidifier on drying was analyzed. Models to predict water mass evolution was developed and validated with experimental data. Drying time in function of ambient conditions could therefore be estimated and solutions to enhance drying were given.

2. Literature review

Pour l'essentiel, cette partie bibliographique reprend les éléments déjà présentés dans les articles précédents.

3. Experiments in a cold room

Experiments were carried out in a cold room (Figure 1) to represent the drying period of a food processing plant. Two types of experiments were performed: one where the evaporation rate of droplets deposited on a stainless steel plate exposed to different ambient conditions was measured, the other where the entire surface of the floor was wet. The first experiment is similar to what happens on the equipment of a food plant, the second one concerns the surface (floor) where the highest water load is observed after the cleaning of a food plant. The ambient conditions (temperature, relative humidity, heat transfer coefficient, water weight) were measured.

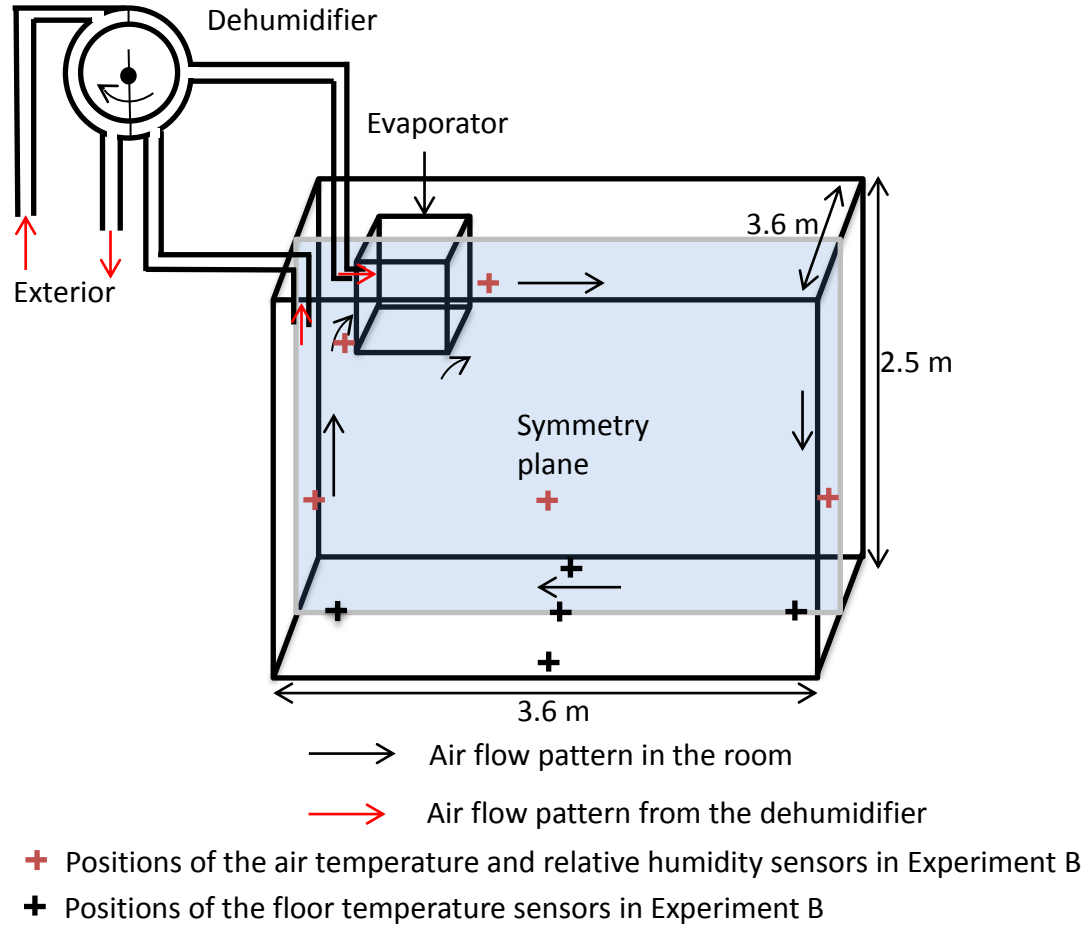

Figure 1: Scheme of the cold room with the air flow patterns (evaporator and dehumidifier)

3.1. Description of the cold room

The dimension of the cold room is 3.6m long, 3.6m wide and 2.5m high. Temperature and relative humidity can be controlled in the room using an evaporator and a dehumidifier located at the ceiling. The evaporator air flow rate (air inlet velocity) can be adjusted using a variable frequency drive.

3.2. Description of the experiments

3.1.1. Experiment A: droplets on stainless steel plate

The aim of this experiment is to mimic the evaporation on equipment in a food processing plant. A stainless steel plate (most common material for equipment) with a surface of 0.5 x 0.5 m² and with 10 cm of thermal insulation underneath (to simplify the heat exchanges) was placed inside the cold room. Water droplets (100 droplets of 0.5 mL) were deposited on it and the evaporation rate on the plate was studied at different ambient conditions: air temperature (5°C to 20°C), relative humidity (30% to 90%) and convective heat transfer coefficient (8 to 14 $W.m^{-2}.K^{-1}$). The conditions studied correspond to the ranges we can find inside a food processing plant (Table 1). During the experiments, the air and plate temperatures, the relative humidity in the room, the water weight and the initial wet surface on the stainless steel plate were measured. To study the influence of the plate position on the evaporation rate, experiments were also performed in different places (positions A, B, C and D, see figure 2).

Table 1: Experimental conditions and value of the evaporation rate during the first period

Studied parameter	Symbol	Experimental conditions				Evaporation rate, 1st period ($x10^{-3}$ $g.s^{-1}$)
		Ta (°C) ± 0.2	Position: h_c ($W.m^{-2}.K^{-1}$) ± 1.1	*RH* (%) ± 3%	β_0 (%)	
RH	1 ◆	5.5	A: 10.1	**31***	23	2.06
				70	24	0.89
				87*	23	0.40
T_a	2 ■	**10.4**	A: 10.1	30	28	3.09
		20.2		31	25	4.68
Air flow rate which influences h_c	3 ▲	5.5	**A: 10.1**	87	23	0.40
		4.4	**A: 11.1**	91	21	0.28
		5.7	**A: 12.7**	91	19	0.37
		5.3	**A: 14.2**	83	20	0.64
Position in the room which influences h_c	4 +	5.8	**B: 10.9**	33	25	2.32
			C: 10.5	33	26	1.99
			D: 8.5	31	23	1.79
High T_a with intermediate RH	5 ■	**20.5**	A: 10.1	**70**	18	1.78
High h_c with low RH	6 ●	5.4	**A: 14.2**	**32**	22	2.83
50 droplets: lower β_0	7 ×	5.5	A: 10.1	30	**7**	0.95
Hydrophobic surface (stainless steel covered with plastic film)	8 ●	5.7	A: 10.1	29	**10**	1.21

* One repetition was performed

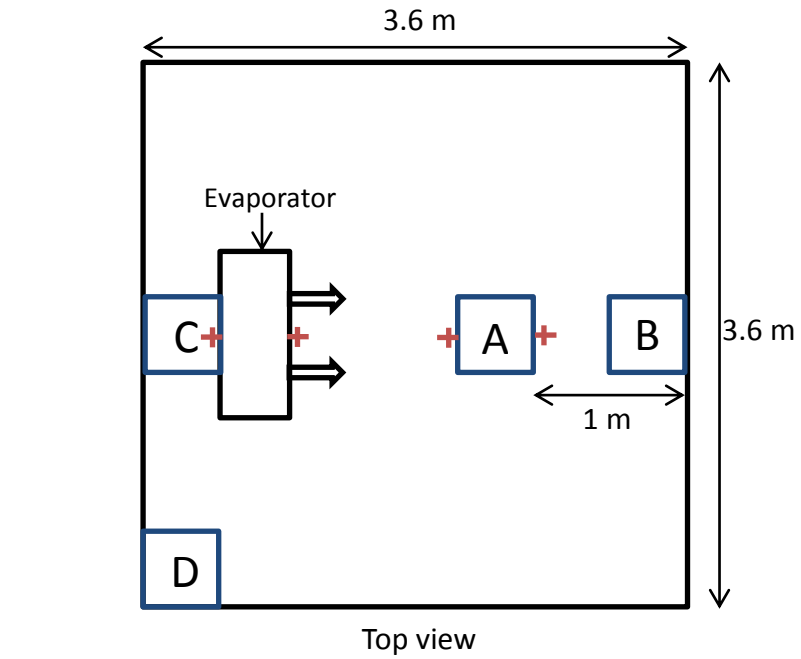

Figure 2: Top view of the cold room with the positions where the water evaporation experiments were performed

3.1.2. Experiment B: floor entirely wet

The aim of this experiment is to reproduce the ambient conditions (temperature, relative humidity, water weight) we can have during the drying process inside a food processing plant without the difficulties we can face in a food plant. For example, the company authorization is necessary and experimental repetition is usually not possible. Moreover, the installation of sensors is limited in time and in position to prevent workers from being disturbed. This implies the results interpretation to be more complicated and some data could be missing.

Inside the laboratory cold room, the initial temperatures (air and walls) were set at 20°C and the thermostat temperature was set a 5°C. The initial relative humidity was around 40-50%. Then, 230 $g.m^{-2}$ of water was deposited on the floor (approximate amount of water remaining after cleaning inside a plant, experimentation performed on site) which represent in total around 3 kg of water. Another experiment was performed with only 1 kg of water initially deposed on the floor which could represent the amount of water on the surface after the technicians removed part of it using squeegee. During the experiment, floor and air temperatures, relative humidity and water weight were measured in the room until all of the water evaporated (procedure explained section 3.3.2.).

To study the influence of a dehumidifier on the ambient conditions and on the drying time, the experiments were performed with and without dehumidifier. For the experiment where the dehumidifier was working, the relative humidity set value was 50%RH during drying. Its characteristics are shown table 2.

Table 2: Technical characteristics of the dehumidifier (Dessica DT-210):

Dehumidification capacity[1] [kg.h^{-1}]	0.6
Dry air flow rate [m^3.h^{-1}]	210
Moist air flow rate [m^3.h^{-1}]	40
Motor power [kW]	1.1

[1] For the inlet condition of 20°C and 60% relative humidity (RH)

3.3. Parameters measurement

3.3.1. Experiment A: droplets on stainless steel plate

Water droplets of 0.5 mL (50 or 100 droplets, using a pipette), were deposited onto the stainless steel plate. The water weight on the plate was recorded every 10 seconds using a balance (± 0.001 g precision) connected to a data-logger (Agilent 34970A). Measurement was carried out until all the water evaporated.

Air temperature was measured using calibrated T-type thermocouples (1 mm diameter, ± 0.2°C precision) in different places: thermocouples were put at the return air, inlet of the evaporator, and two near the plate (10 cm above the plate), shown Figure 2.

Relative humidity was measured in the room during the experiments (using calibrated TESTO 174H hygrometers, ± 3% precision) at the same location than the thermocouples.

Air velocity was measured at the air return and inlet of the evaporator using a hot wire anemometer (TESTO 435-2, range of measurement 0-20 m.s^{-1}, ± 0.03 m.s^{-1} precision). The velocity at the inlet was varied from 2.0 to 4.8 m.s^{-1} which induced respectively an air flow rate from 1000 to 2400 m^3.h^{-1}. The average air velocity was calculated from 60 measured values (every 1s over 1min).

Heat transfer coefficient corresponding to the different inlet air velocity was also measured on the plate at 5 positions and the average value was taken to estimate this coefficient on the plate. It was measured by a fluxmeter equipped with a thermocouple (Trade name Captec, width x height x depth: 4 cm x 4 cm x 450 µm). This fluxmeter was supplied by 10 W of heating power. The fluxmeter temperature, the air temperature (measured at 5 cm from the surface of the fluxmeter) and the measured flux were recorded every second until a steady state was obtained. Then, the mean values were calculated over 20 min of a stabilization period allowing the estimation of the heat transfer coefficient. It is to be noticed that the emissivity of this fluxmeter is close to zero; thus, the radiative exchange can be neglected. For instance, the average value on the plate at the position A for an inlet air velocity of 2 m.s^{-1} was 10.1 (± 1.1) W.m^{-2}.K^{-1}.

3.3.2. Experiment B: floor entirely wet

To measure the water mass, paper towelettes were used to wipe the entire surface of the floor and then weighted using an electronic balance (Sartorius, CPA34001P, ± 0.1 g). The water mass on the floor was measured at different times in order to have its evolution during drying. For that, the experiment was repeated. For instance, in the case where 3 kg of water was deposited initially on the floor, the experiments were repeated 5 times with dehumidifier (wiping the floor at 30 min, 1h, 3h, 5h, 10h after the beginning of the experiment) and 7 times without dehumidifier (at 30 min, 1h, 3h, 5h, 10h , 16h20 and 20h). To be sure of the repeatability of the operating conditions, relative humidity and temperature in the room were measured in all experiments and the same evolution was found. The initial conditions

(temperature and relative humidity) were the same in all the experiments. To avoid as much as possible the variability of the result due to water deposition on the floor, watering can and squeegee were used to cover the whole surface and it was performed by the same person in every experiments.

Temperature and relative humidity was recorded at 5 points in the room every minute during the experiments using calibrated TESTO 174H hygrometers (± 3%RH, ±0.5 °C precision). The sensors were put at the return air, inlet of the evaporator, and three other were put at 1.0m height at different positions in the symmetry plane of the room (0.2 m, 1.8 m, 3.4m, Figure 1). In addition, the floor temperature was recorded using calibrated T-type thermocouples (1 mm diameter, ± 0.2°C precision) with 4 mm of thermal insulation on it.

Using the same fluxmeter (Trade name Captec, width x height x depth: 4 cm x 4 cm x 450 µm) than in experience A, the convective heat transfer coefficient was measured on the floor at 7 different positions to estimate an overall value. For an inlet air velocity of 2 $m.s^{-1}$, the average value on the floor was 10.0 (± 2.5) $W.m^{-2}.K^{-1}$.

4. Evaporation model

In order to predict the water mass evolution, models were developed for water evaporation on a stainless steel plate and for water evaporation on the floor of a test chamber (cold room). These models were validated with the experimental data.

4.1. Model development for the evaporation of water droplets on stainless steel plate

For the evaporation rate on the plate, the model is based on heat balance and Lewis analogy.

The heat balance on a non-heated stainless steel plate (thermal inertia neglected, thermal conductivity of the plate assumed as infinite) is as follows:

$$h \cdot \left(T_a - T_{pl}\right) = \dot{m} \cdot \Delta H_v \tag{1}$$

$$\dot{m} = \beta_c \cdot k \cdot \left(C_{sat(T_{pl})} - C_{wa(T_a)}\right) \tag{2}$$

where β_c is the spherical cap surface of the droplets over the surface of the plate.

The heat transfer coefficient (*h)* can be expressed as the sum of the convective coefficient (h_c*)* and the equivalent heat transfer coefficient from radiation (h_r*)*. Indeed, the heat exchange by convection can be expressed as $h_c\left(T_a - T_{pl}\right)$ and the one by radiation can be approximated by $h_r\left(T_a - T_{pl}\right)$. Even if the surface considered is stainless steel with a low emissivity (0.1), the water on the surface having a high emissivity (0.95) can induce a non-negligible heat transfer by radiation. Thus:

$$h = h_r + h_c \tag{3}$$

where $h_r = 4\sigma\left(\varepsilon_{pl} + \beta\left(\varepsilon_w - \varepsilon_{pl}\right)\right) \cdot (T_a + 273.15)^3$ The convective coefficient (h_c) was determined using a fluxmeter (as explain section 3.3.1); the values are shown on Table 1. The different values of convective coefficient correspond to different air inlet velocity from the evaporator (2.0, 3.0, 4.0, 4.8 $m.s^{-1}$) or position in the room (A, B, C, D) at an air inlet velocity of 2.0 $m.s^{-1}$.

Considering Eq. (1) and (2):

$$h \cdot \left(T_a - T_{pl}\right) = \beta_c \cdot k \cdot \Delta H_v \cdot \left(C_{sat}\left(T_{pl}\right) - C_{wa}(T_a)\right) \quad (4)$$

The mass transfer coefficient k is calculated using the Lewis analogy: $k = \frac{h_c}{\rho . Cp_{air} . Le^{2/3}}$

with $Le = \frac{\alpha}{D} = \frac{18.6 \cdot 10^{-6}}{21.8 \cdot 10^{-6}} \approx 0.85$

where α is the thermal diffusivity of air = $18.6 \cdot 10^{-6}$ m².s^{-1} at 0°C and D the mass diffusivity of water vapor in air = $21.8 \cdot 10^{-6}$ m².s^{-1} at 0°C (Bimbenet et al. 2002).

$C_{sat}(T)$ corresponds to the saturated vapor concentration which is a function of the temperature. It can be determined by the following fitting function for temperature between 0°C and 20°C:

$$C_{sat}(T) = a + b \cdot T + c \cdot T^2 \quad (5)$$

where $a = 4.84 \cdot 10^{-3}$ kg.m^{-3}, $b = 2.94 \cdot 10^{-4}$ kg.m^{-3}.°C^{-1} and $c = 1.58 \cdot 10^{-5}$ kg.m^{-3}.°C^{-2}

From (4) and (5) the expression of the plate temperature can be determined (the equation development is reported in appendix):

$$c' \cdot {T_{pl}}^2 + b' \cdot T_{pl} + a' = 0 \quad (6)$$

where $\delta_1 = \frac{b \cdot \Delta H_v}{\rho . Cp_{air} . Le^{2/3}}$, $c' = -\delta_1 \frac{c}{b} \cdot \beta_c$, $b' = -1 - \delta_1 \cdot \beta_c$ and

$$a' = T_a \left(1 + \delta_1 \left(1 + \frac{c}{b} T_{wb}\right) \beta_c\right) - (T_a - T_{wb}) \left(\frac{h_c}{h} + \delta_1 \left(1 + \frac{c}{b} T_{wb}\right)\right) \beta_c$$

It is to be noted that the solution corresponding to the physical problem is the following one:

$$T_{pl} = \frac{-b' - \sqrt{b'^2 - 4a'c'}}{2c'} \quad (7)$$

Using (1) and (7) the evaporation rate ($\dot{m}$) can be calculated:

$$\frac{dm}{dt} = \dot{m} = \frac{S \cdot \left(T_a - T_{pl}\right) \cdot h}{\Delta H_v} \quad (8)$$

As described by Chandra et al. (1996) the evaporation phenomenon on a stainless steel surface is composed of two periods:

During the first period of the evaporation called "pinning period", the droplet base radius remains constant while the droplet height decreases as well as the contact angle between the liquid and the solid surface. This period is supposed to last as long as the contact angle droplet/solid surface is superior to the receding angle, equal to 10° for water on stainless steel (Chandra et al. 1996). This value of 10° for the receding angle (α_r) corresponds to 15% of the initial water mass (Christophe Doursat, Logan Lecoq, Onrawee Laguerre, Denis Flick "Droplet evaporation on a solid surface exposed to forced convection: experiments, simulation and dimensional analysis", article in submission).

Once the receding angle is reached (the water mass equals 15% of its initial value), the contact angle remains constant and the droplet radius decreases until all of the water is evaporated, which corresponds to the second period of the evaporation process, called "receding period".

Therefore, β remains constant (= β_0) until $m(t) = 0.15 \cdot m_0$, and then decreases with $m(t)$. The wet surface is then proportional to the droplet volume power 2/3. Indeed, the volume droplet is equal to:

$$V_{droplet} = \frac{\pi}{3}\frac{(1-\cos(\alpha))^2(2+\cos(\alpha))}{\sin^3(\alpha)} \cdot r^3 \tag{9}$$

For the second period, the contact angle α is constant, thus the droplet volume is proportional to the cube of the radius. Also, the wet surface (projected surface) is proportional to the square of the radius ($\pi \cdot r^2$).

Therefore, the following evolution for the coefficient β was assumed:

$$\beta(t) = \min\left(\beta_0, \frac{m(t)^{\frac{2}{3}}}{(0.15 \cdot m_0)^{\frac{2}{3}}} \cdot \beta_0\right) \tag{10}$$

The spherical cap surface of the droplet can be calculated using the equation $\beta_c = \frac{2 \cdot \beta}{1+\cos(\alpha)}$. In our case, the initial contact angle of water on stainless steel is rather low (~15°) which induces that the spherical cap surface of the droplets is close to the wet surface:$\beta_c \approx \beta$. Thus, the plate temperature can be directly calculated using the value of β. If the contact angle is higher, its evolution needs to be estimated during this period to calculate β_c. As a first approximation, the contact angle could be taken as the average of the initial contact angle and the receding angle $\left(\alpha = \frac{\alpha_0+\alpha_r}{2}\right)$ to calculate the spherical cap surface (β_c), the plate temperature and the evaporation rate during the first period. This was applied for the experiment where the stainless steel plate was covered with a hydrophobic surface and the initial contact angle was around 45°. In practice, even for an initial contact angle at 45°, the initial spherical cap surface will only be 1.17 times higher than the wet surface ($\beta_{c_0}(\alpha_0 = 45°) = 1.17 \cdot \beta_0$) which will not impact significantly the plate temperature and the evaporation rate.

For the experiments on stainless steel, because $\beta_c \approx \beta$, the plate temperature will remain almost constant as well as the evaporation rate during the first period. Thus, for this period the water mass evolution can be calculated directly using equations (7) and (8). However, during the second period, the plate temperature will increase due to decrease in wet surface until it reaches the air temperature at the end of the evaporation. Therefore, in the second period, the evaporation rate will decrease. Using equations (7), (8) and (10), the water mass evolution during whole evaporation process (period 1 and 2) can be predicted. These equations were implemented using Matlab software (vR2012a; The MathWorks Inc., Natick, MA, USA, Euler method). Results are shown in section 5.

4.2. Model development for the evaporation on a floor entirely wet

In the case of a floor wetted by water, the thermal inertia is not negligible. The heat and mass balances give:

$$m_f \cdot Cp_f \cdot \frac{dT}{dt} = -h \cdot S \cdot (T - T_a) - k \cdot S \cdot \beta \cdot (C_{sat}(T) - C_{wa}) \cdot \Delta H_v \quad (11)$$

$$\frac{dm}{dt} = -k \cdot S \cdot \beta \cdot (C_{sat}(T) - C_{wa}) \quad (12)$$

where *T* is the floor temperature and *m* is the water mass on the floor.

The input parameters such as the convective coefficient *h*, the thermal inertia $m_f \cdot Cp_f$, the initial percentage of wet surface over the total surface β_0 are shown in the results section (5.4.). The air temperature T_a, initially at 20°C, decreases to the thermostat temperature during the process (5°C). Its evolution, measured experimentally (at the air return of the evaporator), is input in the model. The evolution of the vapor concentration in air $C_{wa}\left(= \frac{P_{sat}(T_a) \cdot M_W \cdot RH}{R \cdot T_a}\right)$ is calculated from the experimental data (relative humidity and air temperature at the air return of the evaporator). The concentration of saturated water vapor $C_{sat}(T)$ depends only on the surface temperature which, as in section 4.1., can be fitted using equation (5).

The equations (11) and (12) were implemented using Matlab software (vR2012a; The MathWorks Inc., Natick, MA, USA, Euler method); equation (10) was used to assess the wet surface evolution during drying. This allowed predicting the evolutions of floor temperature and water mass.

5. Results and discussion

5.1. Experiment A: droplets on stainless steel plate

5.1.1. Parameters influence on the evaporation rate

Table 1 shows the experimental evaporation rate results with the corresponding conditions during the first period and Table 3 shows the increase of evaporation rate between the different experiments in the range studied: 31%<RH<87%, 5.4°C<Ta<20.2°C, 8.5 $W.m^{-2}.K^{-1}$<h<14.2 $W.m^{-2}.K^{-1}$ and 7%<β_0<23%. From the results shown in Table 3, it appears that the relative humidity has the most impact on the evaporation rate for the studied conditions. When the relative humidity varies from 87% to 31%, the evaporation rate increases by a factor of 5.2 whereas for the variation of other parameters it increases at most by a factor 2.3. Of course it is to be underlined that, for instance, the temperature range would have been larger than 5 to 20 °C, the evaporation rate might have increased more than for relative humidity. However, the considered ranges correspond to conditions that can be found in a food processing plant. Therefore, it seems that reducing relative humidity by using a dehumidifier is an efficient way to increase significantly the evaporation rate and thus to reduce drying time. Indeed, inside food plant when no dehumidifier is installed, the relative humidity is often above 85% which is very unfavorable for drying. In addition, it can be seen in Table 1 that when the stainless steel plate was covered with plastic, the wet surface was lower (β_0 =10% instead of ~23% for stainless steel) which induced a lower evaporation rate because of lower surface exchange between the droplet and the plate. Therefore, for the same water mass, if water surface is less important, drying will be longer.

Exp.	Conditions				Evaporation rate (1^{st} period) (x10^{-3} g.s^{-1}) $\dot{m}_{min} < \dot{m} < \dot{m}_{max}$	$\frac{\dot{m}_{max}}{\dot{m}_{min}}$
1	h=10.1	T_a=5.5°C	β_0 = 23-24%	**31<RH<87%**	0.40<$\dot{m}$<2.06	5.2
2	h=10.1	RH=29-32%	β_0 = 22-28%	**5.5<Ta<20.2°C**	2.06<$\dot{m}$<4.68	2.3
4, 6	Ta=5.4-5.8°C	RH=31-33%	β_0 = 22-26%	**8.5<h<14.2**	1.79<$\dot{m}$<2.83	1.6
1, 7, 8	h=10.1	T_a=5.5°C	RH=29-31%	**7<β_0<23%**	0.95<$\dot{m}$<2.06	2.2

Table 3: Evaporation rate evolution in the ranges conditions studied

5.1.2. Comparison between model and experimental data

The experimental data for the evaporation rate during the **first period** were first compared to two models:

- The theoretical model presented in section 4.
- An empirical model developed in a previous study (L. Lecoq, D. Flick, O. Laguerre "Study of the water evaporation rate on stainless steel plate in controlled conditions", article in submission) that considers the following equations:

$$\frac{T_a - T_{pl}}{T_a - T_{wb}} = f(\beta_0) \approx \frac{3 \cdot \beta_0}{1 + 2 \cdot \beta_0} \quad (13)$$

$$\dot{m} = \frac{S \cdot f(\beta_0) \cdot (T_a - T_{wb}) \cdot h(v)}{\Delta H_v} \quad (14)$$

The evaporation rate comparison between the results from the empirical model and the experimental data is shown in Figure 3. The comparison shows a rather good agreement with an average relative error $\left(\frac{|Experimental\ value - Theorical\ value|}{Experimental\ value}\right)$ of 16 %.

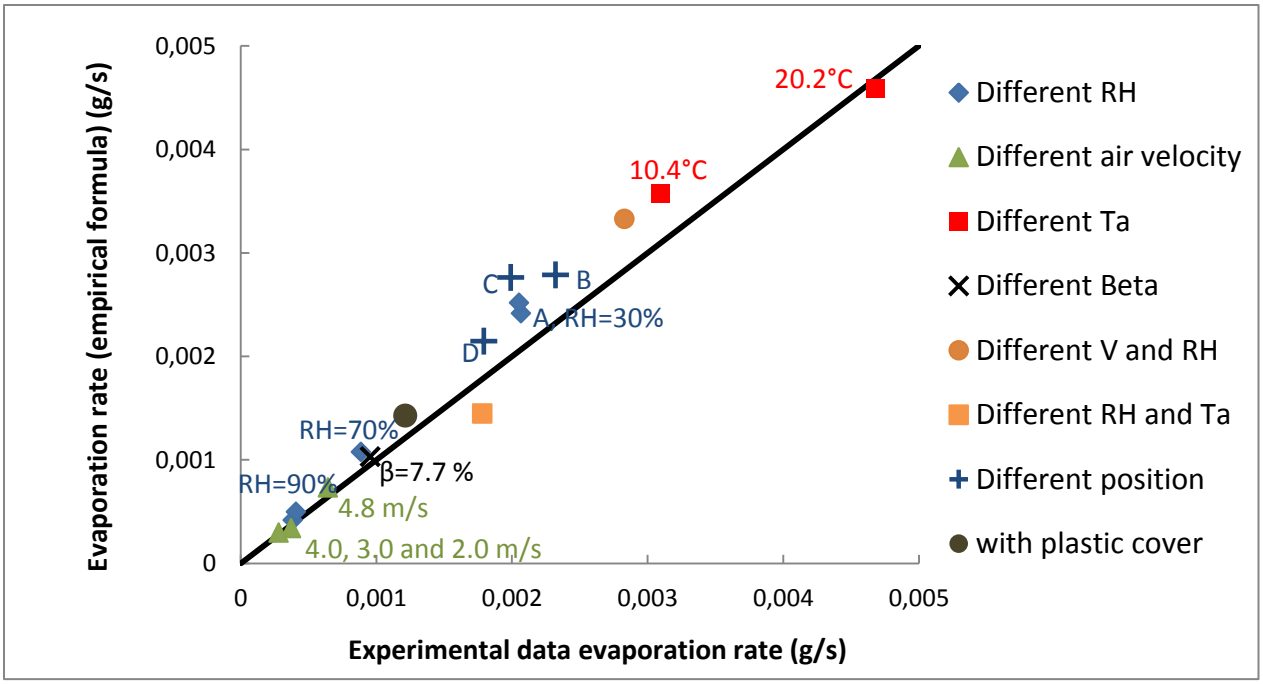

Figure 3: Evaporation rate comparison (1st period) between the experimental data and the empirical model

The evaporation rate comparison between the results from the theoretical model (eq. 7 and 8) and the experimental data is shown in Figure 4. The comparison shows a better agreement than with the empirical model, with a relative error of 9%.

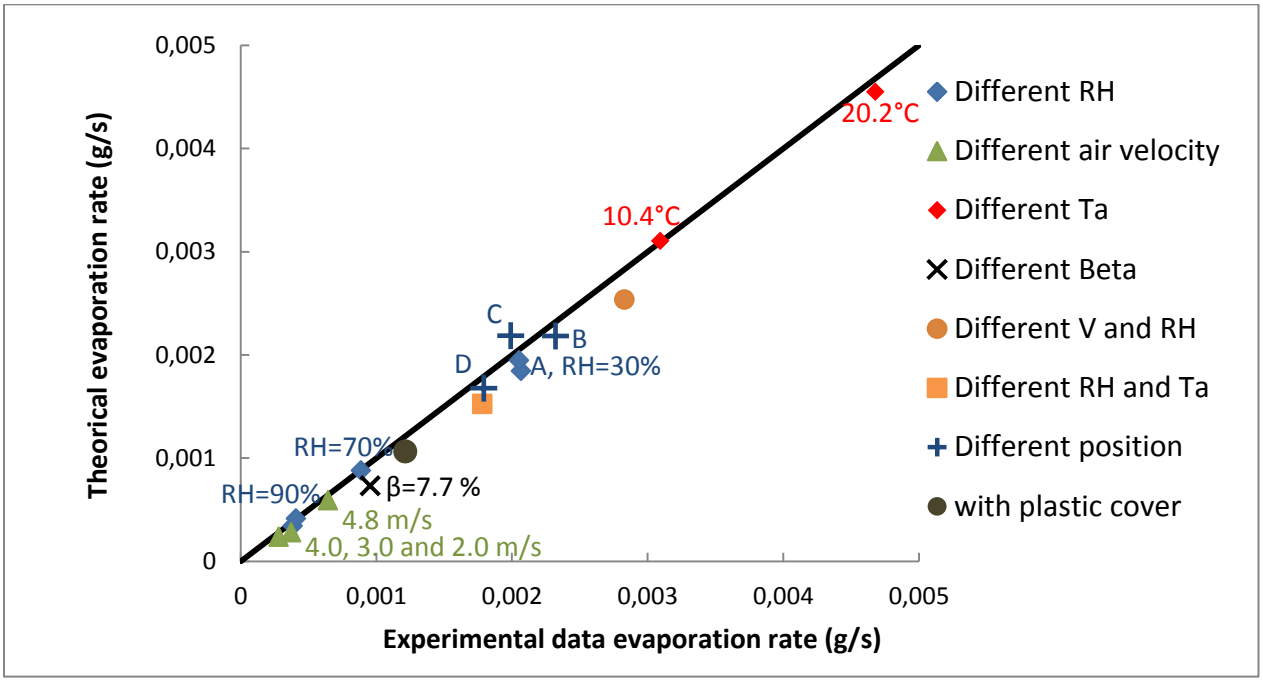

Figure 4: Evaporation rate comparison (1st period) between the experimental data and the theoretical model

The experimental water mass evolution during the **whole process** (period 1 and 2) can also be compared with the prediction of the two models (using equation (10) with equations (7) and (8) for the theoretical model or with equations (13) and (14) for the empirical one). Figure 5 compares the water mass evolutions at different air relative humidity (RH=31, 70, 87%).

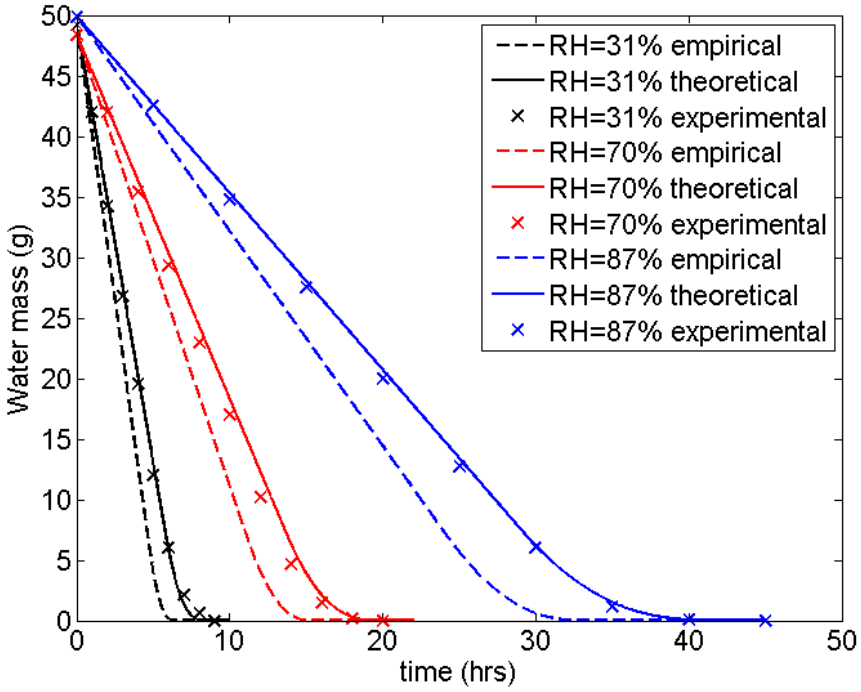

Figure 5: Water mass evolution during evaporation (2 periods): comparison between empirical model, theoretical model and experimental data.

The results for the water mass evolution during the two periods of the evaporation (first r=constant then α=constant) are in good agreement using the theoretical equations whereas the empirical model tends to slightly overestimate the evaporation rate. In the configuration studied (evaporation of water on non-heated stainless steel plate: negligible thermal inertia and very high conductivity) this model can be applied to predict the water mass evolution in function of the ambient conditions during the whole process and therefore predict the drying time.

For other materials the evolution of wet surface versus mass of water can be different so that equation (10) has to be modified. However, if the values of the initial and receding angles are known, the threshold ratio (15% for stainless steel) could be estimated. To apply equation (7) and (8), the material used must still have negligible thermal inertia and high conductivity.

5.2. Experiment B: Floor entirely wet

5.2.1. Water mass evolution

Figure 6 present the evolution of water mass on the floor with and without dehumidifier.

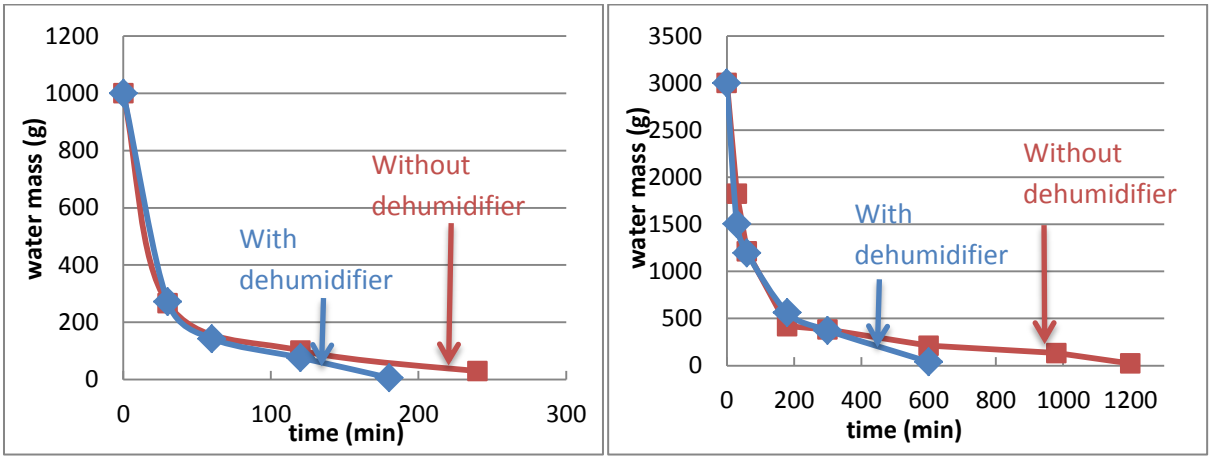

a b

Figure 6: Water mass evolution on the floor with (blue curve) and without dehumidifier (red curve) a- initial water mass: 1kg, b- initial water mass: 3kg

It can be observed that about 80% of the initial water is evaporated after three hours in the experiment with 3 kg and after one hour with 1 kg, either with or without dehumidifier. During this time, the evaporation rate is almost the same with and without dehumidifier. However the difference can be seen for the remaining 20% of water on the floor. The small amount of water remaining is located especially in corners where convection is lower or in areas where there the floor is slightly convex which induces accumulation of water. When we deposited 3 kg of water, after 20 hours, a small amount of water (23 g) was still present. On these areas, if relative humidity is high, which is the case without dehumidifier (RH~90% without dehumidifier, RH~50% with dehumidifier), the evaporation of the remaining water will be much longer as can be observed in Figure 6.

5.2.2. Water content

The evaporation rate evolution (with and without dehumidifier) can be assessed by estimating the difference between water content of air in contact with the floor (saturation value at floor temperature): X_{floor} and the water content in the room (taken at the air return of the evaporator): $X_{air\ return}$.

Indeed, $\dot{m} = k \cdot S \cdot \beta \cdot (C_{sat}(T) - C_{wa}) = k \cdot S \cdot \beta \cdot \rho_a \cdot \left(X_{floor} - X_{air\ return}\right)$

From the experimental data of air temperature and relative humidity at the air return of the evaporator and of floor temperature, $X_{air\ return}$ and X_{floor} were calculated (Figure 7).

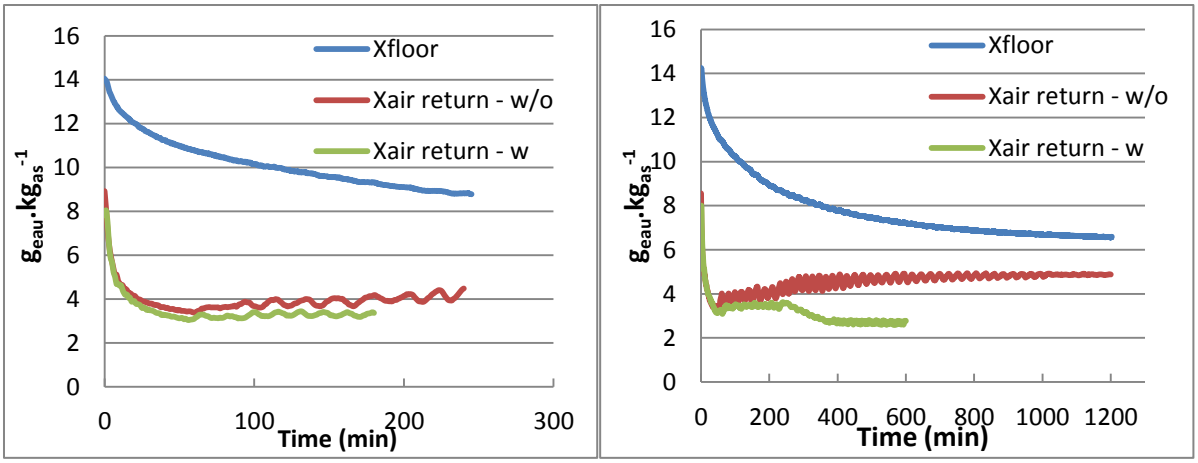

Figure 7: Water content evolution: air in contact with the floor (saturation) and air return to the evaporator, with and without dehumidifier a- initial water mass: 1kg, b- initial water mass: 3kg.
w/o=without dehumidifier
w=with dehumidifier

The water content difference between the floor (saturation) and at the room (air return) determines the evaporation rate: the higher this difference is, the more important the evaporation rate will be. For either 1kg or 3kg of water deposited initially, it can be seen that at the beginning of drying (first two hours), even though the water content at the air return is slightly higher without dehumidifier, the water content difference is quite similar in both cases. This induces almost the same evaporation rate and explains that, for the first two hours, the water mass evolution is almost the same (with or without dehumidifier). Then, the water content drops with dehumidifier.

For 3 kg of water, because the dehumidification capacity of the dehumidifier is rather low (0.6 $kg.h^{-1}$), it could not reduce directly the water content in air due the large amount of evaporated water there is to catch. During the first two hours, about 1.2 kg of water has evaporated. A part of it was caught by the dehumidifier and the rest by the evaporator. Once most of the water was evaporated, the dehumidifier was able to decrease the water content in air which induced the water content difference (between the floor and the air return) to become two times higher than without dehumidifier (Figure 7b at 600 min). This explains the larger evaporation rate with dehumidifier for this period.

5.2.3. Latent and sensible heat power

From the experimental data of air temperature and relative humidity at the air inlet and air return of the evaporator, the sensible heat power ($\dot{m} \cdot Cp_{air} \cdot (T_{air\ return} - T_{air\ blown})$) and latent heat power ($\dot{m} \cdot \Delta H_v \cdot (X_{air\ return} - X_{air\ blown})$) were calculated (Figure 8 & 9). This includes the effect of evaporator and dehumidifier (Figure 1).

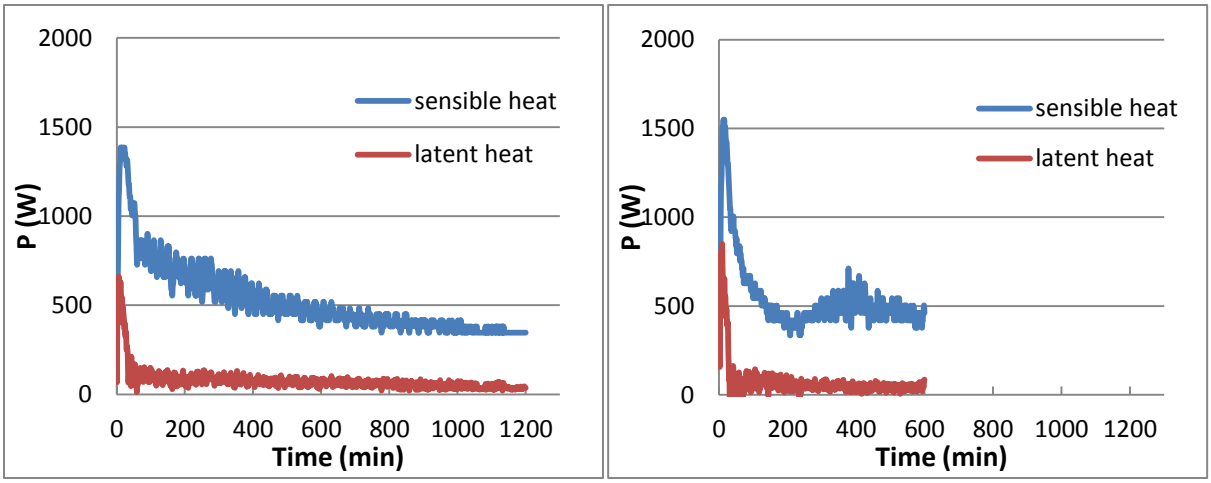

a b

Figure 8: Evolution of the latent and sensible heat power during drying of 3 kg of water, a- without dehumidifier, b- with dehumidifier

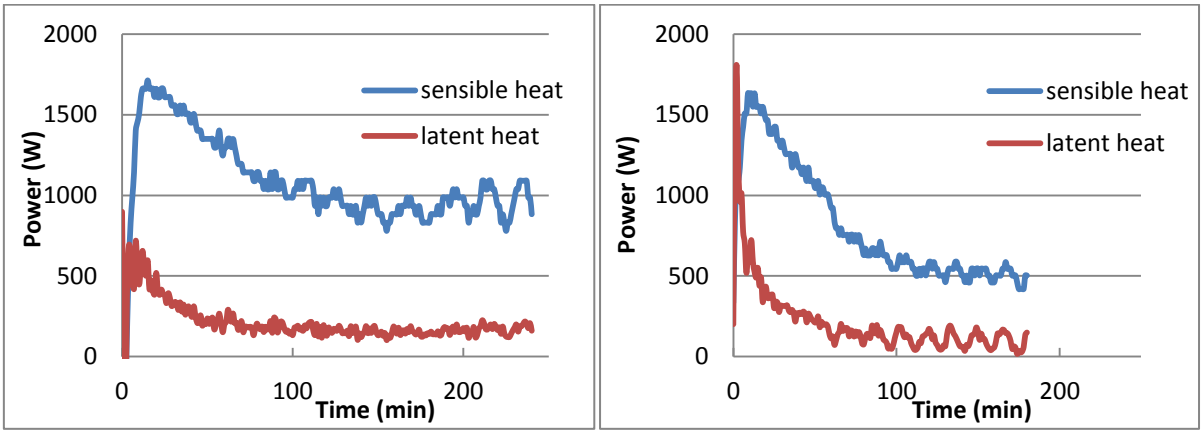

a b

Figure 9: Evolution of the latent and sensible heat power during drying of 1 kg of water, a- without dehumidifier, b- with dehumidifier

It can be observed that for the first 30 min., there was a pick of latent heat power, which corresponds to higher evaporation rate, and it was more important with the dehumidifier than without: ~1800 W / 600 W for 1 kg of water and ~800 W / 600 W for 3 kg of water. Then, the latent heat power decreased in all experiments and reached around the same value after two hours of drying ~100W. Unfortunately, the precision of measurements does not allow differentiating clearly the conditions with and without dehumidifier after two hours with the latent heat power.

The sensible heat power evolves similarly in all experiments, with a maximal power of about 1.5 kW at the beginning in order to reach as fast as possible the thermostat setting (5°C). Once the air temperature is close to 5°C, the evaporator only maintains this temperature and less power is needed. The temperature evolution at the air return of the evaporator is shown Figure 10 (similar in all experiments) to confirm this analyze.

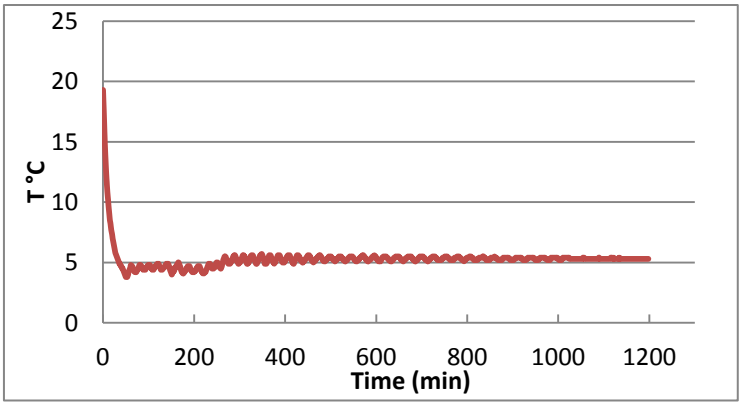

Figure 10: Temperature evolution at the air return of the evaporator (case: 3kg of water, without dehumidifier, similar in all the experiments, other results not shown)

5.2.4 Comparison between the model and the experimental data

The water mass and the floor temperature evolution predicted by the developed model are compared with the experimental data in Figure 11. For this simulation, the parameters were the following:

h=10 W.m^{-2}.K^{-1}, $m_f \cdot Cp_f = 3.3 \cdot 10^6$ J.K^{-1}, $\beta_0 = 1$ and $\beta(t) = \min\left(\beta_0, \frac{m(t)^{\frac{2}{3}}}{(0.15 \cdot m_0)^{\frac{2}{3}}} \cdot \beta_0\right)$

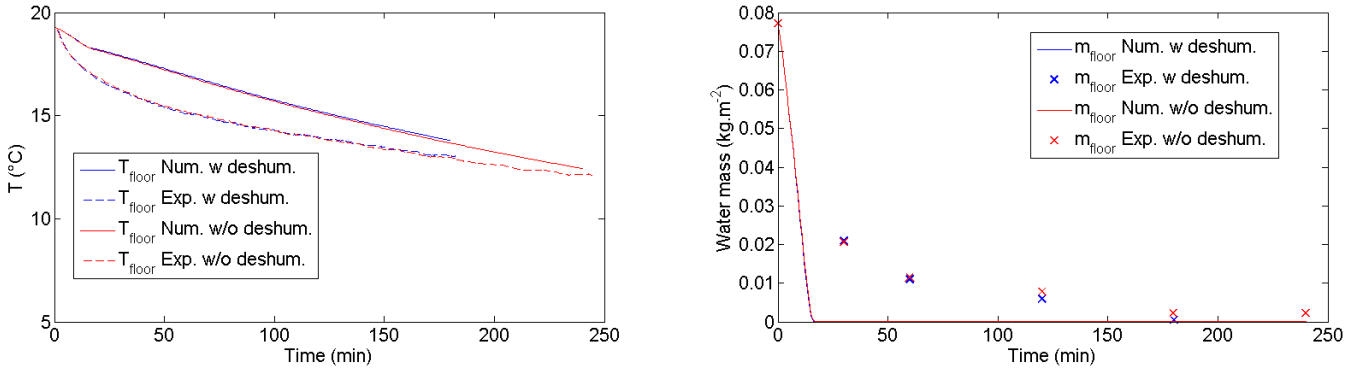

a

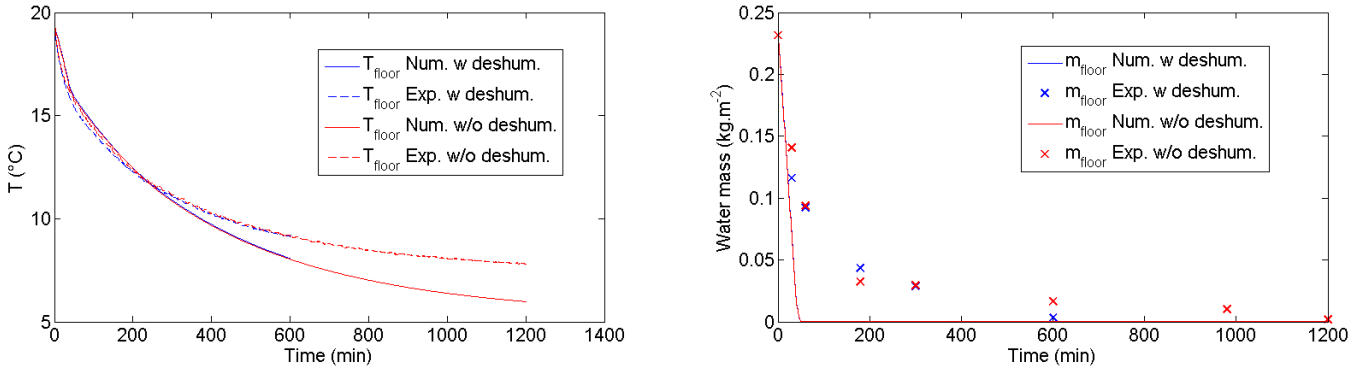

b

Figure 11: Comparison between numerical and experimental results for the floor temperature and the water mass evolution (with and without dehumidifier) a- initial water mass: 1kg, b- initial water mass: 3kg

It can be seen that the floor temperature can be estimated with the model quite well considering the fact that the experimental data measured the temperature at some location at the surface whereas the model considers an average value. However, the water mass evolution predicted by the model decreases much faster than in the experiment and no difference appears with or without dehumidifier. In the model, it was considered that initially the floor is entirely covered by water ($\beta_0 = 1$) and that the floor is perfectly flat. In fact, there are many imperfections. This induces that in some positions water tends to accumulate. Therefore, the water does not cover completely the floor. In addition, due to the variability of initial water load, in some location the wetted surface decreases before 85% of the water is evaporated, as assumed in equation 10. Consequently, this equation and the initial values of β were modified in order to better fit the experimental results. Figure 12 present the evolution for the following modeling assumptions:

h=10 W.m^{-2}.K^{-1}, $m_f \cdot Cp_f = 3.3 \cdot 10^6$ J.K^{-1}, $\beta_0(1\ kg) = 0.2$, $\beta_0(3\ kg) = 0.4$,

$$\beta(t) = \min\left(\beta_0, \frac{m(t)}{0.7 \cdot m_0} \cdot \beta_0\right)$$

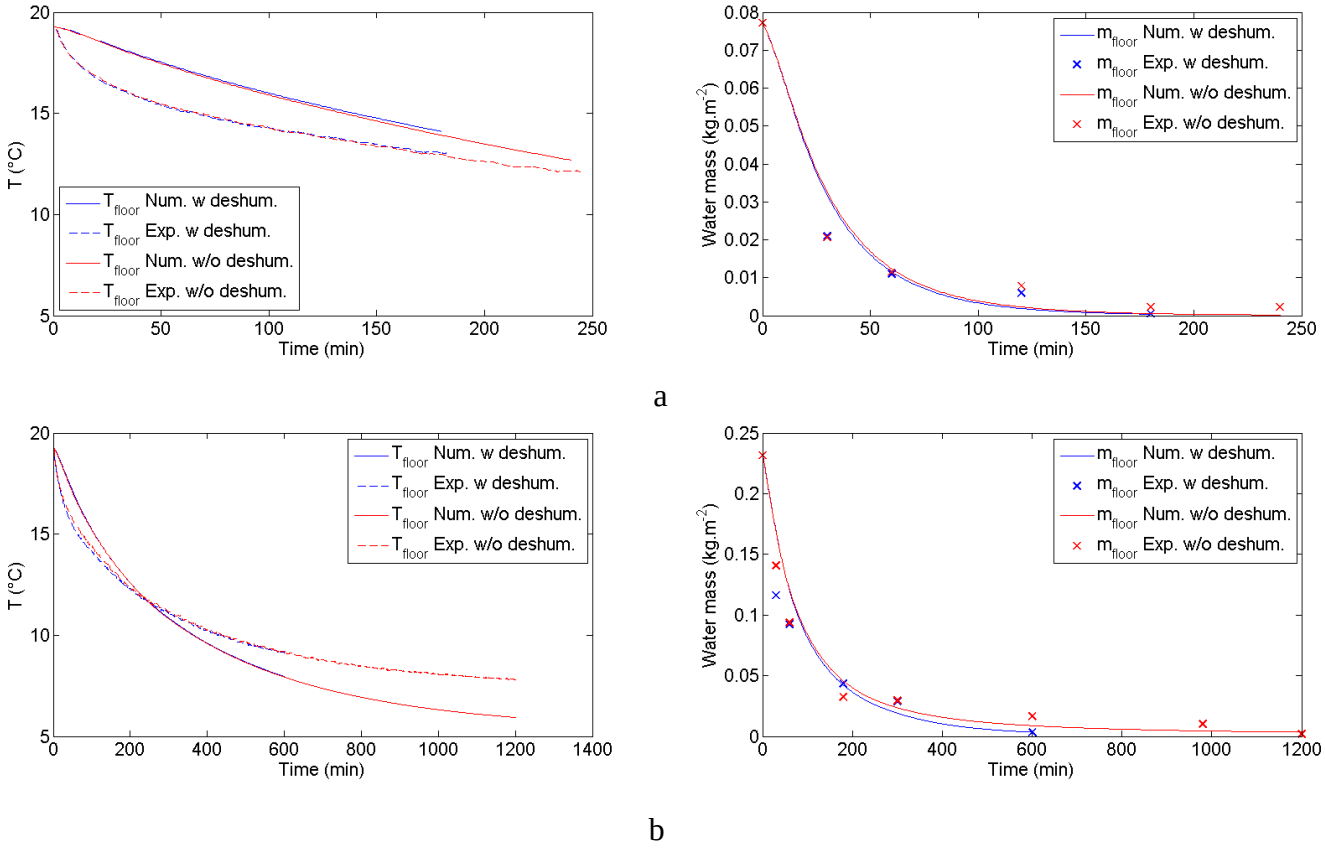

Figure 12: Comparison between numerical and experimental results for the floor temperature and the water mass evolution (with and without dehumidifier) with the following coefficients: $\beta_0(1\ kg) = 0.2$, $\beta_0(3\ kg) = 0.4$, $\beta(t) = \min\left(\beta_0, \frac{m(t)}{0.7 \cdot m_0} \cdot \beta_0\right)$

a- initial water mass: 1kg, b- initial water mass: 3kg

It can be observed that these new modeling assumptions don't have a large impact on the floor temperature. It is slightly higher because evaporation takes place on a smaller part of the floor. However the results for the water mass evolution are much closer to the experimental

data. In addition, because evaporation takes longer, the difference between with and without dehumidifier appears better (especially for the case where 3 kg of water is deposed initially). The initial water repartition has a major impact on evaporation. For the same amount of water, if its repartition is uniform and covers the entire surface ($\beta_0 = 1$, small water film thickness) evaporation is faster than if water is concentrated only at some locations ($\beta_0 < 1$, higher water film thickness) which is the case in our experiments. Therefore, to enhance evaporation inside a food processing plant and lower the drying time of the floor, its flatness and its roughness are factors as important as relative humidity. If the floor is damaged at some locations and allows water to accumulate, drying the floor at these locations will never be possible in two hours (average period of time for drying in food plant) even if there is a dehumidifier working. Water will remain, favoring bacterial development, which is an important issue for food processing plant.

6. Conclusion

Two experiments were performed to study the evaporation of water in conditions close to the ones encountered in a food plant. The first experiment represented the evaporation of water droplets on equipment (stainless steel plate). In this experiment, the most important parameter in the ranges studied was the relative humidity. When it was reduced from 87% to 31%, evaporation rate was multiplied by a factor of 5.2. In order to enhance evaporation, relative humidity should therefore be controlled. A theoretical model was developed which predicts with a good accuracy the water mass evolution and can be applied in various conditions.

The second experiment represents the evaporation on a floor entirely wet (with 230 $g.m^{-2}$ of water or 80 $g.m^{-2}$) where the initial temperature (20°C) and the thermostat temperature (5°C) were set at the values which can be found in a food plant. The relative humidity being one of the most important factors, the influence of a dehumidifier was studied. It was observed that without dehumidifier, water is more and more difficult to evaporate along the process which makes a complete drying impossible in an acceptable time. However when a dehumidifier is working, the water content in air can be maintained at a rather low level which enhances significantly evaporation. In this case, complete drying can be achieved more rapidly. The fact that the dehumidifier used had a relatively small capacity (0.6 $kg.h^{-1}$ for a floor area of 13 m^2), induced that the influence of a dehumidifier was significant only when 80% of the initial water has already evaporated. In addition, it was seen with the model developed for the evaporation of water on the floor that the water surface repartition is important. If water accumulates at some positions where the floor is damaged or badly designed, water will remain even after some hours of drying.

ACKNOWLEDGEMENT

The research leading to this result has received funding from the French National Research Agency (EcoSec Project, ANR-12-ALID-0005-04)

REFERENCES

Bimbenet J.-J., Duquenoy A., Trystram G. 2002. Génie des procédés alimentaires : Des bases aux applications.

Carpentier B., Cerf O. 2011. Review — Persistence of Listeria monocytogenes in food industry equipment and premises. *International Journal of Food Microbiology* 145: 1-8

Chandra S., Marzo M. d., Qiao Y. M., Tartarini P. 1996. Effect of liquid-solid contact angle on droplet evaporation. *Fire Safety Journal* 27: 141-58

Muhterem-Uyar M., Dalmasso M., Bolocan A. S., et, al. 2015. Environmental sampling for Listeria monocytogenes control in food processing facilities reveals three contamination scenarios. *Food Control* 51: 94–107

Vogel B. F., Huss H. H., Ojeniyi B., Ahrens P., Gram L. 2001. Elucidation of Listeria monocytogenes contamination routes in cold-smoked salmon processing plants detected by DNA-based typing methods. *Appl. Environ. Microbiol.* 67: 2586–95

Zoz F., Iaconelli C., Lang E., Iddir H., Guyot S., Grandvalet C., Gervais P., Beney L. 2016. Control of Relative Air Humidity as a Potential Means to Improve Hygiene on Surfaces: A Preliminary Approach with Listeria monocytogenes. *Plos One* 11

APPENDIX

Equations:

Heat balance on a non-heated stainless steel plate (thermal inertia neglected, thermal conductivity of the plate supposed infinite):

$$(h_r + h_c) \cdot (T_a - T_{pl}) = \beta_c \cdot k \cdot \Delta H_v \cdot \left(C_{sat(T_{pl})} - C_{wa(T_a)}\right)$$

corresponds to the saturated vapor concentration which is a function of the local temperature of the surface. It can be determined by the following fitting function for temperature between 0°C and 20°C:

$$C_{sat}(T) = a + b \cdot T + c \cdot T^2$$

where $a = 4.84 \cdot 10^{-3}$ kg.m^{-3}, $b = 2.94 \cdot 10^{-4}$ kg.m^{-3}.°C^{-1} and $c = 1.58 \cdot 10^{-5}$ kg.m^{-3}.°C^{-2}

$$h = h_r + h_c$$

$$h_r = 4\sigma\left(\varepsilon_{inox} + \beta(\varepsilon_{water} - \varepsilon_{inox})\right) \cdot (T_a + 273.15)^3$$

$$\beta c = \frac{S_{cap}}{S}$$

$$h \cdot (T_a - T_{pl}) = \beta_c \cdot k \cdot \Delta H_v \cdot \left(a + b \cdot T_{pl} + c \cdot {T_{pl}}^2 - \left(a + b \cdot T_a + c \cdot {T_a}^2\right) \cdot RH\right)$$

The wet bulb equation gives:

$$h_c \cdot (T_a - T_{wb}) = k \cdot \Delta H_v \cdot (a + b \cdot T_{wb} + c \cdot {T_{wb}}^2 - (a + b \cdot T_a + c \cdot {T_a}^2) \cdot RH)$$

$$\left(a + b \cdot T_a + c \cdot {T_a}^2\right) \cdot RH = -\frac{h_c \cdot (T_a - T_{wb})}{k \cdot \Delta H_v} + a + b \cdot T_{wb} + c \cdot {T_{wb}}^2$$

The relation between β_c and T_{pl} can be expressed by:

$$\beta_c = \frac{h \cdot (T_a - T_{pl})}{k \cdot \Delta H_v \left(a + b \cdot T_{pl} + c \cdot {T_{pl}}^2 + \frac{h_c \cdot (T_a - T_{wb})}{k \cdot \Delta H_v} - \left(a + b \cdot T_{wb} + c \cdot {T_{wb}}^2\right)\right)}$$

$$\beta_c = \frac{(T_a - T_{pl})}{\frac{k \cdot \Delta H_v}{h}\left(b \cdot T_{pl} + c \cdot {T_{pl}}^2 - b \cdot T_{wb} - c \cdot {T_{wb}}^2\right) + \frac{h_c}{h} \cdot (T_a - T_{wb})}$$

$$\beta_c = \frac{(T_a - T_{pl})}{\frac{k \cdot \Delta H_v}{h}\left(b \cdot \left(1 + \frac{c}{b}(T_{pl} + T_{wb})\right)\right) \cdot (T_{pl} - T_{wb}) + \frac{h_c}{h} \cdot (T_a - T_{wb})}$$

To have the plate temperature, the following development is performed:

$$\frac{T_a - T_{pl}}{T_a - T_{wb}} = \frac{\beta_c \left(\frac{h_c}{h} + \frac{b \cdot k \cdot \Delta H_v}{h} \left(1 + \frac{c}{b} \left(T_{pl} + T_{wb} \right) \right) \right)}{1 + \frac{b \cdot k \cdot \Delta H_v}{h} \left(1 + \frac{c}{b} \left(T_{pl} + T_{wb} \right) \right) \cdot \beta_c}$$

$$(T_a - T_{pl}) \cdot \left(1 + \delta_1 \cdot \left(1 + \frac{c}{b} \left(T_{pl} + T_{wb} \right) \right) \cdot \beta_c \right) = \beta_c \left(\frac{h_c}{h} + \delta_1 \cdot \left(1 + \frac{c}{b} \left(T_{pl} + T_{wb} \right) \right) \right) \cdot (T_a - T_{wb})$$

where $\delta_1 = \frac{b \cdot k \cdot \Delta H_v}{h} = \frac{b \cdot \Delta H_v}{\rho . Cp_{air} . Le^{2/3}}$

$$T_{pl} \cdot \left(T_a \cdot \delta_1 \cdot \beta_c \cdot \frac{c}{b} \right) + T_a \left(1 + \beta_c \cdot \delta_1 \left(1 + \frac{c}{b} T_{wb} \right) \right) - {T_{pl}}^2 \cdot \left(\beta_c \cdot \delta_1 \frac{c}{b} \right) - T_{pl} \cdot \left(1 + \beta_c \cdot \delta_1 \left(1 + \frac{c}{b} T_{wb} \right) \right) = (T_a - T_{wb}) \left(\frac{h_c}{h} + \delta_1 \left(1 + \frac{c}{b} T_{wb} \right) \right) \beta_c + \delta_1 \frac{c}{b} \beta_c \cdot (T_a - T_{wb}) \cdot T_{pl}$$

$${T_{pl}}^2 \left(-\delta_1 \frac{c}{b} \cdot \beta_c \right) + T_{pl} \cdot (-1 - \delta_1 \cdot \beta_c) + T_a \left(1 + \delta_1 \left(1 + \frac{c}{b} T_{wb} \right) \beta_c \right) - (T_a - T_{wb}) \left(\frac{h_c}{h} + \delta_1 \left(1 + \frac{c}{b} T_{wb} \right) \right) \beta_c = 0$$

We obtain the following equation

$$c' \cdot {T_{pl}}^2 + b' \cdot T_{pl} + a' = 0$$

where

$$c' = -\delta_1 \frac{c}{b} \cdot \beta_c$$

$$b' = -1 - \delta_1 \cdot \beta_c$$

$$a' = T_a \left(1 + \delta_1 \left(1 + \frac{c}{b} T_{wb} \right) \beta_c \right) - (T_a - T_{wb}) \left(\frac{h_c}{h} + \delta_1 \left(1 + \frac{c}{b} T_{wb} \right) \right) \beta_c$$

With the following expression for the plate temperature T_{pl}:

$$T_{pl} = \frac{-b' - \sqrt{b'^2 - 4a'c'}}{2c'}$$

And the evaporation rate:

$$\dot{m} = \frac{S \cdot \left(T_a - T_{pl} \right) \cdot h}{\Delta H_v}$$

CHAPITRE 5 : ETUDE DU SECHAGE APRES NETTOYAGE DANS UN ATELIER AGRO-ALIMENTAIRE ET DE SON INFLUENCE SUR LA PROLIFERATION BACTERIENNE

5.1. Article 5 : Simplified heat and mass transfer modeling in a food processing plant (Journal of Food Engineering, 171: 1-13)

Simplified heat and mass transfer modeling in a food processing plant

L. Lecoq [abc*], D. Flick [bc], E. Derens [a], H.M. Hoang [a], O. Laguerre [a]

[a] Irstea, UR GPAN, 1 rue Pierre-Gilles de Gennes, 92761 Antony, France

[b] AgroParisTech, UMR1145 Ingénierie Procédés Aliments, F-75005 Paris, France

[c] INRA, UMR1145 Ingénierie Procédés Aliments, F-91300 Massy, France

ABSTRACT

Inside a food production plant, bacteria can grow particularly in zones of high humidity leading to deterioration of food quality and safety. Cleaning and disinfection are currently practiced to reduce this hazard. However it is not always efficient; stagnant water is susceptible to be a source of microbial growth. To prevent this problem, drying must be performed but water may still not entirely evaporate at some locations. In order to optimize the drying process, a simplified heat and mass transfer model was developed in this study. Validation was performed by comparing the predicted water weight evolutions with the ones measured in a food processing plant. From model predictions, it was found that by reducing the air inlet relative humidity from 85% to 50%, the time needed to evaporate 90% of the initial water weight could be reduced by a factor of about 1.5. This shows the interest to dry the inlet air.

Key words: heat transfer, mass transfer, model, food production plant, drying, water residues

Highlights:

►Water residues in food production plants can be a source of microbial growth
►A simplified heat and mass transfer model for a food production plant was developed
►The model predicts well water weight evolutions and air temperature during drying
►This study can help to define optimized conditions to dry food production plants

* Corresponding author: Tel: 33 1 40 96 90 04, Fax: 33 1 40 96 60 75, E-mail: logan.lecoq@irstea.fr

Nomenclature

a	Coefficient of the water content linearization	$kg_{water}.kg_{dry\ air}^{-1}.K^{-1}$
b	Coefficient of the water content linearization	$kg_{water}.kg_{dry\ air}^{-1}$
Cp_a	Specific heat capacity of air	$J.kg^{-1}.K^{-1}$
mC	Heat capacity of materials	$J.K^{-1}$
h	Heat transfer coefficient	$W.m^{-2}.K^{-1}$
k	Mass transfer coefficient	$m.s^{-1}$
Le	Lewis number	Dimensionless
m	Mass of water	kg
$\dot{m}$	Air mass flow rate	$kg.s^{-1}$
$\dot{m}_e$	Water (liquid) supply rate on the equipment	$kg.s^{-1}$
P_{max}	Maximal power of the evaporator	W
$\dot{Q}_e$	Heat produced by the equipment	W
Re	Reynolds number	Dimensionless
RH	Relative humidity	Dimensionless
S	Total surface area	m^2
T	Temperature	°C or K
X	Water content	$kg_{water}.kg_{dry\ air}^{-1}$
α, γ	Air distribution coefficient	Dimensionless
$\beta = \frac{S_{wet}}{S}$	Ratio between wet and total surface	Dimensionless
λ	Thermal conductivity	$W.m^{-1}.K^{-1}$
ρ	Air density	$kg.m^{-3}$
ΔH_v	Heat of water vaporisation	$J.kg^{-1}$

Subscripts

a	air	ext	external	th	thermostat	0	initial time
e	equipment	f	floor	w	wall		

1. Introduction

Listeria Monocytogenes is a serious foodborne pathogen which causes 10 to 20% of fatality (EFSA 2015). Most of the time it is induced by eating contaminated ready-to-eat foods which appears firstly inside the food factories and then could increase along the cold chain. *L. monocytogenes* can grow as long as the water activity is above 0.92, pH between 4.6 and 9.5 and low temperature condition (few degrees below 0°C) (Buchanan et al. 2004). This bacteria can resist against cleaning, especially when only low concentration of disinfection is applied which allows *L. monocytogenes* to adapt to these products (Muhterem-Uyar et al. 2015). Food soil on the floor, hygiene management strategies and equipment design are also important factors (Bridier et al. 2015, Carpentier & Cerf 2011, Ferreira et al. 2014, Gerba 2015, Malley et al. 2015). Thus, cleaning and disinfection must be performed in an efficient way. Stagnant water or high air relative humidity (Likotrafiti et al. 2013) are favorable conditions for bacterial growth. Air dehumidification and water evaporation must be performed properly during drying process (just after cleaning) to limit the contamination. It is thus important to understand the heat and mass transfer phenomena during this drying period to avoid stagnant water and high relative humidity in the plants.

The main objective of this study is to develop a simplified heat and mass transfer model for the drying process in a food plant. This model allows the prediction of the evaporation rate at different positions in the plant (walls, floor and equipment) according to the operating conditions such as temperature, velocity and humidity of the inlet blown air, the initial temperature and water load inside the plant. In this way, the risk zones (warm and humid positions) can be identified. After the model validation by comparing the experimental and calculated water weight and temperature evolutions during the drying process of a food production plant, it can be used to predict the results when some technical improvements are proposed such as the use of dehumidified air or higher air flow rates. The developed model can also be used not only during the drying period but also during the production period.

In the future, this model will be combined with the ones already developed by our team for cold room (Laguerre et al. 2014), refrigerated vehicle (Hoang et al. 2012), display cabinet (Laguerre et al. 2012) and domestic refrigerator (Laguerre & Flick 2010) to describe the product time-temperature history from a food production plant to a domestic refrigerator. These models will be combined with a predictive microbiological model to predict the evolution of microbial load until consumption.

2. Literature review

For better understanding the heat and water exchanges in a production plant, the literature review of two topics was carried out: droplet evaporation on a solid surface and heat/water transfer in refrigerating equipment.

When water droplets are deposited on solid surfaces, different steps occur during evaporation. First the contact angle (air/water/solid) decreases while the surface occupied by water on the solid stays constant. Once this angle reaches a minimal value, it stays constant while the water surface decreases until the end of the evaporation (Chandra et al. 1996, D'agaro et al. 2006). Therefore, the change of evaporation rate when the water surface decreases (Navaz et al. 2008, Vik & Reif 2011) has to be considered. It was observed that air velocity, relative humidity and temperature difference between the air and the water surface have a major role

in evaporation (Raimundo et al. 2014). Low relative humidity makes the evaporation much faster, and as a consequence, less favorable environment for bacterial growth.

Several numerical approaches can be used to predict temperature and velocity in refrigerating equipment. Computational Fluid Dynamic (CFD) approach is often used allowing the understanding of heat and mass transfer phenomenon inside complex environment and the calculation of local parameters: temperature, humidity, air velocity, heat transfer coefficients (Delele et al. 2008, Hoang et al. 2015, Hu & Sun 2000, Hu & Sun 2001). In configurations similar to refrigerated food production plants, non-uniform airflow, temperature and moisture inside the plant was observed (Mirade & Daudin 2006). This uneven distribution of airflow is related to the presence of products and equipment (Ho et al. 2010) which induces a variation in the heat transfer coefficient at different locations (Flick et al. 1999, Mirade 2007). Mirade (2007) carried out 3D simulations (k-ε, k-ω models) in a pilot ripening room (84 m^3, air flow rate 1600 $m^3.h^{-1}$, air temperature 13°C and 86% relative humidity at the blowing duct) filled with cheese-like obstacles (empty cans, 10 cm diameter, 4.4 cm high). Air velocity ranging from 0.05 to 0.40 $m.s^{-1}$, temperature from 13.0 to 14.0°C and relative humidity from 90 to 97% were observed (experimentally and numerically) around and inside the stacks. These variations explain the threefold increase in the heat and water transfer coefficients from one position to another. The product position with maximum/minimum water loss was predicted. The variation of product moisture loss leads to heterogeneity of product quality. The comparison between experimental and numerical results showed good agreement. The CFD approach gives a detailed description of heat and mass exchange phenomena but it requires a high number of cells leading to long calculation time.

In complementarity of the CFD approach, some authors proposed simplified models: cold room (Laguerre et al. 2014, Wang & Touber 1990), domestic refrigerator (Laguerre & Flick 2010), display cabinet (Laguerre et al. 2012) and refrigerated vehicle (Hoang et al. 2012). According to our knowledge, no simplified model is available for a production plant.

3. Experiment in food factory

The experiment was carried out in a production plant of chilled foods during the drying period (Figure 1). The ambient conditions (temperature, relative humidity, air velocity, water weight) were measured. Parts of these data were used for the simplified model construction.

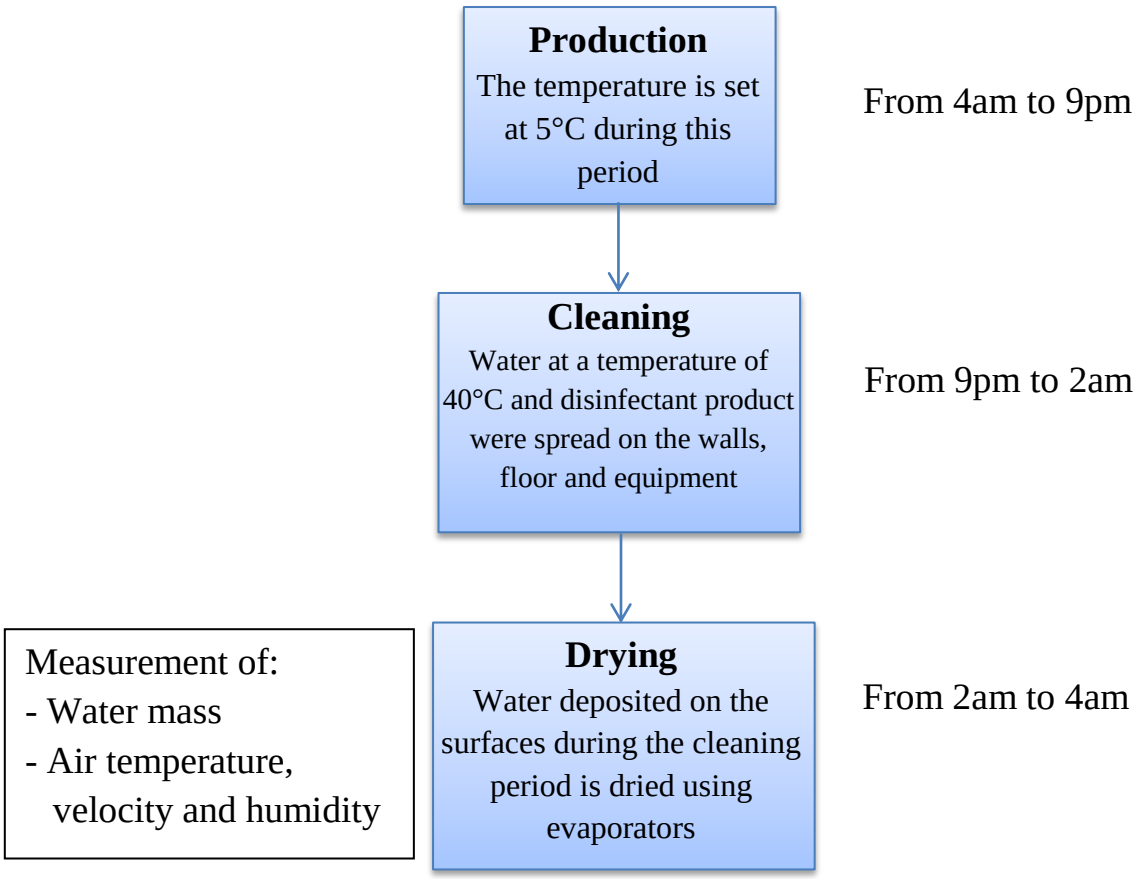

Figure 1: Different daily operations in the production plant investigated

3.1. Description of the production room

The dimension of the production room of chilled products was 17.1m long, 8.2m wide and 3.6m high (Figure 2). Low temperature was maintained in this room using three evaporators located at the ceiling. Air was blown from the center both to the left and the right, the return air was at the bottom of the evaporator. The configuration was almost the same along the room; therefore in the following text, a depth of one meter long was considered. In this section, the air flow rate was 8600 $m^3.h^{-1}$ (cross section of the inlet air 1.2 m^2 and average inlet velocity 2.0 $m.s^{-1}$).

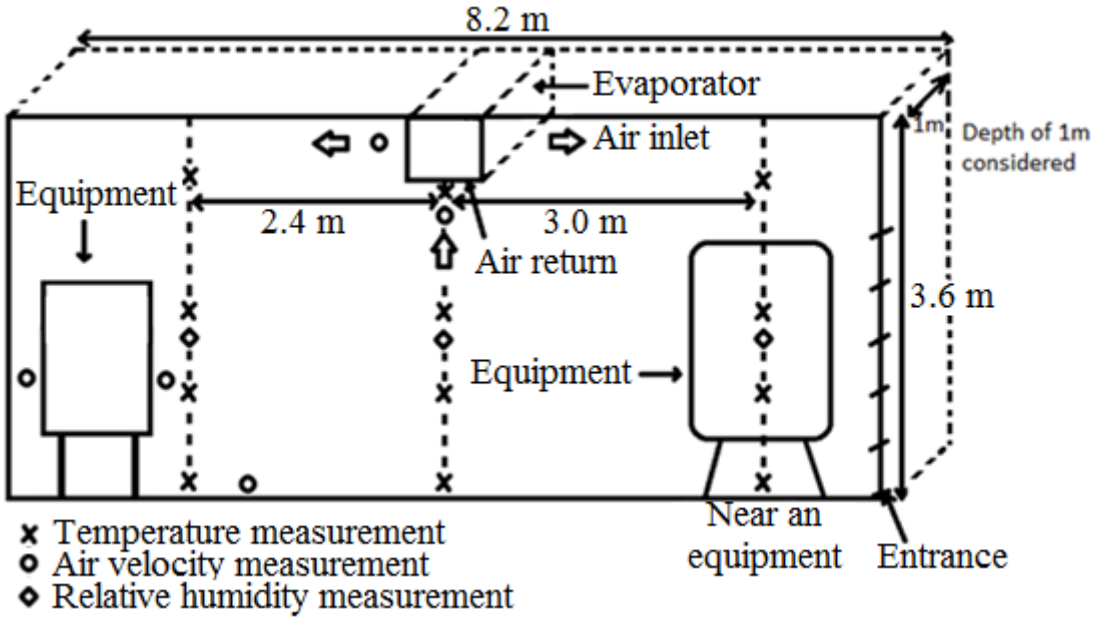

Figure 2: Scheme of the food production room (side view, with the measurement points)

3.2. Water weight measurement

After cleaning by warm water (40°C) in the production room, the water weight at various surfaces: wall, floor and equipment, was measured at different times.

To measure the water weight, paper towelettes were used to wipe a 50cm x 50cm surface on wall, floor and equipment. The same manipulation was repeated every 30 min on neighboring surfaces until 90 min. The evolution of water weight at different positions was followed by weighting the towelettes.

To avoid as much as possible the variability of the result due to water wiping manner, the same person swabbed the wet area several times until that water was totally removed. To ensure that the same surface area was treated, a square frame (50cm x 50cm) was placed on the measurement position before the water swabbing. After swabbing, the towelettes were deposited in a plastic bag, air inside the bag was eliminated by pressing before the bag closing. The towelettes in the bag were weighted, as soon as possible, using an electronic balance (Sartorius, CPA34001P, +/- 0.1 g).

Because of the difficulty to carry out measurements in a real food plant, only one location could be analyzed for each position (wall, floor, equipment) considered as “representative” in spite that the initial water load and the transfer intensity can vary over a surface. The analysis of such heterogeneities is out of the scope of the present study.

3.3. Temperature measurement

Temperature was recorded at 12 points in the room every min only from 70 min to 120 min after the beginning of drying because of the difficulties of measurement. The sensors were put underneath the return air, at 2.4 m and 3.0 m from the room center and at different heights (0.2 m, 1.0 m, 1.8m, 3.0 m, see Figure 2).

3.4. Relative humidity measurement

Relative humidity was measured every minute from 70 min to 120 min (using TESTO 174H hygrometers) at three points in the room at a height of 1.5 m (see Figure 2). These sensors were put at the same positions as the temperature recorders.

3.5. Velocity measurement

Air velocity was measured at five points using a hot wire anemometer (TESTO 435-2, range of measurement 0-20 $m.s^{-1}$): return air grill, in front of evaporator, near the wall, floor and equipment (see Figure 2). These measurements will be used to estimate the convective heat transfer coefficients between air and wall, floor and equipment. The average air velocity was calculated from 60 measured values (every 1s over 1min).

4. Simplified heat and mass transfer model

The model structure based on the data collected from the factory (geometry, air velocity, temperature, humidity, water weight, materials…) is shown in Figure 3. This model allows the prediction of the temperature and water weight evolutions.

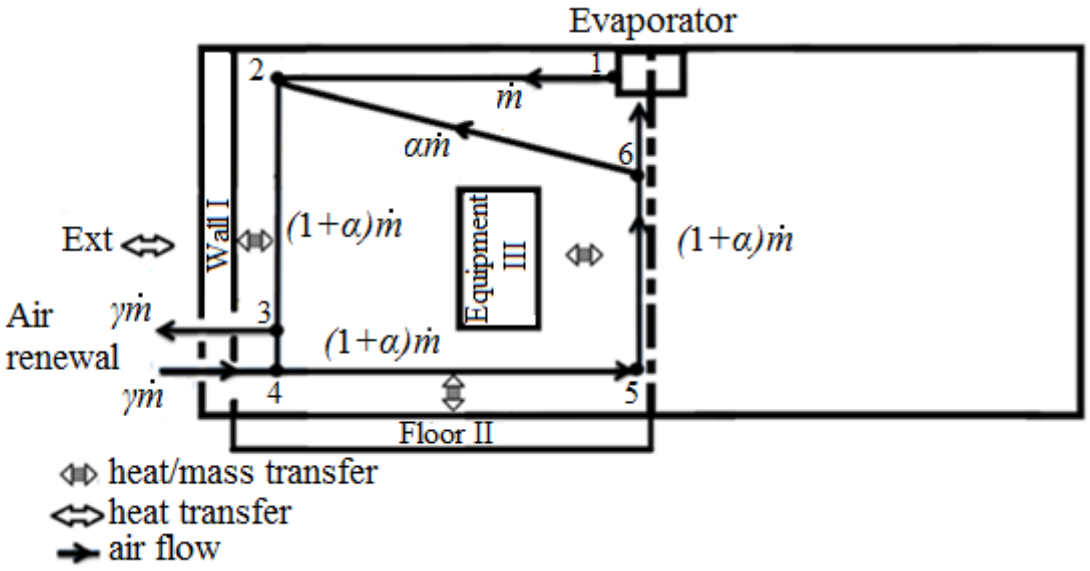

Position	Parameters at the position
1	T_1, X_1
2	T_2, X_2
3	T_3, X_3
4	T_4, X_4
5	T_5, X_5
6	T_6, X_6
I	S_w, $(mC)_w$, T_w, X_w, m_w, k_w, h_w, β_w, S_{ext}, h_{ext}
II	S_f, $(mC)_f$, T_f, X_f, m_f, k_f, h_f, β_f
III	S_e, $(mC)_e$, T_e, X_e, m_e, k_e, h_e, β_e
Ext	T_{ext}, X_{ext}

Figure 3: Simplified airflow, heat and mass transfer model in a food factory (side view)

Only a half of the room is studied considering the same phenomena in the other half (symmetry). Air is blown from the evaporator located on the ceiling, it flows downward near

the wall (I) then toward the center along the floor (II) and finally upward to the return air grill (under the evaporator) along the equipment (III). The entrainment of air by the blown air (which constitutes a wall jet) in front of the evaporator is characterized by the coefficient of air distribution α. The air renewal is characterized by the coefficient γ.

4.1. Heat and mass balance equations

To simplify the model, the thermal inertia of the air was neglected compared to the ones of the wall, floor and equipment. The symbols: ⇚⇛ (Figure 3) in front of the rectangles I, II and III represent the heat and water exchange zones between air/wall, air/floor and air/equipment, respectively. The heat loss through the wall and the air renewal (exchange with external air) were also considered. Heat exchanges by radiation where neglected compared to convection. Indeed the average temperature is relatively low, the emissivities of most of the surfaces (stainless steel equipment for example) are rather low and the temperature difference of the surfaces radiating each on the other is limited at a given time. The heat and water exchanges at several positions are analyzed below and the equations are reported in Tables 1 to 4:

4.1.1. Heat balance on airflow (Table 1)

Mixing of inlet-air (T_1) and return air (T_6): The air near the wall (temperature T_2; water content X_2; mass flow rate $(1+\alpha)\dot{m}$) is a mix of the inlet air (from the evaporator; temperature T_1; water content X_1; mass flow rate $\dot{m}$) and a part of the return air (temperature T_6; water content X_6; mass flow rate $\alpha\dot{m}$).

Heat exchange between the air and the wall (rectangle I): Convective exchange (heat transfer coefficient h_w) takes place between the air (temperature T_2) and the wall (temperature T_w). After this exchange, the air temperature is T_3.

Mixing with the external air (T_{ext}): After the exchange with the wall, the air is partially renewed with external air (temperature T_{ext}; water content X_{ext}; mass flow rate $\gamma\dot{m}$).

Heat exchange between the air and the floor (rectangle II) and between the air and the equipment (rectangle III): the same procedure as that of the wall was applied.

Table 1: Heat balance equations at several positions in air (see Figure 3 for the position)

Position	Balance	Equation
1-2	*Mixing of inlet-air (T_1) and return air (T_6)*	$T_1 + \alpha T_6 = (1+\alpha)T_2$
2-3	*Heat exchange between the air and the wall*	$\delta_w \cdot T_2 - T_3 = -(1-\delta_w)\cdot T_w$ where $\delta_w = e^{-\frac{h_w \cdot S_w}{(1+\alpha)\cdot \dot{m}\cdot Cp_{air}}}$
3-4	*Mixing with the external air (T_{ext})*	$(1+\alpha-\gamma)\cdot T_3 - (1+\alpha)\cdot T_4 = -\gamma \cdot T_{ext}$
4-5	*Heat exchange between the air and the floor*	$\delta_f \cdot T_4 - T_5 = -(1-\delta_f)\cdot T_f$ where $\delta_f = e^{-\frac{h_f \cdot S_f}{(1+\alpha)\cdot \dot{m}\cdot Cp_{air}}}$
5-6	*Heat exchange between the air and the equipment*	$\delta_e \cdot T_5 - T_6 = -(1-\delta_e)\cdot T_e$ where $\delta_e = e^{-\frac{h_e \cdot S_e}{(1+\alpha)\cdot \dot{m}\cdot Cp_{air}}}$

4.1.2. Mass balance on airflow (Table 2)

The same procedure as that of the heat exchanges was applied to develop the water exchange equations.

The evaporation rate is assumed to be proportional to the wet surface and the difference of water concentration in the air in equilibrium with water (at surface temperature) and the air circulating in the vicinity of the surface.

Table 2: Mass balance equations at several positions in air

Position	Balance	Equation
1-2	*Mixing of inlet-air (X_1) and return air (X_6)*	$X_1 + \alpha X_6 = (1+\alpha)X_2$
2-3	*Water exchange between the air and the wall*	$\delta_w' \cdot X_2 - X_3 = -(1-\delta_w') \cdot (a_w.T_w + b_w)$ *where* $\delta_w{}' = e^{-\frac{k_w \cdot \beta_w \cdot S_w \cdot \rho}{(1+\alpha)\cdot \dot{m}}}$
3-4	*Mixing with the external air (Xext):*	$(1+\alpha-\gamma) \cdot X_3 - (1+\alpha) \cdot X_4 = -\gamma \cdot X_{ext}$
4-5	*Water exchange between the air and the floor*	$\delta_f' \cdot X_4 - X_5 = -\left(1-\delta_f'\right) \cdot X_f$ $= -\left(1-\delta_f'\right) \cdot \left(a_f.T_f + b_f\right)$ *where* $\delta_f{}' = e^{-\frac{k_f \cdot \beta_f \cdot S_f \cdot \rho}{(1+\alpha)\cdot \dot{m}}}$
5-6	*Water exchange between the air and the equipment*	$\delta_e' \cdot X_5 - X_6 = -(1-\delta_e') \cdot X_e$ $= -(1-\delta_e') \cdot (a_e.T_e + b_e)$ *where* $\delta_e{}' = e^{-\frac{k_e \cdot \beta_e \cdot S_e \cdot \rho}{(1+\alpha)\cdot \dot{m}}}$

4.1.3. Evaporator (Table 3)

Ideally, the temperature at the return air grill (T_6) is supposed to be the thermostat setting temperature T_{th}, however it is limited by P_{max} which is the maximal power that the evaporator can reach. The evaporator power is equal to the sum of the sensible heat (air cooling) and the latent heat (water vapor condensation).
The relative humidity of the inlet air RH_1 (coming from the evaporator) is assumed to be known (in absence of air dehumidifier, RH_1 is often around 85%). The water content of inlet air can be calculated from RH_1 and T_1.

Table 3: Evaporator

Position	Balance	Equation
1-6	*Power and temperature control*	if; $\dot{m}\left(Cp_{air}(T_{th}-T_1) + \Delta H_v(X_6-X_1)\right) > P_{max}$ $(T_6-T_1) + \frac{\Delta H_v}{Cp_{air}}(X_6-X_1) = \frac{P_{max}}{\dot{m} \cdot Cp_{air}}$ Otherwise: $T_6 = T_{th}$
1	*Relative humidity*	$X_1 - RH_1 \cdot a_1 \cdot T_1 = b_1 \cdot RH_1$

4.1.4. Heat and mass balance on wall, floor and equipment (Table 4)

The variation of the internal energy of the wall depends on the heat exchange by convection with air outside the room and the heat and water exchanges with the air inside the room. The same procedure was applied to the floor and equipment.

Table 4: Heat and mass balances on wall, floor and equipment

Position	Balance	Equation
rectangle I	*Temperature evolution of the wall (rectangle I)*	$\frac{dT_w}{dt} = \frac{h_{ext} \cdot S_{ext}}{(mC)_w}(T_{ext} - T_w) - \frac{(1+\alpha) \cdot \dot{m} \cdot Cp_{air}}{(mC)_w}(T_3 - T_2) - \frac{(1+\alpha) \cdot \dot{m} \cdot \Delta H_v}{(mC)_w}(X_3 - X_2)$
rectangle II	*Temperature evolution of the floor (rectangle II)*	$\frac{dT_f}{dt} = -\frac{(1+\alpha) \cdot \dot{m} \cdot Cp_{air}}{(mC)_f}(T_5 - T_4) - \frac{(1+\alpha) \cdot \dot{m} \cdot \Delta H_v}{(mC)_f}(X_5 - X_4)$
rectangle III	*Temperature evolution of the equipment (rectangle III)*	$\frac{dT_e}{dt} = -\frac{(1+\alpha) \cdot \dot{m} \cdot Cp_{air}}{(mC)_e}(T_6 - T_5) - \frac{(1+\alpha) \cdot \dot{m} \cdot \Delta H_v}{(mC)_e}(X_6 - X_5) + \frac{\dot{Q}_e}{(mC)_e}$ where $\dot{Q}_e$ is the heat generation by the equipment during the production period. Following parameters were defined (eq. 10 to 12, see Appendix): $\tau_i = \frac{(mC)_i}{(1+\alpha) \cdot \dot{m} \cdot Cp_{air}}$ $\tau_{ext} = \frac{(mC)_w}{h_{ext} \cdot S_{ext}}$ $\varepsilon_i = \frac{(mC)_i}{(1+\alpha) \cdot \dot{m} \cdot \Delta H_v}$ where *i=w, f, e*
rectangle I	*Water weight evolution on the wall (rectangle I)*	$\frac{dm_w}{dt} = -(1+\alpha) \cdot \dot{m} \cdot (X_3 - X_2)$
rectangle II	*Water weight evolution on the floor (rectangle II)*	$\frac{dm_f}{dt} = -(1+\alpha) \cdot \dot{m} \cdot (X_5 - X_4)$
rectangle III	*Water weight evolution on the equipment (rectangle III)*	$\frac{dm_e}{dt} = -(1+\alpha) \cdot \dot{m} \cdot (X_6 - X_5) + \dot{m}_e$ where $\dot{m}_e$ is the liquid water introduced at the equipment level during the production period because of rinsing for example.

4.1.5. Wet surface

The coefficient β, defined as the ratio of wet and total surface, varies with time because it depends on the water mass by unit area. Supplementary experiments were carried out to study the evolution of the wet surface during water evaporation. These experiments, conducted inside a wind tunnel, showed that β starts decreasing when the water weight is around 25% of its initial value and tends to zero when all the water is evaporated (Figure 4).

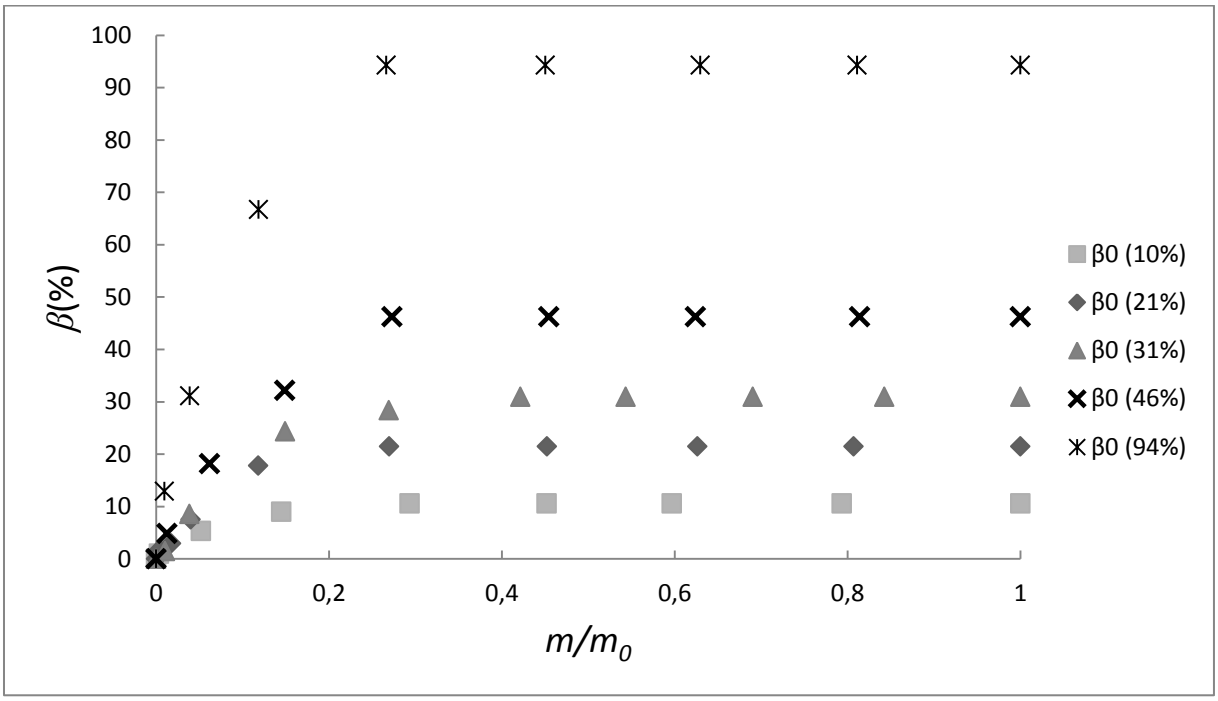

Figure 4: Evolution of the wet surface over the total surface (β) in function of the water weight. Experiments performed inside a wind tunnel at a relative humidity of 51%, air temperature of 4.2°C and airflow velocity of 1.0 m.s^{-1} with different initial values of β_0: 10, 21, 31, 46 and 94%

Therefore, it was assumed that β remains constant (equals β_0) until $m(t) = 0.25 \cdot m_0$, and then β decreases linearly with $\frac{m(t)}{m_0}$:

$$\beta(t) = \min\left(\beta_0, \frac{m(t)}{0.25 \cdot m_0} \cdot \beta_0\right) \quad (1)$$

4.2. Matrix form of the equations

Temperature and water weight for the wall, floor and equipment are summarized in vector $\vec{Y}$. Air temperature and water content constitute vector $\vec{Z}$. The additional heat and water generation during production period are grouped on vector $\vec{W}$:

$$\vec{Y}=\begin{bmatrix} T_w \\ T_f \\ T_e \\ m_w \\ m_f \\ m_e \end{bmatrix} \quad (2) \qquad \vec{Z}=\begin{bmatrix} T_1 \\ T_2 \\ T_3 \\ T_4 \\ T_5 \\ T_6 \\ X_1 \\ X_2 \\ X_3 \\ X_4 \\ X_5 \\ X_6 \end{bmatrix} \quad (3) \qquad \vec{W}=\begin{bmatrix} \dot{Q}_e \\ \dot{m}_e \end{bmatrix} \quad (4)$$

The equations developed previously can be summarized in matrix form by the following equations:

$$\frac{d\vec{Y}}{dt}=\bar{\bar{A}}\vec{Z}+\bar{\bar{B}}\vec{Y}+\vec{C}T_{ext}+\bar{\bar{D}}\vec{W} \quad (5)$$

$$\bar{\bar{E}}\vec{Z}=\bar{\bar{F}}\vec{Y}+\vec{G}T_{ext}+\vec{H}X_{ext}+\vec{I}T_{th}+\vec{J} \quad (6)$$

with $\bar{\bar{A}},\bar{\bar{B}},\vec{C},\bar{\bar{D}},\bar{\bar{E}},\bar{\bar{F}},\vec{G},\vec{H},\vec{I},\vec{J}$ matrices or vectors involving several parameters which depend on the air flow rate, the heat and mass transfer coefficients, the proprieties of the wall, floor, equipment and the air (see Appendix). The percentages of wet surface (β) also appear in some of these matrices.

The equations 5 and 6 were solved using Matlab software (vR2012a; The MathWorks Inc., Natick, MA, USA, Runge-Kutta 2nd order method). The computation time is less than one minute with a computer i5-3570 CPU 340 GHz.

The corresponding matrices of these equations are presented in the appendix.

4.3. Input parameters estimation

4.3.1. Estimation of the air distribution coefficients γ and α

Because of the difficulties to estimate the coefficients α and γ experimentally, they were taken from the literature. The γ coefficient corresponds to the air renewal inside the food production room. For a ham production plant, Billiard (1998) reported an air renewal coefficient γ around 4%. The α coefficient, which characterizes the effect of air distribution in front of the fans of the evaporator, is assumed to be 30% (Rajatnam 1976). These values were used in our simulation. However, to study the impact of these coefficients on the result (shown in section 5.1), two other values were used: 1% and 10% for γ, 10% and 50% for α.

4.3.2. Estimation of the initial water weights, the maximal power and the air relative humidity at the inlet (RH_1)

Only the initial water weight on the floor was measured. For the wall and equipment, the initial water weight was obtained by extrapolation of the measured values (from about 20 min to 90 min). The results are shown in Table 5.

Table 5: Estimated value of the initial water weight and temperature for the wall, floor and equipment.

	m_0/S (g.m^{-2})	T_0 (°C)
Wall	24	15.5
Floor	470	35.0
Equipment	100	39.8

Due to our expertise, the maximal power of the evaporator (P_{max}) is about 3000W. During the drying period, the average air relative humidity is 85% at the air inlet in the room, RH_1 (outlet of evaporator).

4.3.3. Estimation of the initials temperatures (of the wall, floor and equipment)

It was not possible to measure the initials temperatures of the wall, floor and equipment on the day of experiment. To obtain this data, the following approach was considered:

During the cleaning period, water is spread out over the room at a temperature of 40°C (T_{hw}), whereas the air temperature remains around 10°C (Figure 5).

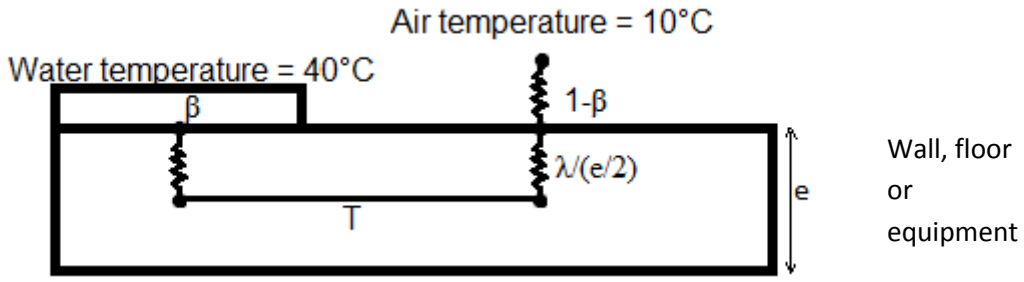

Figure 5: Scheme of the heat transfer phenomena during the cleaning period

Knowing the thermal inertia, the thermal conductivity (λ) and thickness (e) of the wall, floor and equipment, their temperatures can be calculated after five hours, corresponding to the beginning of the drying. The main hypothesis is that during the cleaning period, the water surfaces covering the wall, floor and equipment are equals to the ones at the beginning of the drying period (β_{w0}, β_{f0}, β_{e0}). At the beginning of cleaning, the surfaces are assumed to be near the room temperature during production: 5°C. The equation 7 is solved to obtain the wall, floor and equipment temperatures at the beginning of the drying process (end of cleaning):

$$mC\frac{dT}{dt} = S \cdot \beta \frac{\lambda}{e/2}(T_{hw} - T) + \frac{(1-\beta)\cdot S}{\frac{1}{h} + \frac{e/2}{\lambda}}(T_a - T) \quad (7)$$

The calculated temperatures are shown table 5.

4.3.4. Estimation of the heat and mass transfer coefficients

Additional experiments were conducted in a laboratory test room (length x width x height = 3.4m x 3.4m x 2.5m) inside which air velocities could be controlled. These velocities are of the same order of magnitude as the ones in the production plant. The convective heat transfer coefficient between air/floor and air/walls, *h*, was measured at different air velocities using a convective fluxmeter (Trade name Captec, width x height x depth: 4 cm x 4 cm x 450 µm). This fluxmeter (emissivity <0.1 to avoid the influence of radiation) was equipped with a thermocouple. Constant heating (0.6 W) was supplied to this fluxmeter. Its temperature and the air temperature were recorded and the coefficient *h* was calculated when a steady state was achieved, using equation 8:

$$h = \frac{\dot{q}}{T_{cf} - T_a} \tag{8}$$

where $\dot{q}$ is the measured convective flux at the surface (W.m^{-2}), T_{cf} the temperature measured by the convective fluxmeter (K) and T_a the surrounding air temperature (K). Results relating the heat transfer coefficient to the velocity are shown in Figure 6.

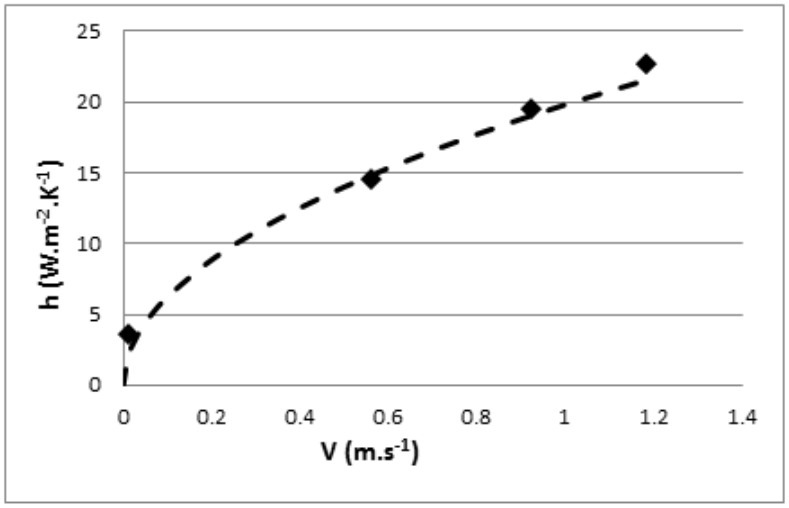

Figure 6: Influence of air velocity on heat transfer coefficient (measurement by fluxmeter inside a laboratory test room).

Thus, by knowing the air velocities, it was possible to estimate the heat transfer coefficient on the different surfaces in the food plant (Table 6).

Table 6: Measured value of the air velocity at the inlet of the evaporator, the return air grill, near the wall, floor, equipment and estimated value of the heat and mass transfer coefficients

	Air velocity ($m.s^{-1}$)	h ($W.m^{-2}.K^{-1}$)	k ($m.s^{-1}$)
Inlet	2.0		
Air return	4.4		
Wall	1.0	20	$17.2 \cdot 10^{-3}$
Floor	0.2	9	$7.7 \cdot 10^{-3}$
Equipment	0.2	9	$7 \cdot 10^{-3}$

The mass transfer coefficients k were calculated using the Lewis analogy:

$$k = \frac{h}{\rho . Cp_{air} . Le^{2/3}} \quad (9)$$

with $Le = \frac{a_{diff}}{D} = \frac{18.6 \cdot 10^{-6}}{21.8 \cdot 10^{-6}} \approx 0.85$

where a_{diff} is the thermal diffusivity of water vapor = $18.6 \cdot 10^{-6}$ $m^2.s^{-1}$ at 0°C and D the mass diffusivity of water vapor in air = $21.8 \cdot 10^{-6}$ $m^2.s^{-1}$ at 0°C (Bimbenet et al. 2002).

4.3.5. Estimation of the coefficients a, b and β

The coefficients a_1, b_1, a_w, b_w, a_f, b_f, a_e, b_e appear (Table 2) because of the linearization of the water content of saturated air versus temperature and are taken from the Antoine equation. They are calculated at each time step. The hypothesis made is that between two time steps of numerical solving, the water content is supposed to increase linearly with the temperature. In our simulation, a time step of one minute was used leading to air temperature increase less than 1°C, therefore this approximation is well verified. The wet surface proportions: β_w, β_f, β_e (Table 2 and equation 1), are also calculated at each time step from the water weights m_w, m_f, m_e.

4.3.6. Other parameters

All the other parameters such as the initial ratios between wet and total surface (β_{w0}, β_{f0}, β_{e0}), the surfaces (S_w, S_f, S_e) or the heat capacities of the wall $(mC)_w$, floor $(mC)_f$ and equipment $(mC)_e$ are shown in Table 7.

Table 7: Numerical values of the simplified model parameters

	β_0(%)	Surface *S* (m²)	Heat capacity *mC* ($J.K^{-1}$)	Thermal conductivity ($W.m^{-1}.K^{-1}$)
Wall	8	3.6	$3.1 \cdot 10^5$	0.9
Floor	100	4.1	$7.1 \cdot 10^5$	0.9
Equipment	20	2.0	$4.8 \cdot 10^4$	26.0

This model can also take into account a heat production ($\dot{Q}_e$) and water supply rate on the equipment ($\dot{m}_e$) during production period. However, in the present study and during drying period, these variables are supposed to be equal to zero.

5. Results and discussion

5.1. Comparison between the experimental and the predicted results

5.1.1. Water weight evolution

The evolutions of the water weight on the wall, floor and equipment obtained with the simplified model were compared to the experimental results obtained in the food production room (Figures 7.a and 7.b).

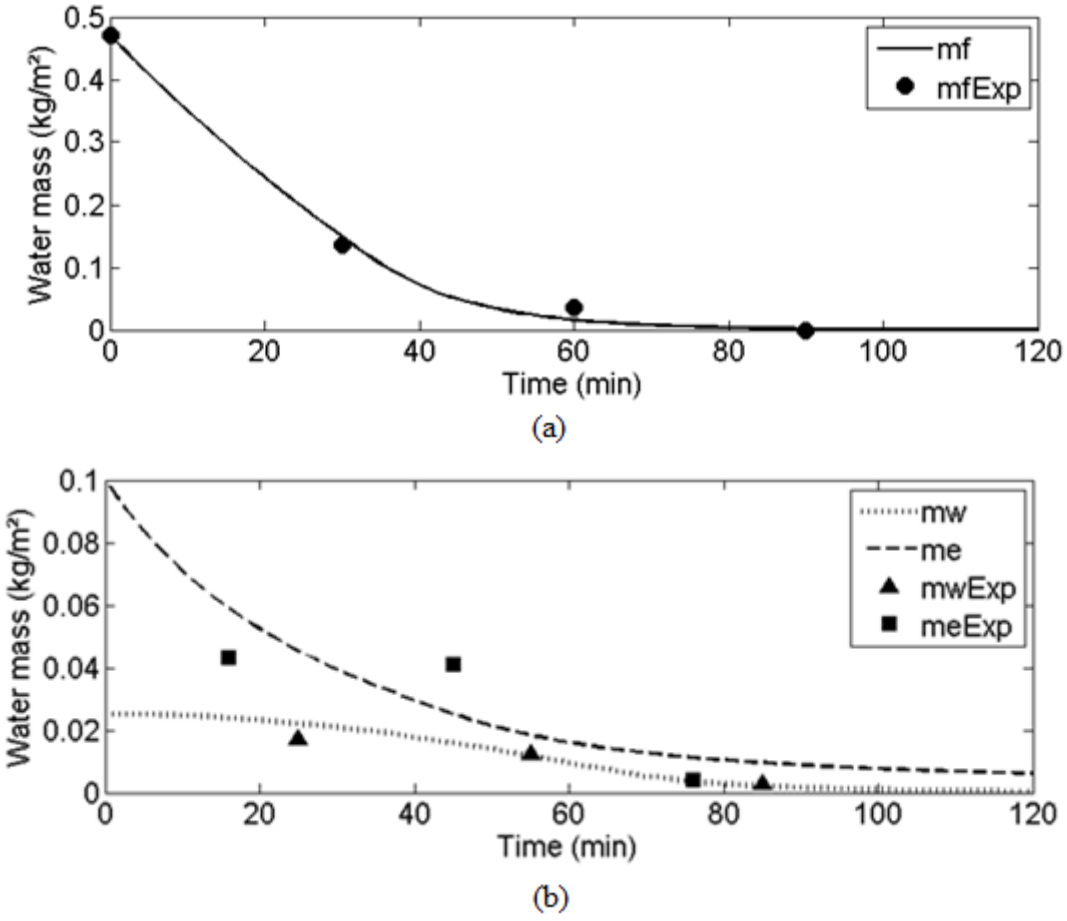

Figure 7: Measured (m Exp) and calculated water weight located on the floor (a) and on the wall and equipment (b) during the drying process (RH=85%)

Even if some data necessary for the model were not obtained experimentally and had to be estimated or taken from the literature, the comparison between these two results is in good agreement. The initial mass of water on the floor is much more significant than on the other surfaces but it decreases much faster. Initially the floor temperature is high (~35°C) because of the hot water used during the cleaning process which wetted the whole surface. The strong thermal inertia of the floor makes its temperature decreases slowly during the drying process, compared to the one of the equipment (Figure 8).

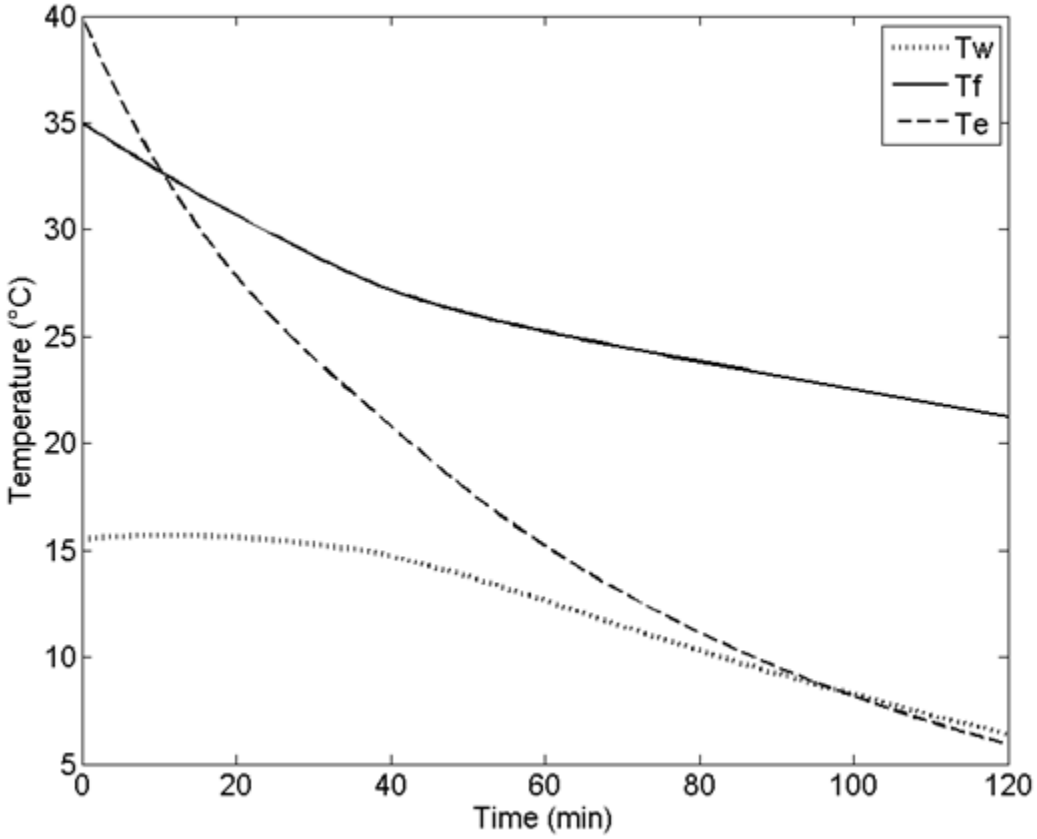

Figure 8: Calculated temperature of the wall, floor and equipment during the drying process.

This phenomenon induces higher evaporation rate on the floor. Indeed, this evaporation rate is influenced by the air velocity over the surface and the temperature difference between the surface and the air. The more significant this difference is, the higher the evaporation rate will be. Even if the equipment temperature is initially higher, it decreases much faster because of a smaller thermal inertia. During the experiment, it was observed that all surfaces were almost dried after about 90min, except for the equipment where water still remain at some locations. Concerning the evaporation on the wall because only a small part was wetted (approximatively 8% of the total surface) the initial temperature is smaller (around 16°C), thus, the difference between the temperature of the wall and the air is not so significant and the evaporation rate is lower than for the other surfaces. The water weight evolution is related to the evolution of the wet surface characterized by the coefficient β (Figure 9). At the beginning of the process, the water surfaces on the wall, floor and equipment are constant. After a certain time, these surfaces decrease. This phenomenon impact directly the water weight evolution (when the water surface decreases, the evaporation rate decreases). It also impacts the water content and the temperature inside the plant.

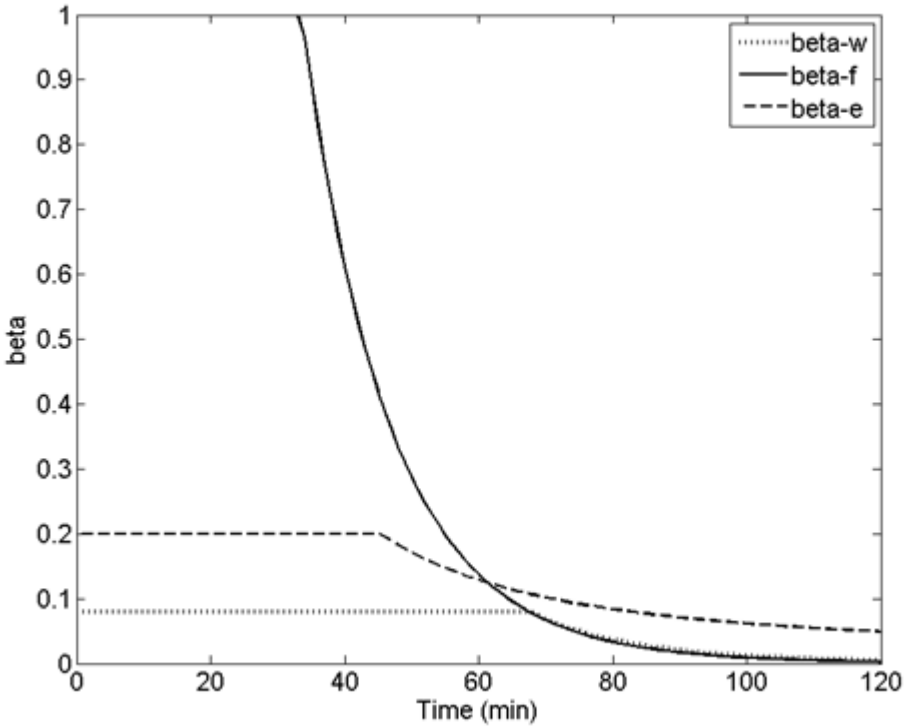

Figure 9: Evolution of the ratio between wet and total surface (β) on the wall, floor and equipment.

5.1.2. Temperature evolution

With the maximal power of the cold production system of the plant (3000 W) the return air reached the thermostat setting temperature (T_{th}=2°C) at ~117 min.

Two parts for the air temperature evolution was distinguished (Figure 10).

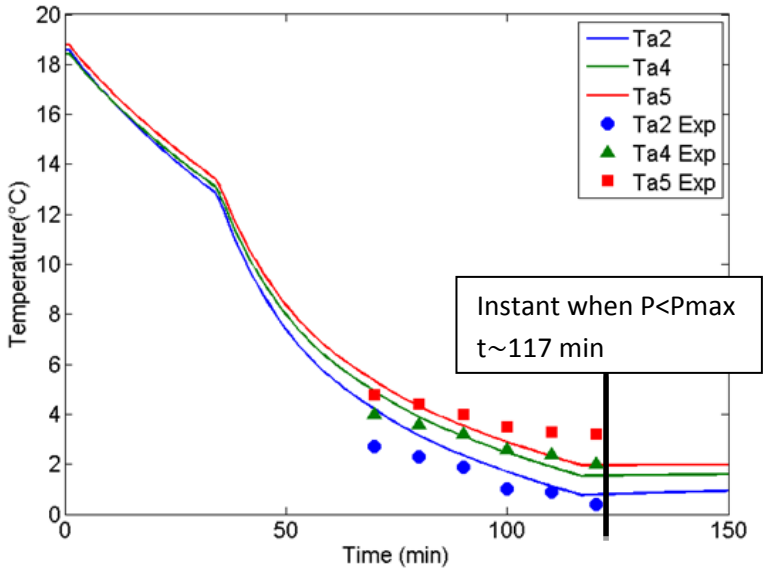

Figure 10: Air temperature evolution during drying period and comparison with experimental data.

In the first part (about 40 min), the whole floor is covered by water and a significant part of the evaporator power is used to condense the water vapor generated by the evaporation (Figure 11).

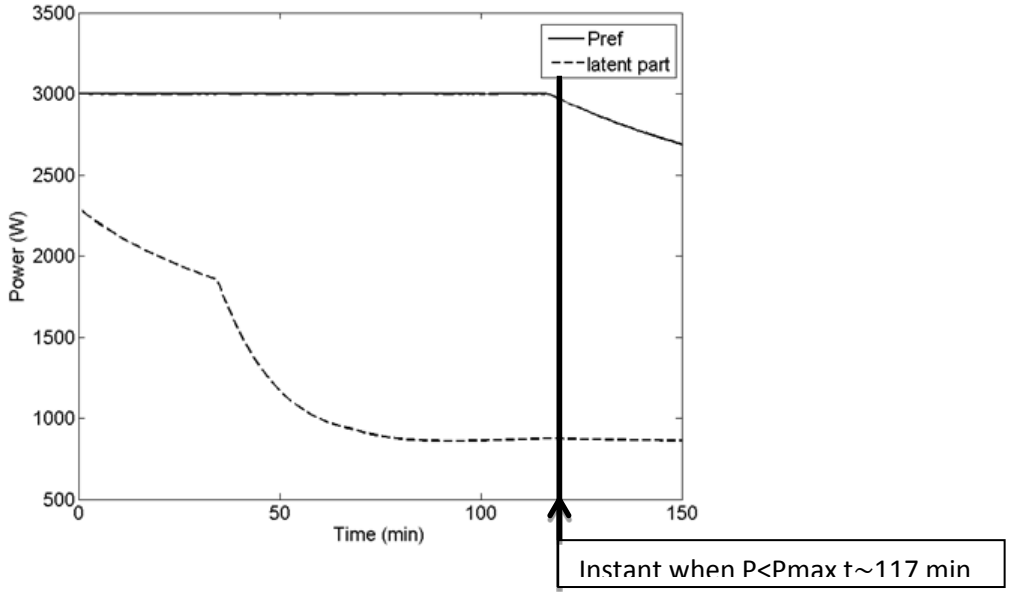

Figure 11: Evaporator power evolution (total and latent part) during drying period.

Then, the surface covered by water on the floor decreases while the evaporator power remains constant. This power is then used mostly to lower the air temperature (and indirectly the wall, floor and equipment temperature), making the temperature decreases faster than the ones in the first part.

For certain temperature measurement positions matching with the ones calculated from the model the air temperature were compared (positions 2, 4 and 5 on Figure 3). The comparison is shown on figure 10 and table 8.

Table 8: Air temperature comparison between the calculated and experimental results

70 min			
	T_2	T_4	T_5
Experimental results	2.7	4.0	4.8
Calculated results	3.5	4.4	5.0
120 min			
	T_2	T_4	T_5
Experimental results	0.4	2.0	3.2
Calculated results	0.4	1.5	1.9

Results are in good agreement, with the same tendency; lower temperatures in front of the evaporator (position 2) and higher temperature near the floor and in return flow (positions 4 and 5).

5.1.3. Influence of the coefficients α and γ

The influence of the coefficient α (air distribution coefficient in front of fans) on the water weight evolution is not significant whatever the values (10%, 30% and 50%, data not shown). The influence of the coefficient γ (air renewal coefficient in the room) is more significant (Figure 12).

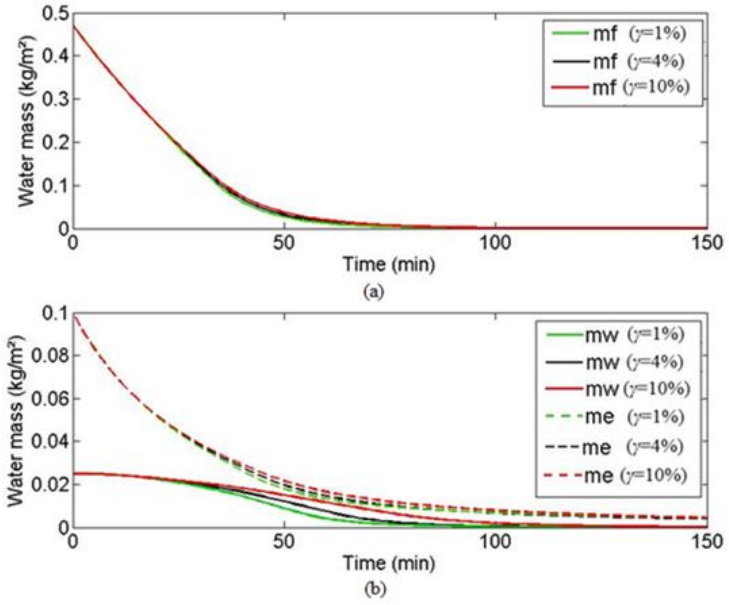

Figure 12: Influence of the coefficient γ (air renewal inside the food production room) on the water weight evolutions on the floor (a) and on the wall and equipment (b).

At a given time, the higher the air renewal, the higher the residual water weight (this influence is more important on the wall and on the equipment than on the floor). This can be explained by the fact that the renewal air contains a larger amount of water vapor than the air in the room.

5.2. Numerical study of the influence of air humidity on the evaporation time

The results previously shown indicate that at the end of the drying period (for inlet air at 85% relative humidity), water can still remain in the plant. This is particularly the case for the equipment which is in contact directly with food and can be a favorable environment to bacterial growth. Even if the amount of water is not much significant, it may be enough to present a risk of contamination. Thanks to the simplified model, the evolution of water weight in the room can be studied with other ambient conditions. The comparison of water weight evolution for 50% and 85% relative humidity at the air inlet is shown in Figure 13.a and 13.b.

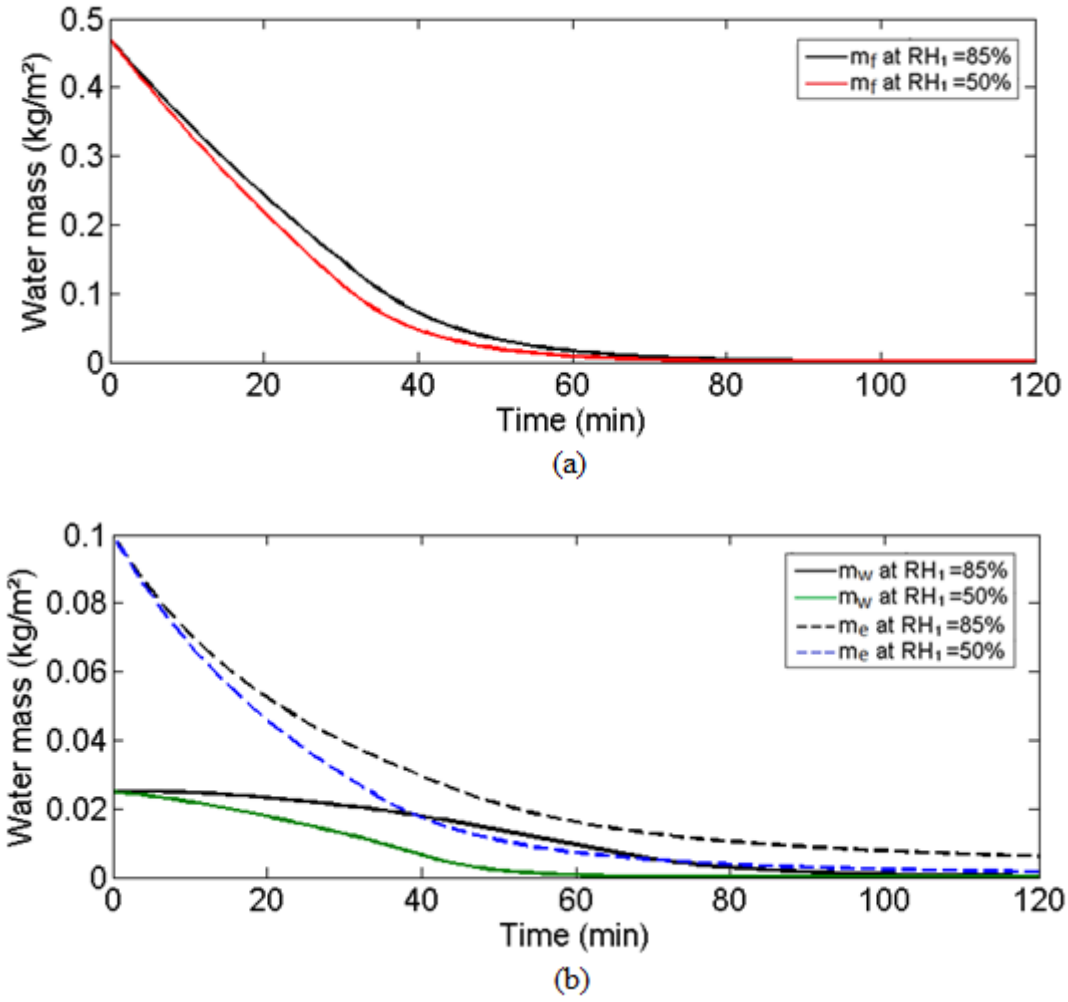

Figure 13: Comparison between the calculated water weights located on the floor (a) and on the wall and equipment (b) during the drying process at 85% and 50% relative humidity.

The result shows that for 50% relative humidity, water evaporation is faster and surfaces are entirely dried after 120 min (end of the drying period). The time needed to evaporate 90% of the initial water is reduced by a factor of about 1.5. This means that reducing relative humidity will trigger less humid surfaces. This numerical study shows the interest of the use of drying device to dehydrate the supply air.

6. Conclusion

Experimental and numerical methodologies were developed to characterize the heat and water transfer inside a food production plant. Air temperature, relative humidity and velocity were measured and the water present on several positions in a production room was weighed at different times. A simplified model was developed based on these observations. This model considers the heat and water exchanges between the air and the wall, floor and equipment inside the plant. It allows the prediction of water weight evolution, temperature of air and surfaces, relative humidity and water content of air during the whole drying process. Rather good agreements between the experimental and predicted values were obtained. This model could be applied to other conditions; only the flow pattern and the characteristics of the plant must be defined (dimensions, materials, air flow rate, air distribution coefficients…).

The main advantage of this model is the short CPU computing time (< 1min). This aspect enables the rapid evaluation of the influence of input parameters, such as the impact of the relative humidity and air temperature at the inlet, air flow rate, evaporator power etc. Inside this food production room, the relative humidity was always rather high (around 80-90%) which induced a low evaporation rate. The model shows that, by imposing the inlet air relative humidity at 50% instead of 85%, the evaporation could be around 1.5 times faster and the equipment could be entirely dried. This means that by reducing relative humidity, the ambient conditions could be more unfavorable for the bacteria survival.

In food plants in general, the implantation of a dehumidifier is done in an empirical way. To our knowledge, no research has been conducted to determine the appropriate conditions (air flow rate, temperature, relative humidity) to dry a food plant in an efficient way (quickly enough). Thus, a detailed study was performed so that it was possible to quantify the impact of the relative humidity of blown air on the drying time at different location.

The developed model has an intermediate complexity between overall engineering calculation and CFD simulation. Without dehumidifier, basic engineering calculation could estimate the overall drying rate from the condensation capacity of the evaporator (refrigerating power divided by latent heat of vaporization) and the drying time is equal to the total initial mass of water divided by the condensation capacity. This assumes however that heat is available to evaporate the water and that mass transfer resistance from the wetted surfaces to the evaporator is negligible. Here, the ‘basic engineering calculations’ and the ‘detailed engineering calculations’ should be distinguished. The first one (basic engineering calculations) based only on the amount of water can underestimate a lot the drying time which also depends on the airflow pattern inside the room, the thermal inertia of the surfaces, the heat/mass transfer intensity near these surfaces. To estimate the drying time reduction due to a dehumidifier, one could add the dehumidification capacity to the condensation capacity. But, this also assumes a non-realistic situation. The second one (detailed engineering calculations), corresponding to our simplified modelling approach, takes into account all these aspects. It is, thus, not only based on the amount of moisture after cleaning but also on some characteristics of the food processing plant (airflow, heating of the surfaces etc.). The lack of the assumption is obvious in figure 11: a variable part, often less than one third of the refrigerating power is used to condense water vapor. The model also clearly shows the difference in water mass evolution between the different surfaces (Figure 12). In spite that the initial water load for equipment is five times lower than that for floor, water is still present on the equipment after two hours (floor was dried after 1h30). This difference is taken into account by the model (higher thermal inertia of the floor).

The best practice to prevent bacteria growth would be to dry all the surfaces (including critical places) as fast as possible. Therefore one should rather oversize the dehumidifier. Most often however, there is no dehumidifier at all in food processing plants. Sometimes even with an expensive oversized dehumidifier, the drying time is too long because of other limiting factors such as low heat/mass transfer coefficient at some positions, too low surface temperature, too low airflow rate. The detailed engineering model developed in our study can help to reduce the drying time in different locations by modifying not only the dehumidifier capacities but also the food processing plant characteristics. Nevertheless, this model is unable to detect in detail critical locations of nearly stagnant air and low evaporation rate. To capture these places like corners, CFD models could be used to determine the locations of low air velocity – low mass transfer coefficient zones. But this would require much more implementation and computation time.

The results obtained in the present study can help to choose an appropriate dehumidifier in function of the food plant characteristics. It can also be used to quickly test new strategies, for example, equipment and inlet air moderate heating. In the future, this simplified model will be combined with a microbiological model to predict the *L. monocytogenes* evolution on the floor, wall and equipment. Such information is of great interest for manufacturers to control the food safety.

Finally, this simplified model of a food processing plant is complementary to other simplified models developed by our team for refrigerated trucks, cold rooms, display cabinets and domestic refrigerators (already published in Journal of Food Engineering). This allows the integration of different steps of the cold chain.

ACKNOWLEDGEMENT

The research leading to this result has received funding from the French National Research Agency (EcoSec Project, ANR-12-ALID-0005-04). The authors would like to thanks Labeyrie Fine Foods for their participation in experimentation in plant.

REFERENCES

Billiard F. 1998. Conception du conditionnement d'ambiance dans l'agro-alimentaire. *Revue générale du froid* 980: 45-48

Bimbenet J.-J., Duquenoy A., Trystram G. 2002. Génie des procédés alimentaires : Des bases aux applications.

Bridier A., Sanchez-Vizuete P., Guilbaud M., Piard J. C., Naïtali M., Briandet R. 2015. Biofilm-associated persistence of food-borne pathogens. *Food microbiology* 45: 167-78

Buchanan R., Lindqvist R., Ross T., Smith M., Todd E., Whiting R. 2004. Risk assessment of Listeria monocytogenes in ready-to-eat foods. *Food and Agriculture Organisation of the United Nations* Microbiological Risk Assessment Series, 4

Carpentier B., Cerf O. 2011. Review — Persistence of Listeria monocytogenes in food industry equipment and premises. *International Journal of Food Microbiology* 145: 1-8

Chandra S., Marzo M. d., Qiao Y. M., Tartarini P. 1996. Effect of liquid-solid contact angle on droplet evaporation. *Fire Safety Journal* 27: 141-58

D'agaro P., Croce G., Cortella G. 2006. Numerical simulation of glass doors fogging and defogging in refrigerated display cabinets. *Applied Thermal Engineering* 26: 1927–34

Delele M. A., Tijskens E., Atalay Y. T., Ho Q. T., Ramon H., Nicolaï B. M., Verboven P. 2008. Combined discrete element and CFD modelling of airflow through random stacking of horticultural products in vented boxes. *Journal of Food Engineering* 89: 33-41

EFSA. 2015. The European Union summary report on trends and sources of zoonoses, zoonotic agents and food-borne outbreaks in 2013. *EFSA Journal* 13: 3991, 162 pp

Ferreira V., Wiedmann M., Teixeira P., Stasiewicz M. J. 2014. Listeria monocytogenes persistence in food-associated environments: epidemiology, strain characteristics, and implications for public health. *Journal of Food Protection* 77: 150–70

Flick D., Alvarez G., Doursat C., Moureh J. 1999. Modélisation des écoulements et des transferts lors du refroidissement de fruits et légumes conditionnés en palettes. *20th international congress of Refrigeration IIR-IIF, Sydney* 6

Gerba C. P. 2015. Quaternary Ammonium Biocides: Efficacy in Application. *Applied and environmental microbiology* 81: 464-69

Ho S. H., Rosario L., Rahman M. M. 2010. Numerical simulation of temperature and velocity in a refrigerated warehouse. *International Journal of Refrigeration* 33: 1015-25

Hoang H.-M., Duret S., Flick D., Laguerre O. 2015. Preliminary study of airflow and heat transfer in a cold room filled with apple pallets: Comparison between two modelling approaches and experimental results. *Applied Thermal Engineering* 76: 367–81

Hoang H.-M., Laguerre O., Moureh J., Flick D. 2012. Heat transfer modelling in a ventilated cavity loaded with food product: Application to a refrigerated vehicle. *Journal of Food Engineering*, 113: 389-98

Hu Z., Sun D.-W. 2000. CFD simulation of heat and moisture transfer for predicting cooling rate and weight loss of cooked ham during air-blast chilling process. *Journal of Food Engineering* 46: 189-97

Hu Z., Sun D.-W. 2001. Predicting local surface heat transfer coefficients by different turbulent k-ϵ models to simulate heat and moisture transfer during air-blast chilling. *International Journal of Refrigeration* 24: 702–17

Laguerre O., Duret S., Hoang M. H., Guillier L., Flick D. 2014. Simplified heat transfer modelling in a cold room filled with food products. *Journal of Food Engineering* in press

Laguerre O., Flick D. 2010. Temperature prediction in domestic refrigerator: association of deterministic and stochastic approaches. *International Journal of Refrigeration* 33: 41-51

Laguerre O., Hoang M. H., Flick D. 2012. Heat transfer modelling in a refrigerated display cabinet: the influence of operating conditions. *Journal of Food Engineering* 108: 353–64

Likotrafiti E., Smirniotis P., Nastou A., Rhoades J. 2013. Effect of relative humidity and storage temperature on the behavior of Listeria Monocytogenes on fresh vegetables. *Journal of Food Safety* 33: 545-51

Malley T. J., Butts J., Wiedmann M. 2015. Seek and Destroy Process: Listeria monocytogenes Process Controls in the Ready-to-Eat Meat and Poultry Industry. *Journal of Food Protection* 78: 436-45

Mirade P. S. 2007. CFD Modeling of Indoor Atmosphere and Water Exchanges during the Cheese Ripening Process. *Computational Fluid Dynamics in Food Processing* CRC Press: 697-726

Mirade P. S., Daudin J.-D. 2006. Computational fluid dynamics prediction and validation of gas circulation in a cheese-ripening room. *International Dairy Journal* 16: 920-30

Muhterem-Uyar M., Dalmasso M., Bolocan A. S., et, al. 2015. Environmental sampling for Listeria monocytogenes control in food processing facilities reveals three contamination scenarios. *Food Control* 51: 94–107

Navaz H. K., Chan E., Markicevic B. 2008. Convective evaporation model of sessile droplets in a turbulent flow—comparison with wind tunnel data. *International Journal of Thermal Sciences* 47: 963-71

Raimundo A., Gaspar A., Oliveira A. V. M., Quintela D. 2014. Wind tunnel measurements and numerical simulations of water evaporation in forced convection airflow. *International Journal of Thermal Sciences* 86: 28-40

Rajatnam N. 1976. Turbulent jets. *Elsevier Scientific Publishing Company* 304 p

Vik T., Reif B. A. P. 2011. Modeling the evaporation from a thin liquid surface beneath a turbulent boundary layer. *International Journal of Thermal Sciences* 50: 2311–17

Wang H., Touber S. 1990. Distributed dynamic modelling of a refrigerated room. *International journal of refrigeration* 13: 214-22

Appendix

Matrices of the simplified model:

$$\bar{\bar{A}} = \begin{bmatrix} 0 & \frac{1}{\tau_w} & -\frac{1}{\tau_w} & 0 & 0 & 0 & 0 & \frac{1}{\varepsilon_w} & -\frac{1}{\varepsilon_w} & 0 & 0 & 0 \\ 0 & 0 & 0 & \frac{1}{\tau_f} & -\frac{1}{\tau_f} & 0 & 0 & 0 & 0 & \frac{1}{\varepsilon_f} & -\frac{1}{\varepsilon_f} & 0 \\ 0 & 0 & 0 & 0 & \frac{1}{\tau_e} & -\frac{1}{\tau_e} & 0 & 0 & 0 & 0 & \frac{1}{\varepsilon_e} & -\frac{1}{\varepsilon_e} \\ 0 & 0 & 0 & 0 & 0 & 0 & 0 & (1+\alpha)\dot{m} & -(1+\alpha)\,\dot{m} & 0 & 0 & 0 \\ 0 & 0 & 0 & 0 & 0 & 0 & 0 & 0 & 0 & (1+\alpha)\,\dot{m} & -(1+\alpha)\,\dot{m} & 0 \\ 0 & 0 & 0 & 0 & 0 & 0 & 0 & 0 & 0 & 0 & (1+\alpha)\,\dot{m} & -(1+\alpha)\,\dot{m} \end{bmatrix} \quad (10)$$

$$\bar{\bar{B}} = \begin{bmatrix} -\frac{1}{\tau_{ext}} & 0 & 0 & 0 & 0 & 0 \\ 0 & 0 & 0 & 0 & 0 & 0 \\ 0 & 0 & 0 & 0 & 0 & 0 \\ 0 & 0 & 0 & 0 & 0 & 0 \\ 0 & 0 & 0 & 0 & 0 & 0 \\ 0 & 0 & 0 & 0 & 0 & 0 \end{bmatrix} \quad (11)$$

$$\vec{C} = \begin{bmatrix} \frac{1}{\tau_{ext}} \\ 0 \\ 0 \\ 0 \\ 0 \\ 0 \end{bmatrix} (12) \qquad \bar{\bar{D}} = \begin{bmatrix} 0 & 0 \\ 0 & 0 \\ \frac{1}{(mC)_e} & 0 \\ 0 & 0 \\ 0 & 0 \\ 0 & 1 \end{bmatrix} (13)$$

$$\bar{\bar{E}} =$$

1	-(1+α)	0	0	0	α	0	0	0	0	0	0
0	δ_w	-1	0	0	0	0	0	0	0	0	0
0	0	(1+α-γ)	-(1+α)	0	0	0	0	0	0	0	0
0	0	0	δ_f	-1	0	0	0	0	0	0	0
0	0	0	0	δ_e	-1	0	0	0	0	0	0
0	0	0	0	0	0	1	-(1+α)	0	0	0	α
0	0	0	0	0	0	0	δ'_w	-1	0	0	0
0	0	0	0	0	0	0	0	(1+α-γ)	-(1+α)	0	0
0	0	0	0	0	0	0	0	0	δ'_f	-1	0
0	0	0	0	0	0	0	0	0	0	δ'_e	-1
0	0	0	0	0	1	0	0	0	0	0	0
$-a_1 RH_1$	0	0	0	0	0	1	0	0	0	0	0

(14)

$$\bar{\bar{F}} =$$

0	0	0	0	0	0
-(1-δ_w)	0	0	0	0	0
0	0	0	0	0	0
0	-(1-δ_f)	0	0	0	0
0	0	-(1-δ_e)	0	0	0
0	0	0	0	0	0
-(1- δ_w')a_w	0	0	0	0	0
0	0	0	0	0	0
0	-(1-δ_f')a_f	0	0	0	0
0	0	-(1-δ_e')a_e	0	0	0
0	0	0	0	0	0
0	0	0	0	0	0

(15)

$$\vec{G} = \begin{bmatrix} 0 \\ 0 \\ -\gamma \\ 0 \\ 0 \\ 0 \\ 0 \\ 0 \\ 0 \\ 0 \\ 0 \\ 0 \end{bmatrix} (16) \qquad \vec{H} = \begin{bmatrix} 0 \\ 0 \\ 0 \\ 0 \\ 0 \\ 0 \\ 0 \\ -\gamma \\ 0 \\ 0 \\ 0 \\ 0 \end{bmatrix} (17) \qquad \vec{I} = \begin{bmatrix} 0 \\ 0 \\ 0 \\ 0 \\ 0 \\ 0 \\ 0 \\ 0 \\ 0 \\ 0 \\ 1 \\ 0 \end{bmatrix} (18) \qquad \vec{J} = \begin{bmatrix} 0 \\ 0 \\ 0 \\ 0 \\ 0 \\ 0 \\ -(1 - \delta'_1)\mathrm{b}_w \\ 0 \\ -(1 - \delta'_2)\mathrm{b}_f \\ -(1 - \delta'_3)\mathrm{b}_e \\ 0 \\ b_1 \cdot RH_1 \end{bmatrix} (19)$$

If the maximal power condition ($\dot{m}\left(Cp_{air}(T_{th} - T_1) + \Delta H_v(X_6 - X_1)\right) < P_{max}$) is not respected, then the equation $(T_6 - T_1) + \frac{\Delta H_v}{Cp_{air}}(X_6 - X_1) = \frac{P_{max}}{\dot{m} \cdot Cp_{air}}$ is applied instead of $T_6 = T_{th}$ and the eleventh line of the matrices E, J and I changes for the following lines:

For E:

$$\left(-1 \quad 0 \quad 0 \quad 0 \quad 0 \quad 1 \quad -\frac{\Delta H_v}{Cp_{air}} \quad 0 \quad 0 \quad 0 \quad 0 \quad \frac{\Delta H_v}{Cp_{air}}\right)$$

For I:

$$(0)$$

For J:

$$\left(\frac{P_{max}}{\dot{m} \cdot Cp_{air}}\right)$$

5.2. Article 6 : Influence of air dehumidification on water evaporation in a food plant (Soumis à International Journal of Refrigeration)

Influence of air dehumidification on water evaporation in a food plant

L. Lecoq [ab*], E. Derens [a], D. Flick [b], O. Laguerre [a]

[a] Irstea, UR GPAN, 1 rue Pierre-Gilles de Gennes, 92761 Antony, France

[b] UMR Ingénierie Procédés Aliments, AgroParisTech, INRA, Université Paris-Saclay, 91300 Massy, France

ABSTRACT

To reduce the proliferation of bacteria inside food plants, cleaning and disinfection are performed daily following production. These operations are followed by drying during which the drying rate should be as high as possible. This study shows the influence of a dehumidifier on the water mass evolution on surfaces during the drying of a food plant. The temperature, relative humidity and water mass evolution were monitored under two conditions: with and without a dehumidifier. Comparison of the results shows that the drying rate is about 1.5 times higher when a dehumidifier is used. These data were used to develop a simplified heat and mass transfer model allowing the prediction of the temperature and drying rate at different locations. The results can help the manufacturer to evaluate the benefits of a dehumidifier and consider the use of other devices to achieve better airflow distribution or greater heat supply for certain surfaces.

Keywords: dehumidifier; food plant; mass transfer; relative humidity; water evaporation

[*] Corresponding author: Tel: +33 1 40 96 90 04, Fax: +33 1 40 96 60 75, E-mail: logan.lecoq@irstea.fr

Nomenclature

Cp_a	Specific heat capacity of air	$J.kg^{-1}.K^{-1}$
C	Water vapor concentration in the air	$kg.m^{-3}$
h	Heat transfer coefficient	$W.m^{-2}.K^{-1}$
k	Mass transfer coefficient	$m.s^{-1}$
m	Mass of water	kg
$m_{w,evap1}$	Mass of water condensed on one evaporator	kg
mC	Heat capacity of materials	$J.K^{-1}$
$\dot{m}$	Air mass flow rate	$kg.s^{-1}$
RH	Relative humidity	Dimensionless
T	Temperature	°C or K
V	Volume of the room	m^3
x	Water content	$kg_{water}.kg_{dry\ air}^{-1}$
ρ	Air density	$kg.m^{-3}$

Subscripts

a	air	*f*	floor	*0*	initial time
e	equipment	*w*	wall		

1. Introduction

Listeria monocytogenes is a serious foodborne pathogen that can cause severe infection called listeriosis and above all occurs in ready-to-eat food products. Product contamination is initially caused by contamination inside the premises of the food processing plant (Autio et al. 1999, Vogel et al. 2001, Wulff et al. 2006). Thereafter, contamination can increase throughout the cold chain and depends on the temperature and residence time of product in the refrigerating equipment (Duret et al. 2014). The product temperature can be determined using heat transfer models where the input parameters such as the product characteristics are known (Flick et al. 2012, Hoang et al. 2012). Legislation requires the absence of *L. monocytogenes* in five 25 g samples of a product before the latter leaves the food plant, and for products placed on the market allows a maximum of 100 CFU g^{-1} during their shelf-life (EC 2005). This implies that many products must be destroyed if contamination occurs in the food plant. Inside the production room, equipment with complex shapes can be difficult to clean, thus enabling bacterial growth to take place. In damaged equipment, cracks on the floor etc., the presence of water and nutrients provide environments in which bacteria can develop (Carpentier & Cerf 2011) and prevent bacteria from being affected by lethal concentrations of chemical products. This in turn enables bacteria to adapt to the disinfectants used, making eradication of bacteria more difficult (Muhterem-Uyar et al. 2015). Residual water and humidity in the premises are determining factors in microbial development, and can be reduced using a dehumidifier.

2. Literature Review

There are many types of dehumidifier (La et al. 2010) for different applications. For human comfort, the use of a dehumidifier makes it possible to slightly reduce and to homogenize the relative humidity inside a building in order to reduce moisture levels and ensure human well-being (Cunningham 2007, Teodosiu et al. 2003, Teodosiu 2013). Kim et al. (2008) carried out an experimental and numerical (3D CFD) study and demonstrated the influence of a dehumidifier in a greenhouse on the relative humidity: a reduction of about 10% (from ~70% to ~60%) was achieved. In a food production plant, the use of a dehumidifier makes it possible to raise the drying rate. However, from our literature review, there have been no studies reporting the influence of dehumidification on the relative humidity in air and on the rate of water evaporation on the surfaces of a food plant. Also, to our knowledge, there are no published data on the water load inside a food processing plant after cleaning and during drying. In most food processing plants, there is no dehumidifier, and when one is used, it is in most cases designed in an empirical manner. In a previous study (Lecoq et al. 2016), an experiment was performed in a food production plant without a dehumidifier in order to study water evaporation on the surfaces (walls, floor and equipment). The relative humidity was rather high (~85%), thus inducing a low evaporation rate during the 2-hour drying period, and water still remained on certain surfaces. A simplified heat and mass transfer model was developed to predict the evaporation rate on these surfaces and a part of the present study is based on this model.

The main objectives of this study are to present an estimation of the water load after cleaning and to analyze the influence of a dehumidifier on the air humidity and the water evaporation rate at different locations in an industrial food plant. The simplified model developed by Lecoq et al. (2016) was adapted to predict the drying rate in the food processing plant under two operating conditions (with and without a dehumidifier).

3. Experiment in a food plant

The experiments were carried out in a chilled food production plant during the drying period (Figure 1). The ambient conditions (temperature, relative humidity, air velocity) and the water mass on several surfaces were measured in two cases: with and without a dehumidifier operating in the room.

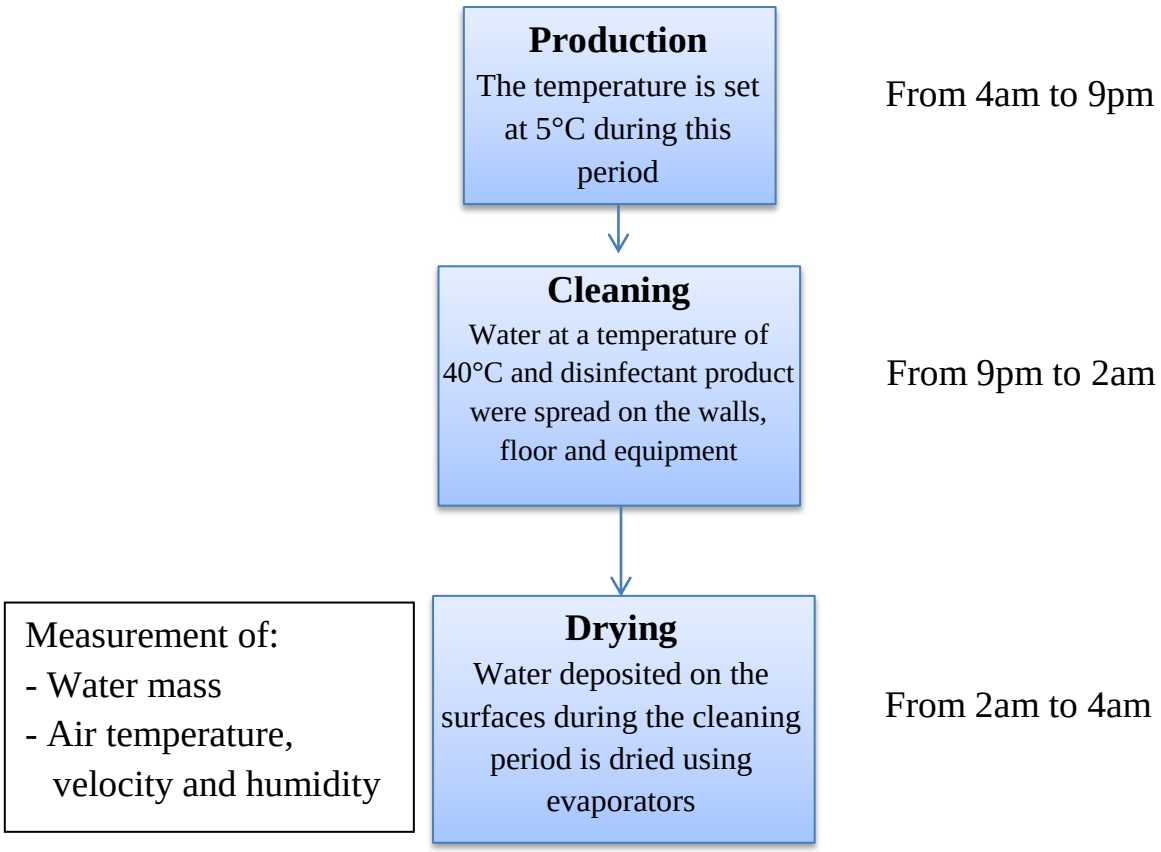

Figure 1: Different daily operations in the production plant investigated

3.1. Production room

The dimensions of the chilled food production room of about 450 m^3 (17.1m long, 8.2m wide and 3.6m high, Figure 2). A low temperature was maintained in this room using two evaporators located in the ceiling. Air from the two evaporators was blown inside air ducts located in the ceiling, and the air was diffused to the left and the right. The two evaporators are referred as Evaporator 1 and Evaporator 2. The equipment in the production room are conveyor production lines, mixing tank and tables and occupied about 20% of the room volume.

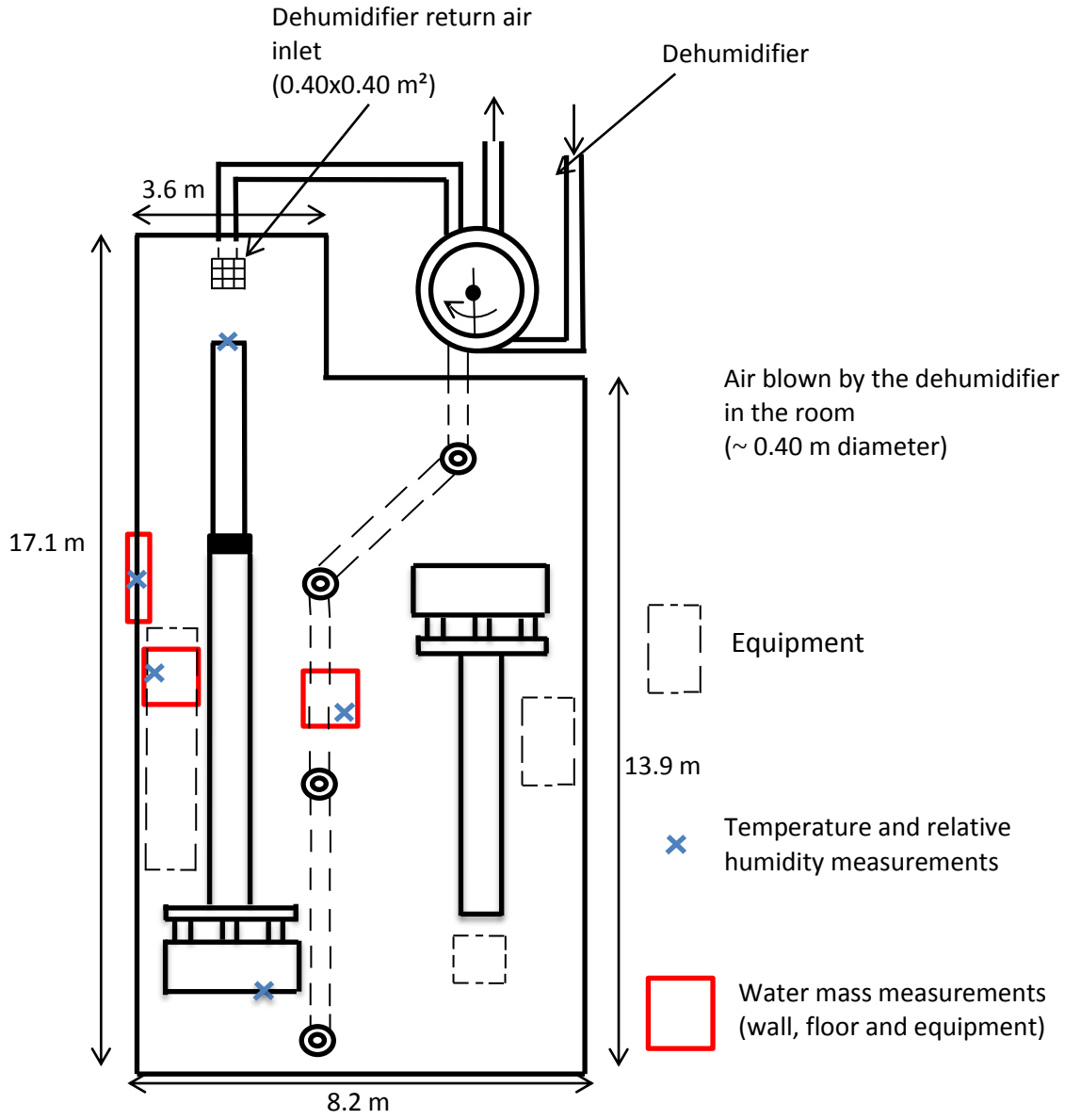

Figure 2: Diagram showing the food production room and the positions of the water mass, temperature and relative humidity measurements

3.2. Evaporator and dehumidifier operating conditions

In this study, it is considered that the drying process starts when the cleaning period ends, which means that no additional water is provided in the room during drying. The following operating conditions specified by the manufacturer are defined bellow:

During the cleaning process, the evaporators were stopped.

For the experiment without a dehumidifier, the first evaporator restarted directly after the end of the cleaning process and the second one after 45 min. The first evaporator was “on” from 0 min. to 20 min., then it was defrosting from 20 min. to 45 min. During this period, the evaporator fan was working, but without cooling.

For the experiment with a dehumidifier, both evaporators restarted 50 min. after the beginning of the drying period. The dehumidifier (desiccant wheel) operated at all times, even during the cleaning process. Its characteristics are shown in Table 1.

Table 1: Technical characteristics of the dehumidifier (Recusorb RZ-081):

Dehumidification capacity[1] [kg.h^{-1}]	19
Dry air flow rate [m^3.h^{-1}] External static pressure [Pa]	3000 400
Moist air flow rate [m^3.h^{-1}] External static pressure [Pa]	1000 200
Cooling capacity [kW]	24
Motor power [kW]	3

[1] For the inlet condition of 20°C and 60% relative humidity (RH). For other conditions, the dehumidification capacity is multiplied by by the coefficient "K" obtained in the following diagram

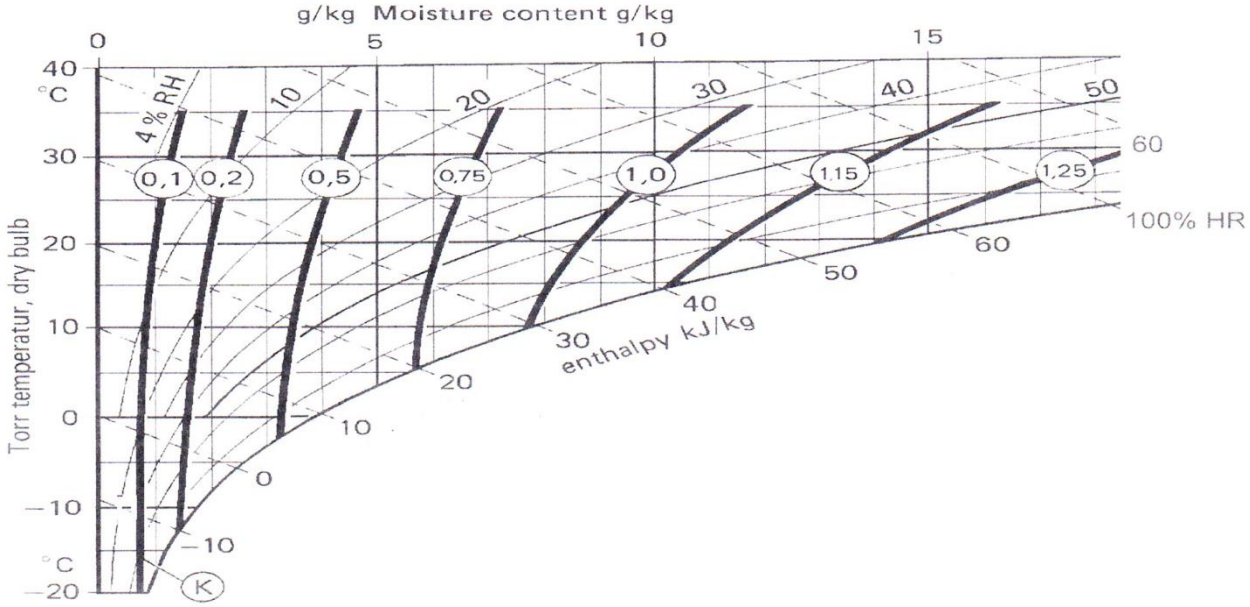

3.3. Parameter measurements

The air and surface temperatures, the relative humidity and the water mass on the surfaces (walls, floor and equipment) were measured during the drying process in both experiments (with and without a dehumidifier).

3.3.1. Water mass measurement

After the cleaning process in the production room, the water mass was measured at different times on various surfaces: floor, walls and equipment. To measure the water mass, paper towels were used to wipe a 25cm x 50cm surface area on the floor. Because there is less water on the walls and on the equipment compared to that on the floor, the wiping was performed on a 50cm x 50cm surface area on these surfaces. A square frame (25cm x 50cm or 50cm x 50cm) was placed on the measuring position prior to water swabbing (Figure 3).

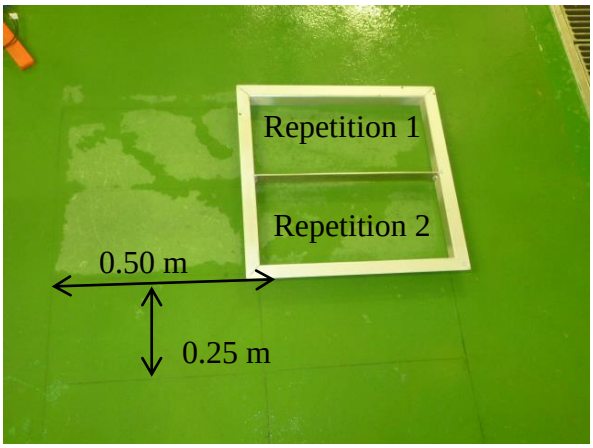

Figure 3: Example of the delimitation for the water mass measurement (on the floor)

After swabbing, the paper towels were deposited in a plastic bag, then the air inside the bag was eliminated by pressing the bag before closing it. The paper towels in the bags were weighed as soon as possible, using an electronic balance (Sartorius, CPA34001P, $\pm$ 0.1 g). On the floor and on the walls, the procedure was repeated. The same procedure was repeated every 30 min. on neighboring surfaces over a 2-hour period. To avoid to the greatest extent possible variability of the results due to manner in which water was wiped, the same person swabbed the wet area several times until the water was totally removed.

Because of the difficulty encountered in the carrying out of measurements in a real food plant, only one location, considered as "representative", could be analyzed for each surface (wall, floor, and equipment) even though the initial water load and the transfer rate can vary from one position to another. The analysis of such heterogeneity is outside the scope of the present study.

3.3.2. Temperature measurements

Temperature was recorded every 30 seconds from the beginning until the end of the drying process using thermistors (Testo 171, $\pm$ 0.2°C). Due to time necessary for installation of the sensors, certain temperature measurements were only performed 30 min. after the beginning of the drying period. The sensors were positioned at the air inlet and outlet (near the outlet of the air duct) of Evaporator 1 and in the middle of the room at several heights: 0.2m, 2.6m and 3.2m (Figure 2). Another sensor was placed near the air blown by the dehumidifier. In addition, surface temperatures were recorded by sticking the sensors on a wall, the floor and equipment. In order to improve the accuracy of the surface temperature measurements, thermal insulation with a thickness of 4 mm was placed on the sensors.

3.3.3. Relative humidity measurements

Relative humidity was recorded every minute using capacitive hygrometers (Testo 174H, $\pm$ 3%) during the entire drying process (as for the temperature measurements, in some cases the relative humidity was only monitored 30 min after the beginning of drying). The sensors were placed at the air inlet and outlet of Evaporator 1 (Figure 2) and also near the air blown by the dehumidifier.

3.3.4. Velocity measurements

Air velocity was measured at the air return grill of Evaporator 2 and the dehumidifier using a hot wire anemometer (Testo 435-2, range of measurement: 0-20 $m.s^{-1}$). It was assumed that the air flow rates of the two evaporators were similar. Using the measured air velocity and the cross section of air duct, the air flow rates were calculated: around 1.2 x 10^4 $m^3.h^{-1}$ for the evaporator, around 3 x 10^3 $m^3.h^{-1}$ for the dehumidifier.

3.4. Laboratory measurements

This study was carried out in complementary of the one undertaken in the food processing plant in which there are several constraints. For example, the company authorization was necessary and experimental repetition was not possible. Moreover, to avoid the disturbance of workers (two technicians were working during the drying process), the installation of sensors was limited in time and in position. Face to these difficulties, an additional experiment was performed in laboratory to study water evaporation in well-controlled conditions.

Water evaporation is a well-known physical phenomenon for single droplet and water film. When droplets are deposited on a solid surface, the phenomena become more complex in terms of heat transfer and evolution of droplet geometries (Chandra et al. 1996, Croce et al. 2005). Some experiments were conducted in controlled conditions (air velocity, temperature and humidity, solid surface characteristics, water repartition, etc…). The evaporation of water droplets deposited on a solid surface was first studied in controlled conditions at laboratory. The experimental device consists of a wind tunnel (length x height x width = 64 cm x 19 cm x 19 cm, Figure 4) made of PVC, except the upper wall, which is made of Plexiglas.

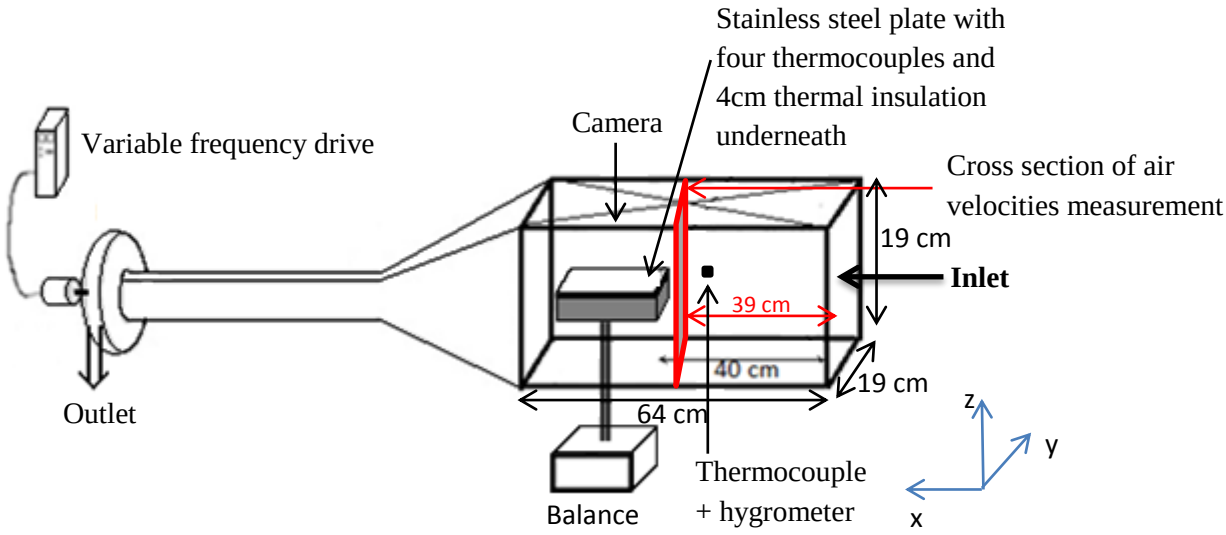

Figure 4: Schematic representation of the experimental setup of a wind tunnel.

This device is located in a test room where temperature and relative humidity can be controlled. In the work zone, a stainless steel plate (15 cm x 15 cm x 0.1 cm) is placed on a balance. Underneath this plate, extruded polystyrene (4 cm thickness) is used as thermal insulation. In this way, the result interpretation is facilitated because the exchange with air is undertaken only between the upper surface of the stainless steel and the air. This plate, wetted by water, was exposed to the following conditions: air temperature (4.2°C), relative humidity (51%) and air velocity (1.0m.s-1). In order to study the wet surface evolution during evaporation, the wet surface on the stainless steel plate was measured using a high definition camera (KAPPA DXP 1154) and a zoom (NavitarTenX) located outside the wind tunnel and

just above the plate and different initial water repartition were studied (β_0= 10, 21, 31, 46 and 94%). The air and plate temperatures were measured using calibrated T-type thermocouples (1 mm diameter, +/- 0.1°C precision), the relative humidity using a capacitive humidity sensor TESTO 174H (+/- 3% precision) in the tunnel and the water weight using an electronic balance (Sartorius, 3410028, +/-0.001 g precision) connected to a data-logger (Agilent 34970A) were also measured.

These experiments allowed determining how the fraction of wetted surface varies: β varies with the water mass by unit area. It was observed that β starts decreasing when the water weight is around 25% of its initial value and tends to zero when all the water is evaporated (results shown in section 5.1.).

4. Experimental results – Comparison with and without dehumidification

4.1. Air temperature and relative humidity evolution

During the first 50 min., as explained in Section 3.2, the evaporators were not operating in a totally similar manner in the two experiments, and this explains a slight difference in the air temperature evolution during this period. Thereafter, both evaporators were operating, which induced a decrease in the temperature at the air inlet (air blown by the evaporator) and thus also in the room (Figure 5).

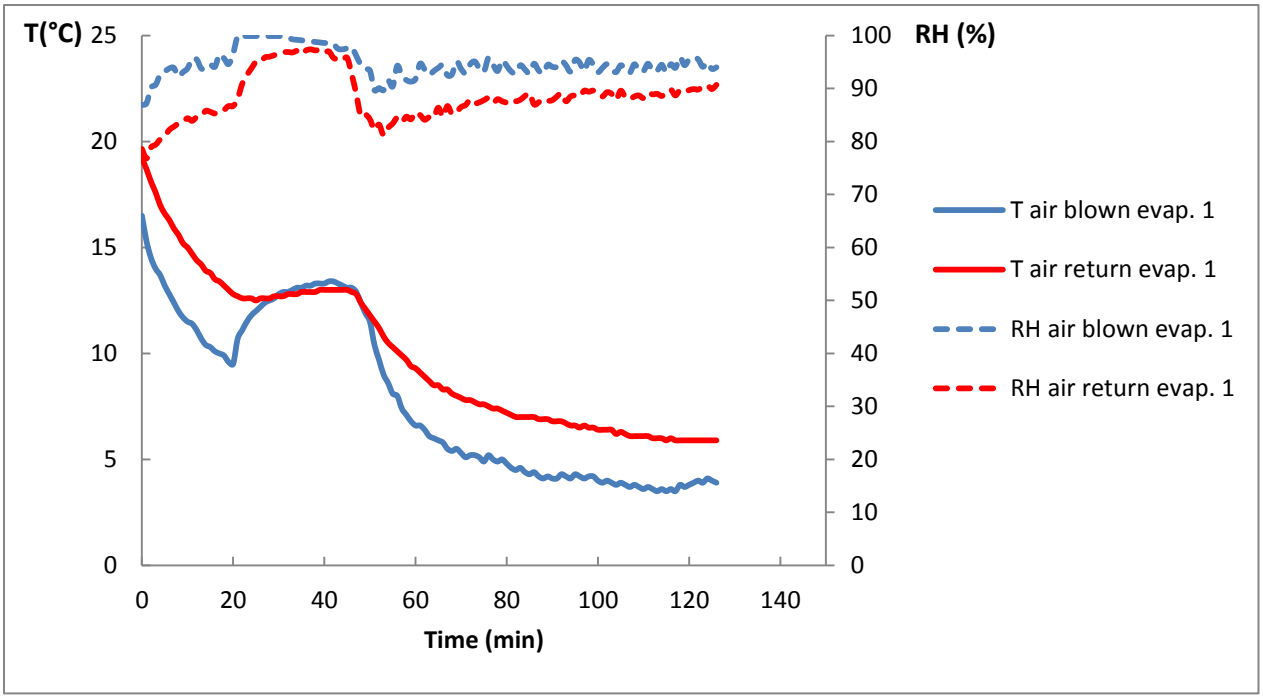

a

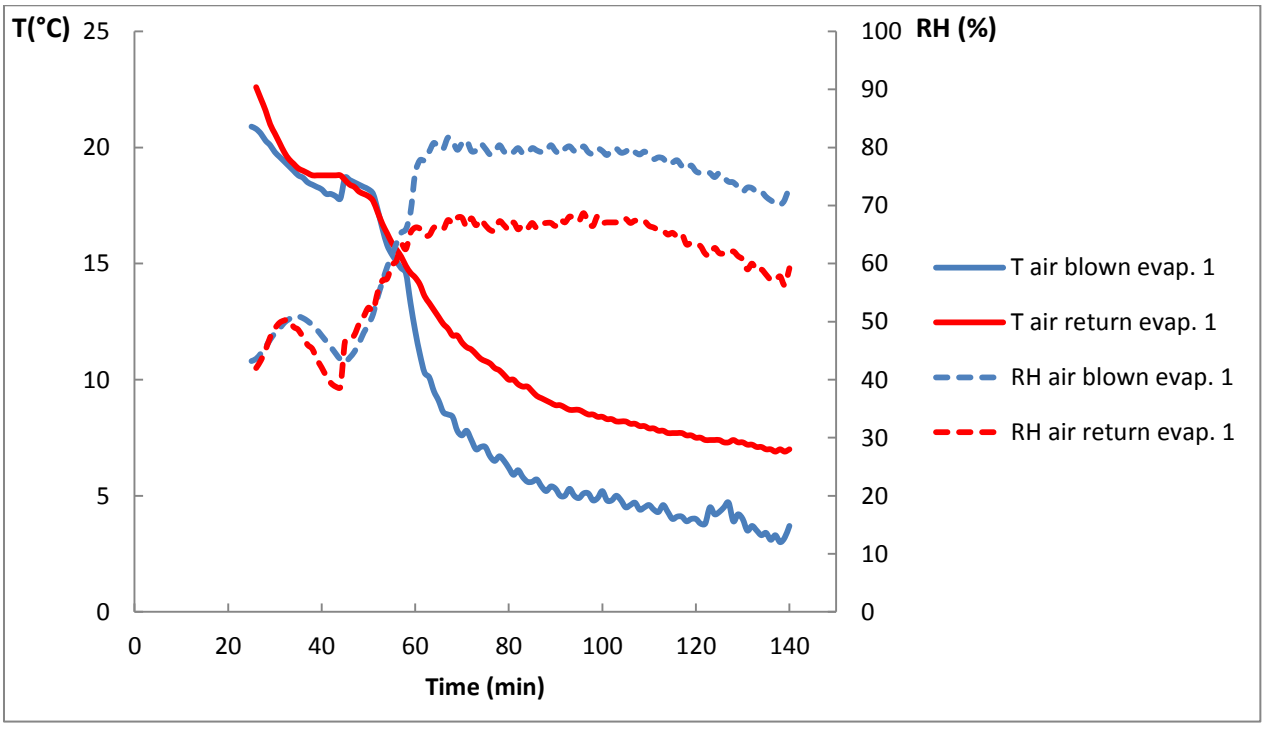

b

Figure 5: Evolution of the air temperature and relative humidity for the air blown and for the return air of Evaporator 1. a- without a dehumidifier b-with a dehumidifier

The air temperature was lower at the air inlet and higher at the evaporator return air (Table 2).

Table 2: Air temperature and relative humidity evolution in the room (°C) measured during the drying period

	Position / Time	Air blown evaporator		Evaporator return air		Air blown dehumidifier	Ambient (0.2m from the floor)		Ambient (2.6m from the floor)		Ambient (3.2m from the floor)	
		w/o[1]	**w[2]**	**w/o**	**w**	**w**	**w/o**	**w**	**w/o**	**w**	**w/o**	**w**
T °C	30 min	13.2	17.8	12.8	17.9	17.0	13.0	15.5	13.1	17.5	12.9	17.4
	60 min	5.9	11.2	8.2	12.9	14.4	9.1	12.4	7.6	12.7	8.1	12.8
	120min	4.0	4.0	5.6	7.1	9.3	5.7	7.7	4.9	5.9	5.1	6.6
		w/o	**w**	**w/o**	**w**	**w**						
RH %	30 min	100	48	96	49	62						
	60 min	92	76	85	66	65						
	120min	96	76	90	63	52						

[1] w/o: without a dehumidifier

[2] w: with dehumidifier

The ambient air temperatures measured in the middle of the room are summarized in this table. The evolution of these temperatures is the same as those at the air inlet and return air inlet of the evaporator, with a temperature of around 6°C at the end of the drying process. The temperature and relative humidity at the return air inlet give a good representation of the overall temperature in the room. At the end of the drying process, the air temperature close to the floor (at a height of 0.2 m) is slightly higher than those at heights of 2.6 m and 3.2 m because of the higher floor temperature (see Section 4.3) that warms up the surrounding air.

Concerning the relative humidity (RH), the difference with and without a dehumidifier is crucial. It can be seen in Figure 5 that without a dehumidifier the RH was around 90% in the room during the whole process. In addition, when the operating evaporator was defrosting over a period of 20 to 45 min, the evaporated water raised the relative humidity of the air (to close to 100%) and the air temperature rose (from ~10°C to ~13°C). In comparison with the conditions present when a humidifier is used, the relative humidity was always below 70% at the evaporator return air inlet. Before the evaporators were switched on (<50 min), the dehumidifier alone was operating, the temperature remained high, and the relative humidity was thus low (~50%). The temperature then decreased, explaining why the relative humidity increased up until 60 min. From 60 min to 120 min, the relative humidity decreased slightly due to the lower relative humidity in the air blown by the dehumidifier (from ~65% to ~52%, Table 2).

Reducing the relative humidity of the air in the room from 90% to 60% enables the water to evaporate faster and thus decreases bacterial survival (Likotrafiti et al. 2013).

4.2. Water content in the room

Knowing the water mass per square meter and the total surfaces of the wall, floor and equipment (Table 3), the water mass remaining on the surfaces at the beginning of the drying process can be estimated. The initial water mass on the floor was more significant without a dehumidifier (~227 $g.m^{-2}$ compared with ~130 $g.m^{-2}$ with a dehumidifier).

Table 3: Initial water mass and surface area

	Initial water mass [1] ($g.m^{-2}$)		Surface area (m^2)
	w/o	**W**	
Wall	14	7	182.2
Floor	227	130	125.5
Equipment	75	78	~80

[1] average of the two repetitions for the floor and the wall

The fact that the dehumidifier was also operating during the cleaning process limits the water remaining during the drying period. In the case without a dehumidifier, the total water remaining at the beginning of the drying process was around 37 kg, whereas it was only about 24 kg with a dehumidifier.

During both experiments, the mass of water condensed on the second evaporator was measured: 6.4 kg without a dehumidifier and 0 kg with a dehumidifier.

The water content of the air in the room during the process can be calculated from the relative humidity and temperature data at the first evaporator return air (Figure 6).

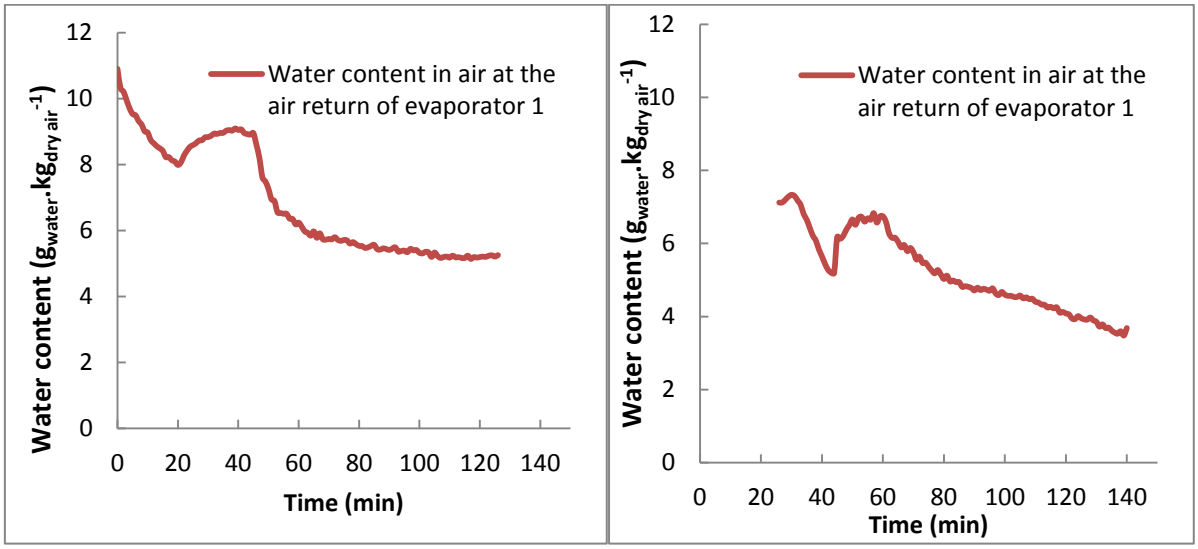

a b

Figure 6: Evolution of the water content in the air at the evaporator return air. a- without a dehumidifier b-with a dehumidifier

The difference in the water content between the beginning and the end of the process was about $5.7 \cdot 10^{-3}$ $kg_{eau}.kg_{air}^{-1}$ without a dehumidifier. Knowing the total volume of the room (~450m^3), the decrease in the mass of water vapor in the air can be estimated using the following equation:

$$m_w = \Delta x * V * \rho \quad (1)$$

where $\Delta x =$ difference in the water content between the beginning and the end of the process.

The decrease in the mass of the water in the air is around 3 kg without a dehumidifier. However, because of technical constraints, the relative humidity and temperature during the first 30 min. of the drying period with a dehumidifier were not measured. Thus, the same calculation cannot be made in this case.

In the case without a dehumidifier, the evaporated water was handled by the two evaporators. It was found experimentally that 6.4 kg of water were handled by the second evaporator. The second evaporator was operating for 70 min. The first evaporator was operating for 100 min. which means that it must have removed approximately 9.1 kg of water during the drying period, considering that the evaporators have the same characteristics. At the end of the process, the two evaporators removed about 15.5 kg of water. Of these 15.5 kg, 3 kg came from the dehumidification of the air and the rest from the water that evaporated on the surfaces. At the beginning of drying period, about 37 kg of water was present on the surfaces. Of the 37 kg, it would appear that about 12.5 kg was collected by the evaporators, an unknown quantity flowed into the sewers, and it could be observed that another amount of water was still present at the end of the drying period (in locations with low air velocity such as in corners).

In the case where a dehumidifier was used, it was found that no water condensed on the evaporator, which suggests that the evaporated water was collected almost entirely by the dehumidifier. Due to technical difficulties, the water collected by the dehumidifier could not be measured experimentally. However, it was observed that even with a dehumidifier, in places such as corners or in complex equipment, water still remained. The dehumidifier, with a maximum capacity of 19 $kg.h^{-1}$ (Table 1), is theoretically able to dry the initial 24 kg of water present on the surfaces within two hours. However, the fact that water remained after two hours means that the evaporation rate is not limited by the capacity of the dehumidifier (which is even greater if we add the capacities of the evaporators). It is limited by the lack of heat required to evaporate water. If additional heat could be provided in the room or directly on the surfaces, even for a short period of time, the evaporated water could be collected by either the dehumidifier or the evaporator, giving rise to a much shorter drying time.

The drying rate in the room, which differs according to the surfaces (wall, floor and equipment), can be studied more accurately using the data on the mass of water collected on these surfaces during the drying process, (shown in section 4.4).

4.3. Surface temperature trends

During the experiment, the surface temperatures (wall, floor and equipment) were recorded near the positions where the water mass measurements were performed. Figure 7 shows that the floor temperature decreased at a slower rate than the temperatures of the wall and equipment during the drying process.

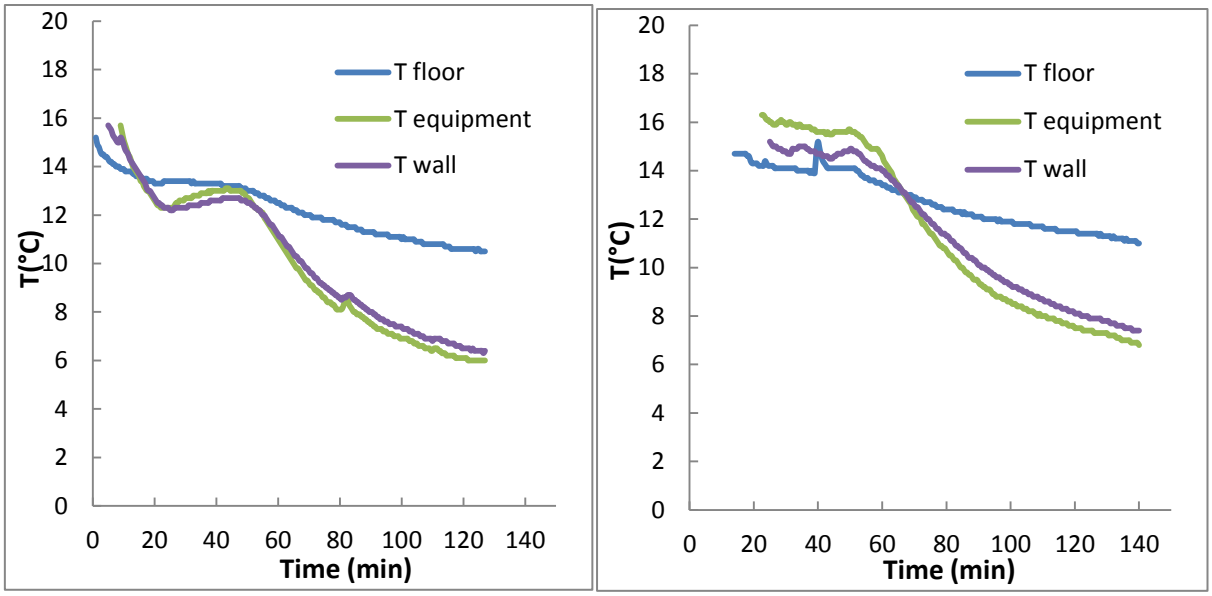

b

Figure 7: Surface temperature evolution of the wall, floor and equipment. a- without a dehumidifier b- with a dehumidifier

This can be explained by the high thermal inertia of the floor (typically 10cm thick concrete) compared with the thermal inertia of the wall and equipment. Indeed, at the end of the drying period, the equipment temperature was close to that of the air (~6°C) while the floor temperature was still above 10°C. Throughout the process, the heat produced by the surfaces becomes lower and lower as they cool. The floor temperature peak that occurred at around 40 min. was due to the replacement of the sensor.

It should be noted that results obtained in the experiments with and without a dehumidifier do not demonstrate a significant difference. The surface temperature trends differ only slightly due to the different air temperature trends during the process.

4.4. Water mass evolution

The masses of water measured on the wall, floor and equipment (as described in Section 3.3.1) during the drying process are presented for both experiments; with and without a dehumidifier, in Figure 8.

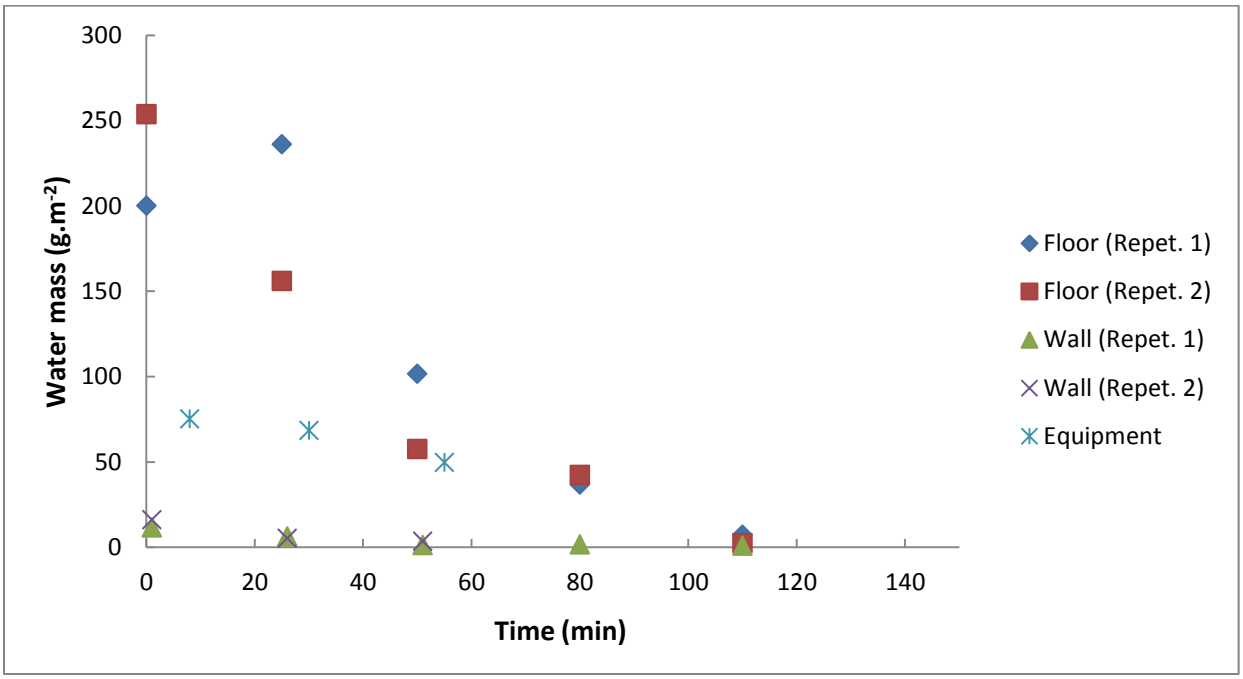

a

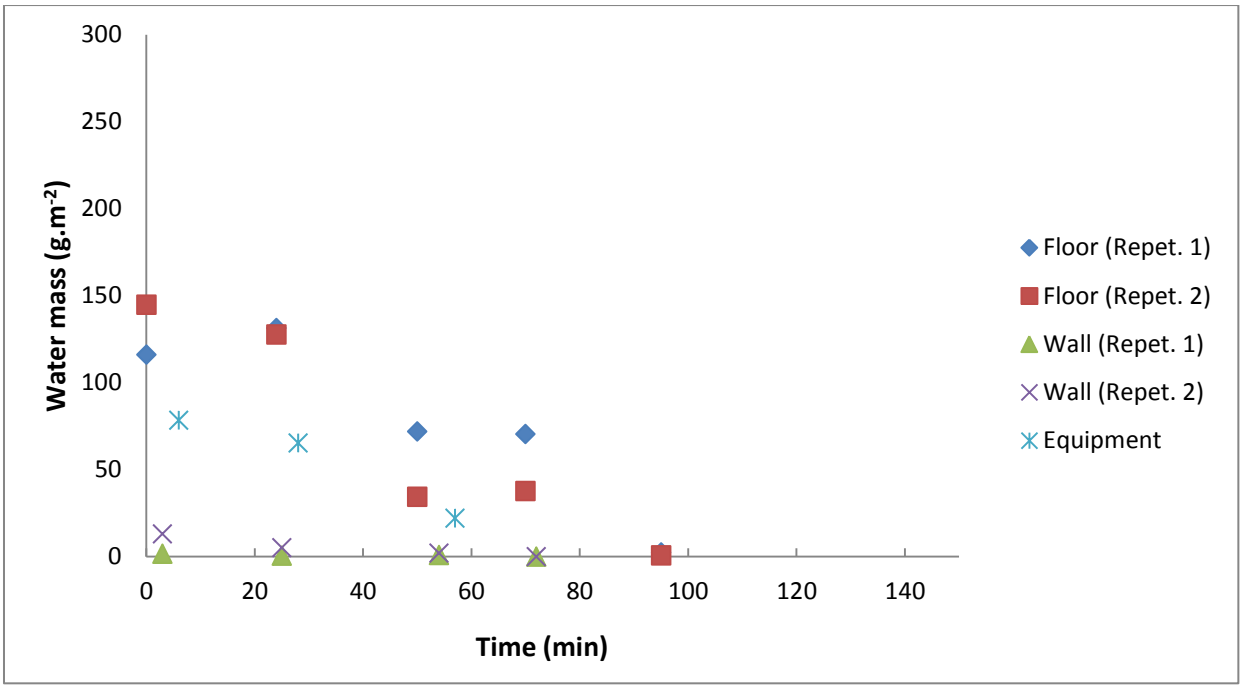

b

Figure 8: Water mass evolution on the wall, floor and equipment a- without a dehumidifier b- with a dehumidifier

In both cases, due to water stagnation on the floor, the initial water mass in this location is much higher than the water mass on the equipment and the wall. However, the water evaporation rate on the floor is higher than that in the other locations because of its high thermal inertia which makes the temperature decrease slower at the level of the floor than at the levels of the wall and the equipment (as explained in Section 4.3).

From Figure 8, the drying time of the surfaces studied can be estimated; without a dehumidifier, the drying time was around 120 min. for the three surfaces, whereas with a dehumidifier, it was approximately 70 min. for the wall and equipment and 100 min. for the floor. However, it was observed during the experiments that in both cases, even after two hours of drying, water could remain in certain positions where the air velocity is low (corners, complex equipment, etc…). It should be emphasized that the water mass evolution presented in Figure 8 gives an order of magnitude only; in fact, the water distribution is heterogeneous.

The influence of the dehumidifier can be directly observed in the water mass evolution. Firstly, the initial amount of water to be evaporated during the drying process is reduced from around 37 kg without a dehumidifier to 24 kg with a dehumidifier (essentially because there was less water on the floor). Secondly, because the relative humidity was much lower, and the evaporation rate on all the surfaces is higher with a dehumidifier; as seen Figure 8, even with the same initial water mass, the wall and the equipment dried faster with a dehumidifier. This gives rise to a shorter drying time. Zoz et al. (2016) carried out an experiment in a hermetic box (0.02 m^3) to study the influence of relative humidity of air in the box on the cultivability of *Listeria monocytogenes*. A relation between them was found (the lower the relative humidity, the faster the microbial inactivation). In this way, the humidity reduction by a dehumidifier is expected to reduce the microbial development. In addition, reducing the drying period would enable production to be started earlier, and this could be important for the manufacturer.

4.5. Analysis of exchange phenomena

The evaporation rate on the surfaces is proportional to the mass transfer coefficient, *k*, and the difference in the water concentration in the air in equilibrium with water (at the surface temperature) $C_{sat(T_{surface})}$, and the air circulating in the vicinity of the surface C_{wa} (Eq. 2).

$$\dot{m}_{evap} \propto k \cdot \left(C_{sat(T_{surface})} - C_{wa}\right) \quad with \quad C_{wa} = C_{sat(T_{air})} * RH \tag{2}$$

The mass transfer coefficient depends on the air velocity near the surfaces induced by ventilation, which was almost the same in the experiments performed with and without a dehumidifier. The water concentration in the air in equilibrium with water increases with the surface temperature and the water concentration in the air decreases as the relative humidity rises. Without a dehumidifier, the relative humidity is rather high (~90%), the evaporation rate is mainly determined by the thermal inertia: it is higher for the floor than for the wall and equipment. With a dehumidifier, the relative humidity decreases, and thus, the increase in the difference in water content ($C_{sat(T_{surface})} - C_{wa}$) induces a higher evaporation rate. In this case, both low relative humidity and thermal inertia are driving forces for the evaporation process.

In addition to the use of a dehumidifier, it is also possible to increase the air flow rate or to heat the surfaces. However, the air flow rate should not be higher than a critical value taking into account the well-being of workers and increasing the air flow rate induces a higher mechanical energy cost. Supplying heat to the surfaces, especially to equipment where a low evaporation rate was observed, could be a way of improving the drying process. Indeed,

because equipment has a low thermal inertia, its temperature decreases fast. Knowing that, as explained in Section 4.2, the dehumidifier and evaporators have sufficient capacity to collect the evaporated water and to allow a higher evaporation rate. A simplified heat and mass transfer model could help forecast, for example, the impact of additional surface heating on the evaporation rate.

5. Simplified heat and mass transfer model

The objectives of the model are to provide a better understanding of the exchange phenomena in the room and to predict the temperatures (air and surfaces), the relative humidity and the water mass evolutions (on the wall, floor and equipment). The model was developed using heat and mass balances, it is, thus, physical-based. Many input parameters were obtained from the food plant characteristics and from measurement in the plant (geometry, air velocity, temperature, humidity, water mass, materials…). The heat transfer coefficients were measured at laboratory scale inside a test chamber where the ventilation is similar to the one in the food plant. Then these values were exploited for the food plant based on velocity measurement near different surfaces. The mass transfer coefficient was estimated using the Lewis analogy. So, the model can be considered as semi-empirical.

5.1. Description of the model

Figure 9 presents schematically the developed zonal model.

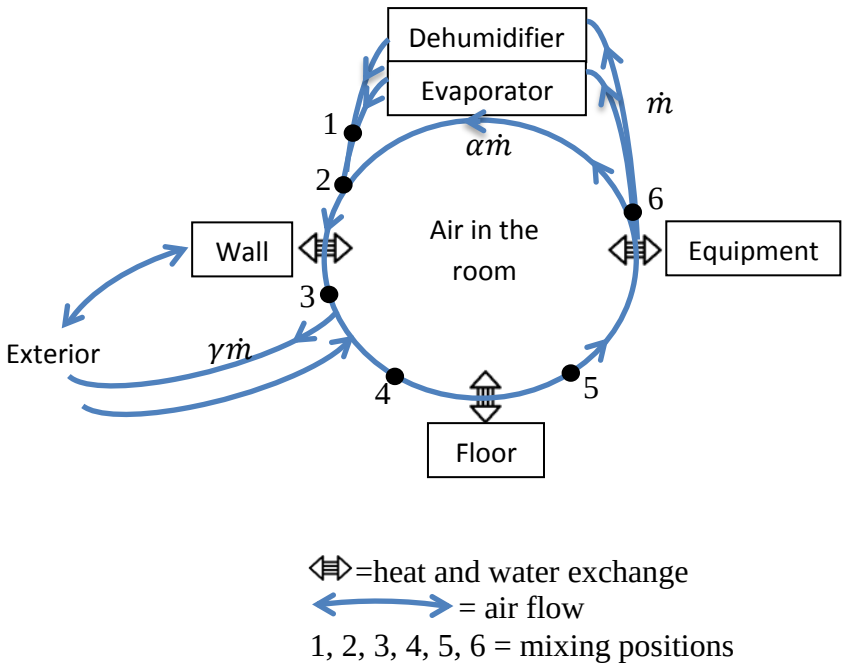

Figure 9: Scheme of the developed zonal model

The symbols: ⇹ represent the heat and water exchanges between air/wall, air/floor and air/equipment, respectively. The heat loss through the wall and the renewal air (exchange with external air) were also considered. The thermal inertia of the air was neglected compared to the ones of the wall, floor and equipment. Heat exchanges by radiation were neglected

compared to convection. Indeed, the average temperature is relatively low, the emissivities of most of the surfaces (stainless steel equipment for example) are rather low and the temperature difference between two radiating surfaces is limited at a given time. The heat and water exchange equations at several positions are presented below. The model is presented in more details in (Lecoq et al. 2016).

Heat and mass exchange between the air and the wall (positions 2 and 3 on Figure 9):

Convective exchange (heat transfer coefficient h_w) takes place between the air (temperature T_2) and the wall (temperature T_w). After this exchange, the air temperature is T_3.

$$(1+\alpha)\cdot\dot{m}\cdot Cp_{air}\cdot dT = h_w(T_w - T)dS_w$$

$$\frac{T_w - T_3}{T_w - T_2} = e^{-\frac{h_w\cdot S_w}{(1+\alpha)\cdot\dot{m}\cdot Cp_{air}}}$$

$$\delta_w\cdot T_2 - T_3 = -(1-\delta_w)\cdot T_w \quad (3)$$

$$\text{where } \delta_w = e^{-\frac{h_w\cdot S_w}{(1+\alpha)\cdot\dot{m}\cdot Cp_{air}}}$$

The evaporation rate is assumed to be proportional to the wet surface and the difference of water concentration in the air in equilibrium with water (at surface temperature) and the air circulating in the vicinity of the surface.

$$(1+\alpha)\cdot\dot{m}\cdot dX = k_w\cdot\beta_w\cdot(\rho\cdot X_w - \rho\cdot X)\cdot dS_w$$

where β_w is the fraction of the wall area which is covered by water and X_w is the water content of saturated air at the temperature of the wall.

$$\frac{X_w - X_3}{X_w - X_2} = e^{-\frac{k_w\cdot\beta_w\cdot S_w\cdot\rho}{(1+\alpha)\cdot\dot{m}}}$$

$$\delta_w'\cdot X_2 - X_3 = -(1-\delta_w')\cdot X_w \quad (4)$$

$$\text{where } \delta_w' = e^{-\frac{k_w\cdot\beta_w\cdot S_w\cdot\rho}{(1+\alpha)\cdot\dot{m}}}$$

The same procedure was applied for the heat and mass exchanges between the air and the floor (positions 4 and 5) and between the air and the equipment (positions 5 and 6).

Heat and mass balance on wall

The variation of the internal energy of the wall depends on the heat exchange by convection with air outside the room and the heat and water exchanges with the air inside the room.

$$\frac{dT_w}{dt} = \frac{h_{ext}\cdot S_{ext}}{(mC)_w}(T_{ext} - T_w) - \frac{(1+\alpha)\cdot\dot{m}\cdot Cp_{air}}{(mC)_w}(T_3 - T_2) - \frac{(1+\alpha)\cdot\dot{m}\cdot\Delta H_v}{(mC)_w}(X_3 - X_2) \quad (5)$$

$$\frac{dm_w}{dt} = -(1+\alpha)\cdot\dot{m}\cdot(X_3 - X_2) \quad (6)$$

The same procedure was applied to the floor and equipment.

The fraction of wetted surface, β, varies with time because it depends on the water mass per unit area. Supplementary experiments were carried out to study the evolution of the wet surface during evaporation of water droplets deposited on a stainless plate in a wind tunnel. This plate was exposed to airflow of 4.2°C, 51% relative humidity and 1.0 m.s^{-1}. The experimental results showed that β starts decreasing when the water mass is around 25% of its initial value ($m(t)/m_0$~0.25) and tends to zero when all the water is evaporated (Figure 10).

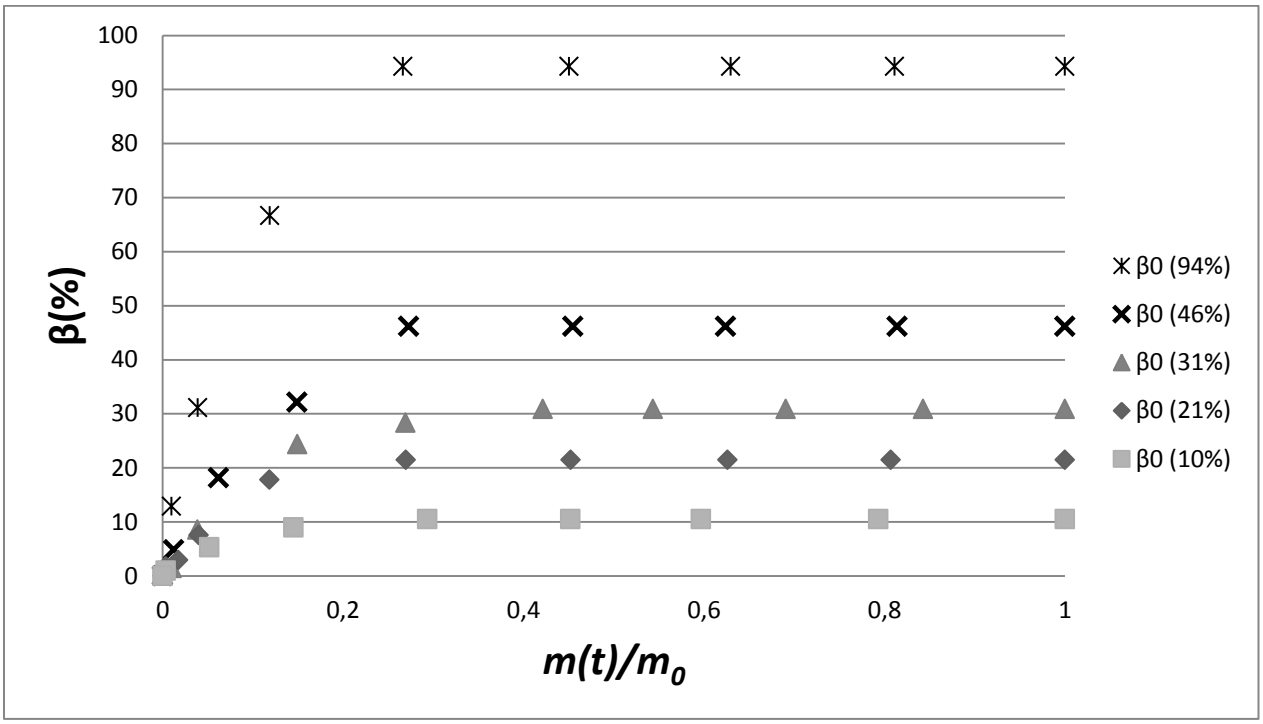

Figure 10: Evolution of the wet surface over the total surface (β) in function of the water mass. Experiments performed inside a wind tunnel with different initial values of β_0: 10, 21, 31, 46 and 94% (4.2°C, 51% air relative humidity and 1.0 m.s^{-1})

Therefore, it was assumed that β remains constant (= β_0) until $m(t) = 0.25 \cdot m_0$, and then β decreases linearly with $m(t)$:

$$\beta(t) = \min\left(\beta_0, \frac{m(t)}{0.25\cdot m_0}\cdot\beta_0\right) \quad (7)$$

In the present study, the air temperature and relative humidity were measured at the air blown by the evaporators and the dehumidifier during the drying process and their evolutions were used as boundary conditions in the model. The characteristic data of the room input in the model (surface areas considered, heat capacities, initial surface temperatures, heat and mass transfer coefficients, wet surface over total surface) are shown in Tables 4 and 5.

Table 4: Numerical values of the simplified model parameters

	Surface S (m²) considered in the 2D model [1]	Heat capacity mC ($J.K^{-1}$)	β_0 (%)
Wall	3.6	$3.1 \cdot 10^5$	8
Floor	4.1	$7.1 \cdot 10^5$	100
Equipment	2.0	$4.8 \cdot 10^4$	50

[1] The 2D model considers a half section of the room with a width of 1 m (the other half is quite symmetrical)

Table 5: Estimated values of the heat/mass transfer coefficients

	Without a dehumidifier		**With a dehumidifier**	
	h ($W.m^{-2}.K^{-1}$)	k ($m.s^{-1}$)	h ($W.m^{-2}.K^{-1}$)	k ($m.s^{-1}$)
	From t=0 to t=45 minutes		From t=0 to t=50 minutes	
Wall	14	$12.3 \cdot 10^{-3}$	7	$6.2 \cdot 10^{-3}$
Floor	6	$5.3 \cdot 10^{-3}$	3	$2.6 \cdot 10^{-3}$
Equipment	6	$5.3 \cdot 10^{-3}$	3	$2.6 \cdot 10^{-3}$
	From t=45 min. until the end of the drying process		From t=50 min. until the end of the drying process	
Wall	20	$17.6 \cdot 10^{-3}$	21	$18.5 \cdot 10^{-3}$
Floor	9	$7.9 \cdot 10^{-3}$	10	$8.8 \cdot 10^{-3}$
Equipment	9	$7.9 \cdot 10^{-3}$	10	$8.8 \cdot 10^{-3}$

It should be noted that the values of the heat/mass transfer coefficients were not the same during the entire drying process and for the two cases (with and without a dehumidifier) due to the fact that the evaporators were not operating at the exact same time intervals. When both evaporators were operating, the air velocities were almost the same as those demonstrated by Lecoq et al. (2015) and the heat transfer coefficients were assumed to be the same. When the dehumidifier or one of the two evaporators was operating (instead of the two evaporators), the heat transfer coefficient was calculated as follows:

$$h_2 = h_1 \cdot \sqrt{\frac{\dot{m}_2}{\dot{m}_1}} \tag{8}$$

where $\dot{m}_1$ is the air flow rate when the two evaporators are operating, h_1 the corresponding heat transfer coefficient, $\dot{m}_2$ the air flow rate in another case (with the dehumidifier or with one of the two evaporators operating) and h_2 the corresponding heat transfer coefficient.

The mass transfer coefficient k was calculated using the Lewis analogy:

$$k = \frac{h}{\rho . Cp_{air} . Le^{2/3}} \tag{9}$$

with $Le = \frac{a_{diff}}{D} = \frac{18.6 \cdot 10^{-6}}{21.8 \cdot 10^{-6}} \approx 0.85$

where a_{diff} is the thermal diffusivity of water vapor = $18.6 \cdot 10^{-6}$ m².s^{-1} at 0°C and D the mass diffusivity of water vapor in air = $21.8 \cdot 10^{-6}$ m².s^{-1} at 0°C (Bimbenet et al. 2002).

The initial surface temperatures were assumed to be 17°C for all the surfaces (due to technical constraints, these temperatures could not be measured at the very beginning of the drying period).

In this model, the main limitation is to consider the floor, the walls and the equipment only as three different zones and each one is represented by an overall temperature, water mass and heat transfer coefficient. In reality, there can still be a small amount of water in a corner of the room, whereas the floor is considered as globally dry by the model. The CFD approach could give more detailed knowledge of heat/mass transfer and airflow, but the implementation is much more complicated and time consuming.

5.2. Model validation

5.2.1. Comparison of the water mass evolution

The evolution of the water mass on the wall, floor and equipment obtained with the simplified model were compared with the experimental results obtained in the food production room (Figure 11).

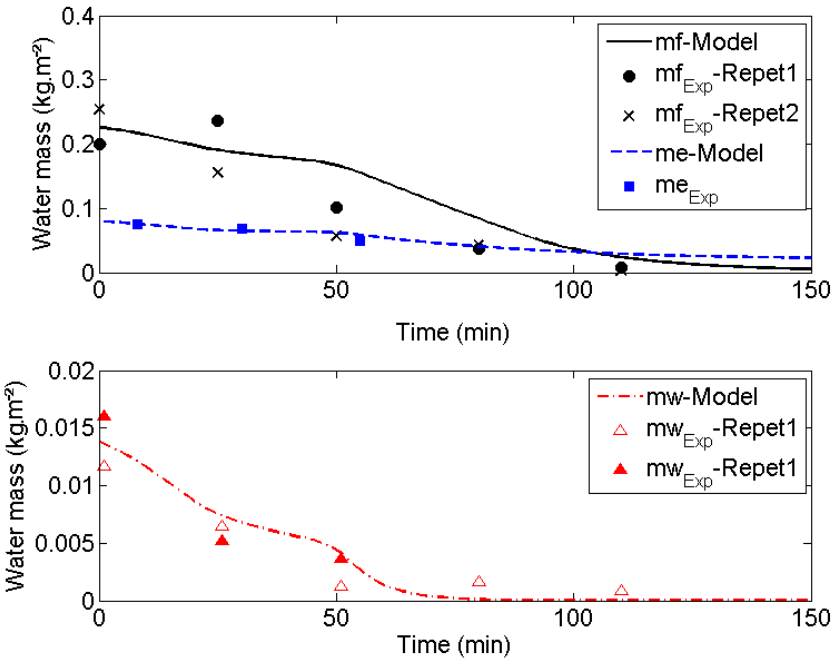

a

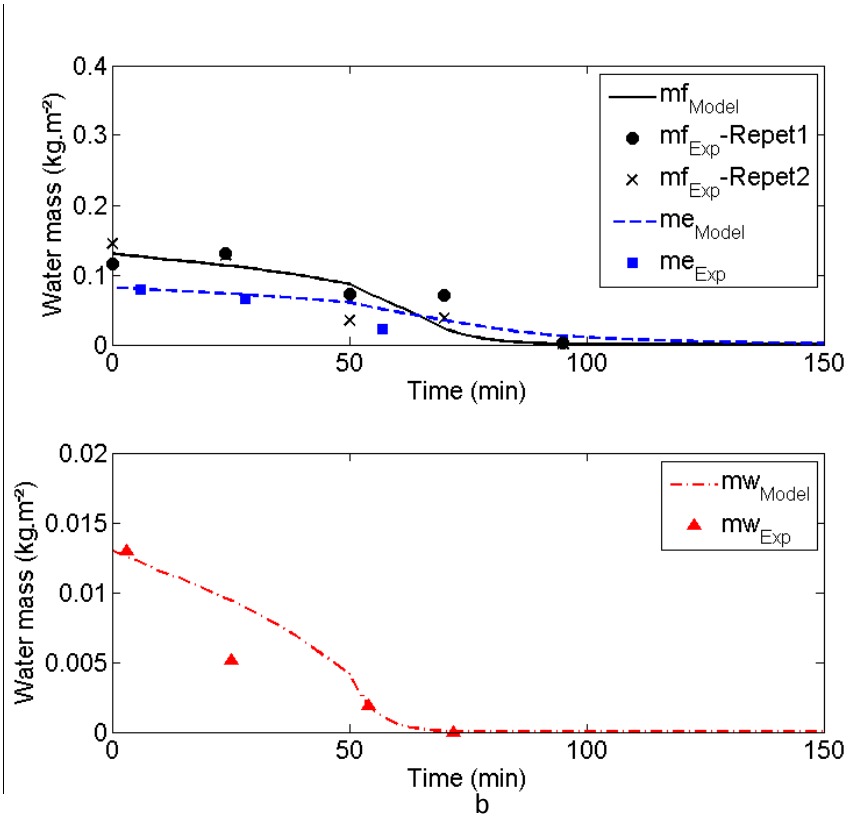

Figure 11: Comparison of the water mass evolution on the floor (mf), equipment (me) and wall (mw) between the experimental and predicted values. a- without a dehumidifier b- with a dehumidifier

Even if all the points do not match the model perfectly, considering that the water distribution is somewhat heterogeneous, the comparisons of the results are in rather good agreement. The influence of the evaporators can also be seen in this figure. During the first 50 min., when only one evaporator (case without a dehumidifier) or no evaporator (case with a dehumidifier) was operating, evaporation was slower.

In the case without a dehumidifier, as explained in Section 4.2, all the water evaporated is condensed on the cooling coils of the evaporators, which means that to evaporate water and prevent the relative humidity from rising, the evaporators must be operating. When the operating evaporator was defrosting over a period of 20 to 45 min. (which means that it stopped cooling), the water evaporated could not condense on the evaporator, and this in turn increased the relative humidity to almost 100%. This induced a much lower evaporation rate over this period (the first 45 min.). Furthermore, when the evaporators are operating, they also provide ventilation in the room, thus speeding up evaporation.

When a dehumidifier was used, both evaporators started operating 50 min. after the beginning of the process. However, as seen in Section 4.2, the dehumidifier alone was able to collect all of the evaporated water (no water condensed on the evaporators). This means that the evaporators promote evaporation alone by adding ventilation in the room, which in turn increases the mass transfer. Indeed, it can be seen from the results given by the model (Figure 11) that when the evaporators are not operating, evaporation is much slower than during the period following the first 50 min. of the process.

5.2.2. Comparison of the surface temperature evolution

The evolutions of the surface temperatures (on the wall, floor and equipment) obtained with the simplified model were compared with the experimental results (Figure 12).

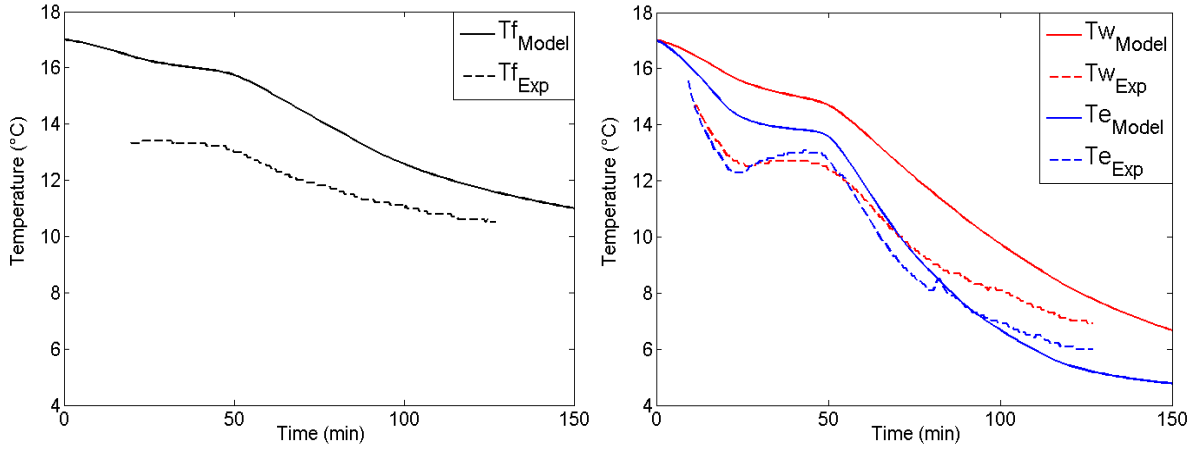

a

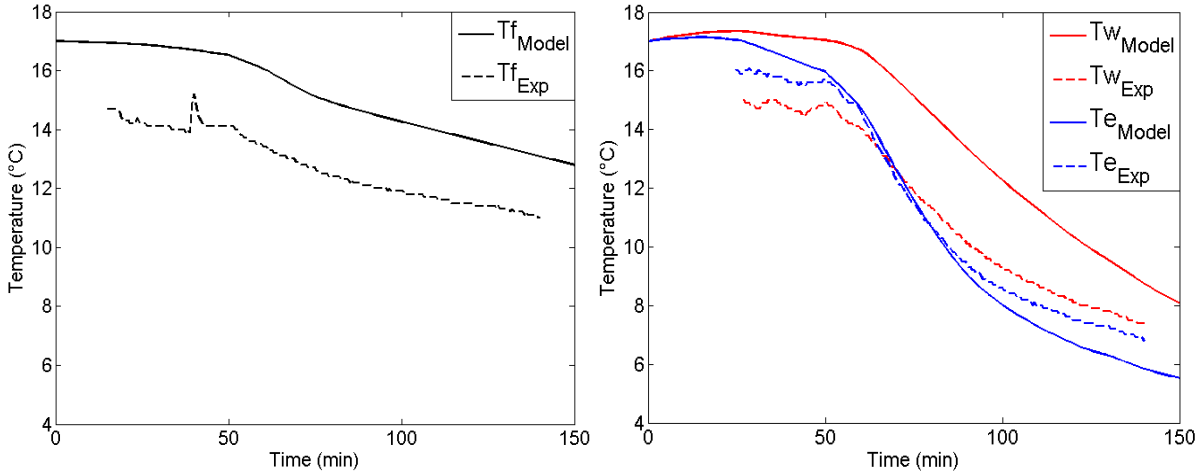

b

Figure 12: Comparison of the surface temperature evolution on the floor, wall and equipment between the experimental (dotted lines) and predicted values (undotted lines). a- without a dehumidifier b- with a dehumidifier

The experimental data provide a local value of the temperatures on the surfaces, which can be heterogeneous. This can explain a difference between the experimental and numerical results. In addition, because we did not have the exact initial surface temperatures (due to experimental difficulties) we estimated a temperature of about 17°C in both cases for the 3 surfaces. However, even if there are differences, the results are still of the same order of magnitude and demonstrate the same trend: a slower decrease in the floor temperature compared with the temperatures of the wall and the equipment.

5.3. Sensible and latent heat power

The sensible heat power ($\dot{m} \cdot Cp_{air} \cdot (T_{air\ return} - T_{air\ blown})$) and the latent heat power ($\dot{m} \cdot \Delta H_v \cdot (X_{air\ return} - X_{air\ blown})$) of the system (evaporators and dehumidifier) were calculated from the model throughout the drying process in both cases (with and without dehumidifier) (Figure 13).

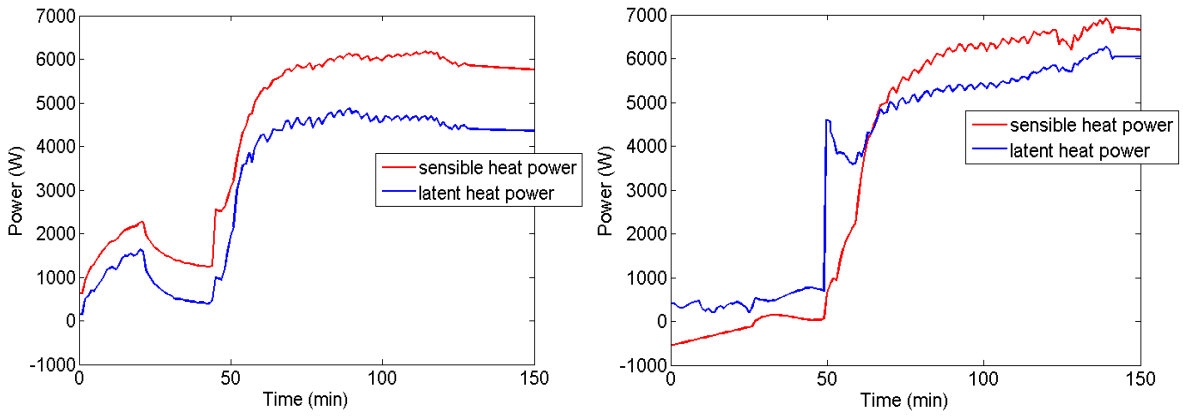

a b

Figure 13: Evolution of the sensible and latent heat power a- without dehumidifier b- with dehumidifier

Without dehumidifier, it can be observed that the sensible and latent heat power are low at the beginning of the process because only one evaporator was running and then defrosting from 20 min to 45 min. Then, both evaporators were running (after 45 min) the sensible and latent heat increased which induced a faster temperature drop (Figure 12) and a much larger evaporation rate (Figure 11).

With dehumidifier, for the first 50 min, only the dehumidifier was running which induced a negative latent heat power because the dehumidifier slightly increases the air temperature. Once the evaporators were running, the latent and sensible heat power increased strongly, inducing, as for the case without dehumidifier, an increase in evaporation rate and a temperature drop (Figure 11 and 12).

The comparison with and without dehumidifier shows that the latent heat power is much higher with dehumidifier (~6000 W against ~4000W at the end of drying) inducing more power to evaporate water. It can also be observed that if the evaporator were running immediately after cleaning, it would increase significantly the latent heat power and thus the evaporation of water.

5.4. Water evaporation prediction with heat supply to the equipment

During the drying process, the simplified model can help predict the drying time, for instance, on equipment when additional heat is provided. Another calculation was performed with 100 W of heating supplied to the equipment during the drying period. The results show that with or without a dehumidifier, the water mass decreases much faster than without any heat supply (Figure 14).

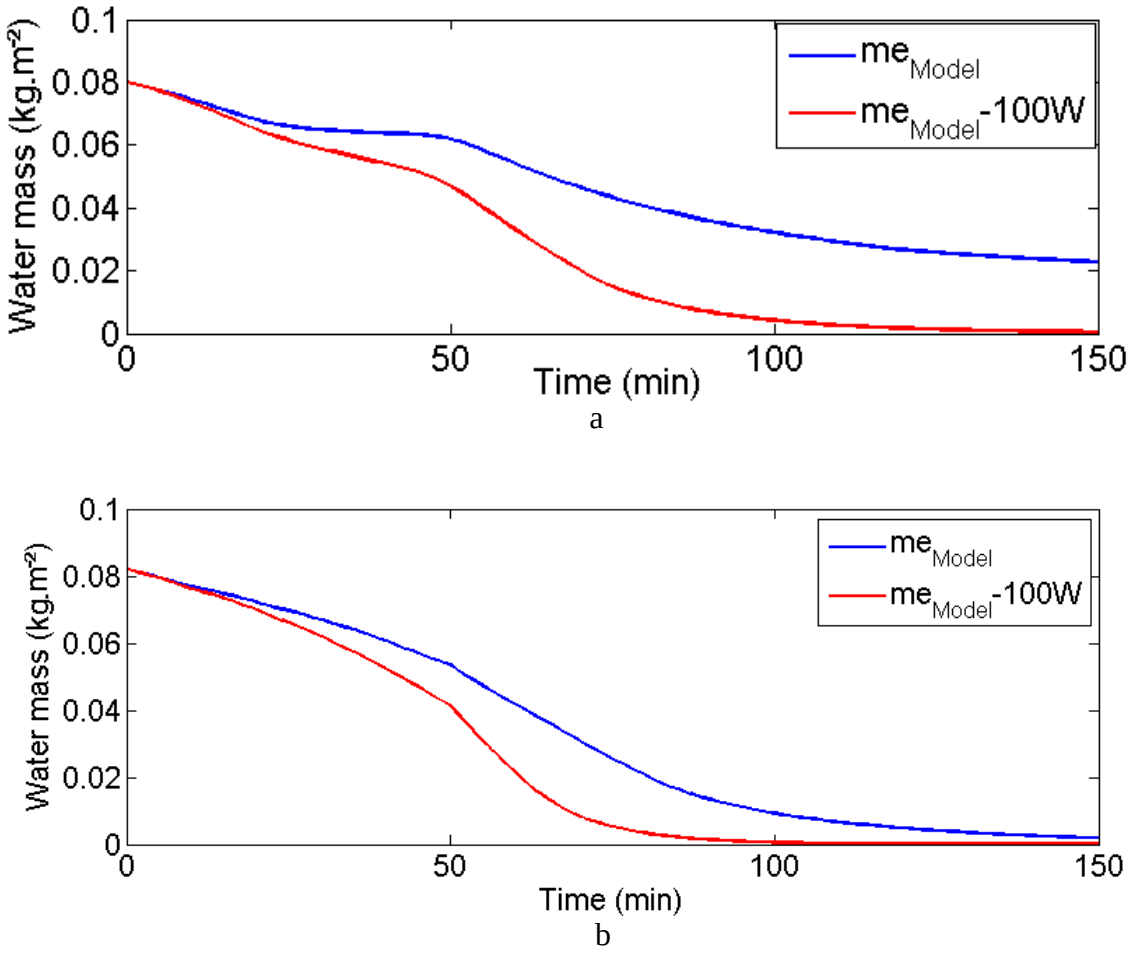

Figure 14: Comparison of the water mass evolution on the equipment with a 100W heat supply (red curve) and without a heat supply (blue curve). a- without a dehumidifier b- with a dehumidifier

This is explained by the fact that the equipment temperature remains rather high when heating is applied: always above 10°C, whereas it decreased to around 6°C when no heat was provided (Figure 15).

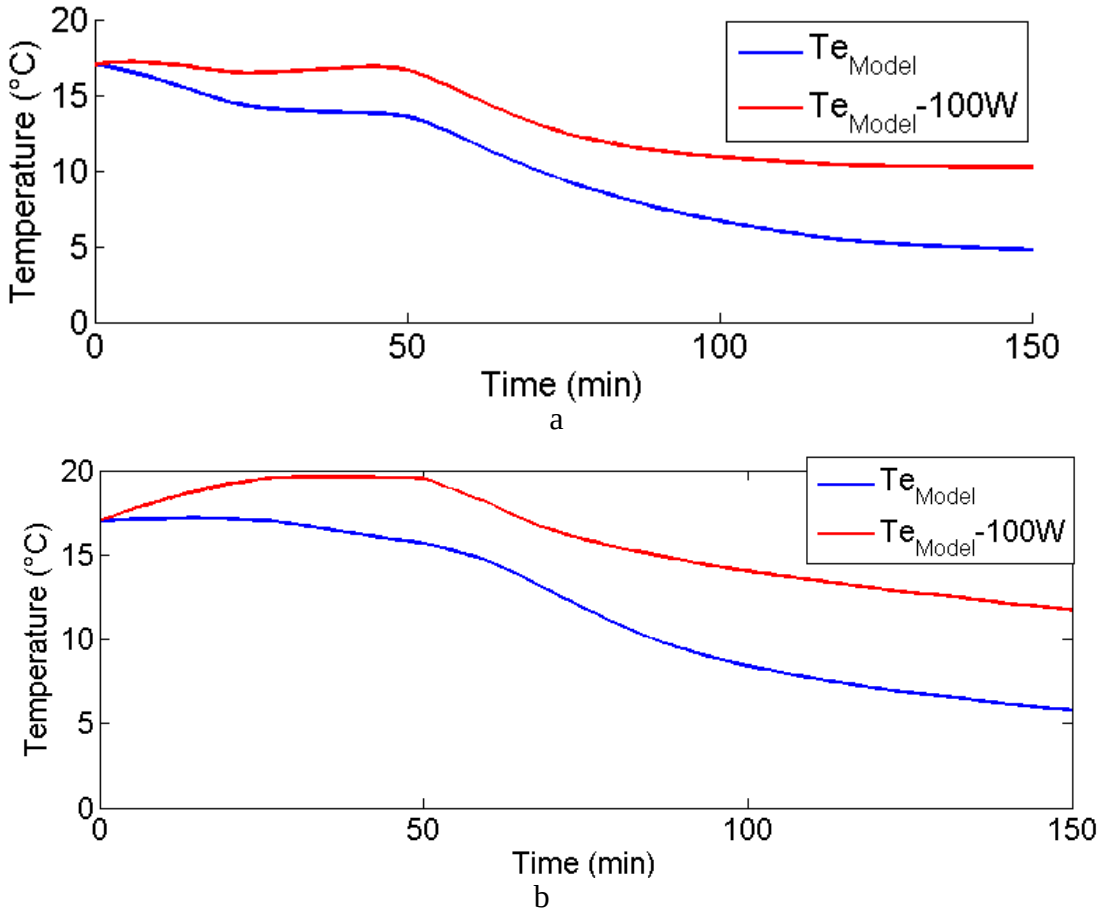

Figure 15: Comparison of the equipment temperature with a 100W heat supply (red curve) and without a heat supply (blue curve). a- without a dehumidifier b- with a dehumidifier

The numerical results show that with a heat supply of 100 W, the time required to dry the equipment is around 130 minutes and 100 minutes respectively without and with a dehumidifier, whereas it is much longer with no heat supply (>150 min). Evaporation is still greater with a dehumidifier due to the lower relative humidity, but the equipment would also be dry without a dehumidifier during the required time interval (approximatively 2 hours) if this amount of heat is provided. However, supplying heat to the equipment does not affect the evaporation rate on the other surfaces (wall and floor, results not shown).

5.5. Generalization of the model for another food processing plant

The developed model is quite directly applicable to a food plant with similar conditions: volume of 450 m^3 corresponding to the average volume of working room in a food plant in France, about 20% of volume occupied by equipment, relative humidity ranged from 60% (with dehumidifier) to 90% (without dehumidifier), air flow rate about 2.4 x 10^4 $m^3.h^{-1}$. The main limitation of applicability for the developed model concerns the air velocity near the surfaces (which determines the heat/mass transfer coefficients): it should be of the same order of magnitude as the one in this study (between 0.3 $m.s^{-1}$ and 2.0 $m.s^{-1}$). If not, additional measurements or simulations have to be performed to estimate these coefficients. The needed parameters for the developed model are reported and explained when it is applied to another plant in Figure 16.

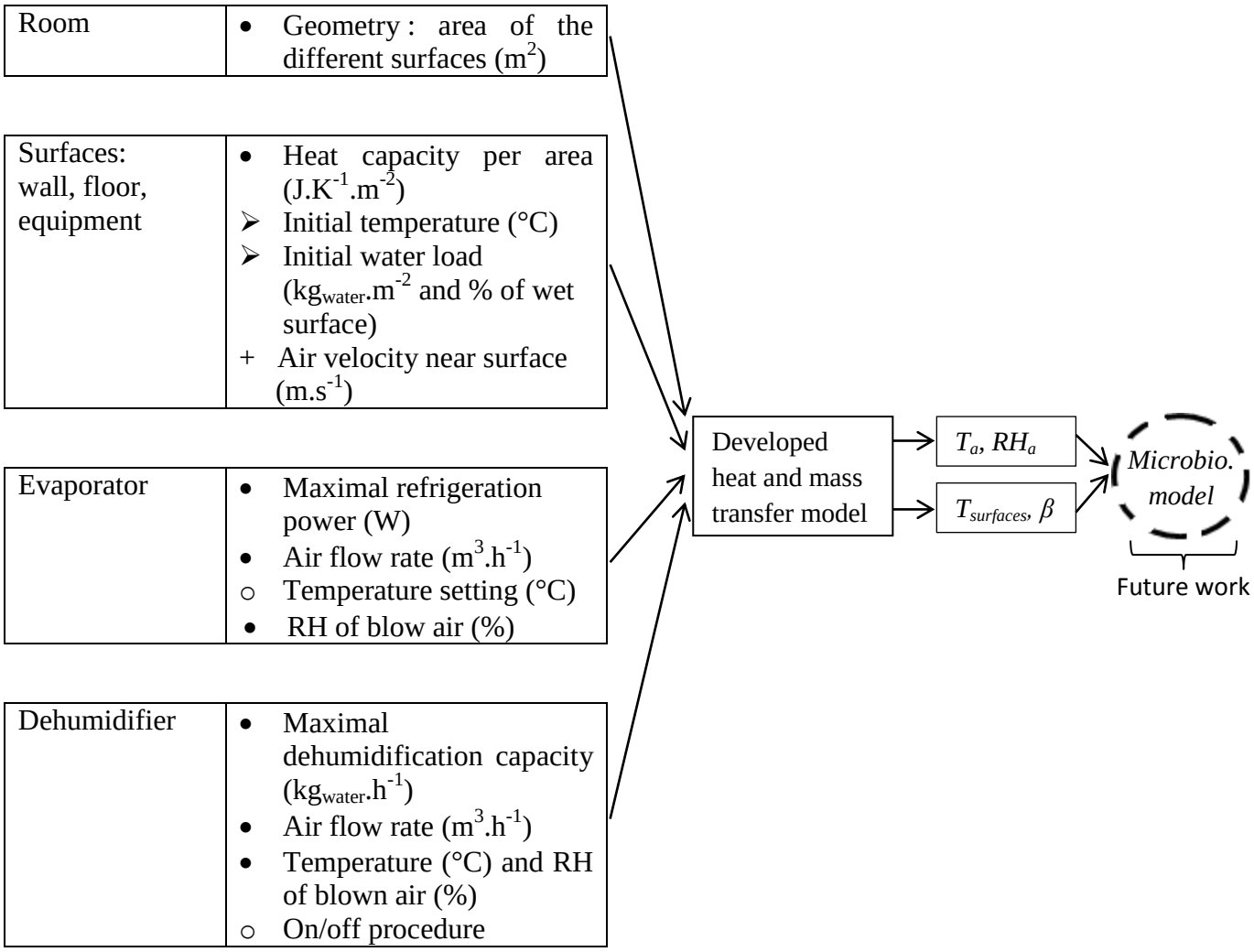

- Estimated from the food plant/evaporator/dehumidifier characteristics
  Can be adapted for another food plant

➢ Depending on the cleaning procedure (measured)

\+ Measured or estimated from CFD simulation
  Have to be measured or simulated (CFD) for another plant

○ Depending on the operating conditions
  Can be changed to study the influence of the operating conditions

Figure 16: Needed parameters for the model in case of application to another food processing plant

6. Conclusion

The value of the use of a dehumidifier in order to reduce the relative humidity in the room has been demonstrated in this study. The dehumidifier also induces a higher evaporation rate on the surfaces. At the positions where water mass measurements were performed, without a dehumidifier, it could take more than two hours to dry the surfaces, whereas most surfaces were dry after 100 minutes with a dehumidifier. However, it should to be underscored that in places where ventilation is low (corners, complex equipment…) the time required to dry these surfaces is longer. From the experimental and numerical methodology developed in this study, it was found that the relative humidity of air blown in the room is the most important factor to enhance drying. With a dehumidifier, the humidity could be reduced from 90% to 60%, this induced the drying rate to be around 1.5 times higher. In addition, in this case, the dehumidifier capacity (~19kg.h^{-1}) was much more significant than the amount of water to catch (~24 kg on the surfaces in two hours). The influence of the dehumidifier and evaporator capacities on the conditions in the room (relative humidity, drying rate…) can be analyzed with the developed model in order to size them correctly. The complexity of the proposed model is between and engineering calculation and CFD modelling. The engineering calculation, based only on the amount of water to be evaporated after cleaning and the maximal dehumidification capacity of the evaporator and dehumidifier, can underestimate the drying time. This time depends on the airflow pattern inside the room, the thermal inertia of the surfaces and the heat/mass transfer intensity near these surfaces. Our simplified modelling approach, takes into account all these aspects. It is, thus, not only based on the amount of moisture after cleaning but also on some characteristics of the food processing plant. The possibility of supplying heat (using heating cables) to the equipment has been discussed using the simplified heat and mass transfer model. The drying time was significantly reduced by supplying heat to this surface. However, there is another point that should be taken into account: the capacity of the evaporators and dehumidifier to collect the evaporated water. If the evaporated water cannot be condensed on an evaporator or a dehumidifier, the relative humidity in the room will keep increasing and fog will be generated. Sizing of the dehumidifier is thus important in order to achieve relatively dry air certain surfaces, other modifications could be tested experimentally or numerically: modifying the air flow pattern during drying, increasing the air flow rate or blowing warm air for instance.

Pathogen or spoilage microorganisms can grow in food plant if they are in favorable conditions especially the presence of liquid water and/or high relative humidity of air. Zoz et al. (2016) found that the lower the relative humidity, the faster the microbial inactivation. In this way, the humidity reduction by a dehumidifier is expected to reduce the microbial development. In order to quantify bacterial growth/inactivation, predictive microbiology can be coupled with the developed heat and mass transfer model. Such models (coupling heat/mass transfer and predictive microbiology) were already implemented for cold chain equipment (bacterial growth versus temperature) (Duret et al. 2014). In the case of a food plant, inactivation versus relative humidity has to be taken into account also once the surfaces are dried. This will be carried out in a future study, based on recent work (Zoz et al. 2016).

To take into account the environmental impact, a life cycle analysis of a dehumidifier could allow estimating the cost and benefice of this installation, it could be done in the future work. Among the benefices is the reduction of the risk of an incident due to bacterial growth. However, this incident in terms of direct cost and trade image would be difficult to assess.

ACKNOWLEDGEMENT

The research leading to this outcome has received funding from the French National Research Agency (EcoSec Project, ANR-12-ALID-0005-04). The authors would like to thank Labeyrie Fine Foods for their participation in experimental work conducted at the plant.

REFERENCES

Autio T., Hielm S., Miettinen M., Sjoberg A. M., Aarnisalo K., Bjorkroth J., Mattila-Sandholm T., Korkeala H. 1999. Sources of Listeria monocytogenes contamination in a cold-smoked rainbow trout processing plant detected by pulsed-field gel electrophoresis typing. *Appl. Environ. Microbiol.* 65: 150–55

Bimbenet J.-J., Duquenoy A., Trystram G. 2002. Génie des procédés alimentaires : Des bases aux applications.

Carpentier B., Cerf O. 2011. Review — Persistence of Listeria monocytogenes in food industry equipment and premises. *International Journal of Food Microbiology* 145: 1-8

Chandra S., Marzo M. d., Qiao Y. M., Tartarini P. 1996. Effect of liquid-solid contact angle on droplet evaporation. *Fire Safety Journal* 27: 141-58

Croce G., D'agaro P., Mora F. D. 2005. Numerical simulation of glass fogging and defogging. *International Journal of Computational Fluid Dynamics* 19: 437-45

Cunningham M. J. 2007. Mould and dust-mites thrive in high relative humidity. *Building and Environment*: 40–41

Duret S., Guillier L., Hoang H.-M., Flick D., Laguerre O. 2014. Identification of the significant factors in food safety using global sensitivity analysis and the accept-and-reject algorithm: application to the cold chain of ham. *International Journal of Food Microbiology* 180: 39–48

EC. 2005. Commission Regulation (EC) no 2073/2005 of 15 November 2005 on microbiological criteria for foodstuffs.

Flick D., Hoang H. M., Alvarez G., Laguerre O. 2012. Combined deterministic and stochastic approaches for modeling the evolution of food products along the cold chain. Part I: Methodology. *International Journal of Refrigeration* 35: 907-14

Hoang H. M., Flick D., Derens E., Alvarez G., Laguerre O. 2012. Combined deterministic and stochastic approaches for modelling the evolution of food products along the cold chain. Part II: A case study. *International Journal of Refrigeration* 35: 915–26

Kim K., Yoon J.-Y., Kwon H.-J., Han J.-H., Son J. E., Nam S.-W., Giacomelli G. A., Lee I.-B. 2008. 3-D CFD analysis of relative humidity distribution in greenhouse with a fog cooling system and refrigerative dehumidifiers. *Biosystems Engineering* 100: 245–55

La D., Dai Y. J., Li Y., Wang R. Z., Ge T. S. 2010. Technical development of rotary desiccant dehumidification and air conditioning: A review. *Renewable and Sustainable Energy Reviews* 14: 130-47

Lecoq L., Flick D., Derens E., Hoang H. M., Laguerre O. 2016. Simplified heat and mass transfer modeling in a food processing plant. *Journal of Food Engineering* 171: 1-13

Likotrafiti E., Smirniotis P., Nastou A., Rhoades J. 2013. Effect of relative humidity and storage temperature on the behavior of Listeria Monocytogenes on fresh vegetables. *Journal of Food Safety* 33: 545-51

Muhterem-Uyar M., Dalmasso M., Bolocan A. S., et, al. 2015. Environmental sampling for Listeria monocytogenes control in food processing facilities reveals three contamination scenarios. *Food Control* 51: 94–107

Teodosiu C., Hohota R., Rusaouën G., Woloszyn M. 2003. Numerical prediction of indoor air humidity and its effect on indoor environment. *Building and Environment* 38: 655-64

Teodosiu R. 2013. Integrated moisture (including condensation) - energy-airflow model within enclosures: Experimental validation. *Building and Environment* 61: 197-209

Vogel B. F., Huss H. H., Ojeniyi B., Ahrens P., Gram L. 2001. Elucidation of Listeria monocytogenes contamination routes in cold-smoked salmon processing plants detected by DNA-based typing methods. *Appl. Environ. Microbiol.* 67: 2586–95

Wulff G., Gram L., Ahrens P., Vogel B. F. 2006. One group of genetically similar Listeria monocytogenes strains frequently dominate and persist in several fish slaughter- and smokehouses. *Appl. Environ. Microbiol.* 72: 4313–22

Zoz F., Iaconelli C., Lang E., Iddir H., Guyot S., Grandvalet C., Gervais P., Beney L. 2016. Control of Relative Air Humidity as a Potential Means to Improve Hygiene on Surfaces: A Preliminary Approach with Listeria monocytogenes. *Plos One* 11

5.3. Article 7 : Influence of the relative humidity on the water drying rate and on microbial growth and inactivation in a food processing plant: Numerical study (Soumis à Journal of Food Engineering)

Influence of the relative humidity on the water drying rate and on microbial growth and inactivation in a food processing plant: Numerical study

L. Lecoq [ab*], L. Guillier[c], L. Fritsch[c], E. Derens[a], H.M. Hoang[a], O. Laguerre[a], D. Flick[b]

[a] Irstea, UR GPAN, 1 rue Pierre-Gilles de Gennes, 92761 Antony, France

[b] UMR Ingénierie Procédés Aliments, AgroParisTech, INRA, Université Paris-Saclay, 91300 Massy, France

[c] Université Paris-Est, Anses, French Agency for Food, Environmental and Occupational Health and Safety, Food Safety Laboratory, 23 avenue du Général de Gaulle, 94706 Maisons-Alfort Cedex, France

ABSTRACT

A heat and mass transfer model was developed to predict, during the drying of a food processing plant, the evolution of the water mass, wet surface, air temperature and relative humidity. The model was previously validated by comparing the predictions with the experimental results obtained in a food processing plant. Then, this model was coupled with a microbiological model to predict the fate of *Listeria monocytogenes* (growth and inactivation) at different locations in the plant (floor, wall and equipment). Simulations were carried out for blown air at 50%, 68% and 85% relative humidity in order to study the influence of air dehumidification in the plant on the drying rate and on the evolution of the microbial load. It was found that bacteria are more likely to develop on equipment when the drying time is longer. A technical solution involving heating of the equipment was proposed and the impact on the wet surface and the evolution of the microbial load was presented.

[*] Corresponding author: Tel: +33 1 40 96 90 04, Fax: +33 1 40 96 60 75, e-mail: logan.lecoq@irstea.fr

Nomenclature

a	Coefficient of the water content linearization	$kg_{water}.kg_{dry\ air}^{-1}.K^{-1}$
b	Coefficient of the water content linearization	$kg_{water}.kg_{dry\ air}^{-1}$
Cp_a	Specific heat capacity of air	$J.kg^{-1}.K^{-1}$
mC	Heat capacity of materials	$J.K^{-1}$
D	Time needed to reduce the bacterial load by a factor of 10	s
fn_{res}	Residual cell density after inactivation	Dimensionless
h	Convective heat transfer coefficient	$W.m^{-2}.K^{-1}$
h_0	Physiological state of the bacteria	Dimensionless
k	Rate of the inactivation reaction	s^{-1}
lag	Lag time of bacteria	h
m	Mass of water	kg
$\dot{m}$	Air mass flow rate	$kg.s^{-1}$
n	*Listeria monocytogenes* count per surface area	m^{-2}
Q	Physiological state of the bacteria	Dimensionless
RH	Relative humidity	Dimensionless
S	Total surface area	m^2
T_{ref}	Reference temperature	°C
$T_{\min}$	Minimal growth temperature	°C
T	Temperature	°C
x	$\log_{10}(\frac{n}{n_0})$	Dimensionless
X	Water content in the air	$kg_{water}.kg_{dry\ air}^{-1}$
α, γ	Air distribution coefficient	Dimensionless
μ_{max}	Maximum growth rate	s^{-1}
μ_{ref}	Maximum growth rate at reference temperature 25°C	s^{-1}
β	Percentage of wet surface with respect to total surface ($\frac{S_{wet}}{S}$)	Dimensionless
ρ	Air density	$kg.m^{-3}$
ΔH_v	Heat of water vaporization	$J.kg^{-1}$

Subscripts

0 initial time e equipment f floor w wall

1. Introduction

Listeria monocytogenes is a major foodborne pathogen that can cause listeriosis, a severe infection with a fatality rate of around 20% (EFSA 2015). Listeriosis occurs following the consumption of contaminated ready-to-eat foods such as cooked ham, cold-smoked salmon, fresh fruit or dairy products (Batz et al. 2012, Fretz et al. 2010, Lambertz et al. 2013, Zhu & Hussain 2014). This pathogen is able to grow as long as the water activity is above 0.92, the pH is between 4.2 and 9.5 and low temperature conditions are present (a few degrees below 0°C) (Buchanan et al. 2004). In addition, *L. monocytogenes* can easily adhere to surfaces such as stainless steel, which is commonly used for equipment in processing plants, and can be transferred to other surfaces, which makes the bacteria ubiquitous in food production plants (Carpentier & Cerf 2011). Equipment with a complex shape can be difficult to disinfect and bacteria are able to take refuge and form biofilms in damaged equipment or cracks on the floor where lethal concentrations of disinfectant cannot be achieved (Carpentier & Cerf 2011). *L. monocytogenes* can thus persist for months in processing plants and can contaminate products even though apparently well performed cleaning and disinfection procedures are applied (Muhterem-Uyar et al. 2015, Vogel et al. 2001). After cleaning and disinfection that usually takes 5 hours, the micro-organism is able to survive or to grow during the drying period (usually 2 hours, e.g. from 2am to 4am) and the production period (e.g. from 4am to 9pm), depending on the ambient conditions in general and the relative humidity in particular. Zoz et al (2016) reported, in a laboratory-scale study, a relationship between the relative humidity and the growth/inactivation of *L. monocytogenes* at different times varying from 0 to 24h. In addition to sanitary measures, better control of processing conditions to prevent contamination of materials and products is crucial (Løvdal 2015). The prediction and the control of ambient conditions, including local air humidity and the presence of water on the different surfaces, are necessary in order to provide more options designed to reduce bacteria growth than disinfection alone.

Subsequent to our previous study on a simplified model of heat and mass transfer applied to a food processing plant (Lecoq et al. 2016), the aim of this study is to integrate a predictive microbiological model in order to assess the growth/inactivation of *L. monocytogenes* on three different surfaces of a food production plant: on the wall, floor and equipment. The influence of the relative humidity of blown air on the water evaporation rate and on microbial fate was studied in order to assess the impact of air dehumidification conditions in processing plants. The proposed approach can be used by manufacturers to identify the possible risks of contamination and to simulate technical solutions that may reduce this risk.

The methodology proposed in this study is original, firstly because few studies have been carried out in order to demonstrate the influence of the relative humidity of the air on the microbial load compared with the influence of temperature. Secondly, heat/mass transfer and predictive microbiology models were associated in order to examine bacterial growth or inactivation on the surfaces under the dynamic conditions present in a food processing plant.

2. Literature review

In practice, it is difficult to assess microbial contamination on large surfaces, above all because of the variability from one location to another. Predictive microbiology is a complementary approach since it provides an estimation of microbial development where microbial experiments would be too labor-intensive. Besides avoiding expensive and time-consuming experiments, predictive microbiology also enables optimization of industrial

processes when conditions encountered in the industry are used as an input factor of the predictive model (VamImpe et al. 1995). According to the recommendation from CAC (Codex Alimentarius Commission, 2007) and the European regulation (2002) on food safety, predictive microbiology can guarantee the quality and safety of food products by forecasting the risk areas and can predict the shelf life of food products (McMeekin & Ross 2002). The model for bacterial growth proposed by Baranyi and Roberts (1994) has become the model the most commonly used to predict microbial growth under dynamic conditions, such as when the air temperature evolves during a process (McKellar & Lu 2004). This deterministic model uses four parameters (n_0, n_{max}, μ_{max} and *lag*) specific to the studied conditions. In addition, to be able to predict microbial evolution, ambient conditions (temperature, relative humidity…) and the evolution of the wet surfaces of a room have to be predicted because of their influence on growth/inactivation rates. Lecoq et al. (2016) developed a simplified heat and mass transfer model to predict the evolution of these parameters.

3. Simplified heat and mass transfer model

The surface temperature, the relative humidity and the absence/presence of water on the surface are determining factors governing microbial development. In food production plants, the temperature and relative humidity vary throughout the day depending on the production phase, cleaning (using water) and drying. The use of a heat and mass transfer model is necessary to estimate the evolution of these parameters (temperature, relative humidity and wet surface area) throughout the process. Through integration of theoretical microbiological models (Baranyi & Roberts 1994) or empirical ones in the heat and mass transfer model, microbial fate (growth or inactivation) can be estimated on surfaces (wall, floor and equipment). The zones presenting high contamination risks can then be highlighted.

The simplified heat and mass transfer model used in this study was developed previously and its validation was performed by comparison with experimental measurements conducted in a food processing plant (Lecoq et al. 2016). The model predicts the surface/air temperature, the relative humidity near the studied area, the water mass and the wet surface evolution at different locations in a food production plant. Only half of the room was studied (Figure 1) and it was considered that the same phenomena were present in the other half (symmetry). Air is blown from the evaporator located on the ceiling, then flows downwards close to the wall (I) then towards the center along the floor (II) and finally upwards to the return air grill (under the evaporator) along the equipment (III). The entrainment of air by the blown air (which constitutes a wall jet) in front of the evaporator is characterized by the coefficient of air distribution α. Air renewal is characterized by the coefficient γ. To simplify the model, the thermal inertia of the air was neglected compared with the inertia of the wall, floor and equipment. The symbols: ⇼ (Figure 1) in front of the rectangles I, II and III represent the heat and water exchange zones between air/wall, air/floor and air/equipment, respectively. Heat loss through the wall and air renewal (exchange with external air) was also considered. Heat exchange by radiation was neglected compared with convection. Indeed, the average temperature is relatively low, the emissivity of most of the surfaces (stainless steel equipment for example) is rather low and the temperature difference between the radiating surfaces is limited at any given time.

Figure 1: Simplified airflow, heat and mass transfer model in a food factory (side view)

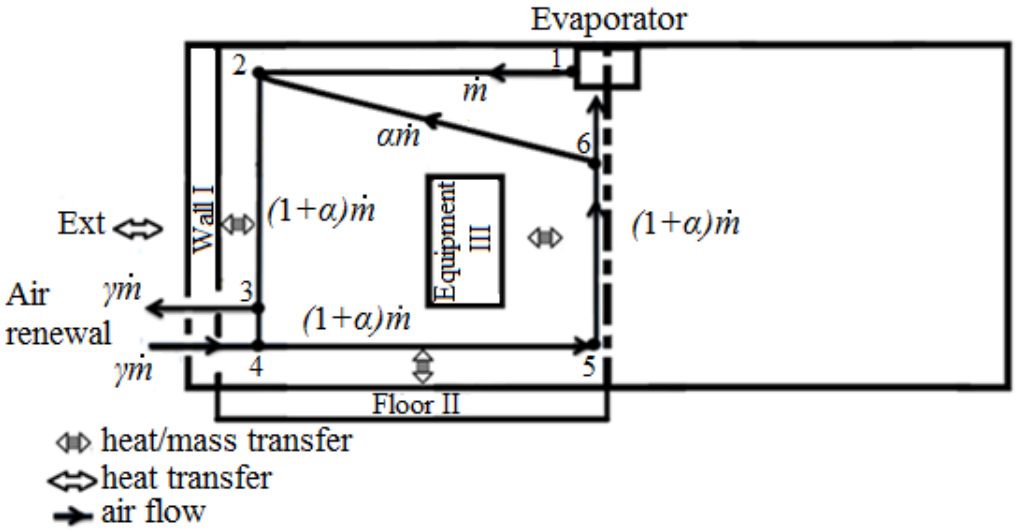

Position	Parameters at the position
1	T_1, X_1
2	T_2, X_2
3	T_3, X_3
4	T_4, X_4
5	T_5, X_5
6	T_6, X_6
I	S_w, $(mC)_w$, T_w, X_w, m_w, k_w, h_w, β_w, S_{ext}, h_{ext}
II	S_f, $(mC)_f$, T_f, X_f, m_f, k_f, h_f, β_f
III	S_e, $(mC)_e$, T_e, X_e, m_e, k_e, h_e, β_e
Ext	T_{ext}, X_{ext}

3.1. Heat and mass balances

Heat and water balances were determined for each point (1 to 6, Figure 1) and for the three surfaces: wall, floor and equipment. For example, concerning the heat and mass exchanges between the air and the wall (rectangle I), convective exchange (heat transfer coefficient h_w) takes place between the air (temperature T_2) and the wall (temperature T_w). Following this exchange, the air temperature is T_3:

$$(1+\alpha)\cdot\dot{m}\cdot Cp_{air}\cdot dT = h_w(T_w - T)dS_w$$

$$\frac{T_w - T_3}{T_w - T_2} = e^{-\frac{h_w\cdot S_w}{(1+\alpha)\cdot\dot{m}\cdot Cp_{air}}}$$

$$\delta_w\cdot T_2 - T_3 = -(1-\delta_w)\cdot T_w \quad (1)$$

where $\delta_w = e^{-\frac{h_w\cdot S_w}{(1+\alpha)\cdot\dot{m}\cdot Cp_{air}}}$

The evaporation rate is assumed to be proportional to the wet surface and the difference in water concentration in the air in equilibrium with water (at surface temperature) and the air circulating in the vicinity of the surface is determined using the following equation

$$(1+\alpha)\cdot\dot{m}\cdot dX = k_w\cdot\beta_w\cdot(\rho\cdot X_w - \rho\cdot X)\cdot dS_w$$

where X_w is the water content of saturated air at the temperature of the wall which is approximated by a linear relation.

$$X_w = a_w\cdot T_w + b_w$$

$$\frac{X_w - X_3}{X_w - X_2} = e^{-\frac{k_w\cdot\beta_w\cdot S_w\cdot\rho}{(1+\alpha)\cdot\dot{m}}}$$

$$\delta_w'\cdot X_2 - X_3 = -(1-\delta_w')\cdot X_w = -(1-\delta_w')\cdot(a_w.T_w + b_w) \quad (2)$$

where $\delta_w' = e^{-\frac{k_w\cdot\beta_w\cdot S_w\cdot\rho}{(1+\alpha)\cdot\dot{m}}}$

For the temperature evolution of the wall (rectangle I):

The variation in the internal energy of the wall depends on the heat exchange by convection with the air outside the room and the heat and water exchange between the air inside the room.

$$\frac{dT_w}{dt} = \frac{h_{ext}\cdot S_{ext}}{(mC)_w}(T_{ext} - T_w) - \frac{(1+\alpha)\cdot\dot{m}\cdot Cp_{air}}{(mC)_w}(T_3 - T_2) - \frac{(1+\alpha)\cdot\dot{m}\cdot\Delta H_v}{(mC)_w}(X_3 - X_2)$$

(3)

$$\frac{dm_w}{dt} = -(1+\alpha)\cdot\dot{m}\cdot(X_3 - X_2) \quad (4)$$

The same heat and mass balances were applied to other points (1 to 6, Figure 1) and for the two other surfaces (floor and equipment). Details concerning the development of the model and a comparison between the predicted water mass evolution and measured values in a food processing plant on the floor, wall and equipment during the drying period (Figure 2) can be found in Lecoq et al. (2016).

Figure 2: Measured (m_{Exp}) and calculated water weight located on the floor (a) and on the wall and equipment (b) during the drying process (RH=85%) (Lecoq et al. 2016)

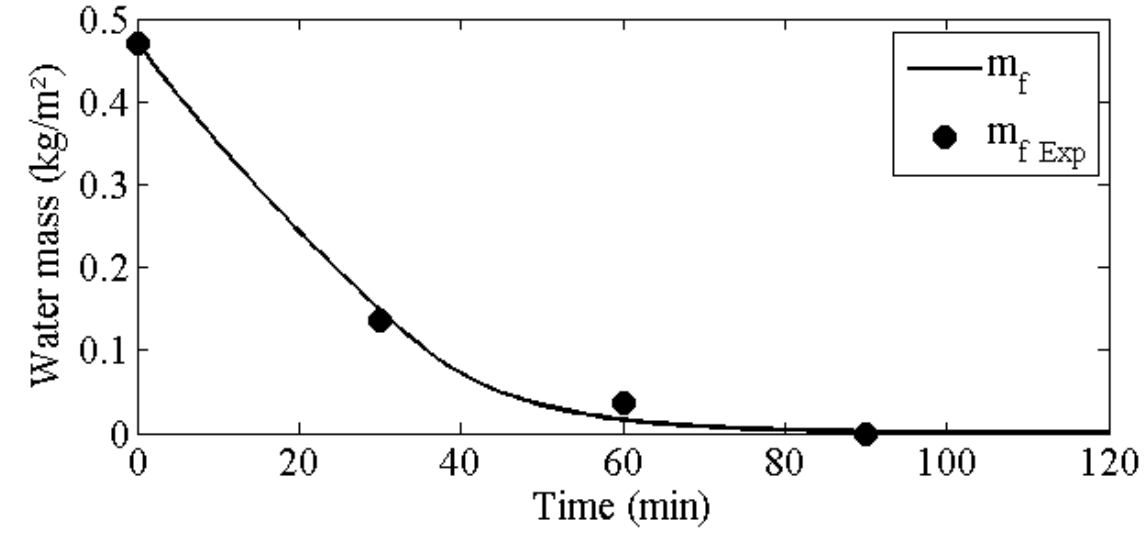

a

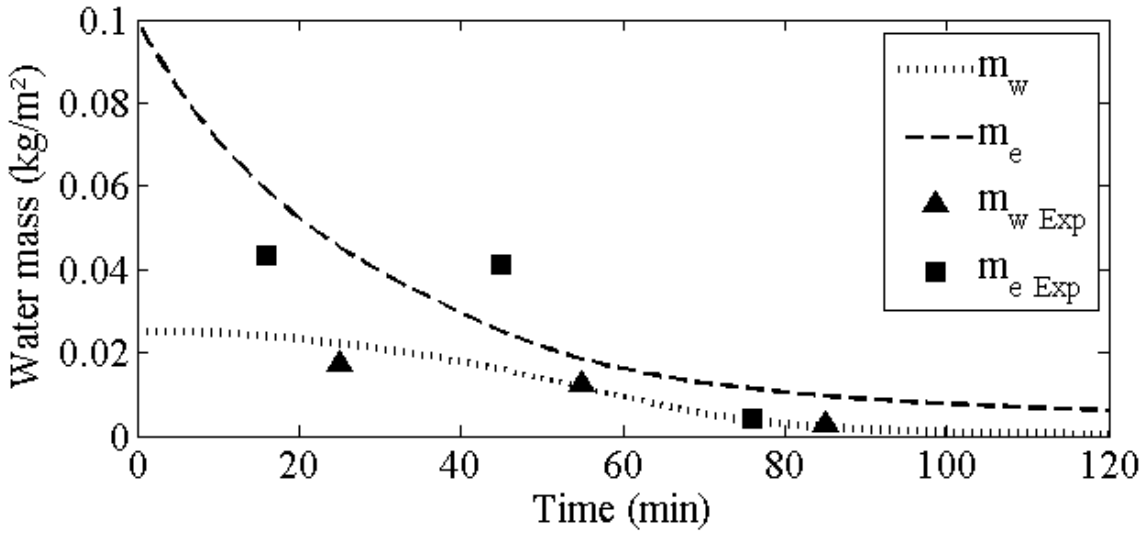

b

3.2. Wet surface (expressed as a percentage) model

The model presented in sub-section 3.1 allows prediction of the surface temperature, the air temperature, the relative humidity and the water mass evolution on the surface. These parameters were used to estimate the percentage of wet surface (β, wet surface with respect to the total surface), a determining factor for microbial load. The surface of wall, floor and equipment were numerically separated into 5000 sub-areas. In accordance with the calculated coefficient β, sub-areas were considered to be dry or wet. For example, at the beginning of the drying process, the floor was considered to be completely wet (β=100%), and thus, all 5000 sub-areas were considered to be wet. The percentage of wet surface gradually decreases. For example, when the β coefficient reaches 50%, 2500 sub-areas are considered as being wet and 2500 dry. This consideration was included in the model using a Boolean function (B). When the sub-area is wet, B is equal to 1, and when the sub-area is dry, B is equal to 0. This function is used in the predictive microbiological model (Section 4).

4. Predictive microbiology

Here, the microbial evolution at the three locations (wall, floor and equipment) of the food plant was studied for one day, starting with the drying period (after cleaning) and finishing at the end of the production period. The bacterial load at the end of the cleaning period is assumed to be known (input parameter of the model) and the evolution (growth or inactivation) of this load throughout the process is then calculated.

4.1. Mathematical model of microbial development

4.2.1. Microbial growth

In a favorable environment, microorganisms can grow exponentially. The presence of water on a surface (or high relative humidity) is necessary for bacterial growth. The influences of inhibition factors such as pH are considered negligible under our conditions. Indeed, even though the pH on the surfaces may vary over time during cleaning, rinsing should guarantee their neutrality (Aziza-Tenenhaus 2007). In a favorable environment for growth, three phases are considered: the lag phase, exponential growth and the stationary phase. In this study, the equations used to describe microbial growth are based on the deterministic model proposed by Baranyi and Roberts (1994). This model uses four parameters to describe bacterial growth; n_0, n_{max}, μ_{max} and *lag*. The lag phase duration (*lag*) can be estimated as follows (Mellefont et al. 2003):

$$lag = \frac{h_0}{\mu_{max}} = \frac{h_0}{\mu_{opt} \cdot \gamma} \tag{5}$$

where h_0 is a parameter characterizing the physiological state of the bacteria. When bacteria are ready for exponential growth, i.e. have already adapted to the growth conditions, there is no lag time. When bacteria have been stressed by conditions they encountered before being placed in conditions favorable for growth, an adaptation period is necessary before exponential growth can occur.

The influence of the environment on bacterial growth is taken into account using the "gamma concept (γ)", developed by Zwietering et al. (1992). Bacterial growth is considered only when B=1 (presence of water in the sub-area) or if the relative humidity is above 92% (Buchanan et al. 2004). Only the surface temperature is considered in the γ function (Tenenhaus-Aziza et al. 2014a):

$$\gamma = \left(\frac{T - T_{min}}{T_{ref} - T_{min}}\right)^2 \tag{6}$$

The following system of equations describes bacterial growth (Baranyi and Roberts (1994):

$$\frac{dn}{dt} = B' \cdot \frac{1}{1 + e^{-Q(t)}} \cdot \mu_{opt} \cdot \gamma \cdot \left(1 - \frac{n}{n_{max}}\right) \cdot n \tag{7}$$

with:

$$B' = \begin{cases} 1 \; if \; (B = 1) \; or \; (B = 0 \; and \; RH > 0.92) \\ 0 \; (B = 0 \; and \; RH < 0.92) \end{cases}$$

$$\frac{dQ}{dt} = B \cdot \mu_{opt} \cdot \gamma \tag{8}$$

$$Q_0 = \ln\left(\frac{1}{e^{h_0} - 1}\right) \quad (9)$$

The parameters in Equations 5 to 9: μ_{opt}, h_0, n_0, n_{max}, T_{min}, T_{ref} obtained from the literature are shown in Table 1. Three physiological states (h_0) were studied: $h_0 = 0$ (representing no adaptation prior to growth), h_0 = 2.0 (representing bacterial stress due to drying) and $h_0 = 3.5$ (representing stress due to disinfection) (Guillier & Augustin 2006b).

Table 1: Values of the parameters used in the model

Parameters	Value used in the model	References
μ_{opt}	0.06 h^{-1} (at T_{ref} =25°C)	(Tenenhaus-Aziza et al. 2014b)
h_0	0 ; 2 ; 3.5	(Guillier & Augustin 2006a)
n_0	1 UFC.m^{-2}	
n_{max}	10^5 UFC.m^{-2}	(Tenenhaus-Aziza et al. 2014b)
T_{ref}	25°C	(Tenenhaus-Aziza et al. 2014b)
T_{min}	-2.3°C	(Augustin et al. 2005a)

Here, $n_0 << n_{max}$ and we will see hereafter that the microbial load does not rise to a great extent, which implies that $1 - \frac{n}{n_{max}} \sim 1$ and that the results are independent of n_0.

4.2.2. Microbial inactivation

Bacterial inactivation is considered when both conditions are respected: B = 0 and relative humidity (just above the surface) is less than 92%.

When bacteria are exposed to lethal conditions, they are not instantaneously inactivated. The first-order kinetics equation used also considers that a fraction of the bacteria resist (residual cell density).

Inactivation can be represented by Equation 10:

$$\frac{dn}{dt} = -(1 - B') \cdot k \cdot \max\left(0, n - fn_{res} \cdot n_{dry}\right) \quad (10)$$

where $k = \frac{\ln(10)}{D}$

fn_{res} = residual cell density

n_{dry} = maximum bacterial load on the sub-area = bacterial load when the sub-area begins to dry

The "max" function in Equation 10 implies that in dry sub-areas, when inactivation takes place, the number of bacteria can only decrease. Without this function, the population could increase if the local relative humidity exceeds 92%.

The empirical equations of the *D* coefficient (Figure 3) and fn_{res} (Figure 4) were developed in this study taking into account recently published experimental data on the inactivation of *L.*

monocytogenes deposited on a surface exposed to different relative humidities at ambient temperature (Zoz et al. 2016). The adjusted equations are shown in Equations 11, 12 and 13.

Figure 3: Influence of the relative humidity on $\log_{10}(D)$, adapted from Zoz et al. (2016)

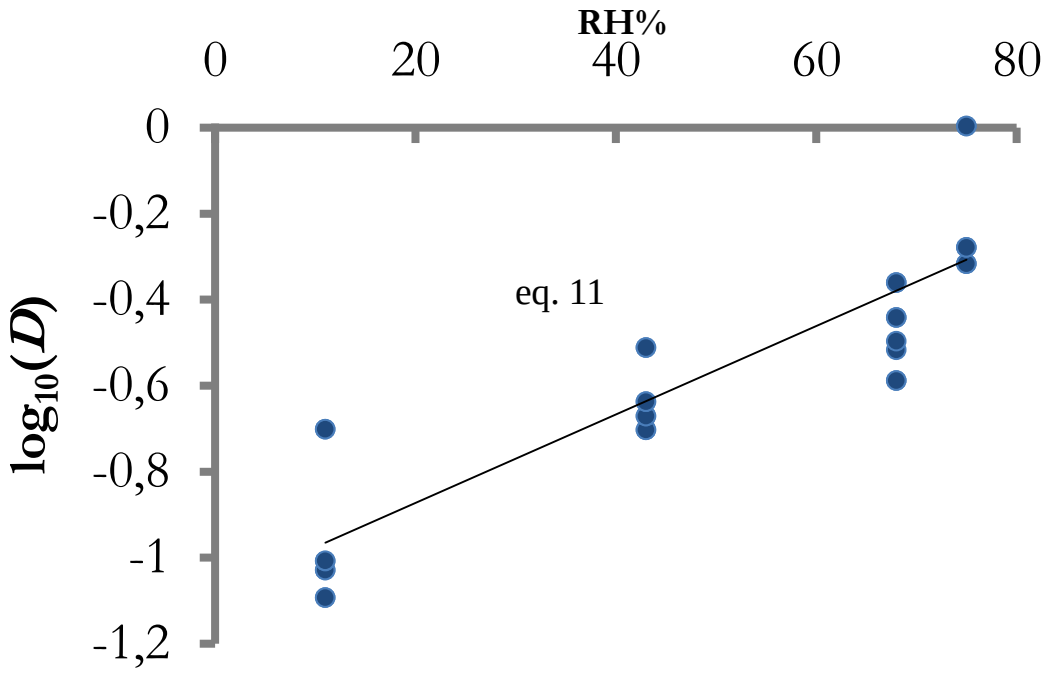

Figure 4: Influence of the relative humidity on $\log_{10}(fn_{res})$, adapted from Zoz et al. (2016)

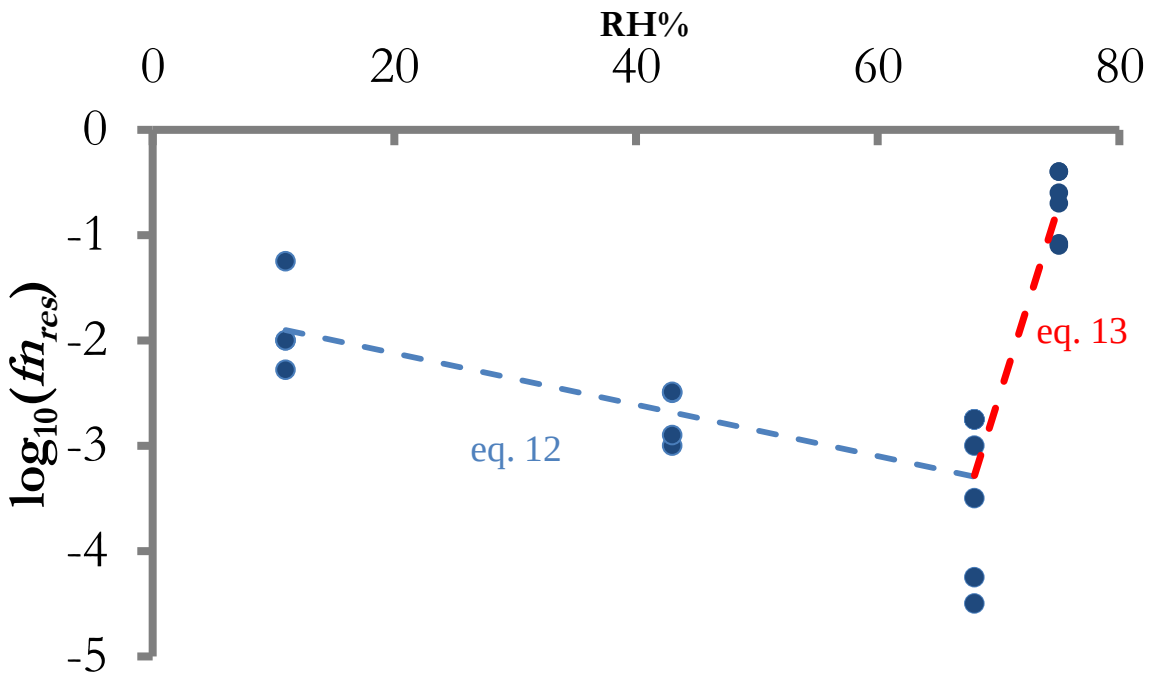

$$D = 3600 \cdot 10^{1.03 \cdot RH - 1.0782} \quad (11)$$

For 11%≤RH≤68%:

$$fn_{res} = 10^{-2.6 \cdot RH - 1.6} \quad (12)$$

For 68%≤RH≤92%:

$$fn_{res} = \min(1, 10^{36.7 \cdot RH - 28.2}) \quad (13)$$

Equation 11 shows that the lower the relative humidity, the faster the microbial inactivation. For example, $D \approx 8$ min. at RH = 20%, $D \approx 33$ min. at RH = 80%. However, Equations 12 and 13 show that the residual cell density (fn_{res}) is not linearly related to relative humidity: fn_{res} reaches a minimum at around 68%. Indeed, Zoz et al. (2016) explains that if RH is too low it tends to preserve bacteria and if RH is too high it doesn't induce sufficient dehydration-related damage. Because of these 2 effects, these authors found that the residual cell density is the lowest for relative humidity of about 68%. For example, from Equation 12 and 13, fn_{res}=8% at RH=20%, fn_{res}=0.5‰ at RH=68%, fn_{res}=100% at RH>77%. Note that when 77%<RH<92%, the microbial load stays constant (no growth and no inactivation).

These equations were implemented using MATLAB software (vR2012a, MathWorks Inc., Natick, MA, USA, Euler method). The computation time was around three minutes when an i5-3570 CPU 340 GHz computer was used. The simulation was carried out for 20 h, representing the drying and production periods. During the production period, it was considered that no water was added to the room, and the thermostat temperature was set at the same value as that during the drying period (5°C).

5. Results and discussion

The influence of several parameters on microbial development was studied: the relative humidity of blown air, the physiological state of bacteria (h_0) and heat supply to the equipment.

5.1. Influence of the relative humidity of blown air on microbial evolution

Three different relative humidities set at the inlet of the evaporator (blown air) of the food production plant were studied: 50%, 68% and 85%. The 68% level corresponds to the minimum residual cell density fn_{res}. It also roughly corresponds to the value measured in a plant when an air drying device (or dehumidifier) was used (measurement performed in a food plant). The 85% level was measured in the plant without a dehumidifier. The 50% level corresponds to a condition that can reasonably be achieved in a food processing plant.

The relative humidity exerts not only an influence on microbial development but also on heat and mass transfer. The evolution of the percentage of wet surface on the floor (β_f), wall (β_w) and equipment (β_e) is predicted and shown in Figure 5 for 50%, 68% and 85% relative humidity. It can be observed that the drying time increases as the relative humidity rises, especially for the wall and equipment. In addition, the equipment seems to be the surface that stays wet the longest, with drying times of around 5 hours, 7 hours and 15 hours for 50%, 68% and 85% relative humidity respectively. This can be explained by the lower thermal inertia (mCp) of the equipment ($4.8 \cdot 10^4$ J.K^{-1}) compared with the wall ($3.1 \cdot 10^5$ J.K^{-1}) and the floor ($7.1 \cdot 10^5$ J.K^{-1}). The initial temperatures of the wall, floor and equipment are estimated to be 15.5°C, 35.0°C and 39.8°C respectively due to the cleaning process (~40°C) over a period of 5 hours (Lecoq et al. 2016). With low thermal inertia, the equipment temperature decreases and rapidly (within two hours) approaches the air temperature (5°C), whereas this decrease takes longer for the other surfaces (Lecoq et al. 2016). Then the equipment can no longer supply the energy (latent heat) required to evaporate the water.

Figure 5: Wet surface evolution at 50%, 68% and 85% of relative humidity at the inlet of the evaporator a: wall (5 hours) b: floor (5 hours) c: equipment (20 hours)

a)

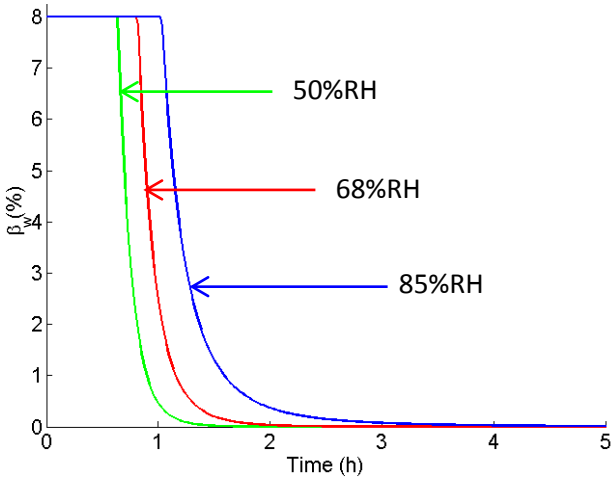

b)

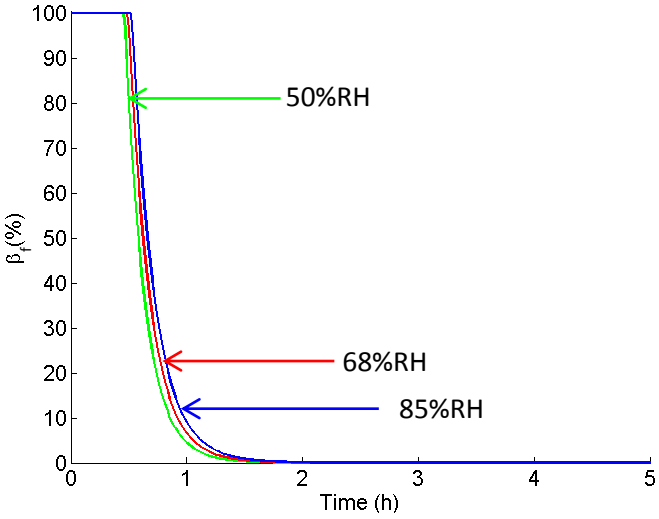

c)

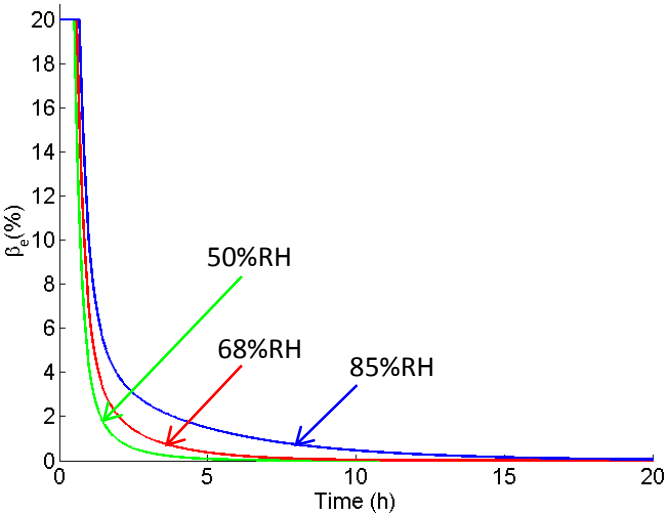

The average microbial evolution ($x = log_{10}\left(\frac{n}{n_0}\right)$) on the floor ($x_f$), wall ($x_w$) and equipment ($x_e$) is shown Figure 6 for 50%, 68% and 85% relative humidity for h_0 = 0. On the wall (Figure 6.a.) and equipment (Figure 6.c.), for relative humidity of 50 and 68%, *L. monocytogenes* decreases from the outset due to the high initial dry area (92% on the wall and 80% on the equipment) where inactivation takes place. On the wet surface, there are fewer living cells than inactivated cells on dry surfaces, which explains the overall decline in the population as a whole. On the floor (Figure 6.b.), slight growth can be observed because the entire surface is covered with water during the first 30 min. The wet surface then decreases, which induces a drop in the *L. monocytogenes* load for 50% and 68% relative humidity. For all the surfaces, the microbial load decreases to about -2.9 logUFC.m^{-2} at 50% RH and -3.3 logUFC.m^{-2} at 68% RH. The higher value at 50%RH means that more bacteria will survive than that at 68%RH (where the residual cell density reaches a minimum) even though the microbial load decreases faster at 50% due to a shorter drying time and a higher rate of inactivation (k). In addition, the *L. monocytogenes* load decreases at a slower rate on the equipment than on the wall and the floor for both 50 and 68% RH, which can be explained by the longer time necessary to dry the equipment. This induces higher contamination risks on the equipment.

Figure 6: Evolution of the *Listeria monocytogenes* load at 50%, 68% and 85% of relative humidity at the inlet of the evaporator for h_0 = 0 a: wall (5 hours) b: the floor (5 hours) c: the equipment (20 hours)

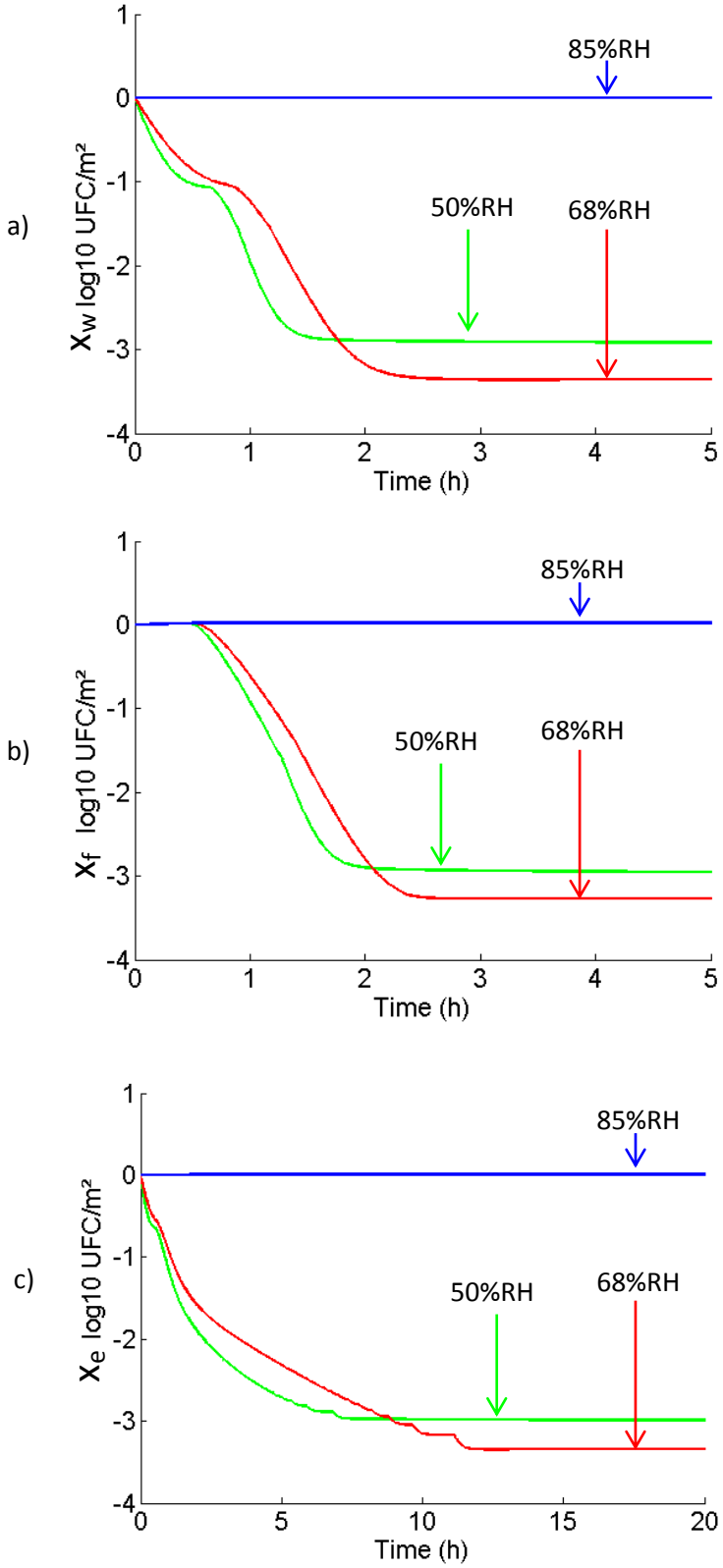

When the relative humidity is set at 85%, only a slight increase in the microbial load can be observed at the beginning (Figure 6). Figure 7 shows the results for *RH* = 85% with a more appropriate scale. The increase in microbial load becomes less marked as the wet surface decreases and then remains constant when the surface is entirely dry. This is due to the log(*D*) value which is very small at this high relative humidity. The microbial load increase is higher on the floor because at the beginning of the process, the floor is entirely covered in water. The characteristic growth time $\left(\frac{1}{\gamma \cdot \mu_{opt}}\right)$ at 5°C is equal to 233 hours, which explains the very small increase in microbial load. However, even if the increase is low for one day ($\frac{n-n_0}{n_0} \approx 6\%$ on the floor, ≈ 1% on the equipment) the accumulation can become problematic over a period of several months in areas where disinfection is not efficient.

From these simulations, it seems that a range of 60-70% RH is an optimal relative humidity range for drying food processing plants, mainly because microbial destruction is the most efficient at that RH level (Zoz et al. 2016).

Figure 7: Evolution of the *Listeria monocytogenes* load at 85% of relative humidity at the inlet of the evaporator on the wall, the floor and the equipment

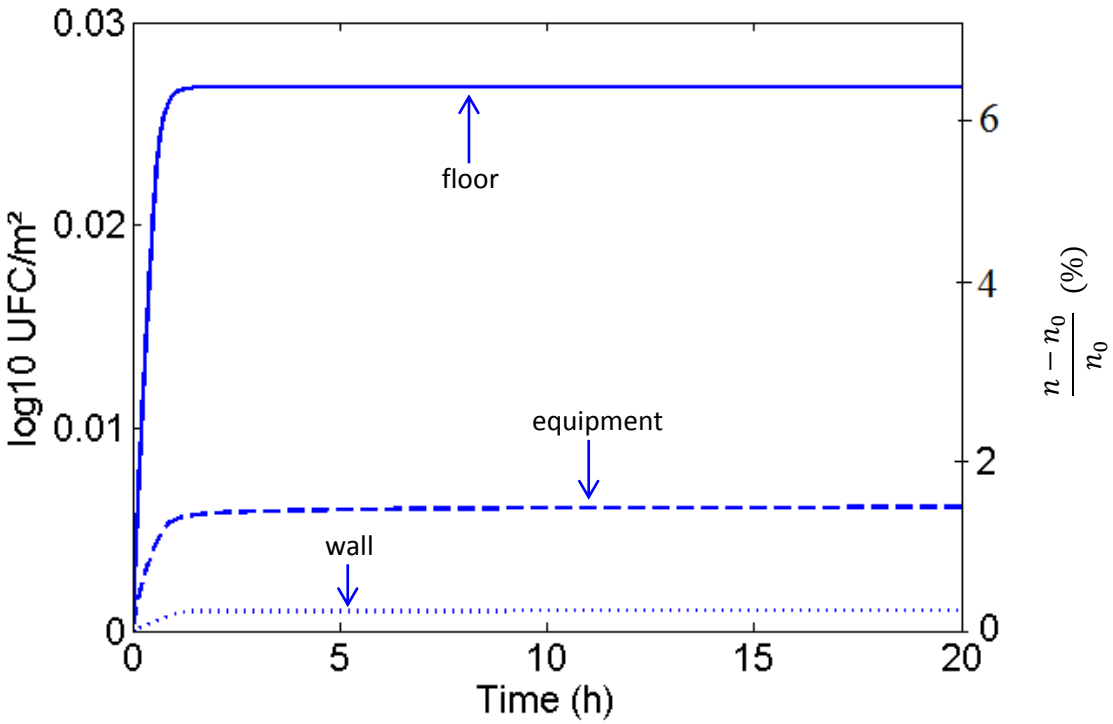

5.2. Influence of the physiological state on microbial evolution

The physiological state of the microorganisms, represented by the coefficient h_0, determines the latency (lag) time interval of microbial growth, and the higher h_0, the greater the lag phase. Three different h_0 values were tested: 0, 2.0 and 3.5 corresponding to different levels of bacterial stress. The influence of this coefficient on the evolution of the microbial load was studied on the floor, where bacterial growth is greatest, for 68% RH during the first 30 min when the floor was entirely wet (Figure 8). It can be observed that with higher h_0, the micro-organism takes longer to grow because of a longer lag time. This implies that when h_0 is equal

to 3.5, growth is almost non-existent because the surface starts drying before the end of the lag time.

Figure 8: Influence of physiological state (h_0) of *Listeria monocytogenes* on the evolution of load on the floor during the first 35 min of drying for 68% relative humidity at the inlet of the evaporator

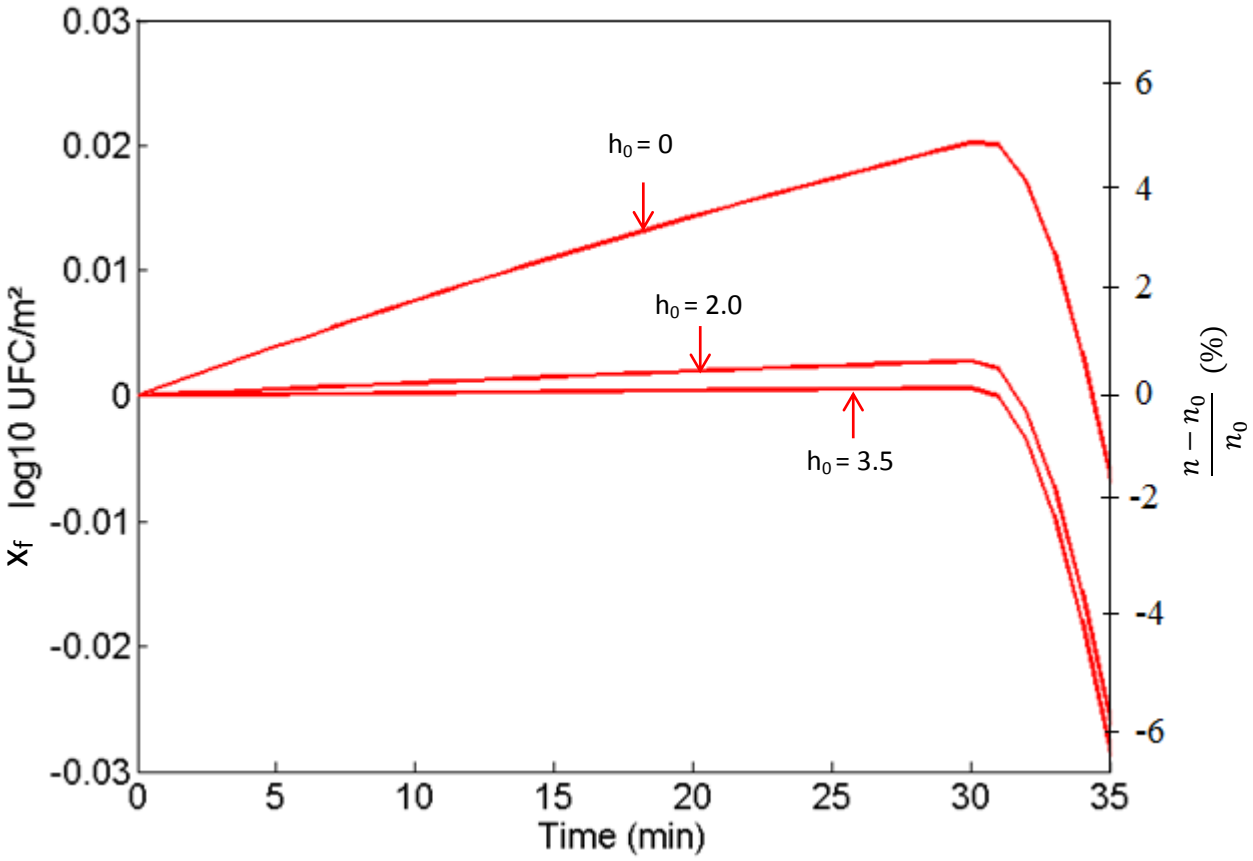

5.3. Influence of heat supply on microbial evolution

Figure 6 shows that microbial inactivation was slowest on the equipment, this being due to the fact that this surface takes longer to dry than the floor and the wall. Due to its low thermal inertia, equipment drying can be enhanced by heat supply. In this study, the impact of 100W heat supply for this equipment on the microbial load evolution was studied. For 68%RH at the inlet of the evaporator, the predicted wet surface (Figure 9a) and the microbial load evolution (Figure 9b) with and without heat supply to the equipment is shown. The surface is dried after about 4 hours with a heat supply and about 8 hours without a heat supply. As a consequence, the microbial load decreases rapidly with a heat supply and attains -3.3 Log UFC.m^{-2} in 5 hours, whereas it takes 12 hours to achieve a similar microbial load reduction without a heat supply. Thus, a heat supply device can be a solution for limiting the contamination risk.

The heat supplied to the equipment does not affect the wall and the floor temperatures (results not shown).

Figure 9: Comparison with and without equipment heating at 68% RH
a: evolution of the wet surface over the total surface of the equipment during the 10 first hours
b: evolution of the population of *Listeria monocytogenes* on the equipment during 20 hours (drying + production)

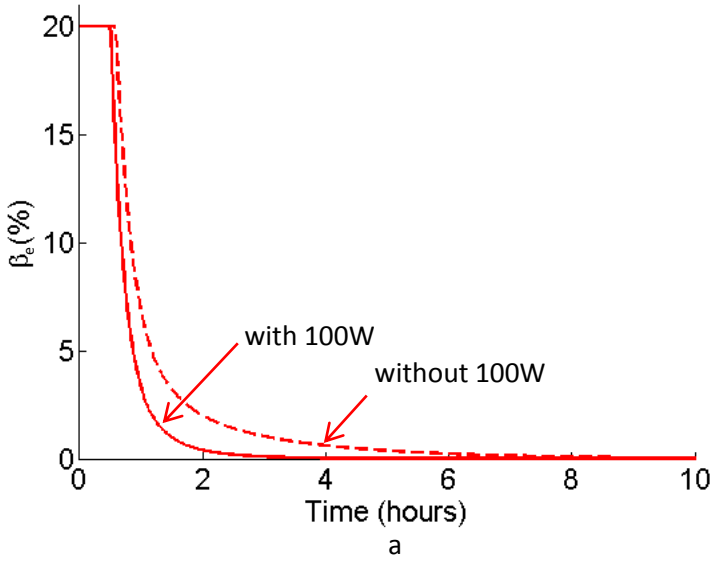

a

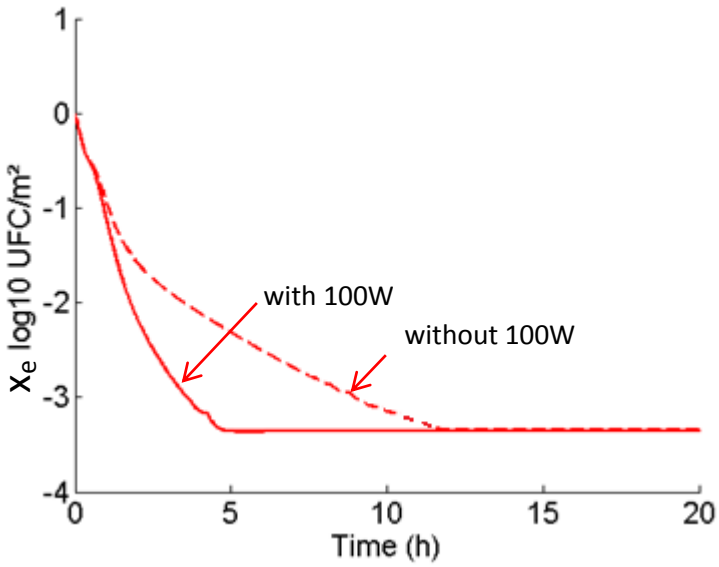

b

6. Conclusion

An approach combining heat/mass transfer and predictive microbiological models, taking into account the wet surface evolution, was developed. The influence of relative humidity (50%, 68% and 85%) at the inlet of the evaporator of a food processing plant on the wet surface and on the evolution of *L. monocytogenes* at different locations (floor, wall and equipment) was numerically studied. Inactivation is faster when the relative humidity is lower because of two phenomena: inactivation kinetics increase and the wet surface decreases faster; thus, inactivation appears earlier in the process. It seems that 60-70% relative humidity in a food processing plant is a good compromise because this relative humidity can be reached using a dehumidifier; lower humidity could lead to higher residual cell density. To inactivate the bacteria on equipment more rapidly, supplying heat in order to increase the drying rate can be a practical solution.

ACKNOWLEDGEMENT

The research leading to this result has received funding from the French National Research Agency (EcoSec Project, ANR-12-ALID-0005-04).

REFERENCES

2002. No 178/2002 of the European parliament and of the council of 28 January 2002 laying down the general principles and requirements of food law, establishing the European Food Safety Authority and laying down procedures in matters of food safety. *(OJ L 31, 1.2.2002)*

Augustin J.-C., Zuliani V., Cornu M., Guillier L. 2005a. Growth rate and growth probability of *Listeria monocytogenes* in dairy, meat and seafood products in suboptimal conditions. *Journal of Applied Microbiology* 99: 1019-42

Augustin J.-C., Zuliani V., Cornu M., Guillier L. 2005b. Growth rate and growth probability of Listeria monocytogenes in dairy, meat and seafood products in suboptimal conditions. . *Journal of Applied Microbiology* 99: 1019-42

Aziza-Tenenhaus F. 2007. Maîtrise des dangers microbiologiques en industrie laitière basée sur un modèle d'appréciation quantitative des risques : application à Listeria monocytogenes dans les fromages à pâte molle au lait pasteurisé. *Thése de doctorat, AgroParisTech, Paris.*

Baranyi J., Roberts T. A. 1994. A dynamic approach to predicting bacterial growth in food. *Journal of Food Microbiology* 23: 277-94

Batz M. B., Hoffmann S., Jr J. G. M. 2012. Ranking the disease burden of 14 pathogens in food sources in the united states using attribution data from outbreak investigations and expert elicitation. *J Food Protect* 75: 1278-91

Buchanan R., Lindqvist R., Ross T., Smith M., Todd E., Whiting R. 2004. Risk assessment of Listeria monocytogenes in ready-to-eat foods. *Food and Agriculture Organisation of the United Nations* Microbiological Risk Assessment Series, 4

CAC. Codex Alimentarius Commission, 2007. Principles and guidelines for the conduct of Microbiological Risk Management (MRM). *CAC/GL* 63-2007

Carpentier B., Cerf O. 2011. Review — Persistence of Listeria monocytogenes in food industry equipment and premises. *International Journal of Food Microbiology* 145: 1-8

EFSA. 2015. The European Union summary report on trends and sources of zoonoses, zoonotic agents and food-borne outbreaks in 2013. *EFSA Journal* 13: 3991, 162 pp

Fretz R., Sagel U., Ruppitsch W., Pietzka A., Stoger A., Huhulescu S., al. e. 2010. Listeriosis outbreak caused by acid curd cheese Quargel, Austria and Germany 2009. *European Surveillance* 15

Guillier L., Augustin J.-C. 2006a. Modelling the individual cell lag time distributions of *Listeria monocytogenes* as a function of the physiological state and the growth conditions. *Int. J. Food Microbiol.* 111: 241-51

Guillier L., Augustin J.-C. 2006b. Modelling the individual cell lag time distributions of Listeria monocytogenes as a function of the physiological state and the growth conditions. *Int. J. Food Microbiol.* 111: 241-51

Lambertz S. T., Ivarsson S., Lopez-Valladares G., Sidstedt M., Lindqvist R. 2013. Subtyping of Listeria monocytogenes isolates recovered from retail ready-to-eat foods, processing plants and listeriosis patients in Sweden 2010. *International Journal of Food Microbiology* 166: 186-92

Lecoq L., Flick D., Derens E., Hoang H. M., Laguerre O. 2016. Simplified heat and mass transfer modeling in a food processing plant. *Journal of Food Engineering* 171: 1-13

Løvdal T. 2015. The microbiology of cold smoked salmon. *Food Control* 54: 360-73

McKellar R. C., Lu X. 2004. Modelling microbial response in food. *Boca Raton, FL, USA : CRC Press.*

McMeekin T. A., Ross T. 2002. Predictive microbiology: providing a knowledge-based framework for change management. *International Journal of Food Microbiology* 78: 133-53

Mellefont L. A., McMeekin T. A., Ross T. 2003. The effect of abrupt osmotic shifts on the lag phase duration of foodborne bacteria. *Int. J. Food Microbiol.* 83: 281-93

Muhterem-Uyar M., Dalmasso M., Bolocan A. S., et, al. 2015. Environmental sampling for Listeria monocytogenes control in food processing facilities reveals three contamination scenarios. *Food Control* 51: 94–107

Tenenhaus-Aziza F., Daudin J. J., Maffre A., Sanaa M. 2014a. Risk-based approach for microbiological food safety management in the dairy industry: The case of Listeria monocytogenes in soft cheese made from pasteurized milk. *Risk Analysis* 34: 56-74

Tenenhaus-Aziza F., Daudin J. J., Maffre A., Sanaa M. 2014b. Risk-based approach for microbiological food safety management in the dairy industry: The case of *Listeria monocytogenes* in soft cheese made from pasteurized milk. *Risk Analysis* 34: 56-74

VamImpe J. F., Nicolaï B. M., Schellekens M., Martens T., Baerdemaeker J. D. 1995. Predictive microbiology in a dynamic environment: a system theory approach. *International Journal of Food Microbiology* 25: 227-49

Vogel B. F., Huss H. H., Ojeniyi B., Ahrens P., Gram L. 2001. Elucidation of Listeria monocytogenes contamination routes in cold-smoked salmon processing plants detected by DNA-based typing methods. *Appl. Environ. Microbiol.* 67: 2586–95

Zhu Q., Hussain M. 2014. Prevalence of Listeria species in fresh salad vegetables and ready-to-eat foods containing fresh produce marketed in Canterbury. New Zealand. *Advances in Food Technology and Nutritional Sciences Open Journal* 1: 5-9

Zoz F., Iaconelli C., Lang E., Iddir H., Guyot S., Grandvalet C., Gervais P., Beney L. 2016. Control of Relative Air Humidity as a Potential Means to Improve Hygiene on Surfaces: A Preliminary Approach with Listeria monocytogenes. *Plos One* 11

Zwietering M. H., Wijtzes T., Wit J. C. D., Riet K. V. 1992. A Decision Support System for Prediction of the Microbial Spoilage in Foods. *Journal of Food Protection* 55: 973-79

CHAPITRE 6 : CONCLUSION – PERSPECTIVES

Pour faire face à la complexité du processus de séchage d'un atelier (grand volume, conditions ambiantes non homogènes, répétition des expérimentations difficiles,…), une méthodologie, basée sur une étude à plusieurs échelles, a alors été développée dans le but d'analyser l'évaporation de l'eau sur une surface. Nous avons étudié d'abord en laboratoire l'évaporation d'une ou plusieurs gouttes d'eau déposées sur une surface, de manière à établir l'influence de différents paramètres. Des corrélations ont été développées, ce qui a permis de prédire le séchage sur les parois d'un atelier et d'identifier celles qui vont rester mouillées à la fin du séchage (principalement les équipements), favorisant ainsi la contamination microbienne.

Les résultats obtenus lors de la thèse ont permis de répondre à plusieurs questions telles que la quantité d'eau initiale dans les ateliers agro-alimentaires après le nettoyage, la cinétique d'évaporation en fonction des conditions ambiantes et l'évolution de la charge microbienne sur différentes surfaces de l'atelier. Ainsi, des solutions techniques ont pu être proposées pour améliorer le séchage.

Pour cela il était nécessaire de comprendre les phénomènes qui interviennent lors de l'étape de séchage. Diverses approches ont été mises en œuvre: expérimentation, modélisation de type mécanique des milieux continus et modélisation simplifiée (approche analytique ou zonale).

6.1. Avancées scientifiques

Une étude portant sur l'évaporation d'eau à quatre échelles différentes a été mise en place lors de cette thèse :

Dans une boîte ventilée. Ceci a permis de mettre en relation l'inactivation microbienne et le séchage en fonction de l'humidité relative (collaboration avec l'UMR PAM Dijon et l'ANSES).

Dans une soufflerie où les conditions ambiantes sont parfaitement maîtrisées. L'influence des conditions ambiantes (HR, h, T_a) et du pourcentage de la surface mouillée (β) sur l'évaporation (évolution de la masse d'eau, m) a été étudiée et des corrélations ont été établies.

Dans une cellule d'essai où les conditions sont moins bien contrôlées par rapport à celles de la soufflerie et se rapprochent d'un atelier agro-alimentaire. Les corrélations développées en soufflerie ont permis de prédire correctement la cinétique d'évaporation à cette échelle (gouttes d'eau sur une surface en inox) justifiant ainsi l'application de celles-ci pour un atelier. Un première modèle pour prédire le séchage d'un sol entièrement mouillé a aussi été mis en place lors de cette étude.

Dans un atelier agro-alimentaire. Un modèle de transfert thermique/massique couplé avec un modèle de microbiologie prévisionnelle a pu être développé grâce aux études précédentes. L'objectif était de prédire l'évolution de la masse d'eau sur trois surfaces : le mur, le sol et un équipement ainsi que l'évolution de la charge bactérienne.

Lors des études à différentes échelles, des modèles plus ou moins détaillés ont permis de prendre en compte que pour des gouttes d'eau déposées sur une plaque, il existe en général 2 périodes de séchage.

Pendant la première période, la cinétique d'évaporation est à peu près constante : l'angle de contact diminue tandis que la surface mouillée reste constante. Pendant la seconde période, la cinétique d'évaporation ralentit : l'angle de contact reste constant tandis que la surface mouillée diminue.

Les études réalisées sont résumées dans le tableau ci-dessous avec les approches employées (expérimentale (Exp.), numérique (Num.) et théorique).

Dispositif	**Phénomènes étudiés**	**Méthodologie** **Exp. / Num. / Théorique**
Boîte ventilée 0.001 m^3	Evaporation d'une goutte Charge microbienne[1]	Exp. *Relation inactivation bactérienne/HR*
Soufflerie 0.02 m^3	Evaporation de plusieurs gouttes	Exp. / Num. *Corrélations prédisant Tplaque et le débit évaporatoire*
Cellule d'essai 30 m^3	Evaporation de plusieurs gouttes	Exp. / Num. / Théorique *Validation des corrélations* *1ère approche modèle simplifié chaleur/masse*
Atelier agro-alimentaire 450 m^3	Séchage d'un atelier 3 surfaces : mur, sol, équipement	Exp. / Num. / Théorique *Développement d'un modèle simplifié chaleur/masse basé sur les résultats soufflerie/cellule* *Couplage microbio. prévisionnelle* [2]

[1] Collaboration UMR PAM (Dijon)

[2] Collaboration ANSES

L'analyse des résultats expérimentaux obtenus en laboratoire (soufflerie et cellule d'essai) ont permis de constater que l'humidité relative de l'air est le paramètre le plus influant sur la cinétique d'évaporation d'eau parmi les 4 paramètres étudiés et dans les plages de valeurs considérées : $31\%<HR<87\%$, $5.4°C<Ta<20.2°C$, $8.5\ W.m^{-2}.K^{-1}<h<14.2\ W.m^{-2}.K^{-1}$ et

7%<β_0<23%. Ces variations correspondent aux plages de valeurs que l'on peut rencontrer en atelier agro-alimentaire. Nous avons constaté que lorsqu'on diminuait l'humidité relative de 87% à 31%, le taux d'évaporation était multiplié par un facteur de 5.2, alors que pour les autres conditions il n'augmentait que de 2.3 au maximum. L'étude de l'influence de la réduction de l'humidité relative par l'implantation d'un déshumidificateur d'air sur le séchage des surfaces d'un atelier agro-alimentaire a alors été réalisée (expérimentalement et numériquement) et a montré l'intérêt d'une telle installation pour accélérer l'évaporation de l'eau sur les parois.

6.2. Avancées technologiques

Dans notre étude, l'installation d'un déshumidificateur a permis de réduire en moyenne l'humidité relative dans l'atelier de 90% à 60%, ce qui entraîne a priori une inactivation microbienne plus importante du fait d'un assèchement rapide des surfaces. Compte tenu de la lourdeur de la mise en place d'analyses microbiologiques dans un atelier, l'impact de la dessiccation sur l'inactivation bactérienne n'a été analysé qu'avec un modèle de microbiologie prévisionnelle. Les paramètres de ce modèle microbiologique ont été déterminés grâce aux expériences réalisées préalablement dans la boîte ventilée à plusieurs humidités relatives imposées par l'UMR PAM. Le modèle d'échanges thermique et massique que nous avons développé permet de prédire, entre autres, la cinétique d'évaporation sur les parois. Ce modèle a été validé en comparant les données numériques avec celles obtenues lors des expérimentations à l'atelier (évolution des masses d'eau, température de parois…). La connaissance de la masse d'eau à sécher et de la cinétique d'évaporation pendant le séchage, permet de déduire la capacité du déshumidificateur (en $kg_{eau}.h^{-1}$) à installer pour évacuer l'eau évaporée. Ceci permet le dimensionnement de l'appareil en fonction des besoins de l'atelier. Il est à noter que l'installation de déshumidificateurs dans les ateliers est rare actuellement et que leur dimensionnement est réalisé de manière empirique.

Il a été observé lors de ces études que ce sont les équipements qui sèchent le plus lentement dans l'atelier du fait de leur faible inertie thermique. Le modèle simplifié développé nous a permis de montrer qu'un apport de chaleur (50 $W.m^{-2}$) au niveau des équipements combiné à l'installation d'un déshumidificateur permettrait de diminuer sensiblement le temps de séchage (passant en dessous du temps imparti de deux heures). De plus, le couplage avec la microbiologie prévisionnelle nous a permis d'en conclure que cela diminuerait aussi fortement la charge microbienne sur cette surface. Cela réduirait ainsi le risque de contamination microbienne sur les équipements, une surface d'autant plus à surveiller car les produits alimentaires seront en contact avec celle-ci. Nous avons appris récemment que cette recommandation avait été suivie avec succès dans un atelier agro-alimentaire sur un équipement qui était problématique.

6.3. Perspectives

Le modèle simplifié développé peut être généralisé à d'autres ateliers en connaissant les paramètres d'entrée qui lui sont propres comme, par exemple, l'aire des parois, l'inertie thermique des surfaces, les vitesses d'air proche des surfaces, la masse d'eau à sécher, les caractéristiques des évaporateurs et du déshumidificateur en fonctionnement (puissance, débit d'air, humidité en sortie), etc…Le modèle simplifié pourrait être complété par une étude CFD dans un atelier agro-alimentaire. Avec une simulation CFD, les champs de vitesse d'air dans la pièce pourraient être analysés en détail, ce qui permettrait d'étudier l'hétérogénéité de l'évaporation sur une surface liée à l'écoulement d'air.

Le modèle simplifié prédit pour l'instant l'évolution de la température, de la masse d'eau et de la charge microbienne sur les parois d'un atelier agro-alimentaire. Il pourra être envisagé par la suite d'y inclure les transferts au niveau du produit pour prédire l'évolution de sa température et de la charge microbienne. Ainsi, ce modèle pourrait être couplé aux modèles déjà développés par Irstea pour des camions frigorifiques, chambres froides, meubles frigorifiques de vente et réfrigérateurs domestiques. L'évolution de la température et de la charge microbienne des produits dans la chaîne du froid, de la production dans un atelier agro-alimentaire au réfrigérateur domestique, pourra être évaluée. Selon le produit étudié, d'autres modèles de qualités pourraient être associés au modèle thermique/massique (couleur, texture, onctuosité,…).

Pour finir, il serait également intéressant de réaliser une analyse coût (installation + fonctionnement) / bénéfice liée à l'installation d'un déshumidificateur. Les bénéfices viennent principalement de la baisse de la contamination dans l'atelier dû au déshumidificateur, impliquant ainsi moins de risque pour les produits. Actuellement, une quantité importante de produit est éliminée à l'usine à cause de sa contamination épisodique. D'après la norme européenne, un produit est considéré comme « à risque » si la contamination dépasse 100 CFU/gramme de produit. Notre étude peut donc contribuer à la lutte contre le gaspillage alimentaire.

Title : experimental characterization and modelling of the evaporation phenomena on surfaces of a cold room

Keywords: food processing plant, evaporation, heat and mass transfer, simplified model, dehumidification

Abstract:

The aim of this Ph.D. thesis is to develop a methodology to predict drying rate on walls in a food processing plant.

This methodology is based on studies at different scales to analyze the heat and mass (water) exchanges in a food plant. Three laboratory studies were performed: a ventilated box (~0.001 m^3), a wind tunnel (~0.02 m^3), a cold room (~30 m^3) and one in a food processing plant (~450 m^3). Numerical (Comsol) and analytical models were developed to predict water evaporation rate on a solid surface (stainless steel, PVC) and validated with experimental data obtained in the wind tunnel and the cold room. For the experimental conditions studied, the results shown that relative humidity was the most influential factor on the evaporation rate.

A simplified heat and mass transfer model was developed to predict the water mass evolution on the walls of a food plant in function of ambient conditions. This model is based on a zonal approach that considers three walls: wall, floor and equipment. The influence of a dehumidifier was studied. The experimental and numerical results showed that the dehumidifier allowed the reduction of relative humidity in the room from 90% to 60% which reduced the drying time by about 1.5 times. It was shown that the equipment dries the slowest due to its low thermal inertia, consequently, water was still remained after 2h (drying duration in the food plant). In order to increase the evaporation rate on the equipment, it was estimated by the model that 50 $W.m^{-2}$ of heat supply could be provided to complete drying.

Finally, this model was coupled to predictive microbiology model where the parameters were identified using the experimental data of the *Listeria monocytogenes* cultivability exposed to different relative humidity in the ventilated box (UMR PAM and ANSES collaboration). The results showed that the inactivation was the highest at 68% of relative humidity and that with the heat supplied to equipment of 50 $W.m^{-2}$, the minimal of bacterial load would be reached after 5 hours instead of 12 hours without heat supply.

Titre : caractérisation expérimentale et modélisation des phénomènes d'évaporation sur les parois d'une enceinte réfrigérée

Mots clés : atelier agro-alimentaire, évaporation, transfert thermique et massique, modèle simplifié, déshumidification

Résumé :

L'objectif de cette thèse est de développer une méthodologie permettant de prédire la cinétique de séchage des parois d'un atelier agro-alimentaire.

Cette méthodologie se base sur des études à différentes échelles dans le but d'analyser les phénomènes liés aux échanges thermique et massique (eau) dans un atelier. Trois études en laboratoire ont été réalisées : dans une boîte ventilée (~0.001 m ^{3}), une soufflerie (~0.02 m^3), une cellule d'essai (~30 m^3) et une étude sur site dans un atelier agro-alimentaire (~450 m^3). Des modèles numériques (Comsol) et analytiques ont été développés permettant de prédire le taux d'évaporation d'eau sur une surface (inox, PVC) et validés avec les données expérimentales obtenues en soufflerie et en cellule d'essai. Pour les conditions expérimentales étudiées, les résultats ont montré que l'humidité relative était le facteur le plus influant sur le taux d'évaporation.

Ces études ont permis le développement d'un modèle simplifié des échanges thermique et massique permettant de prédire l'évolution de la masse d'eau sur les parois d'un atelier en fonction des conditions ambiantes. Ce modèle se base sur une approche zonale en considérant trois parois : un mur, un sol et un équipement. Cela a permis d'étudier l'influence de l'implantation d'un déshumidificateur d'air. Les résultats expérimentaux et numériques ont mis en évidence l'intérêt de l'utilisation d'un tel appareil pour améliorer le séchage des parois. L'humidité relative de l'air dans l'atelier était réduite de 90% à 60% avec un déshumidificateur, ce qui diminuait le temps de séchage d'un facteur 1,5. Il a été montré que l'équipement séchait le plus lentement à cause de sa faible inertie thermique, par conséquent, il restait encore de l'eau même après 2h (durée de séchage de l'atelier). Pour augmenter le taux d'évaporation sur l'équipement, il a été estimé par le modèle qu'un apport de chaleur de 50 W.m^{-2} serait suffisant pour sécher les équipements.

Ce modèle a ensuite été couplé avec un modèle de microbiologie prévisionnelle dont les paramètres ont été identifiés en utilisant les données expérimentales de la cultivabilité de la *Listeria monocytogenes* à différentes humidités relatives dans la boîte ventilée (collaboration l'UMR PAM et l'ANSES). Les résultats ont montré que l'inactivation bactérienne était la plus importante pour une humidité relative aux alentours de 68% et qu'un apport de chaleur à l'équipement de 50 W.m^{-2} permettait d'atteindre un minimum de charge bactérienne au bout de 5 heures au lieu de 12 heures sans apport de chaleur.